3D bioprinted heart patches for cardiac regeneration

Author: Christopher David Roche

Candidature: Doctor of Philosophy

Faculty of Medicine and Health / Northern Clinical School of Medicine

The University of Sydney

A thesis submitted to fulfil requirements for the degree of Doctor of Philosophy

Date: July 2022

Pages: 220

Words: 100,000

PhD Supervisors: A/Prof Meilang Xue[1] and Dr Carmine Gentile[2]

1 University of Sydney and Sutton Research Laboratory, Kolling Institute, Sydney, Australia

2 University of Technology Sydney (primary) and University of Sydney (secondary), Sydney, Australia

Statement of originality

This is to certify that the content of this thesis is my own work. This thesis has not been submitted for any degree or other purposes. Chapters which have already been published in peer reviewed journals have been included in full without alteration as the final published version. All formal post publication correspondences to date are included in the Appendix to this thesis. Where I have collaborated with others, the contribution of those collaborators has been documented and can be found in the *Declarations of the candidate* section of this thesis and in the published contribution statements accompanying each of the published journal articles.

I certify that the intellectual content of this thesis is the product of my own work and that all the assistance received in preparing this thesis and sources have been acknowledged.

Christopher Roche, 12/07/2022

Declarations of the candidate

This thesis contains material which has been published, accepted for publication or is under review. Such material is always introduced with an original summary paragraph written by the candidate (for the purposes of this thesis and not submitted or published elsewhere). Following these summary paragraphs, the published article (or manuscript under review) is then inserted in full (as published or as submitted) with no alterations made. Published accompanying materials (such as Supplementary Materials, Supplementary Figures and Videos associated with each article) are inserted immediately following the article (either directly or as hyperlinks to the source files which were uploaded with the manuscripts for peer review). Where experiments have been pre-registered or where datasets have been uploaded to public repositories the links to these sources are found within their respective published articles.

The following declarations of the candidate have been agreed with the candidate's PhD supervisor regarding the contribution made by the candidate:

The following 11 chapters were written by the candidate for the purposes of introducing and discussing the thesis as a whole and these represent original work which has not been submitted or published elsewhere. Whilst the content is original, some of the concepts in these paragraphs may summarise and be similar to those in published article chapters of the thesis:

- Part 1 – Thesis introduction, hypothesis and aims (Chapter 1.1), Closing remarks Part 1 (Chapter 1.5)
- Part 2 – Introduction to Part 2 (Chapter 2.1), Closing remarks Part 2 (Chapter 2.5)
- Part 3 – Introduction to Part 3 (Chapter 3.1), Closing remarks Part 3 (Chapter 3.4)
- Part 4 – Introduction and relevance to Part 4, (Chapter 4.1), Thesis discussion (Chapter 4.2), Future directions (Chapter 4.3), Thesis conclusion (Chapter 4.4), Thesis take home message (Chapter 4.5)

The rest of the chapters have either been published (1.2, 1.3, 2.2, 2.3, 3.2, 3.3) or are under review (2.4) as peer-reviewed original articles in a scholarly journal. One chapter is in press as a book chapter (1.4). Candidate contribution statements for each of these published/under review chapters are as follows:

1.2 – Current challenges in three-dimensional bioprinting heart tissues for cardiac surgery

Published article: **Roche CD,** Brereton RJL, Ashton AW, Jackson C, Gentile C. Current challenges in three-dimensional bioprinting heart tissues for cardiac surgery. *Eur J Cardiothoracic Surg* 2020;58(3):500–510. https://doi.org/10.1093/ejcts/ezaa093

Contribution: as first author, the candidate researched this narrative review article, wrote the original draft, created the tables and figures (except Figure 6 which was created in liaison with a medical illustrator) and worked on all revised drafts, including the peer review and editing process with the journal. The idea for the article was originally proposed by the candidate's research supervisor and then developed with the candidate. The central image was created by a medial illustrator with guidance from the candidate.

1.3 – Omentum support for cardiac regeneration in ischaemic cardiomyopathy models: a systematic scoping review

Published article: Wang H, **Roche CD**, Gentile C. Omentum support for cardiac regeneration in ischaemic cardiomyopathy models: a systematic scoping review. *Eur J Cardiothorac Surg* 2020;58(6)1118-1129. https://doi.org/10.1093/ejcts/ezaa205

Contribution: as second author of three, the candidate proposed the idea of this narrative review article following discussions with RJL Brereton during work on one of the figures for Chapter 1.2. The candidate then

recruited a first-year medical student (H Wang) and worked closely with that student to learn the skills needed to perform a systematic scoping review. With assistance from the candidate, H Wang defined the search parameters/inclusion criteria. H Wang performed the literature search and screened the 1926 returned article abstracts to produce 35 eligible articles. At this point, H Wang and C Roche independently performed detailed review of each of the 35 screened articles to decide on the final 17 articles for inclusion in the review. H Wang wrote the original draft with guidance from C Roche. C Roche validated the data, completed the article submission process and (when the peer reviewers retuned extensive requests for changes) C Roche did the work of re-writing the manuscript and responding to the reviewers, with occasional proof reading and discussions with C Gentile and H Wang. The data extraction tables originally did not contain numerical data, only descriptions, and C Roche did the work of going to the source articles, extracting the numerical data and creating the data extraction tables as they appear in their final form. The central image was created by a medial illustrator with guidance from all three authors, including the candidate. H Wang and C Roche equally contributed to the PRISMA flowchart in Figure 1. C Roche was in a central supervisory role for the article, with occasional recourse to C Gentile for supervisor-level advice. For the reply letter to the correspondence received via the journal about this article, C Roche wrote the original draft when was subsequently revised in liaison with C Gentile and H Wang and then C Roche did the work of resubmitting this to the journal (Appendix A.2).

1.4 – Generation and applications of cardiac spheroids

Accepted book chapter: **Roche CD**, Polonchuk L, Gentile C. Generation and Applications of Cardiac Spheroids (with editor, *Tissue Engineering and Regeneration* book series)

Contribution: as first author, the candidate researched and wrote the first draft of this invited book chapter for which the title was proposed by the editor of the book series. The candidate then worked on subsequent drafts with his supervisor, C Gentile, and industry partner, L Polonchuk, in supervisory roles.

2.2 – Printability, durability, contractility and vascular network formation in 3D bioprinted cardiac endothelial cells using alginate-gelatin hydrogels

Published article. **Roche CD**, Sharma P, Ashton AW, Jackson C, Xue M, Gentile C. Printability, durability, contractility and vascular network formation in 3D bioprinted cardiac endothelial cells using alginate-gelatin hydrogels. *Front Bioeng Biotechnol* 2021.9;110 https://doi.org/10.3389/fbioe.2021.636257

Contribution: as first author, the candidate led this article which represents the complete *ex vivo* optimisation phase for patches prior to *in vivo* use. The author designed the experiments in liaison with his supervisor, C Gentile, underwent training in the necessary lab techniques and performed all the experiments with the exception of the isolating of cardiac cells from mouse hearts (which was performed by P Sharma who delivered the cells to C Roche who then himself did the work of incorporating them into bioink, 3D bioprinting of patches and subsequent culture, data collection and analysis). C Gentile provided guidance and assistance with confocal microscopy. The candidate wrote the first draft of the manuscript and wrote all subsequent drafts in liaison with supervisors C Gentile, A Ashton, C Jackson and M Xue. The candidate did the work of submitting to journals and responding to the peer reviewer comments. The graphical abstract was created by a medical illustrator with guidance from C Roche and C Gentile. The figures were created by C Roche with input from C Gentile except for Figure 6 (Imaris software 3D rendering) which was created by C Gentile. The 3D rendering video content was created by C Gentile and the video edited into its published form by C Roche.

2.3 – Transplantation of a 3D bioprinted patch in a murine model of myocardial infarction

Published video article: **Roche CD**, Gentile C. Transplantation of a 3D bioprinted patch in a murine model of myocardial infarction. *J Vis Exp* 2020;61675. https://doi.org/10.3791/61675

Contribution: as first author working with one of his supervisors as the only co-author, C Roche proposed the idea of recording the method as a video and performed the video recording or C Gentile performing the surgical method. C Roche wrote the first draft of the accompanying written manuscript (including populating the complete table of materials/equipment) and worked on all subsequent drafts with supervisory guidance

from C Gentile. C Roche worked with the video editor to produce the edited final video and responded to the reviewer comments with guidance from C Gentile.

2.4 – 3D bioprinted alginate-gelatin hydrogel patches containing cardiac spheroids recover heart function in a mouse model of myocardial infarction

Article under Review: **Roche CD**, Lin H, Y Huang, de Bock CE, Beck D, Xue M, Gentile C. 3D bioprinted alginate-gelatin hydrogel patches containing cardiac spheroids recover heart function in a mouse model of myocardial infarction. *Acta Biomaterialia* (under review; submitted 15/03/2022; revised submission 26/06/2022)

Contribution: as first author the candidate underwent training to become competent to perform this experiment (including in use of specialist equipment such as mouse echocardiography and electrical mapping), contributed to the ethics committee application and ongoing liaison with the ethics committee during the experiment, performed the experiment (except the surgery itself, which was performed by C Gentile with C Roche as the anaesthetist), performed all postoperative care for mice and wrote the first draft of the manuscript, except for some of the sections about mRNA genetic profiling (the Figure 7 legend and the relevant method and results paragraphs), first drafts of which were written by D Beck. C Gentile performed the Imaris 3D rendering and confocal microscopy data collection and performed the mRNA isolation with assistance from C Roche. Histology samples were embedded in wax by a technician, H Lin performed picrosirius red histology staining and C Roche performed slicing, H&E and Masson's Trichrome staining and histology data collection and analysis. Flow cytometry was gated by M Xue and H Lin and performed by C Roche and H Lin. All figures, and supplementary figures were created by C Roche except Figure 1 and Videos 1, 2 and 3 (all these presented confocal data and Imaris software 3D rendering of patches, produced by C Gentile), and Figure 7 and Supplementary Figures 9-11 (produced by D Beck).

3.2 – A world first surgical instrument for minimally invasive robotically-enabled transplantation of heart patches for myocardial regeneration: a brief research report

Published article. **Roche CD**, Zhou Y, Zhao L, Gentile C. A world-first surgical instrument for minimally invasive robotically-enabled transplantation of heart patches for myocardial regeneration: a brief research report. *Front Surg* 2021;8:436. https://doi.org/10.3389/fsurg.2021.653328

Contribution: as corresponding author and also as joint first author with Y Zhou, the candidate proposed the original idea of trying to develop robotic minimally invasive surgical instruments to transplant patches (which was an original idea additional to the candidate's thesis proposal at the outset). The candidate developed the idea with the other three co-authors. Y Zhou did the work of creating the computer aided design files and the initial prototyping of instrument parts. C Roche wrote the first draft of the manuscript and all subsequent drafts with some input from supervisors (C Gentile and L Zhao) and in liaison with Y Zhou for specific details. Y Zhou supplied the data for the figure images and video and C Roche processed and edited them into publishable form. C Roche provided the voiceover and editing for the video. C Roche did the submission and responses to the peer reviewers and worked with the production team to produce the final published manuscript.

3.3 – Cardiac patch transplantation instruments for robotic minimally invasive cardiac surgery: initial proof-of-concept designs and surgery in a porcine cadaver

Published article. **Roche CD**, Iyer GR, Nguyen MH, Mabroora S, Dome A, Sakr K, Pawar R, Lee V, Wilson C, Gentile C. Cardiac patch transplantation instruments: world-first designs and prototype testing for robotic minimally invasive cardiac surgery. *Front Robot AI* 2022;8:714356 https://doi.org/10.3389/frobt.2021.714356

Contribution: As corresponding author and first author, C Roche led this multidisciplinary collaborative work. The full contributions of the other team members are found in the supplementary materials for the article (https://www.frontiersin.org/articles/10.3389/frobt.2021.714356/full#supplementary-material). In summary, C Roche provided input from a surgical perspective to teams of robotics and engineering specialists who did the work of producing the computer aided designs of instruments, designing the control systems, in

silico simulations and prototyping of control systems and instruments. C Roche provided supervision, objective setting, problem solving and leadership. C Roche wrote the original draft of the manuscript with input from G Iyer and S Mabroora and wrote all subsequent drafts and did the work of manuscript submission, responding to peer reviewers and the editor. C Roche created the figures and videos from data submitted by other members of the team (except video 2 which was created by G Iyer). C Roche presented the work and submitted it for the awards detailed in the acknowledgements section.

In addition to the statements above, in cases where I am not the corresponding author of a published item, permission to include the published material has been granted by the corresponding author (who is my co-supervisor, Dr Carmine Gentile, in all instances).

Christopher D Roche, 12/07/2022

As supervisor for the candidature upon which this thesis is based, I can confirm that the authorship attribution statements above are correct.

Meilang Xue, 12/07/2022

Acknowledgements

The author would like to acknowledge all the people who gave funding, assistance and/or their time to enable this PhD to happen. This includes (but is not limited to) donors, editors, formal and informal reviewers, the staff of the Kolling Institute, the Royal North Shore Hospital, St Andrew's College, UTS and USYD. This PhD was partly funded through the donations of private citizens, *via* Heart Research Australia (HROz), the Le Gros Legacy Fund New Zealand, the John Loewenthal Scholarship and the Paulette Isabel Jones PhD Completion Scholarship (USYD). The author would like to especially acknowledge the donations of private individuals, without which the PhD would not have been seen through to completion.

Dedication

To my family

Author Affiliations

1 Northern Clinical School of Medicine, University of Sydney, Kolling Institute, St Leonards, Sydney, NSW, Australia

2 School of Biomedical Engineering, Faculty of Engineering and IT, University of Technology Sydney (UTS), Ultimo, Sydney, NSW, Australia

3 Department of Cardiothoracic Surgery, Royal North Shore Hospital, St Leonards, Sydney, NSW, Australia

4 Department of Cardiothoracic Surgery, University Hospital of Wales, Cardiff, UK

5 St Andrews College, University of Sydney, Newtown, NSW 2042, Australia

Supervisory Team

Primary Supervisor: A/Prof Meilang Xue, University of Sydney and Sutton Arthritis Research Laboratory, Kolling Institute, University of Sydney, Sydney, NSW, Australia.

Primary/Secondary Supervisor and Project Leader:* Dr Carmine Gentile, Senior Lecturer, University of Technology Sydney (UTS, primary affiliation) and University of Sydney (secondary affiliation).

Associate Supervisors: Prof Christopher Jackson (University of Sydney and Sutton Arthritis Research Laboratory, Kolling Institute, University of Sydney, Sydney, NSW, Australia) and A/Prof Anthony W Ashton (Northern Clinical School of Medicine, University of Sydney, Kolling Institute, St Leonards, Sydney, NSW, Australia).

*From July 2019, project leader (and initial project supervisor), Dr Carmine Gentile, received a promotion whereby his primary academic affiliation moved from USYD to UTS. Subsequent work took place collaboratively across both university sites with significant parts of the work completed at UTS in the Faculty of Engineering and IT (School of Biomedical Engineering) and using laboratory space in the Faculty of Science (UTS). To fulfil a USYD requirement that named primary supervisors must have primary (not secondary/honorary) USYD affiliation, Dr Gentile was assigned as secondary supervisor for administrative purposes but continued to fulfil a primary supervisor's role in collaboration with A/Prof Meilang Xue. Special thanks also go to Associate Supervisors, Prof Jackson and A/Prof Ashton, who were also briefly in the primary supervisor role (2019) for administrative purposes. The PhD is a true product of academic collaborative spirit and team working.

Abstract (Whole Thesis)

BACKGROUND: epicardial patch transplantation is a promising approach to restore some of the cardiac function lost after myocardial infarction (MI). Advances in 3D bioprinting, 3D cell culture and transplantation methods at surgery have provided hope that this approach could soon benefit heart failure patients. The optimal content of 3D bioprinted patches (the "bioink" extruded by a 3D bioprinter) is not known. Patches containing a suspension of 3D vascularised cardiac spheroids (VCS; 3D aggregates of cells / microtissues) in hydrogel may confer an advantage compared to freely suspended cells or hydrogel without cells. The mechanisms underlying the benefit of epicardial patch transplantation approaches have not been fully elucidated and this is needed for widespread clinical translation. To be fully compatible with cardiothoracic surgical approaches in future, patches should be transplantable by minimally invasive robotic approaches. METHOD: Alginate-gelatin (AlgGel) patches were optimised *ex vivo* for cardiac applications, followed by *in vivo* transplantation of patches in mice modelling MI. For the *ex vivo* optimisation phase, three different bioprinters were used to bioprint patches with different bioink contents which were incubated up to 28 days and analysed. For the *in vivo* phase, new patches were 3D bioprinted using the optimal methods determined in the previous (*ex vivo*) experiments and surgically transplanted to the epicardium in infarcted mice. For these *in vivo* experiments, we cultured mixed cardiac cells: induced pluripotent stem cell derived cardiomyocytes (iCMs), human coronary artery endothelial cells (HCAECs) and cardiac fibroblasts (CFs). Cells were cultured using hanging drops to generate VCS which were suspended in AlgGel to create bioink for 3D bioprinting of patches. Study control groups (*in vivo*) were: the same cells freely suspended in AlgGel, AlgGel without cells, MI without treatment and sham surgery (no MI and no treatment). The primary outcome was cardiac function (left ventricular ejection fraction, LVEF%) measured up to day 28 post surgery. Additional analyses included: electrical mapping, histology, cell quantification by flow cytometry and mRNA (gene expression) profiling. Alongside these experiments, we developed novel surgical robotic minimally invasive instruments designed to transplant similar patches at human scale. We prototyped a heart patch transplanter device and demonstrated its potential utility in a world-first operation on a pig cadaver. RESULTS: *Ex vivo* patches incubated for 28 days allowed for self-organisation of endothelial cells into networks and contractile activity within patches. *In vivo* transplantation of patches in mice modelling MI resulted in a "return to baseline" improvement in median LVEF%. Our results measured median baseline (pre-surgery) LVEF% for all mice at 66%. Post-surgery, LVEF% was 58% for Sham (non-infarcted) and 41% for MI (no treatment) mice. Patch transplantation increased LVEF%: 55% (acellular; p=0.012), 59% (cells; p=0.106), 64% (spheroids; p=0.010). The VCS group was associated with improved electrical mapping profiles, lower infarct sizes, changes in host immune cell numbers and a gene expression (mRNA) profile which was closest to sham mice (with no MI). As proof-of-concept, similar scaled-up AlgGel patches were successfully transplanted in a porcine cadaver using a prototyped robotic minimally invasive surgical instrument. CONCLUSION: Epicardial transplantation of patches improves cardiac function in mice modelling MI. The use of VCS in alginate-gelatin bioink seems to offer advantages compared to freely suspended cells or hydrogel alone. The fact that hydrogel alone without cells confers some restoration of myocardial function suggests that the mechanism is not fully accounted for by the cellular portion of the bioink. Further studies are needed with a focus on whether host immune cell modulation is a key mechanism underlying the benefit of this approach. Since our most successful treatment group (VCS) had a similar transcriptome compared to non-infarcted (sham) mice, further studies should also include transcriptomic analyses to confirm reproducibility of this finding. If it is confirmed that immuno-genetic mechanisms underly patch-based approaches to myocardial protection after MI, this may change the focus of treatment strategies and avoid wasted resources and potentially patient harm (from treatments which are not aligned with the underlying mechanism). Our robotic minimally invasive patch transplantation operation represents a first step on a potential pathway towards transplantation at human surgery (without the need for traditional open surgery). For translatability, patch development should work towards being compatible with robotic and/or minimally invasive transplantation.

3D bioprinted heart patches for cardiac regeneration

Thesis with publication graphical overview

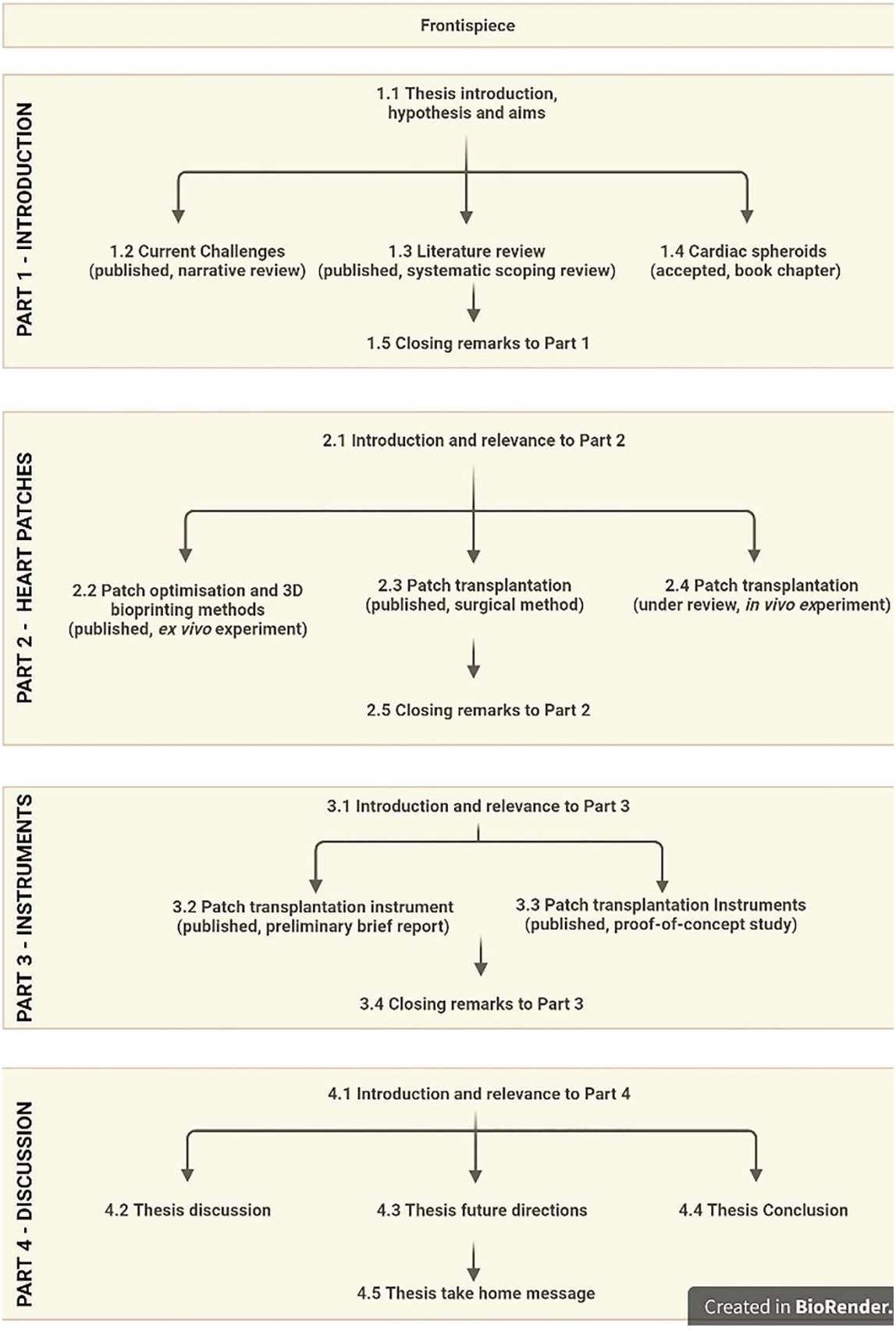

List of Figures

All figures are listed with their short titles. Full figure legends are found in the respective articles/chapters.

1.2 – Current challenges in three-dimensional bioprinting heart tissues for cardiac surgery

Published article: **Roche CD,** Brereton RJL, Ashton AW, Jackson C, Gentile C. Current challenges in three-dimensional bioprinting heart tissues for cardiac surgery. *Eur J Cardiothoracic Surg* 2020;58(3):500–510. https://doi.org/10.1093/ejcts/ezaa093

Figures:

Videos:

1.3 – Omentum support for cardiac regeneration in ischaemic cardiomyopathy models: a systematic scoping review

Published article: Wang H, **Roche CD**, Gentile C. Omentum support for cardiac regeneration in ischaemic cardiomyopathy models: a systematic scoping review. *Eur J Cardiothorac Surg* 2020;58(6)1118-1129. https://doi.org/10.1093/ejcts/ezaa205

Figures:

1.4 – Generation and applications of cardiac spheroids

Accepted book chapter: **Roche CD**, Polonchuk L, Gentile C. Generation and Applications of Cardiac Spheroids (in press, *Tissue Engineering and Regeneration* book series)

Figures:

2.2 – Printability, durability, contractility and vascular network formation in 3D bioprinted cardiac endothelial cells using alginate-gelatin hydrogels

Published article. **Roche CD**, Sharma P, Ashton AW, Jackson C, Xue M, Gentile C. Printability, durability, contractility and vascular network formation in 3D bioprinted cardiac endothelial cells using alginate-gelatin hydrogels. *Front Bioeng Biotechnol* 2021.9;110 https://doi.org/10.3389/fbioe.2021.636257

Figures:

Figure 1. Assessing printability for extrusion 3D bioprinting with AlgGel hydrogels and GelMA.

Figure 2. Durability assessments for 3D bioprinted patches in cell culture medium up to 28 days.

Figure 3. Bioprinted HCAECs and HDFs in AlgGel hydrogel are viable at 28 days.

Figure 4. CD31-positive endothelial cells within a patch containing mouse cardiac spheroids.

Figure 5. CD31-positive endothelial cell organisation within a 3D bioprinted patch containing HCAECs and HDFs.

Figure 6. Lumen evaluation of CD31+ endothelial cells within a 3D bioprinted patch generated with alginate 4%/gelatin 8% hydrogel.

Supplementary Figures:

Supplementary Figure 1. 3D bioprinting platforms used: a custom-made REGEMAT3D model (left column), the ROKIT INVIVO (middle column) and the CELLINK BIO X (right column).

Supplementary Figure 2. 3D bioprinted patch fragmentation.

Supplementary Videos:

Supplementary Video 1. Beating cardiac patches containing mouse vascularised cardiac spheroids in alginate/gelatin hydrogel.

Supplementary Video 2. Three-dimensional rendering of CD31 + endothelial network-like structure within an alginate/gelatin patch containing HCAECs and HDFs.

2.3 – Transplantation of a 3D bioprinted patch in a murine model of myocardial infarction

Published video article: **Roche CD**, Gentile C. Transplantation of a 3D bioprinted patch in a murine model of myocardial infarction. *J Vis Exp* 2020;61675. https://doi.org/10.3791/61675

Video:

Video Article: Transplantation of a 3D Bioprinted Patch in a Murine Model of Myocardial Infarction.

Figures:

Figure 1: A bioprinted cardiac patch applied onto the epicardium of a C57BL6 mouse heart.

Figure 2. Kaplan-Meier survival analysis through 28 days post-MI.

Supplementary Figure:

Supplementary Figure 1. Video still image (video time point 01:54 – 01:55) showing the left auricle (left atrial appendage).

2.4 – 3D bioprinted alginate-gelatin hydrogel patches containing cardiac spheroids recover heart function in a mouse model of myocardial infarction

Article under review: Roche CD, Lin H, Y Huang, de Bock CE, Beck D, Xue M, Gentile C. 3D bioprinted alginate-gelatin hydrogel patches containing cardiac spheroids recover heart function in a mouse model of myocardial infarction. *Acta Biomaterialia* (under review; submission 15/03/2022; revised submission 26/06/2022).

Figures:

Figure 1. Cardiac spheroids and endothelial cell network are present at 28 days in 3D bioprinted patches.

Figure 2. Patch transplantation protects against MI-induced reduction in cardiac function.

Figure 3. Following LAD ligation, no treatment rescued mean CV by day 28.

Figure 4. In mice surviving up to 28 days, the strong correlation between infarct size and LVEF% in the MI group was reduced for the MI+PATCH group and reduced further for the MI+PATCH SPHEROIDS group.

Figure 5. Electrical remodelling of the infarcted LV may be an important mechanism contributing to improved LVEF%.

Figure 6. Immune cell analysis at 28 days post-surgery suggests significant changes in inflammatory cell populations in heart tissue across experimental groups.

Figure 7. Figure 7. The transcriptomic profile of MI+PATCH SPHEROID mice is similar to the one of sham mice (without MI).

Supplementary Figures:

Supplementary Figure 1. Ex vivo detection of electrical activity confirmed electrically active cells after 28 days of patch incubation.

Supplementary Figure 2. Evaluation of cardiac functional outcome measures other than the LVEF%.

Supplementary Figure 3. Mortality data and baseline LVEF% characteristics.

Supplementary Figure 4. Patterns of infarction were variable and may have influenced cardiac function in ways not accounted for by the infarct size measurement alone.

Supplementary Figure 5. A patch remnant captured on histology still adherent to the mouse heart on day 28 post surgery.

Supplementary Figure 6. Day 28 mean CV (n=4 repeat readings per mouse) plotted against mean infarct size values (error bars=SD (only upper bar shown); up to 6 repeats per mouse) in treatment groups and the sham group.

Supplementary Figure 7. No strong trends were identified between macrophages plotted against infarct size or LVEF% for mice in the spheroid group.

Supplementary Figure 8. Supplementary analysis of flow cytometry data for tissue immune cells.

Supplementary Figure 9. Enrichment for canonical pathways.

Supplementary Figure 10. Dilated cardiomyopathy signalling pathway.

Supplementary Figure 11. Enrichment for system development functions.

Supplementary Videos:

Video 1. Visualisation of confocal micrographic data showing cellular structure of a patch (3D rendering).

Video 2. Visualisation of confocal micrographic data showing cellular structure of a patch (3D rendering).

Video 3. Visualisation of confocal micrographic data showing cellular structure of a patch (3D rendering).

3.1 – A world first surgical instrument for minimally invasive robotically-enabled transplantation of heart patches for myocardial regeneration: a brief research report

Published article. **Roche CD**, Zhou Y, Zhao L, Gentile C. A world-first surgical instrument for minimally invasive robotically-enabled transplantation of heart patches for myocardial regeneration: a brief research report. *Front Surg* 2021;8:436. https://doi.org/10.3389/fsurg.2021.653328

Figures:

Figure 1. Lateral and top down views of instrument design.

Figure 2. Close-up angled view and complete lateral view of the distal end of the instrument (the patient end where the patch would be enclosed).

Figure 3. The patch releasing mechanism in close-up.

Figure 4. Curved edges of the arm to reduce risk of injury to surrounding structures inside the chest.

Supplementary Figures:

Supplementary Figure 1. The instrument with the sheath covering the distal arms removed.

Supplementary Figure 2. Control pathways linking the operator's end to the distal arms.

Supplementary Figure 3. Mechanism allowing for adjustment of the rotational angle of the arms.

Supplementary Figure 4. 3D printing parameters for the resin sizing and learning prototyping of individual parts.

Supplementary Video:

Supplementary Video 1. Video walkthrough of patch delivery device, including background and mechanistic demonstration from the computer-aided design (CAD).

3.2 – Cardiac patch transplantation instruments for robotic minimally invasive cardiac surgery: initial proof-of-concept designs and surgery in a porcine cadaver

Published article. **Roche CD**, Iyer GR, Nguyen MH, Mabroora S, Dome A, Sakr K, Pawar R, Lee V, Wilson C, Gentile C. Cardiac patch transplantation instruments: world-first designs and prototype testing for robotic minimally invasive cardiac surgery. *Front Robot AI* 2022;8:714356 https://doi.org/10.3389/frobt.2021.714356

Figures:

Figure 1. The Claw design in detail.

Figure 2. Claw design (open position with plate holder protruding).

Figure 3. “Shell-Beak” design with flexible patch holder connected to the patch dispenser system.

Figure 4. The HeartStamp prototype for cardiac patch transplantation.

Figure 5. SolidWorks design for the HeartStamp device prototype.

Figure 6. Mounting of micro-servo motors onto the rods of the instrument using the Claw design as an example.

Figure 7. A proposed control unit sizing and learning polylactic acid (PLA) prototype.

Figure 8. A new surgical operation for epicardial patch transplantation using the HeartStamp—left anterolateral approach with sheath.

Figure 9. A new surgical operation for epicardial patch transplantation using the HeartStamp—left postero-inferolateral approach without sheath.

Supplementary Figures:

Supplementary Figure S1. The Claw head technical details.

Supplementary Figure S2. Outer body design for the “Claw” minimally invasive heart patch transplantation instrument in early-stage development.

Supplementary Figure S3. Rack and Pinion mechanism technical details.

Supplementary Figure S4. Plate holder technical details.

Supplementary Figure S5. Plate holder working mechanism with combination of linkages.

Supplementary Figure S6. Shell-Beak Design.

Supplementary Figure S7. “Umbrella” Design.

Supplementary Videos:

Supplementary Video S1. Brief overview of robotic keyhole patch transplantation demonstrated with the “Claw” instrument design.

Supplementary Video S2. Video walkthrough for in silico demonstration of instrument Control System 1 using potentiometers, an Arduino microcontroller and servo motors.

Supplementary Video S3. Video walkthrough for in silico demonstration of one subunit of Control System 2.

Supplementary Video S4. Detailed background and video walkthrough for the first-in-kind surgical operation to transplant a patch to the heart using the ‘HeartStamp’ instrument.

List of Tables

All tables are listed with their short titles. Full table legends are found in the respective articles/chapters.

1.2 – Current challenges in three-dimensional bioprinting heart tissues for cardiac surgery

Published article: **Roche CD,** Brereton RJL, Ashton AW, Jackson C, Gentile C. Current challenges in three-dimensional bioprinting heart tissues for cardiac surgery. *Eur J Cardiothoracic Surg* 2020;58(3):500–510. https://doi.org/10.1093/ejcts/ezaa093

Tables:

1.3 – Omentum support for cardiac regeneration in ischaemic cardiomyopathy models: a systematic scoping review

Published article: Wang H, **Roche CD**, Gentile C. Omentum support for cardiac regeneration in ischaemic cardiomyopathy models: a systematic scoping review. *Eur J Cardiothorac Surg* 2020;58(6)1118-1129. https://doi.org/10.1093/ejcts/ezaa205

Tables:

List of Abbreviations

2D or 3D – two or three-dimensional

AlgGel – alginate-gelatin hydrogel

AlloECM – fibroblast derived extracellular matrix hydrogel

Ang-1 – angiopoietin 1

AUD – Australian dollars

bFGF – basic fibroblast growth factor

CABG – coronary artery bypass graft

$CaCl_2$ – calcium chloride

CAD – computer-aided design

CD31 – cluster of differentiation 31

CF – cardiac fibroblast

CFCM – cardiac fibroblast conditional medium

CFR – coronary flow reserve

CM – cardiomyocyte

Cx – circumflex coronary artery

Cx-43 – connexin-43

D1 or 2 – first or second diagonal artery

DMEM – Dulbecco's Modified Eagle Medium

DOX - doxorubicin

EB – embryoid body

EC – endothelial cell

ECM – extracellular matrix

eNOS – endothelial nitric oxide synthase

ES or ESC – embryonic stem cell

FAC – fractional area change

FBS – foetal bovine serum

FDA – food and drug administration

FLIPR – fluorescent imaging plate reader

FPGA – field-programmable gate array

FS – fractional shortening

GBP – Great British pounds

GEA – gastroepiploic artery

GelMA or GELMA – gelatin methacryloyl

HCAEC – human coronary artery endothelial cell

HDF – human dermal fibroblast

HEPES – 4-(2-hydroxyethyl)-1-piperazineethanesulfonic acid

hiPSC-CM – human induced pluripotent stem cell-derived cardiomyocytes

iCM – induced cardiomyocyte

iCS – induced pluripotent stem cell-derived cells (induced cardiac spheroid)

IGF-1 – insulin-like growth factor 1

IMDM – Iscove's modified Dulbecco's medium

iPSC – induced pluripotent stem

iPSC-CM – induced pluripotent stem cell-derived cardiomyocyte

IQR – interquartile range

L-glut – L-glutamine

L-NIO – vinyl-L-NIO hydrochloride (nitric oxide synthase inhibitor)

LAD – left anterior descending coronary artery

LAP – lithium phenyl-2,4,6-trimethylbenzoylphosphinate

LSM – laser scanning microscope

LV – left ventricle

LVEDD – left ventricular end-diastolic diameter

LVEF or LVEF% – left ventricular ejection fraction

LVESD – left ventricular end-systolic diameter

MBF – myocardial blood flow

MCR – maximum capture rate

MI – myocardial infarction

MRI – magnetic resonance imaging

NOS3 – nitric oxide synthase 3

NRF2 – nuclear factor-erythroid factor 2-related factor 2

ns – result not statistically significant

OM1 or 2 – obtuse marginal coronary artery 1 or 2

PCA – printed circuit assembly

PCA – principle component analysis

PCB – printed circuit board

PCL – polycaprolactone

PCR – polymerase chain reaction

PGA – polyglycolic acid

PDGF-β – platelet-derived growth factor-β

PDMS – polydimethylsiloxane

PECAM – platelet endothelial cell adhesion molecule

pen/strep – penicillin/streptomycin

PLA – polylactic acid

RNA – ribonucleic acid

SCN10A – sodium voltage-gated channel alpha subunit 10

shRNA – short hairpin RNA

SMA – smooth muscle actin

TGFβ1 - transforming growth factor beta 1

USD – United States dollars

UV – ultra-violet

VATS – video-assisted thorascopic surgery

VCS – vascularised cardiac spheroid

VEGF – vascular endothelial growth factor

vWF – von Willebrand Factor

List of publications, presentations and awards

Published Manuscripts

- **Roche CD**, Iyer GR, Nguyen MH, Mabroora S, Dome A, Sakr K, Pawar R, Lee V, Wilson C, Gentile C. Cardiac patch transplantation instruments: world-first designs and prototype testing for robotic minimally invasive cardiac surgery. *Front Robot AI* 2022 https://doi.org/10.3389/frobt.2021.714356
- **Roche CD**, Zhou Y, Zhao L, Gentile C. A world-first surgical instrument for minimally invasive robotically-enabled transplantation of heart patches for myocardial regeneration: a brief research report. *Front Surg* 2021;8:436. https://doi.org/10.3389/fsurg.2021.653328
- **Roche CD**, Sharma P, Ashton AW, Jackson C, Xue M, Gentile C. Printability, durability, contractility and vascular network formation in 3D bioprinted cardiac endothelial cells using alginate-gelatin hydrogels. *Front Bioeng Biotechnol* 2021.9;110 https://doi.org/10.3389/fbioe.2021.636257
- **Roche CD**, Brereton RJL, Ashton AW, Jackson C, Gentile C. Current challenges in three-dimensional bioprinting heart tissues for cardiac surgery. *Eur J Cardiothoracic Surg* 2020;58(3):500–510. https://doi.org/10.1093/ejcts/ezaa093
- **Roche CD**, Gentile C. Transplantation of a 3D bioprinted patch in a murine model of myocardial infarction. *J Vis Exp* 2020;61675. https://doi.org/10.3791/61675
- Wang H, **Roche CD**, Gentile C. Omentum support for cardiac regeneration in ischaemic cardiomyopathy models: a systematic scoping review. *Eur J Cardiothorac Surg* 2020;58(6)1118-1129. https://doi.org/10.1093/ejcts/ezaa205

Manuscripts Under Review

- **Roche CD**, Polonchuk L, Gentile C. Generation and Applications of Cardiac Spheroids (invited book chapter – with editor, *Tissue Engineering and Regeneration* book series)
- **Roche CD**, Roche CD, Lin H, Y Huang, de Bock CE, Beck D, Xue M, Gentile C. 3D bioprinted alginate-gelatin hydrogel patches containing cardiac spheroids recover heart function in a mouse model of myocardial infarction. *Acta Biomaterialia* (under review; original submission 15/03/2022; revised submission 26/06/2022)

Presentations

- **Roche CD,** et al. Cardiac patch transplantation instruments: world-first designs and prototype testing for robotic minimally invasive cardiac surgery. Four online presentations: 1) Multimedia poster and pre-recorded 2 min poster presentation, *Biofabrication 2021* (27-29 Sept '21. International Society of Biofabrication); 2) Oral "burster" 5 min presentation, *Third Annual Australian Bioprinting Workshop* (4-5 Oct '21); 3) Oral 45 min presentation *IBJR*, Sydney (7 Oct '21); 4) 'Rising Star Award' 10 min oral presentation plus questions, Sydney Cardiovascular Symposium 2021 (9-10 Dec '21)
- **Roche CD.** Bioprinted heart patches for cardiac regeneration. "Whole thesis" summary oral presentation. Faculty of Medicine and Health Higher Degree by Research Presentations, Sydney University. 16 Nov '21
- **Roche CD.** Bad Advice – Good Advice: Real World Problem Solving in STEMM. Invited Oral Special Session, St Andrew's College Problem Solving Course in Association with McKinsey & Company (28 Jul '21, St Andrew's College, Sydney)
- **Roche CD**, Sharma P, Gentile C. Novel approaches in 3D bioprinting of heart tissues. Poster Presentation, Sydney Cardiovascular Symposium 2019 (27-29 Nov '19, Victor Chang Institute, Sydney)
- **Roche CD**, Sharma P, Gentile C. Novel approaches in 3D bioprinting of heart tissues. Poster Presentation, UTS New Horizons Conference (14-15 Nov '19, UTS, Sydney)
- **Roche CD**. PhD Thesis Proposal (24 Jul '19, Kolling Institute, Northern Clinical School, USyd)
- **Roche CD**. 3D Bioprinted Heart Patches. Invited lecture for international medical students visiting the University of Sydney for the 2019 Young Leaders Program (16 Jul '19, USyd main campus)
- **Roche CD**. Three-minute thesis (28 Jun '19, Kolling Institute, Northern Clinical School, USyd)

Competitive Awards, Prizes and Scholarships

- Winner Cutlers' Surgical Prize for best surgical device invention in the UK that year (£5000GBP) 2022
- Rising Star Award/Presentation for Outstanding Contribution to Cardiovascular Research ($500AUD) 2021
- Paulette Isabel Jones PhD Completion Scholarship, University of Sydney ($7000AUD over 3 months) 2021
- Needlemakers' Company Educational Bursary (£1000GBP to attend RCSeng surgical skills course) 2021
- Nomination for International Society for Biofabrication Asia/Oceania Young Scientist Award 2021
- Project Grant for Adult Stem Cell Research (Catholic Archdiocese Sydney) ($100,000) 2019-20
- Heart Research Australia PhD Scholarship ($90,000AUD over 3 years) 2019-21
- Sir John Loewenthal Scholarship (University of Sydney) ($20,000 over 1 year) 2019-20
- UTS New Horizons Conference Poster Presentation People's Choice Award ($100) 2019

1.1 – Thesis introduction, hypothesis and aims

Background

The goal of this thesis as it was initially being conceptualised in 2019 was to discover if it might be possible to protect the myocardium after a heart attack by transplanting 'heart patches' to the epicardium. Our team considered whether specific techniques might be advantageous for such an approach. Specifically, we considered a new approach combining extrusion 3D bioprinting (to generate hydrogel patches) with clusters of cells (microtissues) called spheroids directly suspended in the hydrogel. The author of the thesis, a practising cardiothoracic surgical trainee in the UK without prior laboratory experience, came to Sydney to team up with laboratory scientists, learn the techniques and access the equipment needed to embark on this project. The resultant thesis herein was the product of a significant multidisciplinary, cross-university collaborative effort.

Additionally, the thesis evolved over time as new challenges were identified during the project which were not foreseen at the outset of the PhD. The most notable example of this is detailed in the final section (Part 3) which describes the invention of robotic surgical instruments to transplant heart patches at relevant human anatomical scale. This award-winning innovative teamwork was borne out of the collaboration of a clinician with cardiothoracic surgical knowledge working with bioengineers and robotics specialists with complementary skills and knowledge.

Introduction

The following thesis introduction, hypothesis and aims were generated and refined in light of the literature reviews performed as part of this thesis (Chapters 1.2, 1.3 and 1.4). Those review chapters complete the Introduction Section (Part 1 of this Thesis) and contain full, detailed exploration of the challenges and techniques outlined in this concise opening Chapter (1.1). Since many of the chapters in this 'thesis-with-publications' have been published as peer-reviewed articles, concise 'Thesis' summaries and/or additional discussions frame those publications which are inserted as published. This allows for important content appropriate for a thesis but not for a published article and also contextualises or connects the published articles/chapters into a coherent whole. The following paragraphs summarise the findings of our literature review process which led to the formation of our hypothesis.

Even today, for patients with a heart attack leading to heart failure, the gold standard treatment is a heart transplant (MacGowan, Crossland, Hasan, & Schueler, 2015). This is waiting-list dependent, requires immunosuppression to prevent organ rejection and carries a high mortality rate of 15% at 1 year (Lund et al., 2017). In this context there has been a strong incentive to develop therapeutics aimed at restoring some of the cardiac function which is lost after myocardial infarction (MI) (Beyersdorf, 2014).

One approach which has shown promise for myocardial regeneration is transplantation of patches to the heart surface (epicardium) (Wang et al., 2021). The mechanisms behind the reproducible improvements in cardiac function with this approach have not yet been fully elucidated (Vagnozzi et al., 2019). Nonetheless, epicardial patch transplantation has been shown to be safe in early human trials (Menasché et al., 2015; Menasché et al., 2018), building on preclinical animal studies which have shown it to be efficacious (Zhou, Zhou, Zheng, Zhang, & Hu, 2010).

Patches may be generated by various methods (Miller et al., 2012), but the now widespread technique of 3D bioprinting promising a method of patch fabrication which is scalable, safe, reproducible and allows for precise control of patch morphology (Maiullari et al., 2018; Zhang et al., 2016).

The substance of the patches themselves in terms of the hydrogel matrices and the cellular content has also been the subject of significant bioengineering research (Mancha Sánchez et al., 2020; Visconti et al., 2010). The perfect hydrogel characteristics have not been determined, but these are often evaluated in terms of

printability or durability and the hydrogel must provide an optimal environment for the cells contained within the gel (Bociaga, Bartniak, Grabarczyk, & Przybyszewska, 2019; Gillispie et al., 2020).

The optimum cellular (or biomaterial) content within the hydrogel "bioink" has also not been determined (Gentile, 2016). In fact, recent research has suggested that the cellular content may not be as important as stimulating a host immune response in the tissue underlying a transplanted patch (Vagnozzi et al., 2019). For example, it remains an open question whether patient-specific (immunocompatible) tissues generated from reprogrammed stem cells (induced pluripotent stem cell-derived cardiac tissue) would be beneficial compared to foreign cells or even acellular biomaterials (Domenech, Polo-Corrales, Ramirez-Vick, & Freytes, 2016).

Recent "3D" cell culture techniques have introduced the idea that culturing cells in 3D (such as in hanging drops) may have benefits over traditional "2D" culture (allowing cells to interact in three dimensions which better recapitulates the physiological microenvironment) (Polonchuk et al., 2017). By mixing cardiac cells in hanging drop cultures they coalesce into 3D aggregates termed "spheroids" (Gentile, 2016). More specifically, if a mixture of cardiomyocytes, endothelial cells and fibroblasts (the most frequent cells in the myocardium) is allowed to culture in 3D, these will form primitive vascular connections and display rhythmic contractile activity (Gentile, 2016). These so-called Vascularised Cardiac Spheroids (VCS) can then be used for various applications, including as the cellular component of cardiac bioink for 3D bioprinting (Mironov et al., 2009). Using these pre-vascularised myocardial microtissues to "print" cardiac patches using a 3D bioprinter is a novel and promising method to overcome several of the pitfalls which have held back progress in regenerating the myocardium.

A pressing and unanswered question for the field of patch-based myocardial regeneration is: if we invent patches which restore myocardial function – how will they actually be transplanted to patients (Wang et al., 2021; Zhu et al., 2021). The field has so far envisaged traditional open surgical approaches to transplant patches by open heart surgery (Chachques et al., 2007; Menasché et al., 2018). It is possible that by the time this therapy is ready for clinical use, minimally invasive and/or robotic surgical transplantation methods will be needed (Christopher David Roche, Zhou, Zhao, & Gentile, 2021; Wang et al., 2021; Zhu et al., 2021).

The thesis herein hypothesises that 3D bioprinting of heart patches using VCS will promote cardiac regeneration:

Part 1 introduces critical background considerations, including: 1) an overview of current challenges for the field; 2) a systematic scoping review which (for the first time) gathers the literature on the technique of omental reinforcement of epicardially transplanted patches; and 3) an in-depth contextual exploration of how VCS can be generated and their wider applications.

Part 2 presents: 1) the optimisation of cardiac patches in the laboratory (including methodological details for patch generation) with an emphasis on printability, durability and vascularisation; 2) the complete surgical method for *in vivo* patch transplantation in a mouse model of MI; and 3) an *in vivo* preclinical study of patches transplanted in mice modelling MI including analyses of functional and structural outcomes.

Part 3 contains early proof-of-concept demonstrations for robotic minimally invasive surgical instruments to transplant patches to the epicardium. This award-winning innovation provides a new way to transplant patches, potentially an important moment in pivoting the field away from its focus on traditional open surgery.

Part 4 discusses the findings presented within this thesis. The relevance of the work and future directions are discussed, including the particular importance of biomedical ethics for this field, the need for mechanistic understandings of why this approach seems to work and the importance of considering the method of patch transplantation for clinical translation.

Taken together, this thesis contributes many new insights for the field of patch-based myocardial regeneration. With an emphasis on 3D bioprinting, VCS (3D cell culture), a feasibility-focused mouse model of MI and robotic minimally invasive surgical instruments, the findings herein will be of interest to a broad multidisciplinary readership. This includes bioengineers optimising biofabrication techniques as well as surgeons seeking technology to restore myocardial function for heart failure patients in the clinic.

1.2 – Current challenges in three-dimensional bioprinting heart tissues for cardiac surgery

Summary:

The following narrative review was published in the *European Journal of Cardio-thoracic Surgery* in 2020. It outlines the current challenges in 3D bioprinting heart patches for cardiac surgical approaches to restoring myocardial function after MI. It includes details of how 3D cell culture, 3D bioprinting and stem cell techniques may be combined in pursuit of the goal of myocardial regeneration. It touches on approaches which have not succeeded in the past (such as direct injection of stem cells), complex issues to do with feasibility of patient-specific tissue compared to tissue which is not patient-specific but may be stored in a "bio-bank". It introduces the important fact that the mechanism behind the benefit of patch-based myocardial regeneration is not yet understood. It presents current best achievements in bioengineered patch contractility and vascularisation. It also explores surgical considerations, for example whether reinforcement of patches with the omentum or suturing of patch bioengineered blood vessels to host vessels might be possible and/or needed for survival of patches. At the time of writing, Altmetric ranks this paper 1st out of 36 articles of a similar age in this journal (and 40th out of 2759 articles in this journal since records began).

European Journal of Cardio-Thoracic Surgery 58 (2020) 500–510
doi:10.1093/ejcts/ezaa093 Advance Access publication 11 May 2020

REVIEW

Cite this article as: Roche CD, Brereton RJL, Ashton AW, Jackson C, Gentile C. Current challenges in three-dimensional bioprinting heart tissues for cardiac surgery. Eur J Cardiothorac Surg 2020;58:500–10.

Current challenges in three-dimensional bioprinting heart tissues for cardiac surgery

Christopher D. Roche [a,b,c,d], Russell J.L. Brereton[b], Anthony W. Ashton[a], Christopher Jackson[a] and Carmine Gentile [a,c,*]

[a] Northern Clinical School of Medicine, University of Sydney, Kolling Institute, St Leonards, Sydney, NSW, Australia
[b] Department of Cardiothoracic Surgery, Royal North Shore Hospital, St Leonards, Sydney, NSW, Australia
[c] Department of Biomedical Engineering, Faculty of Engineering and IT, University of Technology Sydney (UTS), Ultimo, Sydney, NSW, Australia
[d] Department of Cardiothoracic Surgery, University Hospital of Wales, Cardiff, UK

* Corresponding author. Department of Biomedical Engineering, Faculty of Engineering and IT, Building 11, 81 Broadway, Ultimo, NSW 2007, Australia. Tel: +61-2-95144502; e-mail: carmine.gentile@uts.edu.au (C. Gentile).

Received 29 November 2019; received in revised form 27 January 2020; accepted 18 February 2020

Key question

What are the current challenges for 3-dimensional (3D) bioprinting of a functional human myocardial patch for cardiac surgery?

Key finding(s)

Vascularisation and contractility are critical for engraftment and synchronous contraction of 3D bioprinted heart tissue.

Take-home message

Despite current challenges, 3D bioprinting of patient-derived cardiac tissues is a promising approach for creating functional human myocardium.

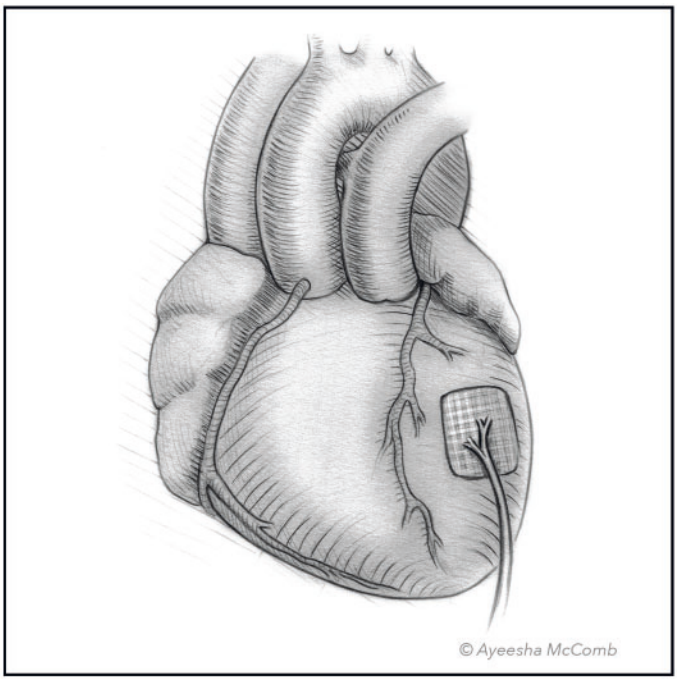

Summary: Previous attempts in cardiac bioengineering have failed to provide tissues for cardiac regeneration. Recent advances in 3-dimensional bioprinting technology using prevascularized myocardial microtissues as 'bioink' have provided a promising way forward. This review guides the reader to understand why myocardial tissue engineering is difficult to achieve and how revascularization and contractile function could be restored in 3-dimensional bioprinted heart tissue using patient-derived stem cells.

Keywords: Bioprinting • Revascularization • Transplantation • Regenerative medicine • Cardiac tissues • Stem cells

ABBREVIATIONS

CFs	Cardiac fibroblasts
CMs	Cardiomyocytes
3D	3-Dimensional
ECM	Extracellular matrix
ECs	Endothelial cells
ESCs	Embryonic stem cells
iPSCs	Induced pluripotent stem cells

INTRODUCTION

With recent advances in the technological triad of induced pluripotent stem cells (iPSCs), 3-dimensional (3D) cardiac microtissues (referred to as 'cardiospheres', 'cardiac spheroids', 'cardiac organoids' [1]) and 3D bioprinting, the enticing prospect has arisen of fabricating cardiac tissues to replace diseased native tissues and to regenerate damaged hearts [2–10].

The incentive for this is strong: in the UK, 30–40% of patients diagnosed with heart failure will die within 1 year of diagnosis with an additional 10% annually thereafter [11]. Moreover, the period before death is associated with a severe disease burden and reduced quality of life [12]. For end-stage patients, the gold standard treatment is a heart transplant [13]. However, this is not suitable for all, carrying significant morbidity and a global mortality rate of ∼15% and 25% at 1 and 5 years, respectively [14]. In addition, there is significant urgency to find a treatment, which is not waiting list dependent, for those patients awaiting a donor. Last year, patients on the Australian heart transplant list had a 56% chance of being transplanted by the end of the year, a 31% chance of being carried over to next year and a 3.5% chance of dying whilst waiting [15]. For the UK, the equivalent figures were 29% transplanted, 55% carried over and 3% dying [16]. The median waiting time for an adult categorized as non-urgent on the UK heart transplant list approaches 3 years [16].

In this context, several new approaches have been developed for regenerating the myocardium [4–7, 9, 10, 17–23]. Recent studies have demonstrated the feasibility for 3D bioprinting of myocardial tissues from patient-derived stem cells; however, limitations of such approaches still remain, including full vascularization and synchronous contractile activity [5, 9, 10]. This review explores why this is difficult and why it is worth pursuing.

CHALLENGES: OVERVIEW

General challenges limiting engineered cardiac tissues include (i) limited tissue survival following transplantation; (ii) limited ability to generate tissue of adequate size; (iii) optimizing the mix of cardiac cell types; (iv) cell sourcing from patients; (v) the immature phenotype of stem cell-derived cardiac cells; (vi) safety concerns for potentially undifferentiated stem cells; and (vii) immunogenicity requiring immunosuppression (Table 1).

Other considerations particularly pertaining to myocardial generation are the need for: (i) a vascular network spanning many orders of magnitude from arterial to capillary level and (ii) a synchronously contractile, electrically conductive tissue.

STEM CELLS AND THEIR NICHE

It is not feasible to use mature, differentiated, adult myocardial cells for the therapeutic regeneration of myocardial tissue, as these cells exhibit reduced viability and proliferation when engrafted [17]. Instead, current approaches prefer stem cells that can be coaxed into desired, fully differentiated forms in response to microenvironmental cues, which can be controlled [4–6]. With the exception of bone marrow transplant, stem cells have not fulfilled their expected clinical potential in regenerative medicine [24]. However, the advent of iPSCs provides a promising cell source for regeneration, including 3D bioprinting of myocardial tissue [5, 9, 25, 26].

It has long been understood that the stem cell microenvironment, called the 'niche', provides cues that determine how tissues develop and function [27–29]. These cues include extracellular matrix (ECM) proteins, temperature and oxygen, which are known to influence tissue growth and stem cell behaviour [28]. Cells in a suboptimal niche may not survive and will perform poorly [28]. Cells implanted directly into diseased host myocardium exhibit poor survival and ability to organize into functional

Table 1: Challenges for the development of bioengineered cardiac tissues

General	Vascularization	Contractility
Cell survival postimplantation in diseased environment	Observation of appropriate vascular tissue maturation without cell destruction or alteration	Integration with host depolarization-repolarization wave without arrhythmogenicity
Host immune response to implanted material	Functional validation of the bioprinted vascular tree	Engineering the correct electrochemical environment for cardiomyocyte maturation
Possible biological scaffold needed with its own biofabrication challenges	Surgical integration with pre-existing host vasculature	Coculture with other cell types for appropriate maturation of stem cell-derived cardiomyocytes
Correct cell mix mimicking mature myocardial tissue	Vascular lumen generation and integration of hierarchical arteriovenous tree segments	Optimization of 3D culture techniques required for formation of cell–cell connections
Expanding cells to an appropriately high number	Stem cell selection for clinically useable vascular cell source	
Reproducibility and scalability to meet demand	Time requirement for vascular tissue maturation *in vitro* (pre) and *in vivo* (post) implantation	
Cost-effectiveness		
Ethics/safety		

3D: 3-dimensional.

tissues, as they lack the appropriate microenvironment [17, 30]. The native heart contains ∼2 billion cardiomyocytes (CMs) and many more of other cell types [31]. The exact cardiac cell ratio is not universally agreed upon; however, fully differentiated adult human ventricular myocardium contains 33% CMs, 24% endothelial cells (ECs) and 43% other cells (including fibroblasts) [32]. To provide a 3D microenvironment for cells to grow before their transplantation, they have been cultured as 3D patches [4, 6, 22]. To further improve cell patch survival, these have been delivered either under host pericardium [33] or matured on vascular host omental tissue before transfer to the epicardium [34].

In addition to the niche, it is important to consider that different stem cell types present their own unique challenges (Table 2) [29].

'Embryonic stem cells' (ESCs) are pluripotent (i.e. they may differentiate into mature cells of any of the 3 original germ cell layers), do not undergo senescence in culture and can self-renew indefinitely [29]. However, whilst harvesting from an embryo raises ethical concerns, the host would also require immunosuppression from their implantation [29, 33] and there is a risk of developing malignancy [29, 35].

Table 2: Limitations of using stem cells for 3D bioprinting myocardial tissue

Stem cell type	Known limitations
Embryonic	Immunosuppression required
	Ethical concerns
	Teratoma formation
Adult	Finite capacity for self-renewal
	Limited mature cell types
	Senescence in culture
Induced pluripotent	Teratoma formation

3D: 3-dimensional.

'Multipotent adult stem cells', such as mesenchymal stem cells from either bone marrow-mesenchymal stem cells or adipose tissue-mesenchymal stem cells, could be readily isolated from the host [29]. This eliminates ethical concerns, and as autografts, there is no need for immunosuppression [29]. However, unlike ESCs, adult stem cells have a limited differentiation repertoire, a finite ability to self-renew and undergo senescence during *in vitro* expansion [29].

Alternatively, somatic cells (skin/blood/urine) can be reprogrammed into iPSCs by transfecting them with a variety of transcription factors [25, 26]. Like adult stem cells, autologous iPSCs are patient specific and not isolated from an embryo [29]. Yet, like ESCs, they self-renew without undergoing senescence and can be coaxed to differentiate into almost any mature cell phenotype in culture [26, 29, 36]. However, iPSCs present the risk of teratoma formation when transplanted if not fully differentiated [29]. An additional risk comes from using a virus to transfect the stem cell factors, which may place the patient at the risk of malignancy [25]. As an alternative, they can be reprogrammed using a non-integrating RNA vector and without the use of a viral vector [25].

3-DIMENSIONAL BIOPRINTING AND BIOINK CHALLENGES

The definition of biofabrication for regenerative medicine is: 'the automated generation of biologically functional products with structural organization from living cells, bioactive molecules, biomaterials, cell aggregates such as microtissues, or hybrid cell-material constructs, through bioprinting or bioassembly and subsequent tissue maturation processes' [37].

In this process, the 3D bioprinter is used to deposit bioink(s) in hydrogels to generate viable and functional tissues, with the end product controlled by the 3D bioprinting platform used [38]. For cardiac tissue, some of the most common systems use extrusion-based bioprinters with pneumatic or screw-driven

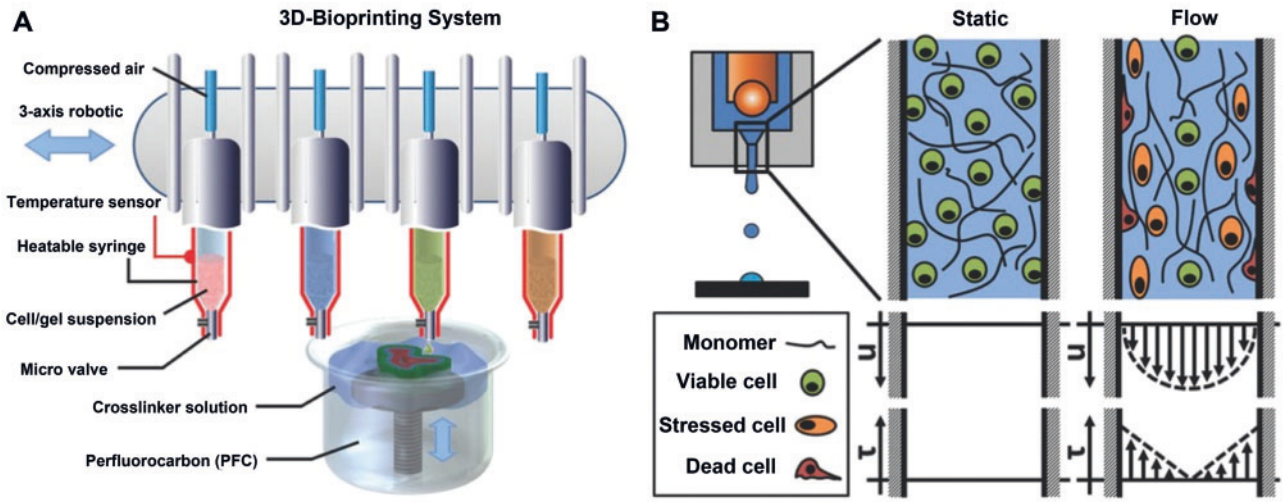

Figure 1: Extrusion-based 3D bioprinting and cell viability. (**A**) Four-nozzle extrusion 3D bioprinting system using pneumatic force to extrude 4 different bioinks. In this example, bioinks are extruded directly into a crosslinker solution, which acts on the bioink to create bonds within the bioprinted structure to retain its shape. (**B**) Downward arrows with greater size indicate greater velocity centrally in the bioink and lower velocity at the periphery, which is in contact with the chamber wall. Upward arrows show resulting shear stress on cells in bioink during 3D bioprinting. Greater shear at the periphery results in stressed cells (orange) and some dead cells (red). Shear stress can be reduced by slowing down the velocity of extrusion, which is readily controlled in 3D bioprinting (reproduced with permission from Blaeser *et al.* [18]). 3D: 3-dimensional.

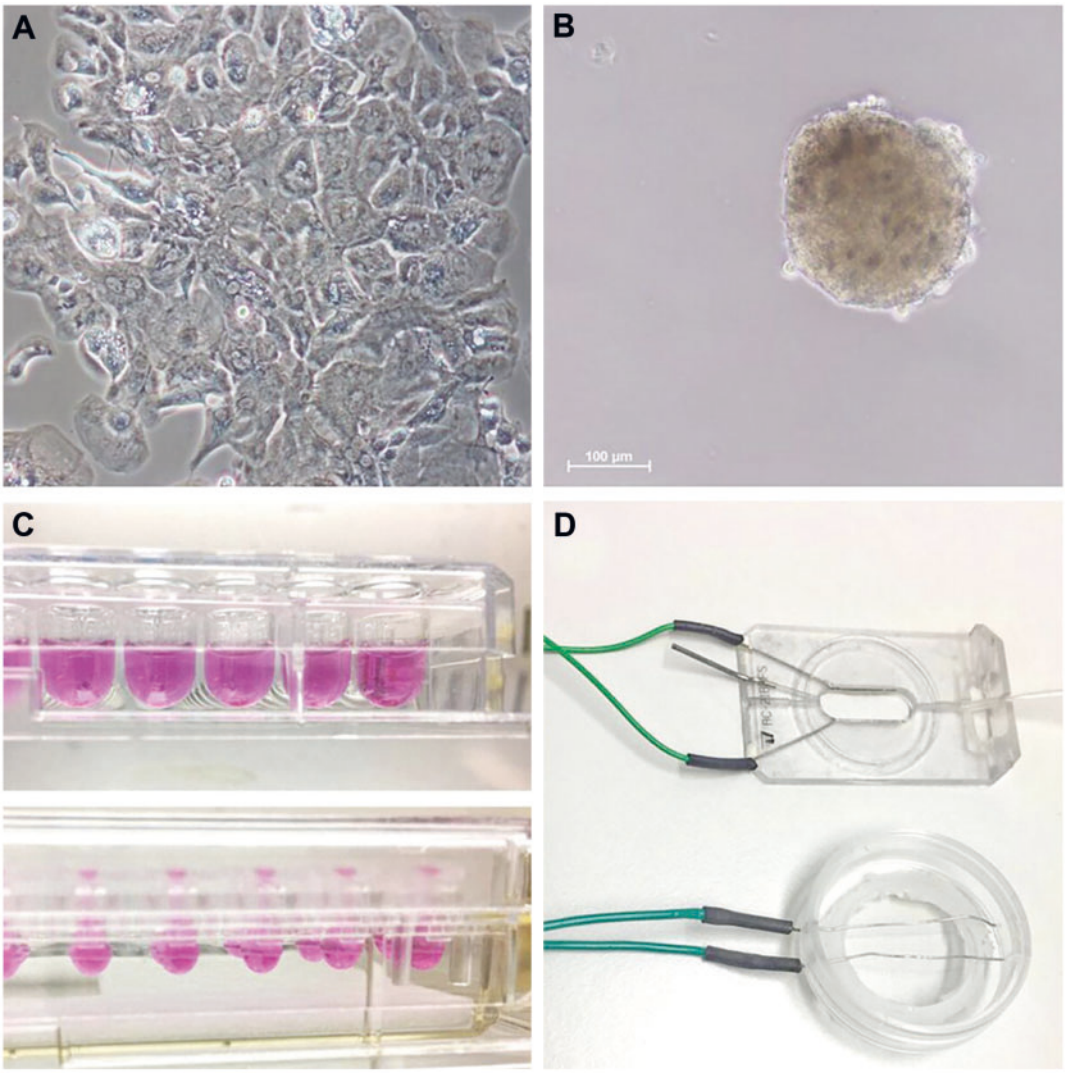

Figure 2: Three-dimensional cardiac microtissue generation and physiology. (**A**) Standard 2-dimensional cell culture of human-induced pluripotent stem cell-derived cardiomyocytes. (**B**) Single (∼200 µm diameter) cardiac spheroid microtissue—a 3-dimensional aggregate of cardiac cells with ability to control spheroid size and cell number and optimize cell–cell interactions, 3-dimensional mechanical signals and extracellular support. (**C**) Two methods for generating cardiac spheroids: U-shaped non-adhesive wells (top panel) and hanging drop cultures (bottom panel). (**D**) Two types of field pacing chambers for providing electrical stimulation to spheroids for the optimal maturation of cardiomyocyte phenotype: a perfusion chamber (above) and culture dish (below) with electrodes to allow for field potential stimulation across cardiac spheroid culture area (modified with permission from Zuppinger [1]).

rotational force to move cellular bioink through a nozzle [3]. The bioprinting method chosen is critical to meet the challenge of delivering cells with minimal shear stress and avoid damaging them in the process (Fig. 1) [18]. A variety of approaches, bioprinters, bioinks and hydrogels to print cells into 3D myocardium have been explored [3, 5].

Ideal bioinks for cardiac regeneration should mimic the native 3D myocardial microenvironment [6, 30]. Bioinks based on cardiac tissue spheroids (which are scaffold free, self-sustainable cell aggregates with a defined diameter and cell number) have been used as building blocks in this process (Fig. 2) [20, 30, 39]. Optimizing cell-specific challenges should be considered when creating cardiac spheroids in bioinks for heart tissue. This includes a clinically relevant scale-up of cell numbers for transplantable bioprinted heart tissues [3, 40]. In addition, mature adult CMs cannot be used for spheroid-based bioinks as they have low adhesive properties and do not form spheroid cultures [41], whereas proliferating neonatal and iPSC-derived CMs (iPSC-CMs) form spheroids within a few days [30]. Furthermore, addition of more adhesive cells to the cellular mix within a spheroid, such as cardiac fibroblasts (CFs), reduces the time for spheroid formation [42]. ECs are a third important cell type found in the human heart, and *in vitro* cardiac spheroids have been generated using a ratio of primary adult CMs:ECs:CFs of 1:3:6, which was optimal for adult CM viability, whereas for CMs derived from iPSCs, a ratio of 2:1:1 was optimal for iPSC-CMs, ECs and CFs, respectively [36, 42].

The use of preformed vascularized microtissues such as spheroids for 3D bioprinting offers the prospect of overcoming many bioink cell-related challenges for tissue engineering of viable and functional myocardium [6, 43]. This includes, but is not limited to, generating a vascular system within the bioink and better integration of physiological contractile function, including speed of contraction, contraction amplitude and calcium transients [1, 44].

In addition to the cellular component, the hydrogel used to support cells in bioink plays a major role in overall patch

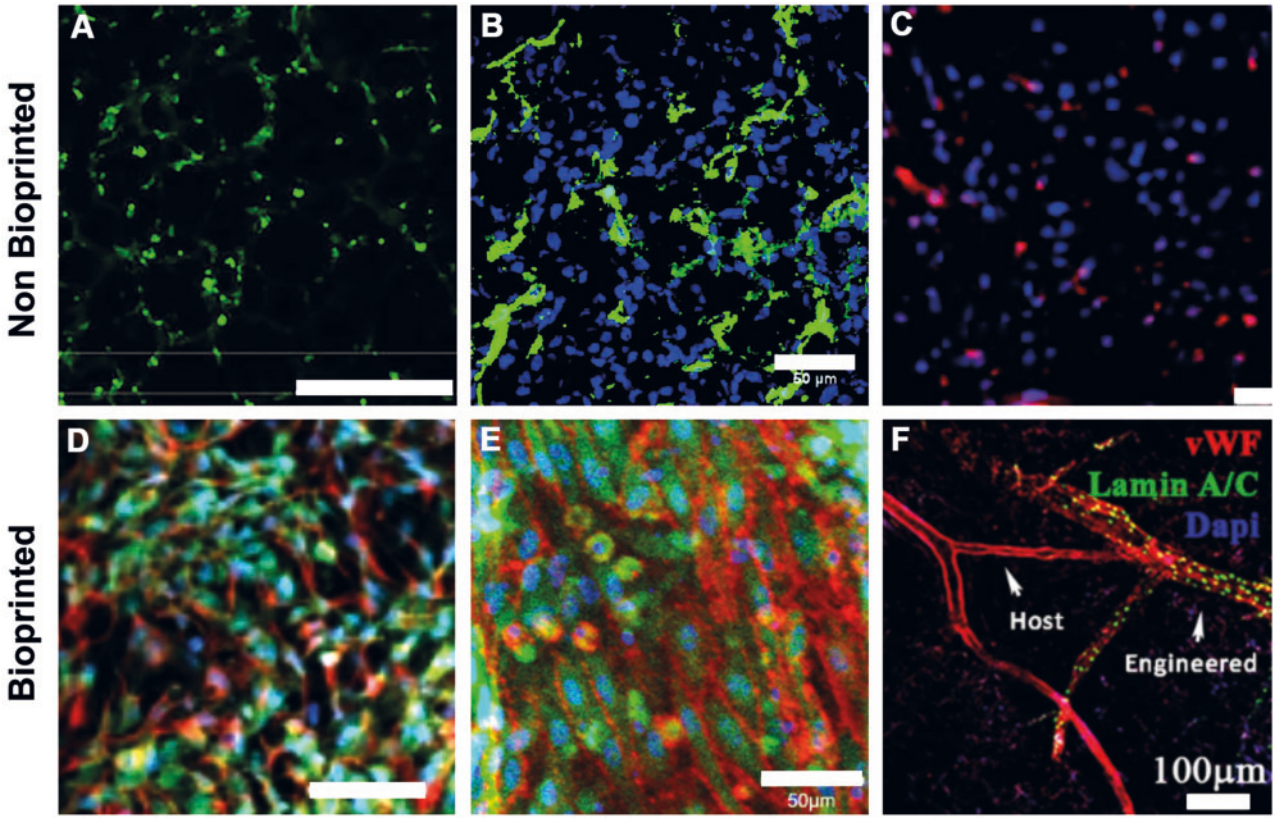

Figure 3: Vascularization in tissue-engineered cardiac patches. (**A**) CD31 expression (green) in a cardiac patch generated by a fibrinogen moulding method and engrafted in pigs (modified with permission from Gao *et al.* [4]). (**B**) CD31 expression (green) in a cardiac patch generated by a net moulding method and engrafted in rats (modified with permission from Yang *et al.* [19]). (**C**) CD31 expression (red) in a fibrin-based cardiac patch generated by a spheroid fusion method and engrafted in mice (modified with permission from Mattapally *et al.* [6]). (**D**) CD31 expression (green) in a cardiac patch generated by a 3-dimensional bioprinting method (modified with permission from Noor *et al.* [5]). (**E**) CD31 expression (red) in a cardiac patch generated by a 3-dimensional bioprinting method (modified with permission from Zhang *et al.* [10]). (**F**) vWF (red) and lamin A/C (green) expressions in a cardiac patch generated by a 3-dimensional bioprinting method and engrafted in mice with the evidence of host-patch anastomosis (modified with permission from Maiullari *et al.* [9]). Scale bar appearances are due to source data. vWF: von Willebrand factor.

geometry, size, survival and function by better mimicking the mechanical properties of the native ECM [45]. Hydrogel/bioink composition determines important characteristics such as biocompatibility, biodegradability, paracrine signalling, non-immunogenicity and stiffness, all of which present optimization challenges [46–48]. To date, the formulation of cardiac bioinks with optimal chemical–mechanical properties to better control the cardiac niche has not been defined [46, 48]. The requirement for a cell-friendly, flowing bioink limits other factors such as the precision and resolution of the print, although this may be improved by applying microfluidic devices to the extrusion nozzles of bioprinters [9, 49]. Whilst the bioink must flow well during the print, it should also be mechanically robust and yet still allow for the tissue to remodel and the cells to interact in the post-printing phase [46].

Several hydrogels have been tested for cardiac tissues, either using natural materials (such as decellularized cardiac ECM [46] and gelatin-based hydrogels combined with fibrinogen, alginate or hyaluronan [47]) or synthetic-origin materials (such as polyurethane) [50]. Decellularized cardiac ECM promotes angiogenesis and cell proliferation but cannot be easily isolated from the same donor heart [46]. Gelatin has excellent rheological properties and biodegradability, but its use is highly temperature dependent [47]. Electrically conductive polymeric hydrogels such as poly(ethylenedioxythiophene) allow for improved cell electroactivity, whilst they present undesired properties such as increased hydrophobicity and reduced elasticity [45, 51]. Other hydrogels may present cell-specific paracrine signalling factors [48]. Therefore, the challenges associated with engineering the optimal hydrogel are of paramount importance and should address several chemical and biomechanical parameters.

VASCULARIZATION

Another major challenge for creating a cardiac patch is engineering a hierarchical vascular tree (Table 1) [10, 39]. The maximum tissue diameter without the development of a necrotic core varies since it depends on cell-specific oxygen consumption, but it generally is common in any cardiac tissue thicker than ~200 μm in diameter [9, 30]. Neovascularization has been attempted by culturing cardiac tissues in highly vascular areas *in vivo*, such as the omentum [34]. Others have used hydrogels from dissolved omentum, with potential use for 3D bioprinted cardiac tissues [5, 44]. However, to date, only capillary-sized, disorganized vasculature has been generated and recreating a fully branched vascular network for cardiac tissue engineering remains a challenge (Fig. 3) [4–6, 9, 10, 19, 49].

Further progress is being made in engineering vascularized tissues by co-culturing CMs with ECs. For example, a microvascular network was achieved in spheroid cultures containing rat ECs, CMs and fibroblasts before their implantation in nude rats [52]. It has been suggested that a better branched vascular network could be achieved by fusing prevascularized spheroids [20, 39, 43]. Vascular network anastomosis between graft and host *in vivo* is critical for new blood flow to promote the engraftment and function of transplanted patches [7, 9, 20, 39, 53]. At a cellular level, such graft–host anastomoses may form directly, for instance by a 'wrap and tap' mechanism whereby graft lumen-forming ECs anastomose with host vasculature by wrapping around host vessels and 'tapping' through the vessel walls, facilitated by matrix metalloproteases [54]. Paracrine signalling including a 'secretome' of cytokines, exosomes and growth factors such as vascular endothelial growth factor is a major regulator of tissue angiogenesis and potentially of cardiac regeneration [4, 9, 23, 48, 55].

The emerging evidence that regenerative transplanted tissue may act by mechanisms other than direct replenishment of lost cells would explain why functional improvement has been seen for patches containing only 8 million cells [4, 33]. It would be advantageous if paracrine mechanisms turned out to be more important than numerical replenishment, as another major challenge is how to expand replacement cells, including non-myocytes (such as ECs and CFs) and myocytes, to a high enough number [3, 40].

An alternative method to bioprinted cardiac tissues is to preform a vascular scaffold. This may be bioprinted in patterns such as networks by depositing cellular bioink [8, 10, 49]. For example, Zhang *et al.* [49] used microfluidic printheads to bioprint ECs within hydrogels. These were fixed in position by ionic and ultraviolet (UV) light crosslinking. The ionic crosslinker (calcium chloride) was added to the alginate scaffold in real time during the print, followed by UV crosslinking of gelatin methacryloyl. Following formation of a vascularized scaffold, CMs were added to the construct to generate cardiac tissue.

CONTRACTILE FUNCTION

For myocardial tissue to first engraft in the host and eventually improve cardiac function, it should not only synchronously contract by itself but also together as a functional syncytium with the host [40]. Electrical properties of cells and tissues, such as cardiac excitation-contraction coupling, calcium transients and cell–cell interactions, are critical [1, 40, 51]. iPSC-CMs do not present the fully mature contractile behaviour typical of adult cells, unless they are cultured with additional cellular and extracellular stimuli, such as electromechanical conditioning, electrical field stimulation and continuous pacing (Fig. 4 and Videos 1 and 2) [21, 56]. Cardiac spheroids from iPSC-CMs spontaneously develop synchronous contractile function, which is linked with improved speed and amplitude of contraction, and calcium transients compared to single-cell cultures [1, 36, 42]. Adding conductive polymers propagates the electrical signal between different areas in a cell culture, providing assistance with current passage in the absence of fully developed cell–cell electrochemical pathways [51, 57]. Overall, physiological contractile function and integration of engineered tissue with the host remain some of the main challenges to overcome (Table 1) [1, 21, 56].

PRECLINICAL SUCCESS

In animal models of myocardial infarction, functional improvement after the engraftment of heart patches generated from cells in moulding devices has already been demonstrated in mice [6], rats [19] and pigs [4]. Direct injection of hydrogel laden with paracrine signalling factors has shown a significant reduction in infarct size from 38% to 16% in a rat model of myocardial infarction [48]. Furthermore, a small rat-sized cardiac ventricle (1/250th the size of a human ventricle) has been tissue-engineered by MacQueen *et al.* [58]. However, this only approximated 100 millionth ($\sim 10^{8}$) of the contractile work of a native human ventricle. Indeed, at ~1%, the ejection fraction of this model was ~1/50th of a normal rat's ejection fraction and the cell density was 10-fold less than normal for a rat. Other studies that used 3D bioprinting reported improved cardiac patch vascularization, automation and precision *in vitro* and *in vivo* in mice [5, 9, 10]. These studies provide examples demonstrating significant preclinical progress and pave the way for human trials and scaled up models.

SURGICAL PERSPECTIVES

Whilst surgical treatment of aortic, coronary and valve disease can now be undertaken with excellent results, repair or reconstruction of the contractile pump element, the myocardium, is currently limited [2]. Excluding infrequently performed procedures such as the Dor (pericardial-lined Dacron endoventricular circular plasty) [59] and Batista (reduction ventriculoplasty) [60] procedures, the only option beyond resynchronization is transplantation [7]. Whether this is human or genetically modified xenotransplantation, the loss of the recipient's heart is obligatory and absolute dependence on the function of the new heart follows. Cellular cardiomyoplasty has been evaluated to allow the augmentation of existing cardiac function but, despite showing some functional merit, has largely been disappointing overall [23].

Early clinical trials using ESC-derived cardiac cells in patients have shown promising results by culturing cells in a patch before transplantation [33, 61]. Following the first case report of a cellular patch applied to a human heart in 2015 [61], the same group reported that transplantation of these patches in 6 patients with heart failure is safe (the ESCORT trial) [33]. Cardiac patches of ~20 cm^2 were surgically applied to the epicardium of patients undergoing coronary artery bypass surgery and secured under a pericardial flap (Fig. 5). As the patches were not 3D bioprinted, the advantages of a scalable manufacturing process were not present; nonetheless, the trial paved the way for more extensive trials testing efficacy.

With prevascularized patches, the study by Maiullari *et al.* [9] showed that host-patch anastomosis in mice is feasible using 3D bioprinted poly(ethylene glycol)-fibrinogen hydrogels embedded with iPSC-CMs and human umbilical vein ECs (Fig. 3F). An augmentative approach may be the use of pro-angiogenic factors to promote vascular fusion between graft and host, similar to that which is observed during vascular development [43].

To progress with the transplantation of thick bioprinted heart tissues with potentially low-calibre vasculature in patients, the surgeon may be tasked with creating a macroscopic anastomosis of the graft to an existing blood supply [53]. This would especially

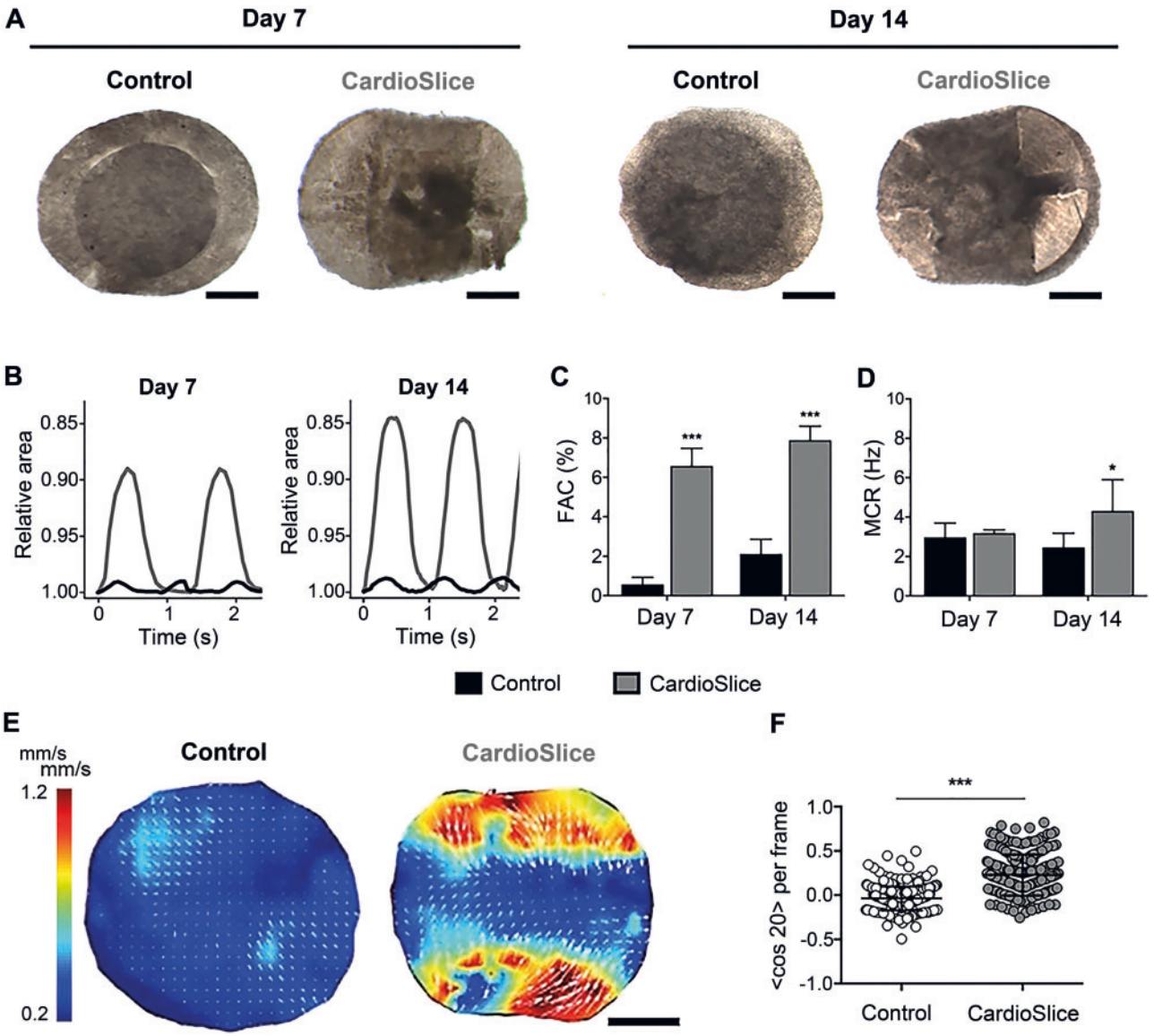

Figure 4: Electrical stimulation of cell culture leads to greater contractility in engineered cardiac tissue. Beating macrotissues were generated by seeding induced pluripotent stem cell-derived cardiomyocytes and human fibroblasts in a 3-dimensional porous scaffold and culturing for 14 days as either control (no electrical stimulation) or 'CardioSlice' (electrical stimulation applied whilst culturing). (**A**) Human cardiac macrotissues after 7 or 14 days of culture, either without (control) or with (CardioSlice) electrical stimulation (scale bars 2.5 mm) (see also Videos 1 and 2). (**B**) Contraction amplitude of control versus CardioSlice bioengineered cardiac tissues. Fractional contraction area (compared to area of the tissue at rest) is represented over time, and control tissue remains close to 1.0 when contracting whereas CardioSlice patches contract to 0.85 (85% of size of tissue at rest). (**C**) The percentage of FAC for control (unstimulated) versus electrically stimulated CardioSlice cardiac macrotissues. (**D**) MCR for control compared to electrically stimulated CardioSlice macrotissues when paced. At 14 days, CardioSlice macrotissues were able to be paced at over 4 Hz, approximately double the MCR of control tissues. (**E**) Beating cardiac macrotissue velocity maps after 14 days of culture. Blue colours and shorter white mini arrows represent lower velocities. Higher velocities (redder areas and longer mini arrows) were observed in CardioSlice macrotissues versus controls (scale bar 2.5 mm). (**F**) Alignment analysis comparing direction of the electrical field vector and subsequent beating direction of bioengineered cardiac tissues. The order parameter cos2θ was used: random distribution gives values close to 0 whereas parallel alignment gives values close to 1 (modified with permission from Valls-Margarit *et al.* [21]). FAC: fractional area change; MCR: maximum capture rate.

be true if naturally forming low-calibre anastomoses to the diseased native myocardial tissue underneath the graft were insufficient. Foreseeably, microsurgical anastomoses may have to be made initially to allow time for naturally occurring graft–host connections to form [53].

One approach to promote host-patch vascular anastomosis could be to use non-diseased, larger-calibre source vessels such as the gastroepiploic or thoracodorsal artery with the tissue cultivated on the omentum or the latissimus dorsi muscle, respectively. Bioengineered tissue could be allowed time to form anastomoses with the underlying tissue, and capillaries formed from ECs within a tissue-engineered cardiac patch can retain patency [53]. Blood flow through the graft could be assessed in advance whilst it lay on its incubating native tissue. Once blood flow and viability of the patch are demonstrated, it should be surgically feasible to then rotate a flap to the myocardium within the pericardium without loss of blood supply (Fig. 6). Conversely, minimally invasive procedures could be used to transplant bioprinted cardiac tissues in innovative ways for cardiac surgical patients [62].

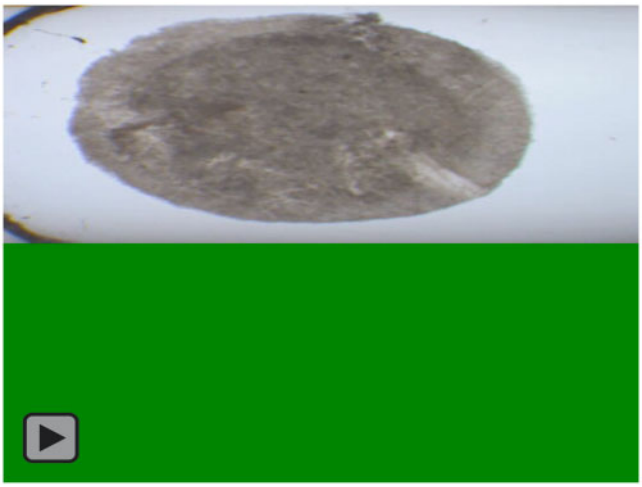

Video 1: Bioengineered human cardiac tissue showing spontaneous beating after 14 days in culture—non-stimulated control tissue shown (reproduced with permission from Valls-Margarit *et al.* [21]).

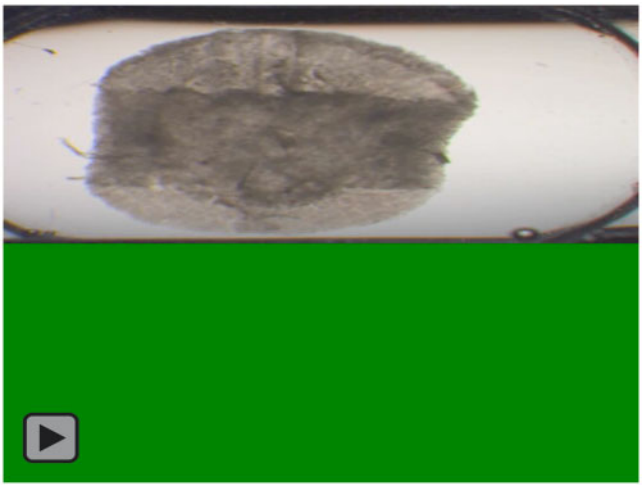

Video 2: Bioengineered human cardiac tissue showing spontaneous beating after 14 days in culture—electrically stimulated (CardioSlice) tissue shown (reproduced with permission from Valls-Margarit *et al.* [21]).

TRANSLATIONAL PERSPECTIVES

As is expected when multiple emerging technologies/techniques (iPSCs, 3D culture, bioprinting) make rapid preclinical gains, translation of the preclinical potential into a useful clinical therapeutic presents specific challenges [40, 63, 64]. Laboratory workflows for autologous iPSCs are appealing in offering a fully patient-specific supply of tissue; however, they can be relatively difficult and resource intensive to achieve for 1 patient per workflow [23]. For translation, workflows need to conform to good manufacturing practice standards, usually making them more challenging, for example, by replacing commonly used xenogeneic laboratory products such as foetal bovine serum with human serum album or carrying out the work in a fully certified good manufacturing practice facility [63, 64]. An alternative, using allogeneic iPSCs from donors, comes with the advantage of potentially being able to cryobank multiple haplotyped iPSCs and iPSC-derived cells or tissues [23, 40]. Having the cells banked in cold storage could allow for a more technically, logistically and economically feasible solution: an 'off-the-shelf' selection of a best-matched tissue at the time of need [23, 40]. However, this would be accompanied with immunosuppression, difficulties acquiring matched tissue (especially for diverse ethnic groups) and a likely need for international coordination for a large enough tissue repository [23, 40].

DISCUSSION

Whilst 3D bioprinting of a fully functional human myocardial patch has not yet been achieved, there are several areas where 3D bioprinting of other tissues has already reached clinical trials. For example, 3D bioprinting of ears of 5 children showed promising results up to 2.5 years of follow-up [65]. However, 3D bioprinting of heart patches presents a different level of complexity.

Important questions remain regarding the application of bioprinted tissue for human cardiac surgery and the patient population it will most benefit [2, 3]. Whether advances in other technologies, such as ventricular assist devices, or even a refined surgical plication technique, could be combined with bioprinted heart tissue in innovative ways remains an open question.

Throughout this review, there has been an assumption that the optimal microenvironment of cardiac tissue should be achieved, but this may not be required and good results may be obtained even in the absence of cells [55, 62]. Recently, a study showed that macrophages may play a major role in cardiac regeneration by inducing inflammation following stem cell injection [66]. It is possible that mechanisms such as this could be implicated in the surprising finding that even acellular patches or hydrogels applied to the heart may have a positive effect on cardiac regeneration via the immune response [55, 62]. Nevertheless, any foreign material or cells within a patch will lead to an immune response with a rim of fibrosis, potentially isolating the graft from the host [40]. Therefore, a better understanding of these mechanisms may be beneficial to developing novel approaches to better couple the graft with the host. These may include the use of either conductive polymers (to allow electroactivity to bypass the fibrotic rim) [57], sacrificial hydrogels disintegrating over time [8, 53] or adjunctive anti-inflammatory and/or 'pro-survival' compounds [67, 68].

It would be critical to compare the cost-effectiveness of a stem cell-derived 3D bioprinted cellular patch to other techniques for long-term treatment but with the price of bioprinters falling rapidly [38], cells derived from patients themselves and workflows utilizing basic laboratory materials [1, 47], there is reason to speculate that 3D bioprinted patient-specific multicellular patches could be a cost-effective surgical therapeutic.

For end-stage cardiac pathology, this is one of the few emerging technologies that provides hope of a cure. It is unique in that it may offer a paradigm-shifting solution for patients with cardiac failure who could otherwise only be 'cured' with a heart transplant. This potential generates considerable media attention which raises specific ethical considerations. These are only recently being elucidated in the bioethical literature, for example, how media hype can inflate expections for desperate patients, which may also create an environment for unscrupulous health providers, or how public misinformation may impact patients' decision-making significantly [63, 69]. Safe translation of animal

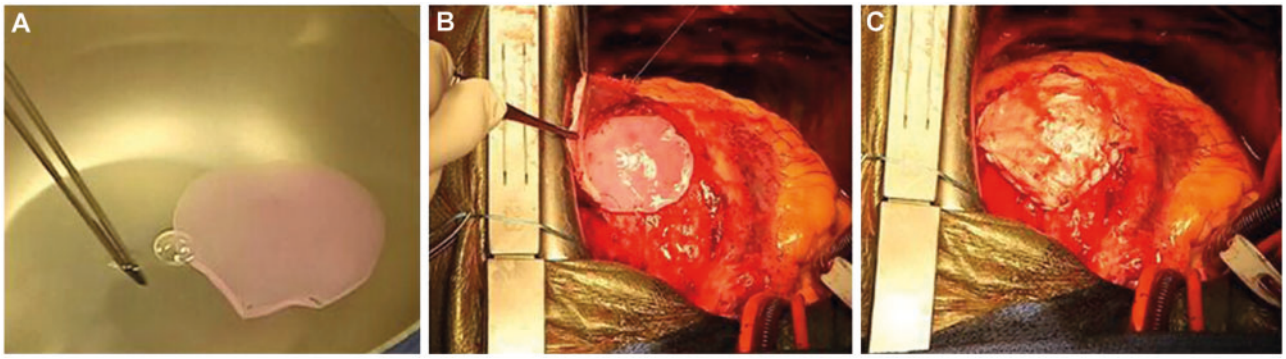

Figure 5: Embryonic stem cell-derived cardiac patches for patients with heart failure undergoing coronary artery bypass grafting (CABG). (**A–C**) A fibrin-based patch infused with allogenic cardiac progenitor cells derived from embryonic stem cells was applied to the epicardial surface of human cardiac failure patients undergoing CABG and shown to be safe in a phase I clinical safety trial (modified with permission from Menasché *et al.* [33]).

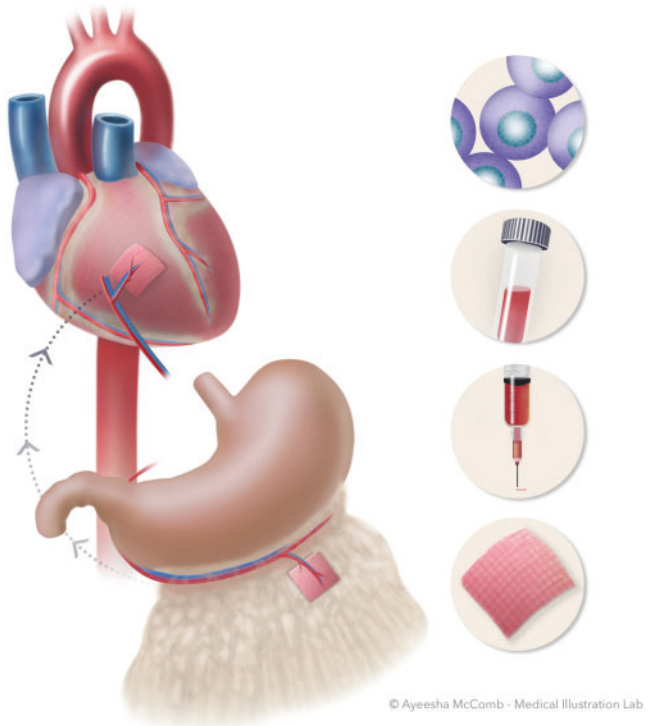

Figure 6: The human body as a natural bioreactor for bioprinted cardiac patch vascularization. Patient-specific induced pluripotent stem cell-derived bioinks obtained by reprogramming cells taken from patient blood could be used to 3-dimensional bioprint cardiac tissue patches. This tissue could be matured on the patient's omentum, anastomosed to the gastroepiploic artery and subsequently rotated onto the epicardial surface to regenerate the myocardium—a waiting list-free and surgically feasible alternative to donor heart allotransplantation.

to human trials may require new 3D bioprinting-specific regulation [69].

CONCLUSION

For patients with non-functional areas of myocardium, 3D bioprinting of personalized heart tissues presents several challenges but also the potential to develop a clinically available approach in the coming years. If successful, this technology has the potential to re-shape the cardiac therapeutic environment, resolve an unmet need for surgical practice and actualize a long-standing desire for surgeons to promote cardiac regeneration in patients.

ACKNOWLEDGEMENTS

The authors thank Ayeesha Clare McComb, Chief Medical Illustrator at Medical Illustrations laboratory, for her work in the design and generation of illustrations for this manuscript.

Funding

Christopher D. Roche was supported by a Sir John Loewenthal Scholarship 2019 (University of Sydney), the Le Gros Legacy Fund New Zealand (PhD012019) and a Heart Research Australia PhD Scholarship (2019-02). Carmine Gentile was supported by a University of Sydney Kick-Start Grant, University of Sydney Chancellor's Doctoral Incentive Programme Grant and a Sydney Medical School Foudation Cardiothoracic Surgery Research Grant.

Conflict of interest: none declared.

Author contributions

Christopher D. Roche: Conceptualization; Data curation; Formal analysis; Funding acquisition; Project administration; Visualization; Writing—original draft; Writing—review & editing. **Russell J.L. Brereton:** Conceptualization; Funding acquisition; Validation; Writing—original draft; Writing—review & editing. **Anthony W. Ashton:** Writing—review & editing. **Christopher Jackson:** Writing—review & editing. **Carmine Gentile:** Conceptualization; Data curation; Formal analysis; Funding acquisition; Project administration; Supervision; Writing—original draft; Writing—review & editing.

REFERENCES

[1] Zuppinger C. Measurement of contractility and calcium release in cardiac spheroids. Methods Mol Biol 2019;1929:41–52.
[2] Beyersdorf F. Three-dimensional bioprinting: new horizon for cardiac surgery. Eur J Cardiothorac Surg 2014;46:339–41.
[3] Puluca N, Lee S, Doppler S, Münsterer A, Dreßen M, Krane M *et al.* Bioprinting approaches to engineering vascularized 3D cardiac tissues. Curr Cardiol Rep 2019;21:90.

[4] Gao L, Gregorich ZR, Zhu W, Mattapally S, Oduk Y, Lou X *et al.* Large cardiac muscle patches engineered from human induced-pluripotent stem cell-derived cardiac cells improve recovery from myocardial infarction in swine. Circulation 2018;137:1712–30.

[5] Noor N, Shapira A, Edri R, Gal I, Wertheim L, Dvir T. 3D printing of personalized thick and perfusable cardiac patches and hearts. Adv Sci 2019; 6:1900344.

[6] Mattapally S, Zhu W, Fast VG, Gao L, Worley C, Kannappan R *et al.* Spheroids of cardiomyocytes derived from human-induced pluripotent stem cells improve recovery from myocardial injury in mice. Am J Physiol Heart Circ Physiol 2018;315:H327–39.

[7] Zhang J, Zhu W, Radisic M, Vunjak-Novakovic G. Can we engineer a human cardiac patch for therapy? Circ Res 2018;123:244–65.

[8] Miller JS, Stevens KR, Yang MT, Baker BM, Nguyen DH, Cohen DM *et al.* Rapid casting of patterned vascular networks for perfusable engineered three-dimensional tissues. Nat Mater 2012;11:768–74.

[9] Maiullari F, Costantini M, Milan M, Pace V, Chirivi M, Maiullari S *et al.* A multi-cellular 3D bioprinting approach for vascularized heart tissue engineering based on HUVECs and iPSC-derived cardiomyocytes. Sci Rep 2018;8:13532.

[10] Zhang YS, Arneri A, Bersini S, Shin SR, Zhu K, Goli-Malekabadi Z *et al.* Bioprinting 3D microfibrous scaffolds for engineering endothelialized myocardium and heart-on-a-chip. Biomaterials 2016;110:45–59.

[11] Hobbs FD, Roalfe AK, Davis RC, Davies MK, Hare R; the Midlands Research Practices Consortium (MidReC). Prognosis of all-cause heart failure and borderline left ventricular systolic dysfunction: 5 year mortality follow-up of the Echocardiographic Heart of England Screening Study (ECHOES). Eur Heart J 2007;28:1128–34.

[12] National Institute for Health and Care Excellence (NICE). Chronic Heart Failure in Adults: Diagnosis and Management. NICE Guideline [NG106], 2018. https://www.nice.org.uk/guidance/ng106 (29 November 2019, date last accessed).

[13] MacGowan GA, Crossland DS, Hasan A, Schueler S. Considerations for patients awaiting heart transplantation—insights from the UK experience. J Thorac Dis 2015;7:527–31.

[14] Lund LH, Khush KK, Cherikh WS, Goldfarb S, Kucheryavaya AY, Levvey BJ *et al.* The registry of the International Society for Heart and Lung Transplantation: thirty-fourth adult heart transplantation report-2017; focus theme: allograft ischemic time. J Heart Lung Transplant 2017;36:1037–46.

[15] Australian and New Zealand Cardiothoracic Organ Transplant Registry (ANZCOTR). 2018 Report. http://www.anzcotr.org.au/pub/e0cc941a/PDFS/ANZCOTR2018_text.pdf (29 November 2019, date last accessed).

[16] UK NHS Blood and Transplant. Organ Donation and Transplantation Annual Activity Report. 2018/2019. https://nhsbtdbe.blob.core.windows.net/umbraco-assets-corp/16537/organ-donation-and-transplantation-activity-report-2018-2019.pdf (29 November 2019, date last accessed).

[17] Reinecke H, Zhang M, Bartosek T, Murry CE. Survival, integration, and differentiation of cardiomyocyte grafts: a study in normal and injured rat hearts. Circulation 1999;100:193–202.

[18] Blaeser A, Duarte Campos DF, Puster U, Richtering W, Stevens MM, Fischer H. Controlling shear stress in 3D bioprinting is a key factor to balance printing resolution and stem cell integrity. Adv Healthcare Mater 2016;5:326–33.

[19] Yang B, Lui C, Yeung E, Matsushita H, Jeyaram A, Pitaktong I *et al.* A net mold-based method of biomaterial-free three-dimensional cardiac tissue creation. Tissue Eng Part C Methods 2019;25:243–52.

[20] Visconti RP, Kasyanov V, Gentile C, Zhang J, Markwald RR, Mironov V. Towards organ printing: engineering an intra-organ branched vascular tree. Expert Opin Biol Ther 2010;10:409–20.

[21] Valls-Margarit M, Iglesias-García O, Di Guglielmo C, Sarlabous L, Tadevosyan K, Paoli R *et al.* Engineered macroscale cardiac constructs elicit human myocardial tissue-like functionality. Stem Cell Reports 2019;13:207–20.

[22] Zhang D, Shadrin IY, Lam J, Xian HQ, Snodgrass HR, Bursac N. Tissue-engineered cardiac patch for advanced functional maturation of human ESC-derived cardiomyocytes. Biomaterials 2013;34:5813–20.

[23] Hatzistergos KE, Selem S, Balkan W, Hare JM. Chapter 17—Cardiac stem cells: biology and therapeutic applications. In: Atala A, Lanza R, Mikos AG, Nerem R (eds). Principles of Regenerative Medicine, 3rd edn. Cambridge, MA, USA: Academic Press, 2019, 247–72.

[24] Curfman G. Stem cell therapy for heart failure: an unfulfilled promise? JAMA 2019;321:1186–7.

[25] Yoshioka N, Dowdy SF. Enhanced generation of iPSCs from older adult human cells by a synthetic five-factor self-replicative RNA. PLoS One 2017;12:e0182018.

[26] Takahashi K, Yamanaka S. Induction of pluripotent stem cells from mouse embryonic and adult fibroblast cultures by defined factors. Cell 2006;126:663–76.

[27] Mawad D, Figtree G, Gentile C. Current technologies based on the knowledge of the stem cells Microenvironments. Adv Exp Med Biol 2017;1041:245–62.

[28] Kimura W, Sadek HA. The cardiac hypoxic niche: emerging role of hypoxic microenvironment in cardiac progenitors. Cardiovasc Diagn Ther 2012;2:278–89.

[29] Campbell M, Surija L, Peceros K, Sharma P, Figtree G, Gentile C. Stem cell spheroids. In: Reis RL (ed). Encyclopedia of Tissue Engineering and Regenerative Medicine. Cambridge, MA, USA: Academic Press, 2019, 387–93.

[30] Gentile C. Filling the gaps between the *in vivo* and *in vitro* microenvironment: engineering of spheroids for stem cell technology. Curr Stem Cell Res Ther 2016;11:652–65.

[31] Adler CP, Costabel U. Cell number in human heart in atrophy, hypertrophy, and under the influence of cytostatics. Recent Adv Stud Cardiac Struct Metab 1975;6:343–55.

[32] Bergmann O, Zdunek S, Felker A, Salehpour M, Alkass K, Bernard S *et al.* Dynamics of cell generation and turnover in the human heart. Cell 2015; 161:1566–75.

[33] Menasché P, Vanneaux V, Hagege A, Bel A, Cholley B, Parouchev A *et al.* Transplantation of human embryonic stem cell-derived cardiovascular progenitors for severe ischemic left ventricular dysfunction. J Am Coll Cardiol 2018;71:429–38.

[34] Dvir T, Kedem A, Ruvinov E, Levy O, Freeman I, Landa N *et al.* Prevascularization of cardiac patch on the omentum improves its therapeutic outcome. Proc Natl Acad Sci USA 2009;106:14990–5.

[35] Tao H, Chen X, Wei A, Song X, Wang W, Liang L *et al.* Comparison of teratoma formation between embryonic stem cells and parthenogenetic embryonic stem cells by molecular imaging. Stem Cells Int 2018;2018: 1–9.

[36] Campbell M, Chabria M, Figtree GA, Polonchuk L, Gentile C. Stem cell-derived cardiac spheroids as 3D *in vitro* models of the human heart microenvironment. In: Turksen K (ed). Stem Cell Niche. Methods in Molecular Biology. Totowa, NJ, USA: Humana Press, 2018, 51–9.

[37] Groll J, Boland T, Blunk T, Burdick JA, Cho DW, Dalton PD *et al.* Biofabrication: reappraising the definition of an evolving field. Biofabrication 2016;8:013001.

[38] Reid JA, Mollica PA, Johnson GD, Ogle RC, Bruno RD, Sachs PC. Accessible bioprinting: adaptation of a low-cost 3D-printer for precise cell placement and stem cell differentiation. Biofabrication 2016;8:025017.

[39] Mironov V, Visconti RP, Kasyanov V, Forgacs G, Drake CJ, Markwald RR. Organ printing: tissue spheroids as building blocks. Biomaterials 2009; 30:2164–74.

[40] Huang NF, Serpooshan V, Morris VB, Sayed N, Pardon G, Abilez OJ *et al.* Big bottlenecks in cardiovascular tissue engineering. Commun Biol 2018; 1:199.

[41] Kim TY, Kofron CM, King ME, Markes AR, Okundaye AO, Qu Z *et al.* Directed fusion of cardiac spheroids into larger heterocellular microtissues enables investigation of cardiac action potential propagation via cardiac fibroblasts. PLoS One 2018;13:e0196714.

[42] Polonchuk L, Chabria M, Badi L, Hoflack JC, Figtree G, Davies MJ *et al.* Cardiac spheroids as promising *in vitro* models to study the human heart microenvironment. Sci Rep 2017;7:7005.

[43] Fleming PA, Argraves WS, Gentile C, Neagu A, Forgacs G, Drake CJ. Fusion of uniluminal vascular spheroids: a model for assembly of blood vessels. Dev Dyn 2010;239:398–406.

[44] Shevach M, Zax R, Abrahamov A, Fleischer S, Shapira A, Dvir T. Omentum ECM-based hydrogel as a platform for cardiac cell delivery. Biomed Mater 2015;10:034106.

[45] Mawad D, Artzy-Schnirman A, Tonkin J, Ramos J, Inal S, Mahat MM *et al.* Electroconductive hydrogel based on functional poly(ethylenedioxy thiophene). Chem Mater 2016;28:6080–8.

[46] Sawkins MJ, Saldin LT, Badylak SF, White LJ. ECM hydrogels for regenerative medicine. In: Berardi AC (ed). Extracellular Matrix for Tissue Engineering and Biomaterials. Stem Cell Biology and Regenerative Medicine. New York, NY, USA: Springer International Publishing, 2018, 27–58.

[47] Wang X, Ao Q, Tian X, Fan J, Tong H, Hou W *et al.* Gelatin-based hydrogels for organ 3D bioprinting. Polymers 2017;9:401.

[48] Waters R, Alam P, Pacelli S, Chakravarti AR, Ahmed RPH, Paul A. Stem cell-inspired secretome-rich injectable hydrogel to repair injured cardiac tissue. Acta Biomater 2018;69:95–106.

[49] Zhang YS, Pi Q, van Genderen AM. Microfluidic bioprinting for engineering vascularized tissues and organoids. J Vis Exp 2017;126:e55957.
[50] Fujimoto KL, Tobita K, Merryman WD, Guan J, Momoi N, Stolz DB *et al*. An elastic, biodegradable cardiac patch induces contractile smooth muscle and improves cardiac remodeling and function in subacute myocardial infarction. J Am Coll Cardiol 2007;49:2292–300.
[51] Mawad D, Mansfield C, Lauto A, Perbellini F, Nelson GW, Tonkin J *et al*. A conducting polymer with enhanced electronic stability applied in cardiac models. Sci Adv 2016;2:e1601007.
[52] Noguchi R, Nakayama K, Itoh M, Kamohara K, Furukawa K, Oyama J *et al*. Development of a three-dimensional pre-vascularized scaffold-free contractile cardiac patch for treating heart disease. J Heart Lung Transplant 2016;35:137–45.
[53] Zhang B, Montgomery M, Chamberlain MD, Ogawa S, Korolj A, Pahnke A *et al*. Biodegradable scaffold with built-in vasculature for organ-on-a-chip engineering and direct surgical anastomosis. Nat Mater 2016;15:669–78.
[54] Cheng G, Liao S, Kit Wong H, Lacorre DA, di Tomaso E, Au P *et al*. Engineered blood vessel networks connect to host vasculature via wrapping-and-tapping anastomosis. Blood 2011;118:4740–9.
[55] Domenech M, Polo-Corrales L, Ramirez-Vick JE, Freytes DO. Tissue engineering strategies for myocardial regeneration: acellular versus cellular scaffolds? Tissue Eng Part B Rev 2016;22:438–58.
[56] Tu C, Chao B, Wu J. Strategies for improving the maturity of human induced pluripotent stem cell-derived cardiomyocytes. Circ Res 2018;123:512–14.
[57] Jiang L, Gentile C, Lauto A, Cui C, Song Y, Romeo T *et al*. Versatile fabrication approach of conductive hydrogels via copolymerization with vinyl monomers. ACS Appl Mater Interfaces 2017;9:44124–33.
[58] MacQueen LA, Sheehy SP, Chantre CO, Zimmerman JF, Pasqualini FS, Liu X *et al*. A tissue-engineered scale model of the heart ventricle. Nat Biomed Eng 2018;2:930–41.
[59] Dor V, Saab M, Coste P, Kornaszewska M, Montiglio F. Left ventricular aneurysm: a new surgical approach. Thorac Cardiovasc Surg 1989;37:11–19.
[60] Batista RJ. Reduction ventriculoplasty. Z Kardiol 2001;90(Suppl 1):35–7.
[61] Menasché P, Vanneaux V, Hagege A, Bel A, Cholley B, Cacciapuoti I *et al*. Human embryonic stem cell-derived cardiac progenitors for severe heart failure treatment: first clinical case report. Eur Heart J 2015;36:2011–17.
[62] Singelyn JM, Sundaramurthy P, Johnson TD, Schup-Magoffin PJ, Hu DP, Faulk DM *et al*. Catheter-deliverable hydrogel derived from decellularized ventricular extracellular matrix increases endogenous cardiomyocytes and preserves cardiac function post-myocardial infarction. J Am Coll Cardiol 2012;59:751–63.
[63] Cossu G, Birchall M, Brown T, De Coppi P, Culme-Seymour E, Gibbon S *et al*. Lancet Commission: stem cells and regenerative medicine. Lancet 2018;391:883–910.
[64] Chimenti I, Gaetani R, Forte E, Angelini F, De Falco E, Zoccai GB *et al*. Serum and supplement optimization for EU GMP-compliance in cardiospheres cell culture. J Cell Mol Med 2014;18:624–34.
[65] Zhou G, Jiang H, Yin Z, Liu Y, Zhang Q, Zhang C *et al*. *in vitro* regeneration of patient-specific ear-shaped cartilage and its first clinical application for auricular reconstruction. EBioMedicine 2018;28:287–302.
[66] Vagnozzi RJ, Maillet M, Sargent MA, Khalil H, Johansen AK, Schwanekamp JA *et al*. An acute immune response underlies the benefit of cardiac stem-cell therapy. Nature 2020;577:405–9.
[67] Laflamme MA, Chen KY, Naumova AV, Muskheli V, Fugate JA, Dupras SK *et al*. Cardiomyocytes derived from human embryonic stem cells in prosurvival factors enhance function of infarcted rat hearts. Nat Biotechnol 2007;25:1015–24.
[68] Romagnuolo R, Masoudpour H, Porta-Sanchez A, Qiang B, Barry J, Laskary A *et al*. Human embryonic stem cell-derived cardiomyocytes regenerate the infarcted pig heart but induce ventricular tachyarrhythmias. Stem Cell Reports 2019;12:967–81.
[69] Hourd P, Medcalf N, Segal J, Williams DJ. A 3D bioprinting exemplar of the consequences of the regulatory requirements on customized processes. Regen Med 2015;10:863–83.

1.3 – Omentum support for cardiac regeneration in ischaemic cardiomyopathy models: a systematic scoping review

Summary:

The following systematic scoping review aimed to capture a snapshot of the state of the literature for epicardial patch-based myocardial repair strategies. Our previous narrative review had encountered the unanswered question of whether reinforcement of patches using the greater omentum is beneficial for structural and functional cardiac outcomes in the host. Since no literature review had previously answered this question we framed our scoping review in terms of omentum support (omentopexy) for epicardial patch-based studies of ischaemic cardiomyopathy. We received a letter to the editor regarding this article which is included, along with our reply, in the Appendix. At the time of writing, Altmetric ranks this paper 7th out of 58 articles of a similar age in this journal (and 252nd out of 2759 articles in this journal since records began).

European Journal of Cardio-Thoracic Surgery 58 (2020) 1118–1129
doi:10.1093/ejcts/ezaa205 Advance Access publication 18 August 2020

REVIEW

Cite this article as: Wang H, Roche CD, Gentile C. Omentum support for cardiac regeneration in ischaemic cardiomyopathy models: a systematic scoping review. Eur J Cardiothorac Surg 2020;58:1118–29.

Omentum support for cardiac regeneration in ischaemic cardiomyopathy models: a systematic scoping review

Hogan Wang [a], Christopher D. Roche [a,b,c,d] and Carmine Gentile [a,c,*]

[a] Northern Clinical School of Medicine, University of Sydney, Kolling Institute, St Leonards, Sydney, NSW, Australia
[b] Department of Cardiothoracic Surgery, Royal North Shore Hospital, St Leonards, Sydney, NSW, Australia
[c] Department of Biomedical Engineering, Faculty of Engineering and IT, University of Technology Sydney (UTS), Ultimo, Sydney, NSW, Australia
[d] Department of Cardiothoracic Surgery, University Hospital of Wales, Cardiff, UK

* Corresponding author. Department of Biomedical Engineering, Faculty of Engineering and IT, University of Technology Sydney (UTS), Building 11, 81 Broadway, Ultimo, Sydney, NSW 2007, Australia. Tel: +61-2-95144502; e-mail: carmine.gentile@uts.edu.au (C. Gentile).

Received 2 February 2020; received in revised form 6 April 2020; accepted 9 May 2020

Key question

What are the effects of the omentum as a support for bioengineered tissue therapy for cardiac regeneration *in vivo*?

Key finding(s)

Omentum-supported bioengineering is associated with superior engraftment, vascularization and functional results *in vivo*.

Take-home message

Bioengineered cardiac tissue seems to benefit from omentum support *in vivo*. This promising tissue may boost progress in cardiac regeneration.

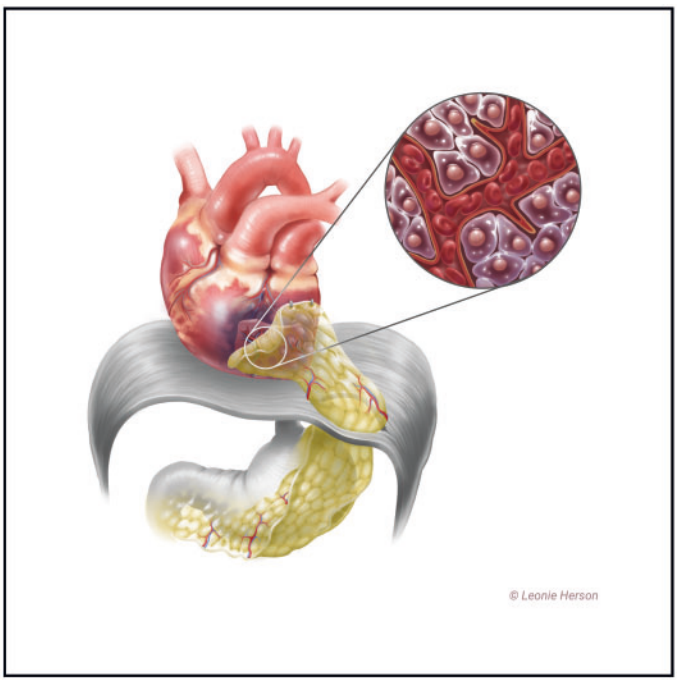

Abstract

OBJECTIVES: Preclinical *in vivo* studies using omental tissue as a biomaterial for myocardial regeneration are promising and have not previously been collated. We aimed to evaluate the effects of the omentum as a support for bioengineered tissue therapy for cardiac regeneration *in vivo*.

METHODS: A systematic scoping review was performed. Only English-language studies that used bioengineered cardio-regenerative tissue, omentum and ischaemic cardiomyopathy *in vivo* models were included.

RESULTS: We initially screened 1926 studies of which 17 were included in the final qualitative analysis. Among these, 11 were methodologically comparable and 6 were non-comparable. The use of the omentum improved the engraftment of bioengineered tissue by improving cell retention and reducing infarct size. Vascularization was also improved by the induction of angiogenesis in the transplanted tissue. Omentum-supported bioengineered grafts were associated with enhanced host reverse remodelling and improved haemodynamic measurements.

CONCLUSIONS: The omentum is a promising support for myocardial regenerative bioengineering *in vivo*. Future studies would benefit from more homogenous methodologies and reporting of outcomes to allow for direct comparison.

Keywords: Omentum • Cardiac regeneration • Omental flap • Omentopexy • *In vivo* models • Vascularization

ABBREVIATIONS

LVEF	Left ventricular ejection fraction
MI	Myocardial infarction

INTRODUCTION

Ischaemic heart disease remains the leading global cause of mortality and is rising in prevalence with population growth, ageing effects and shifting epidemiological trends [1, 2]. For end-stage heart failure patients, transplantation and mechanical circulatory assistance devices are 2 of the limited options to restore a better quality of life [3]. Donor shortage and the limited regenerative potential of myocardium have led to the recent development of numerous cell-based therapies for cardiac tissue engineering [2, 4–10].

The omentum has been used as a support for cardiac bioengineering to overcome some of the challenges in myocardial regeneration, such as poor vascularization and engraftment of bioengineered tissue [2, 11–14]. It has regenerative properties that have been exploited in surgical techniques, such as omental transposition, where the omentum is extended or wrapped around another tissue to promote healing, including the heart in cardio-omentopexy [15]. It is thought that these regenerative capabilities are linked to the presence of angiogenic factors, including vascular endothelial growth factor, basic fibroblast growth factor and an abundance of progenitor cells [16]. Its abundance of collagens, glycosaminoglycans and adhesive proteins is hypothesized to support the morphological, physiological and biochemical properties of bioengineered cardiac tissues to be more akin to native myocardium [17, 18].

Rapid preclinical progress with omental-cardiac support has not previously been collated; therefore, we conducted a systematic scoping review [19]. The primary aim was to determine what is currently known about the effectiveness of the omentum as a biomaterial in regenerative strategies for *in vivo* models of myocardial infarction (MI). The outcomes of interest that will be explored include: (i) engraftment of bioengineered cardiac tissues, (ii) tissue vascularization, (iii) reduction in pathological cardiac remodelling and (iv) functional cardiac and haemodynamic improvement. Gaps in the literature will be identified, and future research directions indicated.

MATERIALS AND METHODS

Eligibility criteria for initial database search

Any English-language study in a peer-reviewed journal reporting on the use of the omentum in bioengineered cardiac tissue was considered in the original database search. Only original scientific articles were included. Conference abstracts, letters, case reports, editorials without a full text and reviews were excluded.

Search strategy and screening process

The databases Embase, Medline, PubMed, Scopus and Web of Science were searched by 1 reviewer (H.W.) from inception until 6 August 2019. The search terms used were: (omentum OR oment*) AND (cardiac OR heart).

Identified studies were imported into bibliographic management software, Endnote X9 (Clarivate Analytics, Philadelphia, PA, USA), and duplicated studies were deleted. One reviewer (H.W.) screened the title and abstract of each citation. For each eligible citation, the full text was obtained and independently screened by 2 reviewers (H.W. and C.D.R.) for the assessment of full-text inclusion. Reference lists of included articles were also searched for additional studies not captured by the original search. Disagreements were resolved by discussion. The criteria for full-text inclusion were as follows:

- The use of the greater omentum as a biomaterial, flap or in omentopexy;
- An ischaemic cardiomyopathy model (animal and/or human tissue);
- The implantation of biomaterials, including non-cardiac cell types, onto the infarcted heart; and
- Implantation efficacy expressed in terms of morphological, biochemical or physiological integration with host tissue.

Data extraction

Extraction tables were used to standardize the collection of data from the included studies (Tables 1–6). One reviewer (H.W.) extracted the data initially, and the second reviewer verified the data (C.D.R.).

RESULTS

Study selection and characteristics of studies

The process of study selection into the review is represented in Fig. 1, a PRISMA flowchart [37]. A total of 17 studies met the inclusion criteria. The 11 comparable studies using a pedicled omental flap technique underwent comparable data extraction (Tables 1–4). Those using non-comparable methodologies [31–33] or control groups [34–36] were separated out and are displayed in Tables 5 and 6, respectively.

Of the 17 selected studies, 6 used a rat MI model [23, 25, 29, 30, 33, 35], 7 used a porcine MI model [20–22, 24, 28, 32, 34], 3 used a rabbit MI model [26, 27, 36] and 1 used a sheep MI model [31].

Table 1: Studies which used a pedicled omental flap as support for bioengineered tissue to regenerate the myocardium

First author	Year	*In vivo* model	Coronary artery for MI	Intervention interval after MI	*N* per group[a]	Bioengineered cardiac tissue	Mode of tissue delivery
Kainuma *et al.* [20]	2015	Pig	LCA	2 weeks	11	Skeletal myoblast cell sheet	Transplantation onto MI/peri-infarct area
Kanamori *et al.* [21]	2006	Minipig	OM1 + 2 Distal D1	1 h	5	Autologous bone marrow-derived mononuclear cells	Injection into MI/peri-infarct area
Kawamura *et al.* [22]	2017	Pig	LAD	1 month	7	Human iPSC cardiomyocyte cell sheets	Transplantation onto MI area
Lilyanna *et al.* [23]	2013	Rat	LAD	2 weeks	11	Fibrin graft containing cord-lining mesenchymal stem cells	Transplantation onto MI area. Attached using fibrin glue
Shudo *et al.* [24]	2011	Minipig	LAD	4 weeks	6	Cell sheets consisting of skeletal myoblast cells	Transplantation onto MI/peri-infarct area
Suzuki *et al.* [25]	2009	Rat	LAD	At initial procedure	10	Myocardial cell sheets	Transplantation onto MI area
Takaba *et al.* [26]	2006	Rabbit	Cx	4 weeks	8	Gelatine hydrogel sheet with bFGF applied	Transplantation onto MI area
Ueyama *et al.* [27]	2004	Rabbit	Cx	At initial procedure	10	Gelatine hydrogel sheet with bFGF applied	Transplantation onto MI area
Yajima *et al.* [28]	2018	Pig	LAD	4 weeks	6	Gelatine compressed sponge immersed in ONO-13301ST (slow-releasing synthetic prostacyclin agonist)	Transplantation onto MI area
Zhang *et al.* [29]	2011	Rat	LCA	3 weeks	17	Autologous tissue patch from left atrial appendage	Transplantation onto MI area
Zhou *et al.* [30]	2010	Rat	LCA	8 weeks	16	Cell patch of polylactic acid-co-glycolic acid polymer seeded with mesenchymal stem cells	Transplantation onto MI area

[a]Defined as the treatment group in which both the bioengineered cardiac tissue and greater omentum were applied.
bFGF: basic fibroblast growth factor; Cx: circumflex coronary artery; D1: first diagonal artery; iPSC: induced pluripotent stem cell; LAD: left anterior descending coronary artery; LCA: left coronary artery; MI: myocardial infarction; OM1 + 2: obtuse marginal coronary artery 1 and 2.

Bioengineering cardiac tissue involved a variety of approaches, including the use of skeletal myoblast cells [20, 24, 25, 31, 34], cells derived from the omentum itself [31, 32], scaffolds for factor delivery [26–28, 33], atrial tissue [29], hepatic tissue [35], uterine tissue [36] and stem cells [21–23, 30].

Fourteen studies transplanted the bioengineered tissue onto the MI and/or peri-infarct area whereas the remaining 3 [21, 31, 32] reported the injection of cells into the same areas.

Effects of omentum support on bioengineered tissue engraftment

Measures of engraftment were reported in 9 methodologically comparable studies (those using a pedicled omental flap to support bioengineered tissue) using various metrics at various time points (Table 2). They were tested between the time period of 7 days to 3 months across these studies, with most reporting effects in 4 weeks or less after treatment.

Transplanted cell retention. In 6 methodologically comparable studies, cell survival was evaluated following transplantation (Table 2) [22, 23, 25, 29, 30, 34]. Only one study [23] found that the omentum had no effects in promoting cell survival. All remaining studies reported greater cell survival and/or decreased apoptosis for omentum-supported treatment compared to bioengineered tissue applied without supportive omentopexy (Table 2).

Cell markers. From all of the 17 selected studies, the most common report of a structural integration marker was the presence of connexin-43, a gap junction protein, critical for propagation of the depolarization impulse between transplanted cells and host myocardium [30, 32, 33, 36]. In 2 of these studies, a higher expression of connexin-43 was observed in omentum-supported groups compared to treatment without omentum [30, 32]. Only one paper reported on the presence of troponin-T and actinin staining to corroborate microscopic observations of distinctive bundled cardiac muscle structures in transplanted tissue [33]. However, this was not compared to their frequency in control groups.

Structural integration. Two of 17 studies described fibre organization of the bioengineered tissue [22, 33]. Omentum-supported neonatal cardiac cells in an alginate scaffold and cardiomyocyte cell sheets transplanted onto ischaemic myocardium both exhibited desirable attributes, such as striation and elongation [22, 33]. Kawamura *et al.* [22] reported that the omentum contributed to the further maturation of induced pluripotent stem cell-derived cardiomyocytes, characterized by larger cells with well-aligned and organized sarcomere structures with positive staining for myosin heavy chain and myosin light chain-2 in the transplanted area at 2 months after omentum-supported treatment.

Infarct size. In the 4 methodologically comparable studies examining changes in infarct size, 2 reported a decrease after

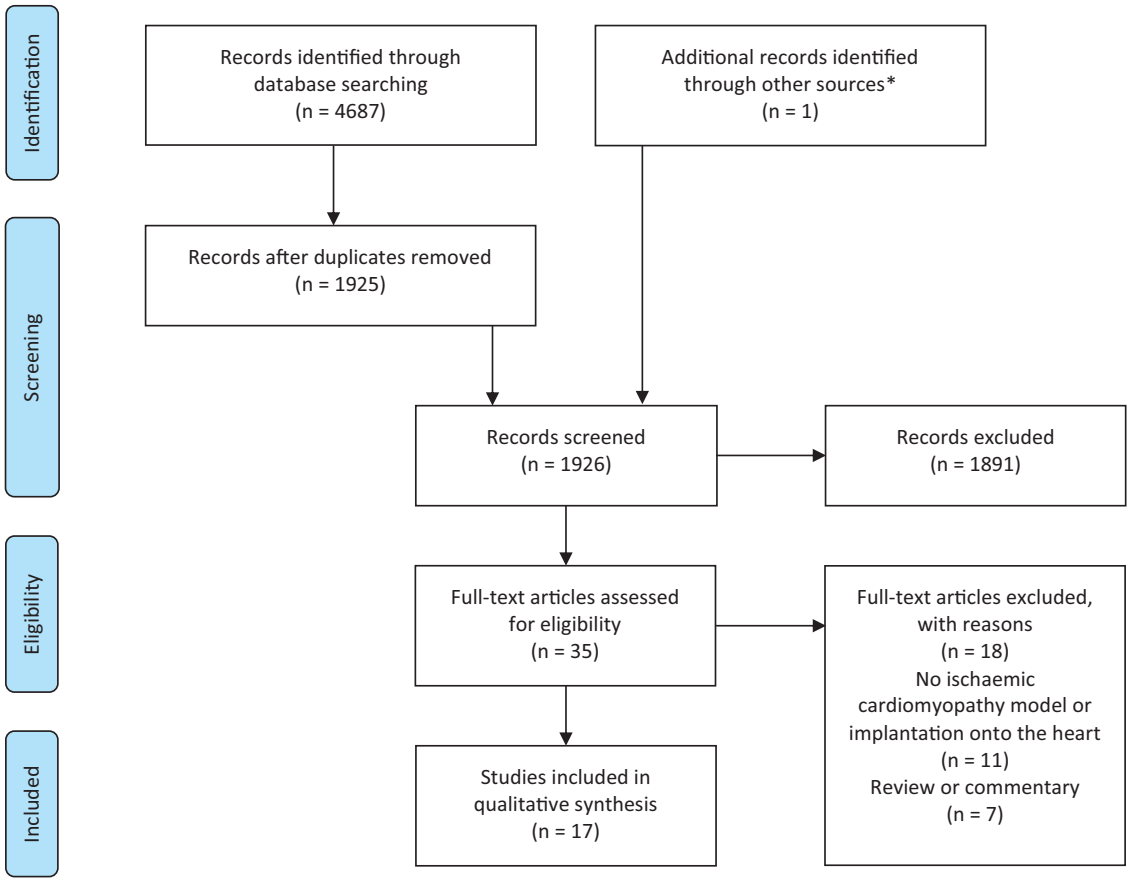

Figure 1: PRISMA flowchart of pathway for papers in the review. *Ueyama *et al.* [27] identified through reference list of an article accepted for full-text assessment.

omentum-supported treatment compared to the control group not using the omentum [24, 27] and 2 reported no difference [23, 29]. Omentum support was shown to increase myocardial wall thickness in 2 methodologically comparable studies [20, 26] and one that did not use a pedicled omental flap [33], although 2 studies showed no significant difference with omental flap support [27, 29]. All studies that examined percentage collagen in the myocardium demonstrated collagen attenuation, leading to decreased cardiac fibrosis, in omentum-supported treatment [20, 30, 35].

Overall results showed that omentum support had a favourable effect on the engraftment of cells for bioengineering strategies to regenerate the heart after MI.

Effects of omentum support on vascularization

Blood vessel formation. Direct blood vessel communication between the bioengineered tissue and omentum was observed in 4 methodologically comparable studies as contributing to a network of vessels that would anastomose with the host myocardium (Table 3 and Fig. 2) [20, 21, 26, 27]. Whilst most comparable studies demonstrated that support with a pedicled omental flap led to greater vessel density in the transplantation area, there were variable reports of whether arteriolar or capillary density was increased (Table 3).

Of all 17 selected studies, 7 reported that arteriolar density was improved [21, 23, 25–28, 35], whilst 5 reported that capillary density had improved [22, 25, 30, 31, 35] and 2 did not specify vessel diameter [20, 33]. No negative relationship between blood vessel density and use of omentum support was reported in any study.

Angiogenic markers. Of all 17 selected studies, many corroborated the observation of increased vascularization with the up-regulated expression of genes related to angiogenesis [20, 22, 24, 25, 28–30, 33, 35]. The most commonly reported up-regulated gene in omentum-supported tissue was vascular endothelial growth factor [20, 22, 24, 25, 30, 35]. There were also reports of increased basic fibroblast growth factor [22, 35] and smooth muscle actin [28, 33].

Blood flow. Taken together, these results suggested that omentum support conveyed a proangiogenic effect. However, despite the potential for this to lead to increased myocardial blood flow or coronary flow reserve, only 2 studies in total reported that treatment supported by the omentum was superior to that of other treatment groups for blood flow [20, 26]. Two studies reported that omentum support made no significant difference to observed blood flow [21, 28].

Effects of omentum-supported bioengineered tissue on cardiac remodelling and function

Remodelling. Eight studies reported that bioengineered tissue supported with a pedicled omental flap decreased cardiac remodelling (Table 4). Seven studies reported a decrease in left

Table 2: Measures of engraftment outcomes of bioengineered cardiac tissue with omentum

First author	Cell retention		Fibre organization and contacts formed		Infarct size, scar and wall changes	
	Omentum-supported bioengineered tissue	Comparison group: bioengineered tissue no omentum support	Omentum-supported bioengineered tissue	Comparison group: bioengineered tissue no omentum support	Omentum-supported bioengineered tissue	Comparison group: bioengineered tissue no omentum support
Kainuma *et al.* [20]	Engrafted area remaining with time Day 7 = 0.3 mm^2 Day 28 = 0.15 mm^2	Day 7 = 0.07 mm^2 Day 28 = 0.05 mm^2			Collagen content 8% LV wall thickness 912 μm Myocyte size 16 μm	13% 688 μm 20 μm
Key findings	∼3–4× increased area of grafted cells remained *in situ* with omentum support[a]				Scar collagen attenuation, less thick LV wall, reduced hypertrophy with omentum support	
Kawamura *et al.* [22]	Cell % survival rate 1 month = 90% 3 months = 58%	 1 month = 61% 3 months = 24%	Myosin heavy chain/myosin light chain-2 positive (striated filaments) Present	 Not reported		
Key findings	Improved grafted cell survival with omentum support[a]		Well-organized sarcomere structure in cells with omentum support (not compared to control)			
Lilyanna *et al.* [23]	Bioluminescence photon emission flux of labelled live donor cells (photons/s) Day 1 = 6.5×10^7 Day 14 = 1.5×10^5	 Day 1 = 7.6×10^7 Day 14 = 6.8×10^5			Scar size (LV cross sectional area % containing fibrosis) 34.7%	 35.7%
Key findings	Donor cell attrition rate *in vivo* over time comparable with or without omentum support				Minimal difference in scar with or without omentum support	
Shudo *et al.* [24]					Infarct area ∼6%	 ∼11%
Key findings					Infarct size (infarcted LV/total LV estimated by computer-based planimetry of Masson trichrome-staining) reduced with omentum support[a]	
Suzuki *et al.* [25]	Cardiomyocyte survival 46% Cell sheet thickness 120 μm	 31% 70 μm				
Key findings	Improved graft survival with omentum support					
Takaba *et al.* [26]					Dynamic % wall thickening of infarct region 49%	 41%
Key findings					% fractional wall thickening (assessed by cine MRI for quantitative wall motion) increased with omentum support	
Ueyama *et al.* [27]					Infarct size 10% LV circumference 48 mm Scar circumference 16 mm Infarct area wall thickness 2.5 mm (ns)	 16% 56 mm 24 mm 2.0 mm (ns)
Key findings					Reduced infarct size, dilatation and scar. No significant difference in wall thickness	
Zhang *et al.* [29]	Atrial tissue patch graft presence after 4 weeks *In situ*	 Not seen			Scar thickness ∼0.4 mm (ns) Infarct size ∼38% (ns)	 ∼0.35 mm (ns) ∼39% (ns)

Continued

Table 2: Continued

First author	Cell retention		Fibre organization and contacts formed		Infarct size, scar and wall changes	
	Omentum-supported bioengineered tissue	Comparison group: bioengineered tissue no omentum support	Omentum-supported bioengineered tissue	Comparison group: bioengineered tissue no omentum support	Omentum-supported bioengineered tissue	Comparison group: bioengineered tissue no omentum support
Key findings	Troponin-stained graft survived with omentum support but did not without omentum support				No significant difference in scar thickness or infarct size with or without omentum support[a]	
Zhou *et al.* [30]	Quantification PCR of grafted cells[b] Week 1 = 14.1 units Week 4 = 2.6 units	Week 1 = 3.8 units Week 4 = 1.2 units	Connective protein Cx-43 expression[c] 0.23 units	0.19 units	Collagen (scar) density 16%	26%
Key findings	Cell survival rate *in vivo* over time improved with omentum support		Higher levels of Cx-43 suggested enhanced structural coupling of transplanted cells to host myocardium. Sham group (baseline) level = 0.31; MI with no treatment group level = 0.11		Reduced % fibrillar collagen in the infarction zone (semiquantitatively measured by picrosirius red staining under polarized light microscopy)	

[a]Numerical data extrapolated from graphical figure.
[b]Units expressed as ratio of optical density under UV light compared to reference sample at the same time.
[c]Cx-43 protein expression determined by western blot. Units expressed as ratio to the level of β-actin which was run on all blots.
Cx-43: connexin-43; LV: left ventricle; MI: myocardial infarction; MRI: magnetic resonance imaging; ns: result not statistically significant; PCR: polymerase chain reaction; UV: ultra-violet.

ventricular end-diastolic diameter in the range of 2–25%, and 5 studies reported a decrease in left ventricular end-systolic diameter in the range of 10–27% (Table 4). For reverse remodelling, the study that reported the most beneficial effect did not involve a pedicled omental flap, but rather pre-vascularization of a cardiac patch on the omentum, supplemented with angiogenic factors, before transplanting the patch without omentopexy onto the heart [33]. Nevertheless, combining bioengineered tissue with an omental flap favoured reverse remodelling, especially at 4 weeks or later after intervention (Table 4).

Function. The most common measure of functional improvement reported was the left ventricular ejection fraction (LVEF). Omentum-supported bioengineered tissue improved the LVEF by up to 82% as a relative increase on absolute values compared to controls receiving bioengineered tissue alone (Table 4). Conversely, omentopexy alone without a bioengineered tissue was not enough to significantly improve LVEF [25, 29]. Results for fractional shortening and fractional area change were reported with less frequency than LVEF with only 3 studies reporting a significant increase in fractional shortening [26, 29, 30] and 1 study reporting an increase in fractional area change [27] with omentum support (Table 4).

DISCUSSION

This is the first review that systematically evaluates the effects of omentum support for bioengineering of cardiac tissues in MI models *in vivo*. Although all the included studies demonstrated that the omentum conferred a benefit in at least one of the outcomes assessed (engraftment, vascularization, remodelling, function), only a few studies reported on all outcomes. Furthermore, a few did not contain optimal control groups. This makes it difficult to draw conclusions of how effective the omentum is compared to controls or other bioengineering strategies. Our results highlight the variability of methodologies and results between studies (such as the treatment modality combined with the omentum, the model of MI and the outcome measures). This limits the extent to which the benefit of the omentum can be compared across studies.

The synergistic proangiogenic potential of omentum-supported bioengineered tissue was instrumental in most studies to promoting greater vascularization than bioengineered treatment or omentopexy alone. The development of a microvasculature between the coronary and gastroepiploic circulation was reported (Fig. 2) [20, 21, 26, 28]. The up-regulation of several angiogenic genes and proteins (e.g. vascular endothelial growth factor and smooth muscle actin) suggested that angiogenesis and vessel maturation are supported by the omentum (Table 3). However, most studies demonstrated that enhanced vascularization of the bioengineered tissue did not ultimately correlate with increased myocardial blood flow [20, 21, 28, 34]. Therefore, additional studies are needed to make progress from these results before they can be translated into clinical trials.

As shown in Table 4, bioengineered tissues with omentum support reported positive effects on cardiac function at 4 weeks in 6 studies. Suzuki *et al.* [25] reported an improvement at 1 week, and Kawamura *et al.* [22] reported an improvement at 3 months. All studies reporting a significant positive effect on function (Table 4) also reported enhanced vascularization (Table 3). Five studies reported both improved engraftment and cardiac function (Tables 2 and 4). Altogether, this suggests that both vascularization and engraftment are required for a cardiac functional improvement. Furthermore, 2 studies [25, 29] showed that the omentum by itself did not significantly improve cardiac function. Despite promising functional results, future studies would benefit from observations of long-term outcomes as some measurements, such as LVEF, have limited prognostic power in predicting clinical benefit across long time horizons.

Table 3: Measures of vascularization outcomes of bioengineered cardiac tissue with omentum

First author	Blood vessel character		Blood vessel dynamics		Up-regulated vascular markers in omentum-supported tissue
	Omentum-supported bioengineered tissue	Comparison group: bioengineered tissue no omentum support or omentopexy alone	Omentum-supported bioengineered tissue	Comparison group: bioengineered tissue no omentum support or omentopexy alone	
Kainuma *et al.* [20]	*Total* CD31+ endothelial cells (mature and immature vessels) ~425 cells/mm^2	~275 cells/mm^2	1st branching order vessel diameter ~225 μm	~170 μm	VEGF (endothelial cells) PDGF-β (pericytes) Ang-1 (endothelial cells) Tie-2 (angioblasts) VE-cadherin (adult endothelial cells) PECAM (CD31) (endothelial cells)
	Functionally mature vessels (CD31+/Lecithin+) ~375 cells/mm^2	~225 cells/mm^2	2nd–4th branch vessel diameter No difference	No difference	
	Structurally mature vessels (CD31+/SMA+) ~120 cells/mm^2	~30 cells/mm^2	Resistance vessels (3rd–4th order) ~2–3× more vessels	~2–3× fewer vessels	
	% Maturation (structurally mature vessels/total) ~31%	~12%	Acetylcholine challenge (resistance vessel diameter dilation) 28% (3rd order vessels) 32% (4th order vessels)	18% (3rd order vessels) 21% (4th order vessels)	
	Gastroepiploic-coronary anastomoses Present	(Absent)[b]	Dobutamine challenge (resistance vessel diameter constriction) 31% (3rd order vessels) 34% (4th order vessels)	9% (3rd order vessels) 29% (4th order vessels)	
	Gastroepiploic-coronary anastomotic tight junctions Present	(Absent)[b]	Global CFR change (ratio pre:post-treatment) 1.3	0.9	
	Gastroepiploic-coronary anastomotic ink leakage Minimal	(Widespread)[b]	MBF (resting or stressed) No difference	No difference	
Key findings	1. Increase in total vascularity and mature vascularity peri-infarct at 28 days with omentum support[a] 2. Anastomoses formed between omental and coronary circulation only if bioengineered tissue omentum-supported		1. Greater number and responsiveness of resistance vessels (3rd–4th order in descending hierarchy of calibre) 2. Increase in global CFR change and no change in MBF pre- to post-treatment with omentum support[a]		Up-regulation of multiple vascular molecular markers suggesting increased vascular cellularity with omentum support
Kanamori *et al.* [21]	Arteriole (>50 μm) density 27/mm^2	18/mm^2	Regional MBF (infarct or non-infarct wall, resting or stressed) No difference	No difference	
	Capillaries (<50 μm) density 109/mm^2 (ns)	88/mm^2 (ns)	Regional MBF ratio infarct: non-infarct wall (resting or stressed) No difference	No difference	
	Gastroepiploic-coronary anastomoses via omentum-supported tissue Present	No comparison data			
Key findings	1. Arteriole density increased but no significant difference for capillaries (<50 μm) 2. Anastomoses formed between omental and coronary circulation via omentum-supported bioengineered tissue		No difference in regional MBF (assessed by spectrophotometry of coloured microsphere cardiac injection with femoral arterial blood reference sampling) with omentum support compared to bioengineered tissue without omentum support		
Kawamura *et al.* [22]	Capillary density 111 units/mm^2	51 units/mm^2			VEGF (endothelial cells) bFGF (fibroblasts/angiogenesis)
Key findings	Increased capillary density at the transplanted area (assessed by semiquantitative immunohistochemistry for vWF) with omentum support				Up-regulation of markers suggesting increased endothelial cells and angiogenesis with omentum support
Lilyanna *et al.* [23]	Functional blood vessels as % of LV scar area 18%	8%			
	Structural blood vessels 6/hpf (400×)	3/hpf (400×)			
Key findings	Increased vascularity with functional staining (infused DiI+ vessels[c]) and structural staining (Masson's trichrome) with omentum support				
Shudo *et al.* [24]	Capillary density 170/mm^2	125/mm^2			VEGF (endothelial cells) vWF (endothelial cells)
Key findings	Increased capillaries (anti-vWF antibody immunolabelled capillaries) with omentum support				Up-regulation of markers suggesting increased endothelial cells

Continued

Table 3: Continued

First author	Blood vessel character		Blood vessel dynamics		Up-regulated vascular markers in omentum-supported tissue
	Omentum-supported bioengineered tissue	Comparison group: bio-engineered tissue no omentum support or omentopexy alone	Omentum-supported bioengineered tissue	Comparison group: bio-engineered tissue no omentum support or omentopexy alone	
Suzuki *et al.* [25]	Small vessels				VEGF (endothelial cells)
	70/hpf	20/hpf			vWF (endothelial cells)
Key findings	Increased small vessels observed (anti-vWF antibody immunolabelled vessels) with omentum support[a]				Up-regulation of markers suggesting increased endothelial cells
Takaba *et al.* [26]	Arteriole (>50 μm) density		Regional MBF		
	31 vessels/mm^2	26 vessels/mm^2	2.8 ml/min/g	2.3 ml/min/g	
	Gastroepiploic-coronary anastomoses via omentum-supported tissue		Regional MBF drop on clamping gastroepiploic artery pedicle		
	Present	No comparison data	2.8–1.9 ml/min/g	No comparison data	
Key findings	1. Increased arterioles (anti-SMA antibody immunolabelled arterioles) with omentum support 2. Anastomoses formed between omental and coronary circulation via omentum-supported bioengineered tissue		1. Infarct regional MBF increased with omentum support 2. Clamping gastroepiploic pedicle for omentum-supported bioengineered tissue caused 32% drop in host infarct regional MBF		
Ueyama *et al.* [27]	Arteriole (20–100 μm) density		Subjects with LV collateral vessels on angiography via gastroepiploic artery pedicle		
	23/mm^2	14/mm^2	7/7	(2/7)[b]	
			Collateral vessel description		
			Rich	(Poor)[b]	
			Patent collateral vessel proportion (angiographic score)		
			0.8	(0.1)[b]	
Key findings	Increased arterioles (anti-SMA antibody immunolabelled arterioles) with omentum support		Dye injection into gastroepiploic pedicle at immediate post-mortem angiography showed favourable collateral vessel patency for omentum-supported bioengineered tissue compared to omentopexy alone		Up-regulation of markers suggesting increased endothelial cells
Yajima *et al.* [28]	Arteriole (CD31+/SMA+) density		Global MBF		CD31 (endothelial cells)
	31/mm^2	20/mm^2	∼1.3 (ns)	∼1.0 (ns)	SMA (smooth muscle cells)
	Capillary (CD31+) density		Territorial and regional MBF		VEGF (endothelial cells) (ns)
	∼98/mm^2 (ns)	∼90/mm^2 (ns)	No difference	No difference	bFGF (fibroblasts/ angiogenesis) (ns)
	Vessels >100 μm diameter		CFR proportional change on occlusion of Cx artery with gastroepiploic pedicle not occluded		
	∼1.5/mm^2 (ns)	∼1.2/mm^2 (ns)	∼1.0	(∼0.7)[b]	
Key findings	Increased arteriole (CD31+ and SMA+ vessels) density and no difference for capillaries (CD31+ vessels) or >100 μm diameter vessels in peri-infarct area with omentum support[a]		1. No significant difference in MBF with omentum support 2. On clamping the Cx coronary artery for subject animals with LAD infarcts there was no change in CFR with omentum-supported bioengineered tissue compared to a 30% drop in CFR with omentopexy alone without bioengineered tissue		Up-regulation of markers suggesting increased endothelial cells
Zhang *et al.* [29]	Capillary (VEGF+) density				VEGF (endothelial cells) (ns)
	∼48/0.2 mm^2 (ns)	∼28/0.2 mm^2 (ns)			
Key findings	No difference in capillary (VEGF+ vessels) density with omentum support versus bioengineered tissue alone[a]				No difference in up-regulation of VEGF
Zhou *et al.* [30]	Microvessel (vWF+) density				VEGF (endothelial cells)
	226/mm^2	109/mm^2			
Key findings	Increased vessel (anti-vWF antibody immunolabelled microvessels) density with omentum support				Up-regulation of VEGF suggesting increased endothelial cells

[a]Numerical data extrapolated from graphical figure.

[b]Comparison to bioengineered tissue without omentum support is not applicable for this assay as no connection to gastroepiploic circulation is possible in this group. Therefore control group result is for omentopexy alone (no bioengineered tissue).

[c]DiI is $DiIC_{18}$ (1,1′-dioctadecyl-3,3,3′,3′-tetramethylindocarbocyanine perchlorate) fluorescent dye.

Ang-1: angiopoietin 1; bFGF: basic fibroblast growth factor; CFR: coronary flow reserve; Cx: circumflex coronary artery; LV: left ventricle; MBF: myocardial blood flow; ns: result not statistically significant; PDGF-β: platelet-derived growth factor-β; PECAM: platelet endothelial cell adhesion molecule; SMA: smooth muscle actin; VEGF: vascular endothelial growth factor; vWF: von Willebrand factor.

Table 4: Cardiac functional outcomes of bioengineered tissue with omentum support compared to bioengineered tissue without omentum support[a]

First author	LVEDD % decrease	LVESD % decrease	LVEF % increase	FS % increase	FAC % increase	Measurement interval after treatment
Kainuma *et al.* [20]	10% (ns)[b]	13% (ns)[b]	12% (ns)[b]			2 weeks
	16%[b]	16%[b]	24%[b]			4 weeks
Kawamura *et al.* [22]			5% (ns)			1 month
			8% (ns)			2 months
	25%	26%	16%			3 months
Lilyanna *et al.* [23]			15% (ns)	15% (ns)	6% (ns)	4 weeks
Shudo *et al.* [24]	24% (ns)[b]	36%[b]	26%[b]			4 weeks
	25% (ns)[b]	27%[b]	22%[b]			8 weeks
Suzuki *et al.* [25]	0% (ns)[b]		3%[b]			1 week
	10% (ns)[b]		8%[b]			4 weeks
	12%[b]		18%[b]			8 weeks
Takaba *et al.* [26]	-3% (ns)[b]		82%	5% (ns)[b]		4 weeks
	2%			36%		8 weeks
Ueyama *et al.* [27]	26%[b]				26%[b]	2 weeks
	21%				41%	4 weeks
Yajima *et al.* [28]	5% (ns)	14% (ns)	34% (ns)			4 weeks
Zhang *et al.* [29]	8%	10%	10%	6.3%		4 weeks
Zhou *et al.* [30]	13%	12%	13%	11%		4 weeks

[a]Data expressed as % decrease or % increase (whichever is the desirable outcome) between the absolute values for the omentum-supported and non-omentum-supported groups.
[b]Numerical data extrapolated from graphical figure.
FAC: fractional area change; FS: fractional shortening; LVEDD: left ventricular end-diastolic diameter; LVEF: left ventricular ejection fraction; LVESD: left ventricular end-systolic diameter; ns: result not stastically significant.

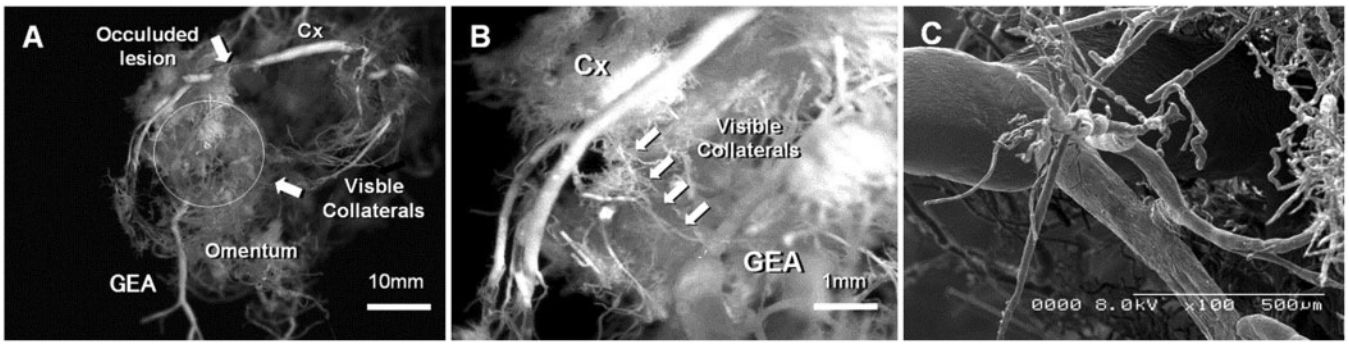

Figure 2: Collateral blood vessel formation between the Cx and the GEA in omentum-supported bioengineered tissue applied to the heart in a rabbit model of Cx infarction. (**A**) The whole specimen (scale bar = 10 mm). (**B**) Collateral formation between occluded Cx and GEA (scale bar = 1 mm). (**C**) Scanning electron micrograph of collaterals between occluded Cx and GEA. Reproduced with permission from [36]. Cx: circumflex coronary artery; GEA: gastroepiploic artery.

Limitations

Limitations of this review include those inherent to the scoping review methodology, namely that other relevant studies may not have been included. Aside from those not in English, there remain innovative *in vitro* studies utilizing the omentum for bioengineered cardiac tissue that fell outside the scope of this review because they were not tested *in vivo*. Most studies captured by our scoping review used a pedicled omental flap, which is feasible in human surgery. This is perhaps why it featured so prominently and may lend itself to a smooth translation from the laboratory into clinical practice. However, only 17 publications out of 1926 were admissible for the lack of translation of *in vitro* work into *in vivo* experiments, which highlights a gap between scientists and clinicians. This should be addressed in all future studies to facilitate translating preclinical *in vivo* studies to human trials.

The tendency towards positive results from the studies found in this review may also present a publication bias. No studies in this review reported a detrimental effect and only a few reported no overall difference as a result of omentum support. This was despite the cardiac and diaphragmatic impairment that an omentopexy might cause in animal models. The results may also present attrition bias whereby animals that died as the result of the initial grafting procedure were not analysed. Furthermore, preclinical studies that pioneer new techniques are susceptible to scientific design weaknesses such as operator skill variability, tweaking of methods during experiments, non-randomization of animal subjects, small sample sizes and non-blinding of researchers [38]. Future *in vivo* experiments should explicitly address all of these points, adhering to an established experimental planning guideline, uploading protocols to un-editable repositories before work begins and including more systematic reporting on cardiac and respiratory functional outcomes beyond the LVEF.

Table 5: Studies that did not use an omental pedicled flap method

First author	Year	MI model *in vivo*	Coronary artery for MI	Intervention interval after MI	Subjects (*n*)/group	Bioengineered cardiac tissue	Method utilizing omentum	Mode of tissue delivery
Bourahla *et al.* [31]	2010	Sheep	LAD (distal) D2	3 weeks	10	Omental cells or skeletal myoblast cells	Isolation and expansion of autologous omental mesothelial cells	Injection into MI area
De Siena *et al.* [32]	2010	Pig	LAD	45 min	13	Human fat omentum-derived stromal cells	Isolation and expansion of human fat omentum-derived stromal cells	Injection into proximal MI border zone
Dvir *et al.* [33]	2009	Rat	LAD	1 week	11	Alginate-based cardiac patch containing neonatal cardiac cells and pro-survival and angiogenic factors (stromal cell-derived factor-1, IGF-1, VEGF)	Cardiac patch was vascularized on the omentum	Transplantation onto MI area

D2: second diagonal coronary artery; IGF-1: insulin-like growth factor 1; LAD: left anterior descending coronary artery; MI: myocardial infarction; VEGF: vascular endothelial growth factor.

Table 6: Studies that did not use a control group allowing for the comparison of bioengineered tissue with or without omentum support

Author	Year	MI model *in vivo*	Coronary artery for MI	Intervention interval after MI	Subjects (*n*)/group	Bioengineered cardiac tissue	Method utilizing omentum	Mode of tissue delivery
Kainuma *et al.* [34]	2018	Minipig	LAD (distal)	4 weeks	2	Skeletal myoblast cell sheet	Pedicled omentum flap	Transplantation onto MI area using transphrenic peritoneoscopy-assisted omentopexy
Shao *et al.* [35]	2008	Rat	LAD	30 min	11	Hepatic tissue resected from the left lobe of the liver	Pedicled omentum flap	Transplantation onto MI area
Taheri *et al.* [36]	2008	Rabbit	LAD	At initial procedure	6	Autologous graft using uterine segment	'Reinforcement' of myometrial patches	Transplantation onto MI area

LAD: left anterior descending coronary artery; MI: myocardial infarction.

The omentum has also been used in non-cardiac tissues for the promotion of regeneration and superior bioengineering techniques. In particular, the pedicled omental flap has been used *in vivo* for spinal wound repair [39] and synthetic patch reconstruction of the anterior abdominal wall [40]. Hepatocytes on biodegradable scaffolds [41] and tracheal [42] tissue have also been shown to grow successfully on the omentum. The common mechanism behind the regenerative potential of the omentum is likely due to its numerous paracrine factors and immunological mediators promoting the optimal stem cell niche [43]. A deeper understanding of the mechanisms regulating non-cardiac tissue regeneration may lead to future innovative approaches in cardiac bioengineering.

CONCLUSION

The omentum is a promising tissue for cardiac bioengineering. It has demonstrated its ability to enhance transplanted cell engraftment, vascularization and host cardiac function. The mechanisms that confer functional cardiac benefit are not fully understood and require further experimental consideration. Future studies that examine these mechanisms and outcomes would benefit from a more homogenous approach to methodology that promotes a more detailed understanding of mechanistic processes and outcomes, which is important for clinical translation.

ACKNOWLEDGEMENTS

The authors thank Yulia Ulyannikova, Academic Liaison Librarian, University of Sydney for her guidance on the design of the literature search. They also thank Leonie Herson for her work in the design and generation of the central image.

Funding

C.D.R. was supported by a Sir John Loewenthal Scholarship 2019 (University of Sydney), the Le Gros Legacy Fund New Zealand

[PhD012019] and a Heart Research Australia Scholarship [PhD2019-02]. C.G. was supported by a University of Sydney Kick-Start Grant, University of Sydney Chancellor's Doctoral Incentive Programme Grant, a Sydney Medical School Foundation Cardiothoracic Surgery Research Grant, UTS Seed Funding and the Catholic Archdiocese of Sydney Grant for Adult Stem Cell Research (2019).

Conflict of interest: none declared.

Author contributions

Hogan Wang: Conceptualization; Data curation; Formal analysis; Investigation; Methodology; Resources; Software; Validation; Visualization; Writing—original draft; Writing—review & editing. **Christopher D. Roche:** Conceptualization; Data curation; Formal analysis; Funding acquisition; Investigation; Methodology; Project administration; Supervision; Validation; Writing—review & editing. **Carmine Gentile:** Conceptualization; Data curation; Funding acquisition; Methodology; Project administration; Supervision; Writing—review & editing.

Reviewer information

European Journal of Cardio-Thoracic Surgery thanks Claudia Heilmann, Luiz Felipe P. Moreira and Peter Zilla for their contribution to the peer review process of this article.

REFERENCES

[1] Naghavi M, Abajobir AA, Abbafati C, Abbas KM, Abd-Allah F, Abera SF *et al*. Global, regional, and national age-sex specific mortality for 264 causes of death, 1980–2016: a systematic analysis for the Global Burden of Disease Study 2016. Lancet 2017;390:1151–210.

[2] Roche CD, Brereton RJL, Ashton AW, Jackson C, Gentile C. Current challenges in three-dimensional bioprinting heart tissues for cardiac surgery. Eur J Cardiothorac Surg 2020;doi:10.1093/ejcts/ezaa093.

[3] Boilson BA, Raichlin E, Park SJ, Kushwaha SS. Device therapy and cardiac transplantation for end-stage heart failure. Curr Probl Cardiol 2010;35:8–64.

[4] Reis LA, Chiu LLY, Feric N, Fu L, Radisic M. Biomaterials in myocardial tissue engineering. J Tissue Eng Regen Med 2016;10:11–28.

[5] Duan B. State-of-the-art review of 3D bioprinting for cardiovascular tissue engineering. Ann Biomed Eng 2017;45:195–209.

[6] Sui R, Liao X, Zhou X, Tan Q. The current status of engineering myocardial tissue. Stem Cell Rev Rep 2011;7:172–80.

[7] Chachques JC, Lila N, Soler-Botija C, Martinez-Ramos C, Valles A, Autret G *et al*. Elastomeric cardiopatch scaffold for myocardial repair and ventricular support. Eur J Cardiothorac Surg 2020;57:545–55.

[8] Chachques JC, Trainini JC, Lago N, Cortes-Morichetti M, Schussler O, Carpentier A. Myocardial assistance by grafting a new bioartificial upgraded myocardium (MAGNUM trial): clinical feasibility study. Ann Thorac Surg 2008;85:901–8.

[9] Menasché P, Vanneaux V, Hagège A, Bel A, Cholley B, Parouchev A *et al*. Transplantation of human embryonic stem cell–derived cardiovascular progenitors for severe ischemic left ventricular dysfunction. J Am Coll Cardiol 2018;71:429–38.

[10] Menasché P, Vanneaux V, Hagège A, Bel A, Cholley B, Cacciapuoti I *et al*. Human embryonic stem cell-derived cardiac progenitors for severe heart failure treatment: first clinical case report. Eur Heart J 2015;36:2011–7.

[11] Tee R, Lokmic Z, Morrison WA, Dilley RJ. Strategies in cardiac tissue engineering. ANZ J Surg 2010;80:683–93.

[12] Noor N, Shapira A, Edri R, Gal I, Wertheim L, Dvir T. 3D printing of personalized thick and perfusable cardiac patches and hearts. Adv Sci 2019;6:1900344.

[13] Chachques JC, Pradas MM, Bayes-Genis A, Semino C. Creating the bioartificial myocardium for cardiac repair: challenges and clinical targets. Expert Rev Cardiovasc Ther 2013;11:1701–11.

[14] Vunjak-Novakovic G, Tandon N, Godier A, Maidhof R, Marsano A, Martens TP *et al*. Challenges in cardiac tissue engineering. Tissue Eng Part B Rev 2010;16:169–87.

[15] O'Shaughnessy L. Surgical treatment of cardiac ischaemia. Lancet 1937;229:185–94.

[16] Litbarg NO, Gudehithlu KP, Sethupathi P, Arruda JA, Dunea G, Singh AK. Activated omentum becomes rich in factors that promote healing and tissue regeneration. Cell Tissue Res 2007;328:487–97.

[17] Shevach M, Soffer-Tsur N, Fleischer S, Shapira A, Dvir T. Fabrication of omentum-based matrix for engineering vascularized cardiac tissues. Biofabrication 2014;6:024101.

[18] Soffer-Tsur N, Shevach M, Shapira A, Peer D, Dvir T. Optimizing the biofabrication process of omentum-based scaffolds for engineering autologous tissues. Biofabrication 2014;6:035023.

[19] Peters MDJ, Godfrey CM, Khalil H, McInerney P, Parker D, Soares CB. Guidance for conducting systematic scoping reviews. Int J Evid Based Healthc 2015;13:141–6.

[20] Kainuma S, Miyagawa S, Fukushima S, Pearson J, Chen YC, Saito A *et al*. Cell-sheet therapy with omentopexy promotes arteriogenesis and improves coronary circulation physiology in failing heart. Mol Ther 2015;23:374–86.

[21] Kanamori T, Watanabe G, Yasuda T, Nagamine H, Kamiya H, Koshida Y. Hybrid surgical angiogenesis: omentopexy can enhance myocardial angiogenesis induced by cell therapy. Ann Thorac Surg 2006;81:160–7.

[22] Kawamura M, Miyagawa S, Fukushima S, Saito A, Miki K, Funakoshi S *et al*. Enhanced therapeutic effects of human iPS cell derived-cardiomyocyte by combined cell-sheets with omental flap technique in porcine ischemic cardiomyopathy model. Sci Rep 2017;7:8824.

[23] Lilyanna S, Martinez EC, Vu TD, Ling LH, Gan SU, Tan AL *et al*. Cord lining-mesenchymal stem cells graft supplemented with an omental flap induces myocardial revascularization and ameliorates cardiac dysfunction in a rat model of chronic ischemic heart failure. Tissue Eng Part A 2013;19:1303–15.

[24] Shudo Y, Miyagawa S, Fukushima S, Saito A, Shimizu T, Okano T *et al*. Novel regenerative therapy using cell-sheet covered with omentum flap delivers a huge number of cells in a porcine myocardial infarction model. J Thorac Cardiovasc Surg 2011;142:1188–96.

[25] Suzuki R, Hattori F, Itabashi Y, Yoshioka M, Yuasa S, Manabe-Kawaguchi H *et al*. Omentopexy enhances graft function in myocardial cell sheet transplantation. Biochem Biophys Res Commun 2009;387:353–9.

[26] Takaba K, Jiang C, Nemoto S, Saji Y, Ikeda T, Urayama S *et al*. A combination of omental flap and growth factor therapy induces arteriogenesis and increases myocardial perfusion in chronic myocardial ischemia: evolving concept of biologic coronary artery bypass grafting. J Thorac Cardiovasc Surg 2006;132:891–9.

[27] Ueyama K, Bing G, Tabata Y, Ozeki M, Doi K, Nishimura K *et al*. Development of biologic coronary artery bypass grafting in a rabbit model: revival of a classic concept with modern biotechnology. J Thorac Cardiovasc Surg 2004;127:1608–15.

[28] Yajima S, Miyagawa S, Fukushima S, Sakai Y, Isohashi K, Watabe T *et al*. A prostacyclin agonist and an omental flap increased myocardial blood flow in a porcine chronic ischemia model. J Thorac Cardiovasc Surg 2018;156:229–41.e14.

[29] Zhang C, Hou J, Zheng S, Zheng Z, Hu S. Vascularized atrial tissue patch cardiomyoplasty with omentopexy improves cardiac performance after myocardial infarction. Ann Thorac Surg 2011;92:1435–42.

[30] Zhou Q, Zhou JY, Zheng Z, Zhang H, Hu SS. A novel vascularized patch enhances cell survival and modifies ventricular remodeling in a rat myocardial infarction model. J Thorac Cardiovasc Surg 2010;140:1388–96.e1–3.

[31] Bourahla B, Shafy A, Meilhac O, Elmadbouh I, Michel JB, Chachques JC. Mesothelial cells vs. skeletal myoblasts for myocardial infarction. Asian Cardiovasc Thorac Ann 2010;18:153–60.

[32] De Siena R, Balducci L, Blasi A, Montanaro MG, Saldarelli M, Saponaro V *et al*. Omentum-derived stromal cells improve myocardial regeneration in pig post-infarcted heart through a potent paracrine mechanism. Exp Cell Res 2010;316:1804–15.

[33] Dvir T, Kedem A, Ruvinov E, Levy O, Freeman I, Landa N *et al*. Prevascularization of cardiac patch on the omentum improves its therapeutic outcome. Proc Natl Acad Sci USA 2009;106:14990–5.

[34] Kainuma S, Nakajima K, Miyagawa S, Fukushima S, Saito A, Harada A *et al*. Novel regenerative therapy combined with transphrenic peritoneoscopy-assisted omentopexy. Interact CardioVasc Thorac Surg 2018;26:993–1001.

[35] Shao ZQ, Kawasuji M, Takaji K, Katayama Y, Matsukawa M. Therapeutic angiogenesis with autologous hepatic tissue implantation and omental wrapping. Circ J 2008;72:1894–9.
[36] Taheri SA, Yeh J, Batt RE, Fang Y, Ashraf H, Heffner R *et al*. Uterine myometrium as a cell patch as an alternative graft for transplantation to infarcted cardiac myocardium: a preliminary study. Int J Artif Organs 2008;31:62–7.
[37] Moher D, Liberati A, Tetzlaff J, Altman DG; The PRISMA Group. Preferred reporting items for systematic reviews and meta-analyses: the PRISMA statement. PLoS Med 2009;6:e1000097.
[38] Sade RM, Rylski B, Swain JA, Entwistle JWC, Ceppa DP, Blitzer D *et al*.; Members of the Cardiothoracic Ethics Forum who contributed to this work. Transatlantic editorial: institutional investigations of ethically flawed reports in cardiothoracic surgery journals. Eur J Cardiothorac Surg 2020;57:617–19.
[39] Sambri A, Gasbarrini A, Cialdella S, De Iaco P, Boriani S. Pedicled omental flaps in the treatment of complex spinal wounds after en bloc resection of spine tumors. J Plast Reconstr Aesthet Surg 2017;70:1267–71.
[40] Uchibori T, Takanari K, Hashizume R, Amoroso NJ, Kamei Y, Wagner WR. Use of a pedicled omental flap to reduce inflammation and vascularize an abdominal wall patch. J Surg Res 2017;212:77–85.
[41] Lee H, Cusick RA, Utsunomiya H, Ma PX, Langer R, Vacanti JP. Effect of implantation site on hepatocytes heterotopically transplanted on biodegradable polymer scaffolds. Tissue Eng 2003;9:1227–32.
[42] Li J, Xu P, Chen H, Yang Z, Zhang Q. Improvement of tracheal autograft survival with transplantation into the greater omentum. Ann Thorac Surg 1995;60:1592–6.
[43] Behfar A, Crespo-Diaz R, Terzic A, Gersh BJ. Cell therapy for cardiac repair—lessons from clinical trials. Nat Rev Cardiol 2014;11:232–46.

1.4 – Generation and applications of cardiac spheroids

Summary:

The following book chapter was invited by the editor of *Tissue Engineering and Regeneration* and is currently with the editor pending publication. This chapter provides detailed context about (vascularised) cardiac spheroids, including the different methods by which they can be generated and the different applications they have been used for. A central hypothesis of this thesis is that there is a benefit to using cardiac spheroids in bioink for 3D bioprinting of patches (rather than freely suspended cells not precultured in spheroids). The importance of this chapter to the thesis is therefore that it provides a detailed description of what cardiac spheroids are. The chapter shows that there are many methods to generate spheroids, each with advantages and disadvantages (for this thesis the method we chose to use is the hanging drop culture). The chapter also shows that cardiac spheroids have been used for other applications (such as disease modelling and drug testing) whereas our use of cardiac spheroids for direct suspension in bioink is a novel avenue which has not been fully explored for these so-called “mini-hearts”.

Generation and Applications of Cardiac Spheroids

Christopher D Roche[1], Liudmila Polonchuk[2] and Carmine Gentile[1,3*]

[1]Sydney Medical School, The University of Sydney, Sydney, New South Wales 2000, Australia
[2]Roche Pharma Research and Early Development, Roche Innovation Center Basel, F. Hoffmann-La Roche Ltd., 4070 Basel, Switzerland
[3]School of Biomedical Engineering/FEIT, University of Technology Sydney, Sydney, New South Wales 2007, Australia

*Corresponding author: Dr Carmine Gentile, PharmD/PhD, FAHA, School of Biomedical Engineering/Faculty of Engineering and IT, UTS, Building 11, Level 8, Room 311, 81 Broadway, Ultimo, NSW 2007, Australia. Phone +61(2)9514 4502; Email: carmine.gentile@uts.edu.au

Contents

Abstract

This chapter describes the methods for the optimal engineering of cardiac spheroids as well as their applications. As 3D cardiac cell aggregates, they are scaffold-free self-sustainable cultures with a defined diameter and cell number. They can be generated from either primary cells or stem cells, in the optimum microenvironmental "*niche*". Commonly known as "*mini-hearts*", their applications include: *i)* disease modelling; *ii)* drug screening and cardiac safety testing as high-throughput assays. Patient-derived spheroids may also represent a significant contemporary breakthrough in the field of *iii)* cardiac regenerative medicine, a field in which the clinical incentive is strong. In this rapidly evolving field, cutting-edge techniques such as the use of cardiac spheroids amalgamated into a cardiac "bio-ink" for use in novel 3D bioprinting processes makes it tempting to speculate that new cardiac spheroid-derived therapeutic options may be on the horizon for patients. Cardiac spheroids represent a novel and exciting *in vitro* model of the heart, presenting many opportunities to advance cardiac knowledge and therapeutics.

Keywords: cardiospheres, mammospheres, micromasses, microtissues, 3D cell culture, cardiac organoids

1 Introduction

3D cellular culture of cardiac cells is a rapidly evolving multidisciplinary field with significant potential to re-shape the cardiac clinical and research landscape. Three-dimensional cultures better approximate the biochemistry and physiology of tissues and organs (Wu, Giri, Sun, & Wirtz, 2014). *Cardiac spheroids*, also known as *cardiac organoids* (amongst several other names), are 3D aggregates of cardiac cells which are scaffold-free self-sustainable systems with a defined diameter and cell number (Gentile, 2016). These specialised microtissues have been in use for many years (Gahwiler, 1999; Halbert, Bruderer, & Lin, 1971; Sperelakis, 1978; Yechiel & Barenholz, 1986) but have recently received increasing attention as new technologies have impacted both the techniques of their generation and also the applications for which they are being used (Chimenti et al., 2017; Kelm & Fussenegger, 2004).

There are many methods for their generation, including (but not limited to) hanging drop cultures (Yang et al., 2019), microwells (Noguchi et al., 2016), rotary spinner flasks (Bursac et al., 1999; Gettler, Zakhari, Gandhi, & Williams, 2017), suspension in specialised media (Leung, Lesher-Perez, Matsuoka, Moraes, & Takayama, 2015), microfluidics (Khademhosseini et al., 2007) and bioprinting (Mehesz et al., 2011; Moldovan, Hibino, & Nakayama, 2017; Ong et al., 2017). These techniques are not exclusive and are being combined in different innovative ways, for example by combining either microwells and rotating devices (Hookway, Butts, Lee, Tang, & McDevitt, 2016; Nguyen et al., 2014), or microfluidics and bioprinting technology (H. Zhao et al., 2018) (**Fig. 1**).

Spheroid cultures are being employed for several *in vitro* and *in vivo* applications, such as: *i)* disease modelling; *ii)* drug screening; *iii*) and cardiac safety testing; *iv)* 3D bioprinting of cardiac tissues; and *v)* cardiac regeneration.

The future directions in both their methods of generation and applications are exciting and rapidly evolving. Progress is being made towards full, scalable automation for spheroid generation (Mehesz et al., 2011; Moldovan et al., 2017; Tung et al., 2011). Generation of personalised cardiac spheroids from patient-derived cells offer the prospect of patient-specificity, notably in cardiotoxicity and therapeutic response testing as well as patient-specific regenerative cardiac tissue fabrication (M. Campbell, Chabria, Figtree, Polonchuk, & Gentile, 2018). This chapter will also allow for a broad discussion on the engineering of spheroids beyond the use of cardiac cells, with concepts including tissue vascularisation potentially applicable to other spheroid types, such as liver, kidney, brain and cancer spheroids.

In highlighting some of the methods of cardiac spheroid generation and the applications of cardiac spheroids, before discussing some of the emerging paradigms and future directions this rapidly-evolving field is likely to take, this chapter aims to guide the reader to better understand the potential cardiac spheroids have to shape clinical and pre-clinical cardiovascular research.

2 Generation of Cardiac Spheroids

2.1 Hanging Drop Cultures

The first description of a hanging drop culture dates to 1907 with frog neural cells (Gahwiler, 1999). Hanging drop cultures in their simplest form can be generated from pipetting cellular fluid onto a petri dish and inverting the dish (Foty, 2011). Cells aggregate at the bottom of the drop and adhere to each other forming a spheroid (Leung et al., 2015). One of the first

application of this procedure in the cardiac field was described by Anna Wobus who used it for embryonic stem (ES) cell differentiation (Wobus, Wallukat, & Hescheler, 1991). For a more advanced culturing technique, specialised hanging drop plates can be used such as the Perfecta 3D® 96-well hanging drop plate (3D Biomatrix, MI, USA) (Polonchuk et al., 2017). For higher throughput, 384-well hanging drop plates (Tung et al., 2011) and 850 well hanging drop devices, Elplasia™ Mpc 350 (Kuraray Co., Ltd., Tokyo, Japan), have been described (Yang et al., 2019).

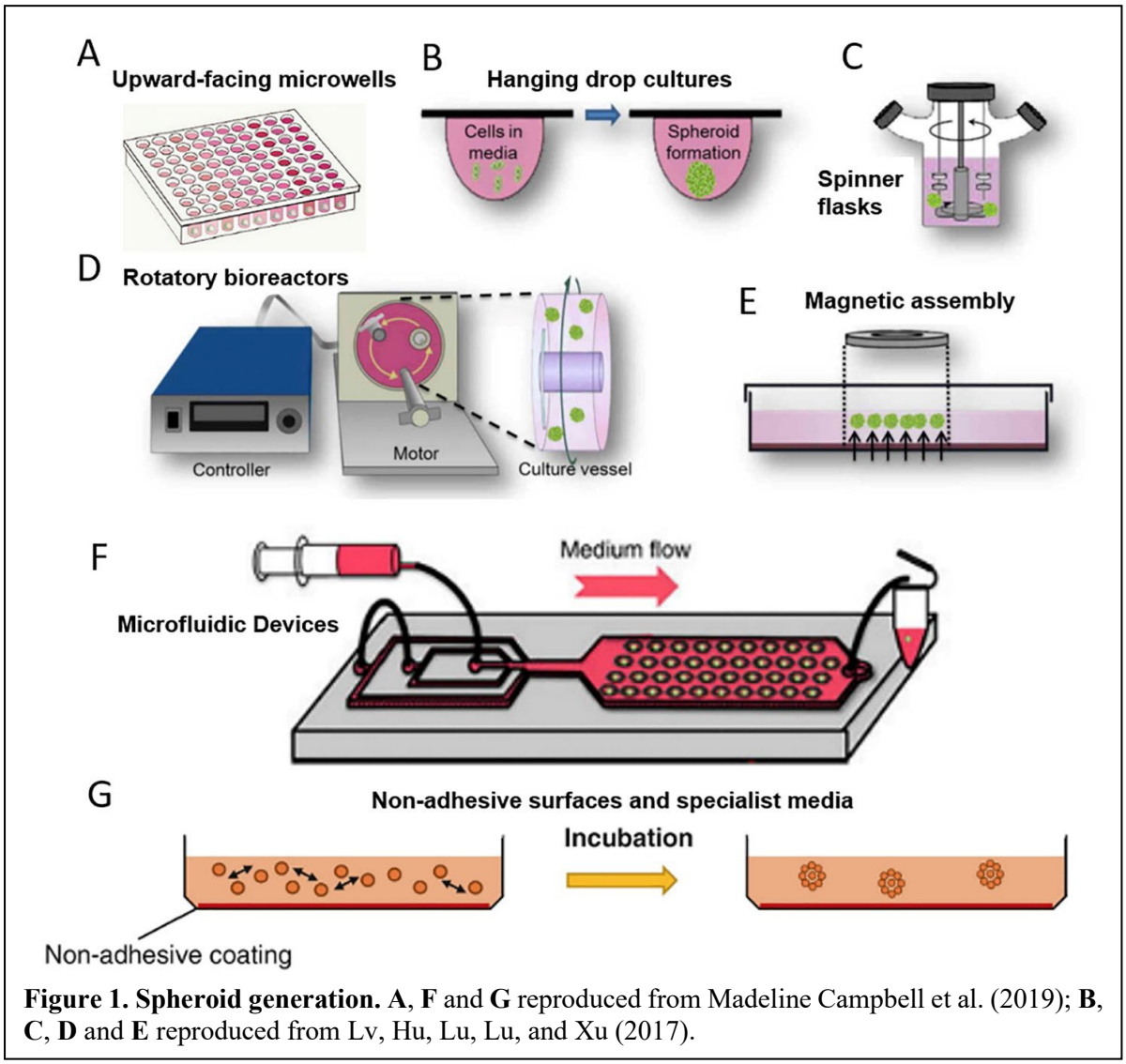

Figure 1. Spheroid generation. A, **F** and **G** reproduced from Madeline Campbell et al. (2019); **B**, **C**, **D** and **E** reproduced from Lv, Hu, Lu, Lu, and Xu (2017).

Additionally to dedicated hanging drop devices, the inversion of a low-adhesive plate with U bottom wells in it can generate spheroids. This method combines the upward-facing low adhesive surface (*microwell*) method initially, followed by the downward-facing hanging drop method, in the same hydrophobic polystyrene plate (Neto et al., 2015). Another similar published method used a generally hydrophobic plate but with wettable areas where the fluid-based cellular material would aggregate into spheroids which were then inverted to turn them into hanging drops (Oliveira et al., 2014).

The formation and control of spheroids in hanging drops has been well-studied and continues to yield interesting results. For example, altering the composition of the cell media by adding varying concentrations of methylcellulose and/or collagen controls spheroid circularity and compaction in hanging drops, with optimal conditions determined by the cellular composition

of the spheroid (Leung et al., 2015). Others have reported the significant differences in cell behaviour within spheroids by cell type, for instance with endothelial cells migrating to the periphery of the hanging spheroid culture (Kelm & Fussenegger, 2004).

2.2 Microwells and Low-Adhesive Surfaces

It has long been known that culturing cells in flat monolayer sheets on *low-adhesive surfaces* such as polystyrene causes them to eventually dissociate from the surface and aggregate into 3D clusters (Halbert et al., 1971). To keep spheroids compartmentalised and facilitate uniform generation, microwell arrays specifically designed for spheroid formation are readily available and 96-well plates with coated low adhesive wells are commonly chosen to successfully generate cardiac spheroids (Koudan et al., 2017; Mattapally et al., 2018; Noguchi et al., 2016). Alternatively, moulds can be used to generate a pattern of imprinted cylindrical recesses in non-adhesive hydrogel sheets (such as *agarose*) which can then be used to generate cardiac spheroids, or, by altering the recess shape from cylindrical to elliptical, to generate fusions of spheroids into more elongated rows of 3D microtissues (Kim et al., 2018).

The specific methodologies employed for ideal cardiac spheroid generation are variable as spheroid formation is influenced by several factors. For instance, the shape of the wells (*U-shaped* or *V-Shaped* are frequently chosen but other shapes are available) determines the success of spheroid generation for specific cardiac cell lines. Bartulos et al. (2016) showed that cardiac progenitor cells expressing ISL1-LIM–homeodomain transcription factor (a protein expressed by cardiac progenitor cells involved in the development of all four cardiac chambers) will not form spheroids in V shaped wells, or in hanging drops, but will form spheroids in U shaped wells. In the same study, highlighting how microwell array spheroid culture lends itself to manipulation of the spheroid-generating process, it was shown that addition of the rho-associated protein kinase (ROCK) inhibitor, Y27632, halved the time taken for spheroids to form in the microwells from 24 to 12 hours.

It has been observed that the generation of spheroids in microwells is the product of the balance between cell-to-cell adhesion forces and cell-to-microwell adhesion forces (Hookway et al., 2016). Furthermore, as cells may change inside the spheroid over time, for example from induced-pluripotent stem cells (iPSCs) to iPSC-derived cardiomyocytes (iPSC-CMs), they have different interactions with the microwells as they change phenotype, suggesting the choice of the microwell plate may also need to be optimised to better match the cell type as cell maturation progresses (Hookway et al., 2016).

In another experiment which manipulated upward-facing low adhesive spheroid culture, Lee et al. (2015) generated and edited small spheroids (microspheres) on *AggreWell™ 400 inserts* (Stem Cell Technologies, Vancouver, Canada) which contain 1200 spheroid-generating wells per insert. In this study human embryonic stem cells formed *embryoid bodies,* or *EBs* (spheroids formed from embryonic stem cells, or ESCs, which may develop into mature cells from any of the three germ cell layers) interspersed with polycaprolactone (PCL) or PCL and gold. EBs were then transferred into standard microwell arrays where they were differentiated into cardiomyogenic spheroids through the addition of specific cytokines. The AggreWell™ spheroid culture plates required centrifugation for cells to populate the wells. Their method highlights that the combined use of more than one technique allows for precise control and manipulation of the spheroid generation process.

2.3 Rotation and Spinner Flasks

The use of rotational force has been employed in diverse ways to generate spheroids. In a non-cardiac example, spheroids of chondrocytes and polyglycolic acid (PGA) were generated in a *rotating bioreactor* both within the Earth's gravity and in space where zero-gravity conditions yielded more spherical spheroids (Freed, Langer, Martin, Pellis, & Vunjak-Novakovic, 1997). For those without access to NASA-built rotating bioreactors, *standard spinner flasks* with a magnetic rotating bar at the base have been used to culture cardiac spheroids PGA scaffolds suspended from the flask's bung into the swirling media to which cells are added (Bursac et al., 1999). Others have used standard conical (*Erlenmeyer*) flasks on a *gyratory agitator*, rotating 20mls of media containing cells at 75rpm, which can be stepped up for larger volumes to a 100ml stirred (spinner) flask (*Stirred DASbox minibioreactor* (Eppendorf, Hamburg, Germany)) (Kempf et al., 2014). It has also been shown that by taking spheroids generated in a centrifuged microwell array and placing them in 10mls of media in a 10cm circular dish on a rotatory orbital shaker in an incubator spheroids can be forced to aggregate in the centre of the swirling media (Hookway et al., 2016; Kinney, Saeed, & McDevitt, 2012). It has been argued that rotatory bioreactors are a promising method for scaling up to large scale production of cardiac spheroids (Kempf et al., 2014) as well as for control of multicellular coaggregation of cardiac spheroids, for example with human pluripotent stem cell-derived cardiomyocytes and cardiac fibroblasts (Hookway et al., 2016).

2.4 Cell Media Formulations

The knowledge that cellular clustering and spheroid formation depends on the interaction of the specific growth media used and the cell type being cultured is perhaps intuitive and has been well established for some time (Moscona & Moscona, 1952). The media used in the techniques outlined above interacts with cardiac spheroids and can be altered to control spheroid formation (Leung et al., 2015).

Messina et al. (2004) described cardiosphere-growing medium, a mixture of IMDM, DMEM/F-12, B27, mercaptoethanol, epidermal growth factor, basic fibroblast growth factor, cardiotrophin-1, thrombin, antibiotics and L-Glut, used as part of a cardiosphere generation method which has been repeated since (Davis et al., 2009; Smith et al., 2007). In a modification of this method, Chen et al. (2013) added cardiac fibroblast conditional medium (CFCM) which contains cardiac fibroblast paracrine factors obtained by incubating the medium with cardiac fibroblasts before use. They also manipulated the isolation of cardiac progenitor (*Sca-1*$^{+}$) cells used to form cardiac spheroids by a magnetic indirect antibody labelling and separation process and allowed cardiac spheroids to form on a poly-D-lysine-coated dish. Further illustrating how the media can be manipulated in innovative ways to generate spheroids, Parfenov et al. (2018) described a method which did not label the spheroids (in this case they used sheep chondrocytes) but used paramagnetic media containing gadolinium (Gd^{3+}) and an externally applied magnetic field to levitate the unlabelled chondrospheres to generate 3D living tissue constructs.

When generating cardiac spheroids from cardiac progenitor cells, it is also known that the choice of supplements added to the media influences cardiosphere culture and even seemingly

subtle modifications to the media used to generate cardiospheres may have profound effects (Chimenti et al., 2014). Chimenti et al. (2014) observed that when replacing the commonly-used xenobiotic medium supplement, foetal bovine serum (FBS), with gamma-irradiated FBS from three different supplying companies, whilst the products were supposedly similar, two of the suppliers' formulations caused a significant reduction of the number of successful spheroid cultures. In absence of the media supplement B27 the absolute cell number of cardiospheres was decreased but the size of the cardiospheres increased. Removing B27 from the media also caused a 10-fold reduction of cardiosphere expression of *c-kit* suggesting a reduction in the phenotypic stemness of the cardiac progenitor cells being used.

2.5 Microfluidics

Microfluidic techniques, which employ the flow of small volumes of fluids to generate and manipulate microtissues, offer the ability to both generate and test cardiac spheroids in the same microfluidic process. This is appealing, especially for high-throughput testing, as it skips the step of moving the cardiospheres from the generating platform to the testing platform (Vadivelu, Kamble, Shiddiky, & Nguyen, 2017). Some have argued that, just as 3D cellular culture models are superior to monolayer culture for drug testing, the flow which is integral to a microfluidic system is necessary to properly evaluate human cellular responses on a more physiological basis than fluid-static cultures allow (Moya, Tran, & George, 2013). Others have shown that microfluidic systems where the cellular aggregates generated are not explicitly three-dimensional (i.e. monolayers) can be used (Kobuszewska et al., 2017; Qian et al., 2017).

A basic microfluidic device, or chip, for generation of spheroids can use U-shaped traps and as cellular fluid flows past, the cells collect in the traps and the low adherent coating of the traps causes cells to aggregate into spheroids. This method has been described for fibroblasts and human hepatoma cells (Fu et al., 2014). Another device used a "hanging" microfluidic system which could generate hanging drop style spheroids whilst passing fluidic flow through the spheroids to deliver nutrients (Frey, Misun, Fluri, Hengstler, & Hierlemann, 2014).

One of the appeals of microfluidic devices is the ability to generate 3D cardiac spheroids and then introduce a drug within the same platform. One group used a vacuum-assisted microfluidic chamber to achieve this, generating 3D cardiac microtissues from induced pluripotent stem cell-derived cardiomyocytes (iPSC-CMs) and rat cardiac fibroblasts in fibrin-based hydrogel solution (Visone et al., 2019). The cell-hydrogel solution was injected and beating cardiac 3D microtissues aggregated. After this they performed experiments with injections of doxorubicin, sotalol and verapamil into the chambers and were able to obtain results on the same cardiac spheroids generated within the unit. It is worth noting that this technique does not require the assembled cardiac tissues to be spheroidal. For example, Mathur et al. (2015) demonstrated a microfluidic chamber where hiPSC-CMs could be assembled into beating elongated structures in rows which performed well as biomimetic cardiac organoids when tested with various compounds.

Highlighting the use of combined techniques for spheroid generation, Osidak et al. (2019) added a turnstile-valve microfluidic device to the dispensing part of a bioprinter which allowed for precise control of alternating passage of pre-formed spheroids through the nozzle and detection of spheroid deposition by a sensor. For the primary use of a microfluidic-bioprinter combination to form spheroids *de novo*, H. Zhao et al. (2018) combined a microfluidic device

with a 3D bioprinter and demonstrated the ability to control the spatial architecture within spheroids, even infusing their spheroids with a tai-chi inspired emblem.

2.6 Bioprinting and Spraying

3D bioprinting as a method of spheroid generation is appealing as it has the potential to allow for scalable, uniform, automated mass production of spheroids. As well as the example presented by H. Zhao et al. (2018) (**Fig. 2**), true direct 3D bioprinting of cellular spheroids has been described by Jakab et al. (2008). Their 3D bioprinter, custom made by nScrypt (Orlando, FL, USA), is piston-driven and extrudes spheroids through a micropipette nozzle. The spheroids themselves are generated in a previous step in their method by a custom-built apparatus which pushes cells through a 500µm diameter micropipette and slices off cylinders with a height:diameter ratio of 1:1 which subsequently round-off into spheroids. These pure cellular spheroids without supporting hydrogel material are extruded from one nozzle of their bioprinter as spheroids whilst another nozzle of the same bioprinter extrudes collagen type 1 as hydrogel patches of 1cm x 1cm x 0.2cm into which the spheroids can be deposited.

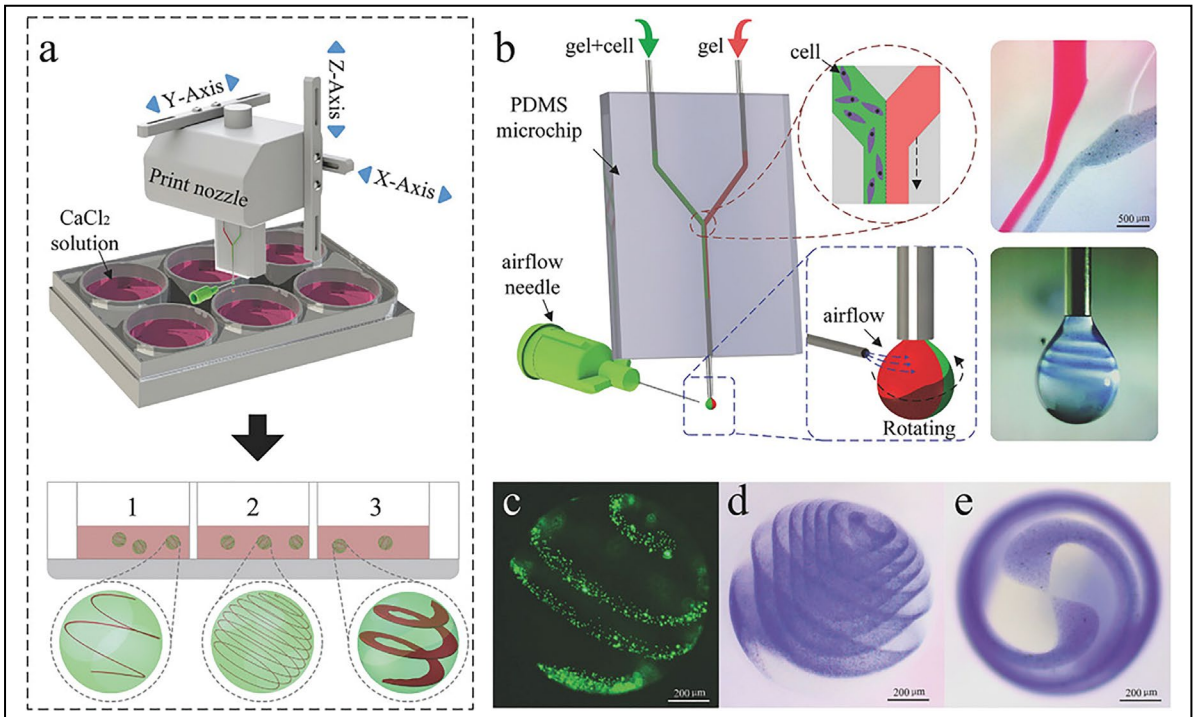

Figure 2. 3D bioprinting of spheroids with a microfluidic device and airflow injector at the print nozzle allows for precise geospatial control of depositional patterns within spheroids. (a) 3D printer with microfluidic device and airflow injector at the print nozzle opening. In this example, spheroids are printed into a 6-well plate containing crosslinking solution of calcium chloride ($CaCl_2$) Subsequent patterning within spheroids is shown in lower image with spheroids suspended in media having different spiral-shaped patterning within them. (b) Magnified diagrammatic representation of the cell-laden bioink (green) fusing with acellular bioink (red) in a PDMS microfluidic device. The airflow needle spins the spheroid at the point of deposition allowing for precise geometrical patterning of cells within a spheroid. Reproduced from H. Zhao et al. (2018).

Another interesting example, which falls outside the definition of bioprinting but has similarities of mechanism and appeal for spheroid generation, was put forward by Munarin and

Coulombe (2015) in the form of the Var J30 Bead Generator (Nisco, Switzerland). This machine was used to jet spray 'microspheres' of alginate into a gelling bath which were then incorporated into a scaffold used for cardiac regeneration. The microsphere diameters could be controlled and were typically 100µm (range between 50 and 450µm), similar in size to typical spheroids. Whilst the spheroids generated in this experiment were not cellular themselves, when engrafted onto rat hearts they provided a scaffold for host cardiac cells to grow around. The method was not attempted with cells, but with manipulation it could foreseeably provide inspiration for a novel jet-spray method of primary cellular spheroid generation in the future as it has been shown that even stem cells can survive bioelectrosprays and aerodynamically-assisted bio-jetting without gross cellular damage (Mongkoldhumrongkul, Flanagan, & Jayasinghe, 2009).

For primary, high-throughput bioprinting/bio-depositing of cellular spheroids, Mehesz et al. (2011) have described a method which produced more uniform diameter spheroids than standard hanging drop culture using an eight-channel dispenser, the epMotion 5070 automated pipetting system (Eppendorf, Hamburg, Germany). Using that system yielded 5856 spheroids in 12 pipetting movements. Similar experiments for robotic bioprinting of cells into spheroids are underway, including those with cardiac cells specifically, using contemporary bioprinters such as the 'Rastrum' (Inventia Life Sciences, Sydney, Australia) and peer-reviewed data for cardiac spheroid-depositing technologies are anticipated.

In addition to direct 3D bioprinting of spheroids, automated, spheroid-handling systems have been designed (Blakely, Manning, Tripathi, & Morgan, 2015) which is in keeping with the vision of fully automated, scalable microtissue production where the 3D bioprinter is supported by an automated production-line (Mironov, Kasyanov, & Markwald, 2011). Ongoing research is yielding novel techniques such as the Kenzan ('mountain of needles') technique which uses a biological 3D printer, the 'Regenova' (Cyfuse Biomedical, Tokyo, Japan), for spheroids based on a robotic aspirator of spheroids initially cultured in a standard 96-well microarray. The robotic arm then places the spheroids onto microneedles which allows for precise deposition of the spheroids in a subsequent step in the process to generate secondary spheroid-based structures (Moldovan et al., 2017).

3 Applications of Cardiac Spheroids

3.1 Cardiac Regeneration

Whilst bioprinting is currently emerging as a cutting-edge method to generate spheroids *de novo* from deposition of cell-laden material, it is also one of the applications for spheroids once they have been formed (Mironov et al., 2009). In a method conceptually similar to the 'Kenzan' method described above, Ong et al. (2017) used a 3D bioprinter to print cardiac spheroids onto a needle array. The adjacently positioned spheroids were then allowed to fuse to form a spontaneously-beating cardiac patch. In one notable (non-cardiac) example, Bulanova et al. (2017) passed preformed spheroids through a bioprinter to generate a functional mouse thyroid gland organoid.

Not all methods of spheroid-based cardiac regeneration utilise a 3D bioprinter, as illustrated by trials which aim to directly inject cardiospheres or similar cardiosphere-derived cells into the heart (Chakravarty et al., 2017; Makkar et al., 2012; Tseliou et al., 2013; Yee et al., 2014) or

incorporate them into formed heart patches first (Noguchi et al., 2016). Clinical trials such as the CArdiosphere-Derived aUtologous stem CElls to reverse ventricUlar dySfunction (CADUCEUS) trial showed that autologous cardiosphere-derived cell injection is safe in humans (Makkar et al., 2012) and paved the way for other trials such as the ALLogeneic Heart STem Cells to Achieve Myocardial Regeneration (ALLSTAR) Trial (Chakravarty et al., 2017) and the Halt Cardiomyopathy Progression (HOPE)-Duchenne trial for patients with Duchenne Muscular Dystrophy with cardiac fibrosis (Taylor et al., 2019). These trials utilised a method of intracoronary injection cardiosphere-derived cells generated from deceased human donors.

Others have sought to pre-form cardiac patches before implantation, such as Noguchi et al. (2016) who generated beating heart patches by culturing spheroids in a microarray and then transferring them to a gyrating, standard low-adhesive petri dish. The cardiospheres in that study were formed from co-culture of rat neonatal ventricular cardiomyocytes, human dermal fibroblasts and human cardiac microvascular endothelial cells and the resulting patch contained some microvascular channels within the patch. Mattapally et al. (2018) generated spheroids from hiPSC-CMs and embedded them in a fibrin patch before engrafting them in mice with myocardial infarction. They observed a high (>25%) engraftment rate and a cardiac functional improvement, a significant part of which they attributed to a paracrine mechanism. Interestingly, as they worked with cardiac spheroids of 800µm diameter without them developing necrotic cores, they challenged the conventional belief that spheroids should not be able to exceed around 200µm diameter before central apoptosis and necrosis occurs. Using a similar method in a porcine model, Gao et al. (2018) used cardiac spheroids to generate larger heart patches (4cm × 2cm × 1.25mm) which were found to show a functional improvement in large animals with myocardial infarction. It is perhaps worth noting here that the most advanced studies along these lines, with large cellular patches implanted in humans (Menasché et al., 2015; Menasché et al., 2018), did not used a spheroid-based approach and seeded cells directly into fibrin-based patches. Nonetheless, it has been argued that spheroid-based approaches may ultimately have more success as the attrition rate may be lessened when compared to isolated cardiac cells and cardiac spheroids as building blocks for heart regeneration by preformed macroscopic tissue is considered a promising method (Mironov et al., 2009).

3.2 Disease Modelling

The use of cardiac spheroids for disease modelling and pathophysiology testing is not a new idea (Yechiel & Barenholz, 1986). One of the reasons for recent anticipation in the various fields which employ cardiac spheroids is that with the advent of induced pluripotent stem cells (iPSCs) (Takahashi & Yamanaka, 2006; Yoshioka & Dowdy, 2017; Yoshioka et al., 2013), it is possible to use patient-specific stem cells to generate cardiac spheroids or similar 3D microtissues of non-spheroidal morphology which are specific to and compatible with a given patient (M. Campbell et al., 2018; Cashman, Josowitz, Johnson, Gelb, & Costa, 2016). For instance, primary cells of a patient with a genetic disease causing cardiac pathology may be obtained with relative ease from the skin or elsewhere, can be reprogrammed to revert to stemness and then cultured towards expressing a desired mature cardiac phenotype(Cashman et al., 2016).

Techniques using cardiac patient-specific cells have mainly been described as part of methods which combine 3D and monolayer techniques, where it has been demonstrated that human dermal fibroblasts taken from the skin of patients with inherited cardiac conditions can be

reprogrammed to generate iPSC-CMs which retain the genotype and phenotype for that disease (Cashman et al., 2016; Goldfracht et al., 2019; Itzhaki et al., 2011; Maizels et al., 2017). In one notable example, iPSC-CMs were injected into moulds to generate large (2 million patient-specific iPSC-CMs per 4mm outer-diameter mould) engineered heart tissue rings (Zimmermann et al., 2002), for patient and disease-specific modelling of the long QT syndrome and catecholaminergic polymorphic ventricular tachycardia (Goldfracht et al., 2019).

As testing on 3D tissues *in vitro* becomes more widespread, it may be that, beyond cardiac spheroids, tubular myocardial structures (Amano et al., 2016; Cashman et al., 2016), even whole beating miniature ventricles (MacQueen et al., 2018) provide enhanced (although increasingly complex and difficult to utilise) models for 3D tissue disease modelling. However, with spheroids able to recapitulate the 3D microenvironment with only a few thousand cells, their smaller size, large number of repeats, relative ease of use and potential for scalable automation makes them appealing alternatives to large constructs and it is envisaged this will have significant implications for both patient-specific and non-patient-specific disease testing (M. Campbell et al., 2018; Eglen & Reisine, 2019).

For disease models which do not have to be patient-specific, access to human stem cell derived cardiac spheroids (as opposed to having to obtain primary cardiac tissue) is opening up the field of 3D tissue for modelling of pathophysiological processes such as cardiac fibrosis (Figtree et al., 2017) (**Fig. 3**). The way in which cardiospheres are used for disease modelling can be employed in diverse ways. This is illustrated by the work of Ebert et al. (2007) who cultured mouse embryonic stem cells into spheroidal EBs in hanging drops to study cardiac ischaemia-reperfusion. When cultured in this way, this cell type is known to differentiate towards a cardiomyocyte phenotype (Maltsev, Wobus, Rohwedel, Bader, & Hescheler, 1994). The cells in this case were observed to be contracting and were labelled with superparamagnetic fluorescent microspheres. They were injected directly into mouse hearts following ischaemia and then tracked by MRI to model reperfusion. This study serves as a useful illustration that there are not always clear boundaries between definitions of what is or is not a cardiac spheroid or between methods that work with spheroids and those that do not: there was no definitive moment when the EBs became cardiac spheroids and when the cardiac spheroids dissociated into individual cells as they were subsequently plated in a T75 flask, infused with magnetic microspheres, aspirated, injected into the mouse ventricles and observed to complete the model of cardiac ischaemia-reperfusion.

3.3 Drug Screening and Cardiac Safety Testing

Accounting for all processes and lost capital opportunity costs, bringing a drug to market has been estimated to cost $1.8 billion US dollars per drug and take an average time of 13.5 years (Paul et al., 2010). For cardiovascular drugs the success rate for a compound making it from phase I trials to regulatory approval has been found to be 8.7% (DiMasi, Feldman, Seckler, & Wilson, 2010). In the USA between 1980 and 2009, 3.5% of drugs approved for market had to be withdrawn due to safety concerns which became apparent after introduction of the drug to the market (Qureshi, Seoane-Vazquez, Rodriguez-Monguio, Stevenson, & Szeinbach, 2011).

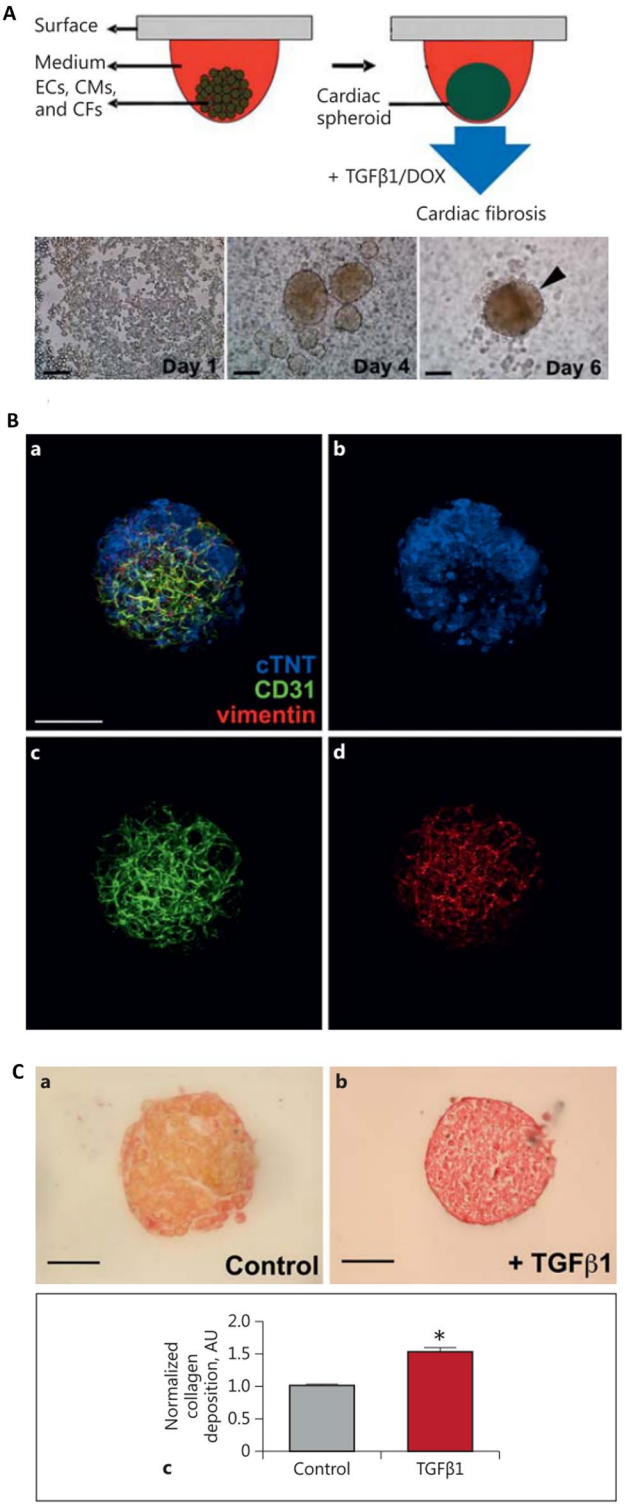

Figure 3. Cardiac Spheroids as a model of cardiac fibrosis. (**A**) Generation and treatment of vascularised cardiac spheroids (VCSs) with pro-fibrotic TGFβ1 and/or doxorubicin. (**B**) Confocal microscopy images of a VCS stained for markers of cardiomyocytes (blue), endothelial cells (green) and cardiac fibroblasts (red). (**C**) TGFβ1 upregulates collagen deposition in VCSs (PicroSirius Red staining). Reproduced from Figtree, Bubb, Tang, Kizana,

On this backdrop, the appeal of novel 3D models which can model the effect of compounds on tissues in the laboratory in a biomimetic, reliable and inexpensive way is evident. For example, testing of compounds on cardiac spheroids presents the opportunity for early prediction and prevention of the hugely wasteful investment in drugs which then have to be removed from the market due to cardiotoxicity discovered at the end of the drug development process.

Evidence that 3D culture is superior to 2D for this purpose is mounting (Neto et al., 2015; Polonchuk et al., 2017; Tomlinson et al., 2019; Tung et al., 2011) and is not just applicable to cardiac spheroids. For instance, it has been shown that 3D spheroids formed from mouse fibroblast L929 cells in hanging drop culture show a greater resistance to doxorubicin, an anticancer drug with cardiotoxic effects, than 2D cultures (Neto et al., 2015). More closely recapitulating the human heart, Polonchuk et al. (2017) showed that co-cultured 'mini beating hearts' could be used for drug testing and toxicity pathophysiology assay (**Fig. 4**). Their group generated cardiac spheroids from hanging drops composed of a mix of human coronary artery endothelial cells, cardiac fibroblasts derived from induced pluripotent stem cells (iPSCs) and either human primary adult cardiomyocytes harvested from patients undergoing cardiac surgery or iPSC-derived cardiomyocytes from reprogrammed stem cells. With this physiologically relevant model they were able to determine that endothelial nitric oxide synthase was implicated in the mechanism of

doxorubicin toxicity. They also confirmed that for these cells a 2D (monolayer) model obtained different results.

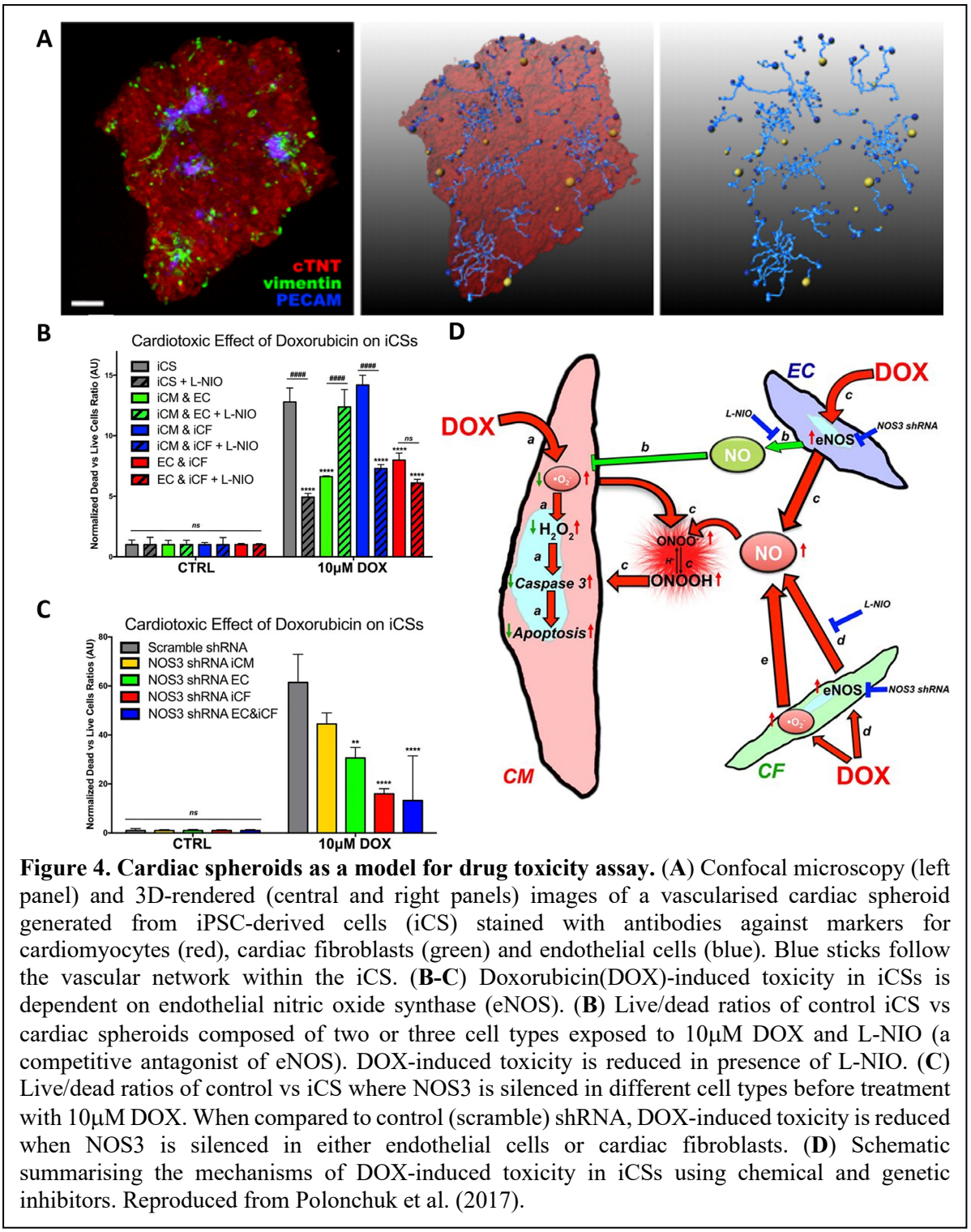

Figure 4. Cardiac spheroids as a model for drug toxicity assay. (**A**) Confocal microscopy (left panel) and 3D-rendered (central and right panels) images of a vascularised cardiac spheroid generated from iPSC-derived cells (iCS) stained with antibodies against markers for cardiomyocytes (red), cardiac fibroblasts (green) and endothelial cells (blue). Blue sticks follow the vascular network within the iCS. (**B-C**) Doxorubicin(DOX)-induced toxicity in iCSs is dependent on endothelial nitric oxide synthase (eNOS). (**B**) Live/dead ratios of control iCS vs cardiac spheroids composed of two or three cell types exposed to 10μM DOX and L-NIO (a competitive antagonist of eNOS). DOX-induced toxicity is reduced in presence of L-NIO. (**C**) Live/dead ratios of control vs iCS where NOS3 is silenced in different cell types before treatment with 10μM DOX. When compared to control (scramble) shRNA, DOX-induced toxicity is reduced when NOS3 is silenced in either endothelial cells or cardiac fibroblasts. (**D**) Schematic summarising the mechanisms of DOX-induced toxicity in iCSs using chemical and genetic inhibitors. Reproduced from Polonchuk et al. (2017).

Tomlinson et al. (2019) have provided further evidence that cardiac spheroids can unlock findings which monolayer cultures overlook due, for example, to monolayer cultures lacking the intercellular crosstalk and relationship between cells and extracellular matrix which are important, especially when testing the effects of compounds. Highlighting that cardiac spheroids can be used for more complex drug testing than simply adding a cardiotoxic agent and measuring its effect, they tested cardiac spheroids with doxorubicin combined with

dexrazoxane (a cardioprotective agent which is co-administered with doxorubicin to reduce the risk of cardiotoxicity in selected patients). They observed a cardioprotective effect in their cardiospheres and also co-administered other agents, the NRF2 activators bardoxolone-methyl (CDDO-me) and sulforaphane, showing that the model could be used for complex multi-compound testing. Trastuzumab (Herceptin) has also been tested in a similar cardiac spheroid model and the model was able to elucidate an *in vivo* mechanism dependent on trastuzumab's effect on resident human cardiac stem cells.

Interestingly, the latest publication of Blinova et al. (2019) reported no significant correlation between the subject-specific iPSC-derived cardiomyocyte APD and QT responses to the same blocking drugs, dofetilide and moxifloxacin. Among various factors affecting correlation, using 3D cardiac spheroids instead of the monolayer cultures should be considered for future studies of patient-specific responses in the "clinical trial in a dish".

Another important driver for this bio-mimetic technology is the ability to test toxins and perform experiments where damage to cells is the primary endpoint (Forsythe et al., 2018). Drug-induced cardiotoxicity is one of the main reasons for compound withdrawal from development. Current regulatory mandated assays do not capture the complexity of arrhythmia or the *in vivo* animal studies cannot be extrapolated to humans. The strategy that integrates human iPS-cardiomyocytes engineered into a 3D system replicating cardiac physiology presents an opportunity to develop a robust, physiologically relevant *in vitro* functional assay. This better predicts clinical outcomes while limiting animal usage, improving preclinical decision making and reducing development costs.

3.4 High-throughput Assay and Automation

To fully realise the potential of cardiac spheroids as a paradigm-shifting methodology for drug testing, it is necessary to turn the testing platform into a high-throughput, scalable and low-cost alternative to traditional methods. To this end, (non-cardiac) spheroids of cancer cell lines in 384-well hanging drop plates have been combined with automated liquid dispensing robots to demonstrate high-throughput, automated assay by adding anti-cancer drugs (Tung et al., 2011).

One of the limitations of high-throughput assay is how to continue with full automation at the data analysis phase. Progress is being made in this aspect, for example Sirenko et al. (2017) have described automated confocal microscopy and 3D Ca^{2+} oscillation (flux) assay using fast kinetic fluorescence imaging (FLIPR, FortéBio, CA, USA) to automatically analyse cardiac spheroids in 96 or 384-well plates. The CellOPTIQ®platform from Clyde Bioscience, which can be used for cardiomyocytes in various formats, combines the three cardinal measurements in cardiac assessments by recording voltage, calcium and contraction in one experiment using standard 96 well plates and modern voltage sensitive optical sensors.

Besides optically-based methods and technologies, the 3D self-rolled biosensory arrays present a promising approach to study cardiac electrophysiology of human electrogenic spheroids in an organ-on-e-chip platform in the future (Kalmykov et al., 2019).

4 Discussion and Future Perspectives

Whilst it is increasingly evident that cardiac spheroids represent an important advance from monolayer techniques, every system has advantages and disadvantages and monolayer techniques may remain preferable in certain situations. For example, Bursac, Parker, Iravanian, and Tung (2002) have argued that, when studying electrical propagation, monolayer provides certainty that the entire signal is produced from only one layer of cells which allows for direct comparison with computer simulations and 2D theoretical models.

Even single cell testing can yield important insights, as illustrated by a recent study of patient and disease-specific cells using iPSC-CMs derived from skin cells of a patient with Brugada syndrome and the SCN10A mutation (El-Battrawy et al., 2019). The experimental model chosen was effective for the study of single cell phenotype and single-cell ion channel behaviour but did not account for cell-cell interactions, hormone and neural regulating factors.

Beyond spheroids, for truly comprehensive study in 3D, it may be that even more physiologically relevant tissues than spheroids are required, such as fused cardiac spheroids in rows (Kim et al., 2018), filamentous fibres mimicking heart muscle (Huebsch et al., 2016; Ma et al., 2018; Y. Zhao et al., 2019), larger constructs such as slices of heart tissue cut with a microtome (Kang et al., 2016), 5mm diameter discoids (Bursac et al., 1999), doughnut-shaped engineered heart tissue (Eschenhagen et al., 2002; Schlick et al., 2019; Tiburcy, Meyer, Soong, & Zimmermann, 2014), or even miniature whole heart chamber models (MacQueen et al., 2018). Indeed, high-throughput techniques including automated analysis of Ca2+ transients have been described in ring-contractile 3D-engineered heart tissue with inner diameter 2mm, outer diameter 4mm and height 5mm (Hansen et al., 2010; Stoehr et al., 2014; Tiburcy et al., 2017). In addition, the 'Biowire II' model of cylindrical trabecular strips of heart tissue presented by Y. Zhao et al. (2019) was able to generate chamber-specific (atrial and ventricular) results and they observed that to model polygenic disease such as left ventricular hypertrophy, it will be critical to be able to provide a chronic increased workload to the cardiac tissue at least over many months which their model was able to sustain. On a smaller scale, which combines the ease of use associated with cardiac spheroids with the biomimetic physiology of larger engineered heart tissue constructs, the Micro-Heart Muscle (μHM) array developed by Huebsch et al. (2016) may offer an insight into a future in which 3D cardiac tissue culture will combine ease of generation and analysis with ever closer recapitulation of native cardiac structure and physiology.

Eventually, the purpose and the mechanistic question will determine the model to be utilized in specific studies. And the recent FDA white paper co-authorized by academic and industrial experts outlines the general validation principles for the models to be used e.g. in the safety pharmacology field (Li, 2019).

5 Conclusions

Replicating the native myocardium *in vitro* requires departure from standard 2D cell culture and combining concepts in tissue engineering, material science and cardiomyocyte biology. 3D culture of cells provides a more biomimetic model than traditional non-3D methods. Cardiac spheroids can be generated using diverse methods which can be combined either in series within the same experiment or within the same apparatus using elements of different generation techniques combined together in innovative ways.

Cardiac spheroids have opened up new avenues in cardiac regeneration, disease modelling and compound testing. As a model, cardiac spheroids are well-suited to techniques which test patient-specific or disease specific cells. Due to their ease of use and their advantages compared to non-3D techniques, they occupy a space between 2D culture techniques and more complicated macro-structural tissue engineered constructs which are currently more difficult to fabricate and use. In future, it is envisaged that cardiac spheroids combined with scalable automatic techniques will dramatically change the way cardiac tissues can be engineered, cardiac diseases can be modelled and cardio-active compounds can be tested.

6 Acknowledgements

The writing of this chapter was supported by the Sir John Loewenthal Scholarship (University of Sydney) and a Heart Research Australia Scholarship to CDR, and by the Kick-Start Grant, CDIP Grant and a Cardiothoracic Surgery Research Grant from the University of Sydney to CG.

7 References

Amano, Y., Nishiguchi, A., Matsusaki, M., Iseoka, H., Miyagawa, S., Sawa, Y., . . . Akashi, M. (2016). Development of vascularized iPSC derived 3D-cardiomyocyte tissues by filtration Layer-by-Layer technique and their application for pharmaceutical assays. *Acta Biomater, 33*, 110-121. doi:10.1016/j.actbio.2016.01.033

Bartulos, O., Zhuang, Z. W., Huang, Y., Mikush, N., Suh, C., Bregasi, A., . . . Qyang, Y. (2016). ISL1 cardiovascular progenitor cells for cardiac repair after myocardial infarction. *JCI Insight, 1*(10). doi:10.1172/jci.insight.80920

Blakely, A. M., Manning, K. L., Tripathi, A., & Morgan, J. R. (2015). Bio-Pick, Place, and Perfuse: A New Instrument for Three-Dimensional Tissue Engineering. *Tissue Eng Part C Methods, 21*(7), 737-746. doi:10.1089/ten.TEC.2014.0439

Blinova, K., Schocken, D., Patel, D., Daluwatte, C., Vicente, J., Wu, J. C., & Strauss, D. G. (2019). Clinical Trial in a Dish: Personalized Stem Cell-Derived Cardiomyocyte Assay Compared With Clinical Trial Results for Two QT-Prolonging Drugs. *Clin Transl Sci*. doi:10.1111/cts.12674

Bulanova, E. A., Koudan, E. V., Degosserie, J., Heymans, C., Pereira, F. D., Parfenov, V. A., . . . Mironov, V. A. (2017). Bioprinting of a functional vascularized mouse thyroid gland construct. *Biofabrication, 9*(3), 034105. doi:10.1088/1758-5090/aa7fdd

Bursac, N., Papadaki, M., Cohen, R. J., Schoen, F. J., Eisenberg, S. R., Carrier, R., . . . Freed, L. E. (1999). Cardiac muscle tissue engineering: toward an in vitro model for electrophysiological studies. *Am J Physiol, 277*(2), H433-444. doi:10.1152/ajpheart.1999.277.2.H433

Bursac, N., Parker, K. K., Iravanian, S., & Tung, L. (2002). Cardiomyocyte cultures with controlled macroscopic anisotropy: a model for functional electrophysiological studies of cardiac muscle. *Circ Res, 91*(12), e45-54.

Campbell, M., Chabria, M., Figtree, G. A., Polonchuk, L., & Gentile, C. (2018). Stem cell-derived cardiac spheroids as 3D in vitro models of the human heart microenvironment. In J. Walker (Ed.), *Methods in Molecular Biology* (2018/08/31 ed., pp. 1-9): Humana Press.

Campbell, M., Surija, L., Peceros, K., Sharma, P., Figtree, G., & Gentile, C. (2019). Stem cell spheroids. In R. L. Reis (Ed.), *Encyclopedia of Tissue Engineering and Regenerative Medicine* (pp. 387-393). Oxford: Academic Press.

Cashman, T. J., Josowitz, R., Johnson, B. V., Gelb, B. D., & Costa, K. D. (2016). Human Engineered Cardiac Tissues Created Using Induced Pluripotent Stem Cells Reveal Functional Characteristics of BRAF-Mediated Hypertrophic Cardiomyopathy. *PLoS One, 11*(1), e0146697. doi:10.1371/journal.pone.0146697

Chakravarty, T., Makkar, R. R., Ascheim, D. D., Traverse, J. H., Schatz, R., DeMaria, A., . . . Henry, T. D. (2017). ALLogeneic Heart STem Cells to Achieve Myocardial Regeneration (ALLSTAR) Trial: Rationale and Design. *Cell Transplant, 26*(2), 205-214. doi:10.3727/096368916x692933

Chen, L., Pan, Y., Zhang, L., Wang, Y., Weintraub, N., & Tang, Y. (2013). Two-step protocol for isolation and culture of cardiospheres. *Methods Mol Biol, 1036*, 75-80. doi:10.1007/978-1-62703-511-8_6

Chimenti, I., Gaetani, R., Forte, E., Angelini, F., De Falco, E., Zoccai, G. B., . . . Giacomello, A. (2014). Serum and supplement optimization for EU GMP-compliance in cardiospheres cell culture. *J Cell Mol Med, 18*(4), 624-634. doi:10.1111/jcmm.12210

Chimenti, I., Massai, D., Morbiducci, U., Beltrami, A. P., Pesce, M., & Messina, E. (2017). Stem Cell Spheroids and Ex Vivo Niche Modeling: Rationalization and Scaling-Up. *J Cardiovasc Transl Res, 10*(2), 150-166. doi:10.1007/s12265-017-9741-5

Davis, D. R., Zhang, Y., Smith, R. R., Cheng, K., Terrovitis, J., Malliaras, K., . . . Marbán, E. (2009). Validation of the cardiosphere method to culture cardiac progenitor cells from myocardial tissue. *PLoS One, 4*(9), e7195. doi:10.1371/journal.pone.0007195

DiMasi, J. A., Feldman, L., Seckler, A., & Wilson, A. (2010). Trends in Risks Associated With New Drug Development: Success Rates for Investigational Drugs. *Clinical Pharmacology & Therapeutics, 87*(3), 272-277. doi:10.1038/clpt.2009.295

Ebert, S. N., Taylor, D. G., Nguyen, H. L., Kodack, D. P., Beyers, R. J., Xu, Y., . . . French, B. A. (2007). Noninvasive tracking of cardiac embryonic stem cells in vivo using magnetic resonance imaging techniques. *Stem Cells, 25*(11), 2936-2944. doi:10.1634/stemcells.2007-0216

Eglen, R. M., & Reisine, T. (2019). Human iPS Cell-Derived Patient Tissues and 3D Cell Culture Part 2: Spheroids, Organoids, and Disease Modeling. *SLAS Technol, 24*(1), 18-27. doi:10.1177/2472630318803275

El-Battrawy, I., Albers, S., Cyganek, L., Zhao, Z., Lan, H., Li, X., . . . Akin, I. (2019). A cellular model of Brugada syndrome with SCN10A variants using human-induced pluripotent stem cell-derived cardiomyocytes. *Europace*. doi:10.1093/europace/euz122

Eschenhagen, T., Didie, M., Munzel, F., Schubert, P., Schneiderbanger, K., & Zimmermann, W. H. (2002). 3D engineered heart tissue for replacement therapy. *Basic Res Cardiol, 97 Suppl 1*, I146-152.

Figtree, G. A., Bubb, K. J., Tang, O., Kizana, E., & Gentile, C. (2017). Vascularized cardiac spheroids as novel 3D in vitro models to study cardiac fibrosis. *Cells Tissues Organs, 204*(3-4), 191-198. doi:10.1159/000477436

Forsythe, S. D., Devarasetty, M., Shupe, T., Bishop, C., Atala, A., Soker, S., & Skardal, A. (2018). Environmental Toxin Screening Using Human-Derived 3D Bioengineered Liver and Cardiac Organoids. *Front Public Health, 6*, 103. doi:10.3389/fpubh.2018.00103

Foty, R. (2011). A simple hanging drop cell culture protocol for generation of 3D spheroids. *J Vis Exp, 6*(51), 2720. doi:10.3791/2720

Freed, L. E., Langer, R., Martin, I., Pellis, N. R., & Vunjak-Novakovic, G. (1997). Tissue engineering of cartilage in space. *Proc Natl Acad Sci U S A, 94*(25), 13885-13890. doi:10.1073/pnas.94.25.13885

Frey, O., Misun, P. M., Fluri, D. A., Hengstler, J. G., & Hierlemann, A. (2014). Reconfigurable microfluidic hanging drop network for multi-tissue interaction and analysis. *Nat Commun, 5*, 4250. doi:10.1038/ncomms5250

Fu, C. Y., Tseng, S. Y., Yang, S. M., Hsu, L., Liu, C. H., & Chang, H. Y. (2014). A microfluidic chip with a U-shaped microstructure array for multicellular spheroid formation, culturing and analysis. *Biofabrication, 6*(1), 015009. doi:10.1088/1758-5082/6/1/015009

Gahwiler, B. H. (1999). Nerve cells in culture: the extraordinary discovery by Ross Granville Harrison. *Brain Res Bull, 50*(5-6), 343-344.

Gao, L., Gregorich, Z. R., Zhu, W., Mattapally, S., Oduk, Y., Lou, X., . . . Zhang, J. (2018). Large cardiac muscle patches engineered from human induced-pluripotent stem cell-derived cardiac cells improve recovery from myocardial infarction in swine. *Circulation, 137*(16), 1712-1730. doi:10.1161/circulationaha.117.030785

Gentile, C. (2016). Filling the gaps between the in vivo and in vitro microenvironment: engineering of spheroids for stem cell technology. *Curr Stem Cell Res Ther, 11*(8), 652-665.

Gettler, B. C., Zakhari, J. S., Gandhi, P. S., & Williams, S. K. (2017). Formation of Adipose Stromal Vascular Fraction Cell-Laden Spheroids Using a Three-Dimensional Bioprinter and Superhydrophobic Surfaces. *Tissue Eng Part C Methods, 23*(9), 516-524. doi:10.1089/ten.TEC.2017.0056

Goldfracht, I., Efraim, Y., Shinnawi, R., Kovalev, E., Huber, I., Gepstein, A., . . . Gepstein, L. (2019). Engineered heart tissue models from hiPSC-derived cardiomyocytes and cardiac ECM for disease modeling and drug testing applications. *Acta Biomater, 92*, 145-159. doi:10.1016/j.actbio.2019.05.016

Halbert, S. P., Bruderer, R., & Lin, T. M. (1971). In vitro organization of dissociated rat cardiac cells into beating three-dimensional structures. *J Exp Med, 133*(4), 677-695. doi:10.1084/jem.133.4.677

Hansen, A., Eder, A., Bonstrup, M., Flato, M., Mewe, M., Schaaf, S., . . . Eschenhagen, T. (2010). Development of a drug screening platform based on engineered heart tissue. *Circ Res, 107*(1), 35-44. doi:10.1161/circresaha.109.211458

Hookway, T. A., Butts, J. C., Lee, E., Tang, H., & McDevitt, T. C. (2016). Aggregate formation and suspension culture of human pluripotent stem cells and differentiated progeny. *Methods, 101*, 11-20. doi:10.1016/j.ymeth.2015.11.027

Huebsch, N., Loskill, P., Deveshwar, N., Spencer, C. I., Judge, L. M., Mandegar, M. A., . . . Conklin, B. R. (2016). Miniaturized iPS-Cell-Derived Cardiac Muscles for Physiologically Relevant Drug Response Analyses. *Sci Rep, 6*, 24726. doi:10.1038/srep24726

Itzhaki, I., Maizels, L., Huber, I., Zwi-Dantsis, L., Caspi, O., Winterstern, A., . . . Gepstein, L. (2011). Modelling the long QT syndrome with induced pluripotent stem cells. *Nature, 471*(7337), 225-229. doi:10.1038/nature09747

Jakab, K., Norotte, C., Damon, B., Marga, F., Neagu, A., Besch-Williford, C. L., . . . Forgacs, G. (2008). Tissue engineering by self-assembly of cells printed into topologically defined structures. *Tissue Eng Part A, 14*(3), 413-421. doi:10.1089/tea.2007.0173

Kalmykov, A., Huang, C., Bliley, J., Shiwarski, D., Tashman, J., Abdullah, A., . . . Cohen-Karni, T. (2019). Organ-on-e-chip: Three-dimensional self-rolled biosensor array for electrical interrogations of human electrogenic spheroids. *Sci Adv, 5*(8), eaax0729. doi:10.1126/sciadv.aax0729

Kang, C., Qiao, Y., Li, G., Baechle, K., Camelliti, P., Rentschler, S., & Efimov, I. R. (2016). Human Organotypic Cultured Cardiac Slices: New Platform For High Throughput Preclinical Human Trials. *Scientific Reports, 6*, 28798. doi:10.1038/srep28798

Kelm, J. M., & Fussenegger, M. (2004). Microscale tissue engineering using gravity-enforced cell assembly. *Trends Biotechnol, 22*(4), 195-202. doi:10.1016/j.tibtech.2004.02.002

Kempf, H., Olmer, R., Kropp, C., Ruckert, M., Jara-Avaca, M., Robles-Diaz, D., . . . Zweigerdt, R. (2014). Controlling expansion and cardiomyogenic differentiation of human pluripotent stem cells in scalable suspension culture. *Stem Cell Reports, 3*(6), 1132-1146. doi:10.1016/j.stemcr.2014.09.017

Khademhosseini, A., Eng, G., Yeh, J., Kucharczyk, P. A., Langer, R., Vunjak-Novakovic, G., & Radisic, M. (2007). Microfluidic patterning for fabrication of contractile cardiac organoids. *Biomedical Microdevices, 9*(2), 149-157. doi:10.1007/s10544-006-9013-7

Kim, T. Y., Kofron, C. M., King, M. E., Markes, A. R., Okundaye, A. O., Qu, Z., . . . Choi, B. R. (2018). Directed fusion of cardiac spheroids into larger heterocellular microtissues enables investigation of cardiac action potential propagation via cardiac fibroblasts. *PLoS One, 13*(5), e0196714. doi:10.1371/journal.pone.0196714

Kinney, M. A., Saeed, R., & McDevitt, T. C. (2012). Systematic analysis of embryonic stem cell differentiation in hydrodynamic environments with controlled embryoid body size. *Integr Biol (Camb), 4*(6), 641-650. doi:10.1039/c2ib00165a

Kobuszewska, A., Tomecka, E., Zukowski, K., Jastrzebska, E., Chudy, M., Dybko, A., . . . Brzozka, Z. (2017). Heart-on-a-Chip: An Investigation of the Influence of Static and Perfusion Conditions on Cardiac (H9C2) Cell Proliferation, Morphology, and Alignment. *SLAS Technol, 22*(5), 536-546. doi:10.1177/2472630317705610

Koudan, E. V., Korneva, J. V., Karalkin, P. A., Gladkaya, I. S., Gryadunova, A. A., Mironov, V. A., . . . Bulanova, E. A. (2017). The Scalable Standardized Biofabrication of Tissue Spheroids from Different Cell Types Using Nonadhesive Technology. *3D Printing and Additive Manufacturing, 4*(1), 53-60. doi:10.1089/3dp.2016.0044

Lee, T. J., Kang, S., Jeong, G. J., Yoon, J. K., Bhang, S. H., Oh, J., & Kim, B. S. (2015). Incorporation of gold-coated microspheres into embryoid body of human embryonic stem cells for cardiomyogenic differentiation. *Tissue Eng Part A, 21*(1-2), 374-381. doi:10.1089/ten.TEA.2014.0015

Leung, B. M., Lesher-Perez, S. C., Matsuoka, T., Moraes, C., & Takayama, S. (2015). Media additives to promote spheroid circularity and compactness in hanging drop platform. *Biomater Sci, 3*(2), 336-344. doi:10.1039/c4bm00319e

Li, Z., Mirams, G., Yoshinaga, T., Ridder, B., Han, X., Chen, J., Stockbridge, N., Wisialowski, T., Damiano, B., Severi, S., Morissette, P., Kowey, P., Holbrook, M., Smith, G., Rusmusson, R., Liu, M., Song, Z., Qu, Z., Leishman, D., Steidl-Nichols, J., Rodriguez, B., Bueno-Orovio, A., Zhou, X., Passini, E., Edwards, A., Morotti, S., Ni, H., Grandi, E., Clancy, C., Vandenberg, J., Hill, A., Nakamura, M., Singer, T., Polonchuk, L., Greiter-Wilke, A., Wang, K., Nave, S., Fullerton, A., Sobie, E., Paci, M., Musuamba, F.T.,, and Strauss, D. . (2019). General Principles for the Validation of Proarrhythmia Risk Prediction Models: an Extension of the CiPA In Silico Strategy. . *Clinical Pharmacology & Therapeutics*.

Lv, D., Hu, Z., Lu, L., Lu, H., & Xu, X. (2017). Three-dimensional cell culture: A powerful tool in tumor research and drug discovery. *Oncol Lett, 14*(6), 6999-7010. doi:10.3892/ol.2017.7134

Ma, Z., Huebsch, N., Koo, S., Mandegar, M. A., Siemons, B., Boggess, S., . . . Healy, K. E. (2018). Contractile deficits in engineered cardiac microtissues as a result of MYBPC3 deficiency and mechanical overload. *Nat Biomed Eng, 2*(12), 955-967. doi:10.1038/s41551-018-0280-4

MacQueen, L. A., Sheehy, S. P., Chantre, C. O., Zimmerman, J. F., Pasqualini, F. S., Liu, X., . . . Parker, K. K. (2018). A tissue-engineered scale model of the heart ventricle. *Nat Biomed Eng, 2*(12), 930-941. doi:10.1038/s41551-018-0271-5

Maizels, L., Huber, I., Arbel, G., Tijsen, A. J., Gepstein, A., Khoury, A., & Gepstein, L. (2017). Patient-Specific Drug Screening Using a Human Induced Pluripotent Stem Cell Model of Catecholaminergic Polymorphic Ventricular Tachycardia Type 2. *Circ Arrhythm Electrophysiol, 10*(6). doi:10.1161/circep.116.004725

Makkar, R. R., Smith, R. R., Cheng, K., Malliaras, K., Thomson, L. E., Berman, D., . . . Marban, E. (2012). Intracoronary cardiosphere-derived cells for heart regeneration after myocardial infarction (CADUCEUS): a prospective, randomised phase 1 trial. *Lancet, 379*(9819), 895-904. doi:10.1016/s0140-6736(12)60195-0

Maltsev, V. A., Wobus, A. M., Rohwedel, J., Bader, M., & Hescheler, J. (1994). Cardiomyocytes differentiated in vitro from embryonic stem cells developmentally express cardiac-specific genes and ionic currents. *Circ Res, 75*(2), 233-244.

Mathur, A., Loskill, P., Shao, K., Huebsch, N., Hong, S., Marcus, S. G., . . . Healy, K. E. (2015). Human iPSC-based cardiac microphysiological system for drug screening applications. *Sci Rep, 5*, 8883. doi:10.1038/srep08883

Mattapally, S., Zhu, W., Fast, V. G., Gao, L., Worley, C., Kannappan, R., . . . Zhang, J. (2018). Spheroids of cardiomyocytes derived from human-induced pluripotent stem cells improve recovery from myocardial injury in mice. *Am J Physiol Heart Circ Physiol, 315*(2), H327-h339. doi:10.1152/ajpheart.00688.2017

Mehesz, A. N., Brown, J., Hajdu, Z., Beaver, W., da Silva, J. V., Visconti, R. P., . . . Mironov, V. (2011). Scalable robotic biofabrication of tissue spheroids. *Biofabrication, 3*(2), 025002. doi:10.1088/1758-5082/3/2/025002

Menasché, P., Vanneaux, V., Hagege, A., Bel, A., Cholley, B., Cacciapuoti, I., . . . Larghero, J. (2015). Human embryonic stem cell-derived cardiac progenitors for severe heart failure treatment: first clinical case report. *Eur Heart J, 36*(30), 2011-2017. doi:10.1093/eurheartj/ehv189

Menasché, P., Vanneaux, V., Hagege, A., Bel, A., Cholley, B., Parouchev, A., . . . Larghero, J. (2018). Transplantation of human embryonic stem cell-derived cardiovascular progenitors for severe ischemic left ventricular dysfunction. *J Am Coll Cardiol, 71*(4), 429-438. doi:10.1016/j.jacc.2017.11.047

Messina, E., De Angelis, L., Frati, G., Morrone, S., Chimenti, S., Fiordaliso, F., . . . Giacomello, A. (2004). Isolation and expansion of adult cardiac stem cells from human and murine heart. *Circ Res, 95*(9), 911-921. doi:10.1161/01.Res.0000147315.71699.51

Mironov, V., Kasyanov, V., & Markwald, R. R. (2011). Organ printing: from bioprinter to organ biofabrication line. *Curr Opin Biotechnol, 22*(5), 667-673. doi:10.1016/j.copbio.2011.02.006

Mironov, V., Visconti, R. P., Kasyanov, V., Forgacs, G., Drake, C. J., & Markwald, R. R. (2009). Organ printing: tissue spheroids as building blocks. *Biomaterials, 30*(12), 2164-2174. doi:10.1016/j.biomaterials.2008.12.084

Moldovan, N. I., Hibino, N., & Nakayama, K. (2017). Principles of the Kenzan method for robotic cell spheroid-based three-dimensional bioprinting. *Tissue Eng Part B Rev, 23*(3), 237-244. doi:10.1089/ten.TEB.2016.0322

Mongkoldhumrongkul, N., Flanagan, J. M., & Jayasinghe, S. N. (2009). Direct jetting approaches for handling stem cells. *Biomed Mater, 4*(1), 015018. doi:10.1088/1748-6041/4/1/015018

Moscona, A., & Moscona, H. (1952). The dissociation and aggregation of cells from organ rudiments of the early chick embryo. *J Anat, 86*(3), 287-301.

Moya, M., Tran, D., & George, S. C. (2013). An integrated in vitro model of perfused tumor and cardiac tissue. *Stem Cell Res Ther, 4 Suppl 1*, S15. doi:10.1186/scrt376

Munarin, F., & Coulombe, K. L. (2015). A novel 3-dimensional approach for cardiac regeneration. *Conf Proc IEEE Eng Med Biol Soc, 2015*, 1741-1744. doi:10.1109/embc.2015.7318714

Neto, A. I., Correia, C. R., Oliveira, M. B., Rial-Hermida, M. I., Alvarez-Lorenzo, C., Reis, R. L., & Mano, J. F. (2015). A novel hanging spherical drop system for the generation of cellular spheroids and high throughput combinatorial drug screening. *Biomater Sci, 3*(4), 581-585. doi:10.1039/c4bm00411f

Nguyen, D. C., Hookway, T. A., Wu, Q., Jha, R., Preininger, M. K., Chen, X., . . . Xu, C. (2014). Microscale generation of cardiospheres promotes robust enrichment of cardiomyocytes derived from human pluripotent stem cells. *Stem Cell Reports, 3*(2), 260-268. doi:10.1016/j.stemcr.2014.06.002

Noguchi, R., Nakayama, K., Itoh, M., Kamohara, K., Furukawa, K., Oyama, J., . . . Morita, S. (2016). Development of a three-dimensional pre-vascularized scaffold-free contractile cardiac patch for treating heart disease. *J Heart Lung Transplant, 35*(1), 137-145. doi:10.1016/j.healun.2015.06.001

Oliveira, M. B., Neto, A. I., Correia, C. R., Rial-Hermida, M. I., Alvarez-Lorenzo, C., & Mano, J. F. (2014). Superhydrophobic chips for cell spheroids high-throughput generation and drug screening. *ACS Appl Mater Interfaces, 6*(12), 9488-9495. doi:10.1021/am5018607

Ong, C. S., Fukunishi, T., Nashed, A., Blazeski, A., Zhang, H., Hardy, S., . . . Hibino, N. (2017). Creation of Cardiac Tissue Exhibiting Mechanical Integration of Spheroids Using 3D Bioprinting. *J Vis Exp*(125). doi:10.3791/55438

Osidak, E. O., Karalkin, P. A., Osidak, M. S., Parfenov, V. A., Sivogrivov, D. E., Pereira, F., . . . Domogatsky, S. P. (2019). Viscoll collagen solution as a novel bioink for direct 3D bioprinting. *J Mater Sci Mater Med, 30*(3), 31. doi:10.1007/s10856-019-6233-y

Parfenov, V. A., Koudan, E. V., Bulanova, E. A., Karalkin, P. A., F, D. A. S. P., Norkin, N. E., . . . Mironov, V. A. (2018). Scaffold-free, label-free and nozzle-free biofabrication technology using magnetic levitational assembly. *Biofabrication, 10*(3), 034104. doi:10.1088/1758-5090/aac900

Paul, S. M., Mytelka, D. S., Dunwiddie, C. T., Persinger, C. C., Munos, B. H., Lindborg, S. R., & Schacht, A. L. (2010). How to improve R&D productivity: the pharmaceutical industry's grand challenge. *Nature Reviews Drug Discovery, 9*, 203. doi:10.1038/nrd3078

Polonchuk, L., Chabria, M., Badi, L., Hoflack, J. C., Figtree, G., Davies, M. J., & Gentile, C. (2017). Cardiac spheroids as promising in vitro models to study the human heart microenvironment. *Sci Rep, 7*(1), 7005. doi:10.1038/s41598-017-06385-8

Qian, F., Huang, C., Lin, Y. D., Ivanovskaya, A. N., O'Hara, T. J., Booth, R. H., . . . Wheeler, E. K. (2017). Simultaneous electrical recording of cardiac electrophysiology and contraction on chip. *Lab Chip, 17*(10), 1732-1739. doi:10.1039/c7lc00210f

Qureshi, Z. P., Seoane-Vazquez, E., Rodriguez-Monguio, R., Stevenson, K. B., & Szeinbach, S. L. (2011). Market withdrawal of new molecular entities approved in the United States from 1980 to 2009. *Pharmacoepidemiol Drug Saf, 20*(7), 772-777. doi:10.1002/pds.2155

Schlick, S. F., Spreckelsen, F., Tiburcy, M., Iyer, L. M., Meyer, T., Zelarayan, L. C., . . . Rehfeldt, F. (2019). Agonistic and antagonistic roles of fibroblasts and cardiomyocytes on viscoelastic stiffening of engineered human myocardium. *Prog Biophys Mol Biol, 144*, 51-60. doi:10.1016/j.pbiomolbio.2018.11.011

Sirenko, O., Hancock, M. K., Crittenden, C., Hammer, M., Keating, S., Carlson, C. B., & Chandy, G. (2017). Phenotypic Assays for Characterizing Compound Effects on Induced Pluripotent Stem Cell-Derived Cardiac Spheroids. *Assay Drug Dev Technol, 15*(6), 280-296. doi:10.1089/adt.2017.792

Smith, R. R., Barile, L., Cho, H. C., Leppo, M. K., Hare, J. M., Messina, E., . . . Marban, E. (2007). Regenerative potential of cardiosphere-derived cells expanded from percutaneous endomyocardial biopsy specimens. *Circulation, 115*(7), 896-908. doi:10.1161/circulationaha.106.655209

Sperelakis, N. (1978). Cultured heart cell reaggregate model for studying cardiac toxicology. *Environ Health Perspect, 26*, 243-267. doi:10.1289/ehp.7826243

Stoehr, A., Neuber, C., Baldauf, C., Vollert, I., Friedrich, F. W., Flenner, F., . . . Hansen, A. (2014). Automated analysis of contractile force and Ca2+ transients in engineered heart tissue.

American journal of physiology. Heart and circulatory physiology, 306(9), H1353-H1363. doi:10.1152/ajpheart.00705.2013

Takahashi, K., & Yamanaka, S. (2006). Induction of pluripotent stem cells from mouse embryonic and adult fibroblast cultures by defined factors. *Cell, 126*(4), 663-676. doi:10.1016/j.cell.2006.07.024

Taylor, M., Jefferies, J., Byrne, B., Lima, J., Ambale-Venkatesh, B., Ostovaneh, M. R., . . . Victor, R. G. (2019). Cardiac and skeletal muscle effects in the randomized HOPE-Duchenne trial. *Neurology, 92*(8), e866-e878. doi:10.1212/WNL.0000000000006950

Tiburcy, M., Hudson, J. E., Balfanz, P., Schlick, S., Meyer, T., Chang Liao, M. L., . . . Zimmermann, W. H. (2017). Defined Engineered Human Myocardium With Advanced Maturation for Applications in Heart Failure Modeling and Repair. *Circulation, 135*(19), 1832-1847. doi:10.1161/circulationaha.116.024145

Tiburcy, M., Meyer, T., Soong, P. L., & Zimmermann, W. H. (2014). Collagen-based engineered heart muscle. *Methods Mol Biol, 1181*, 167-176. doi:10.1007/978-1-4939-1047-2_15

Tomlinson, L., Lu, Z. Q., Bentley, R. A., Colley, H. E., Murdoch, C., Webb, S. D., . . . Sharma, P. (2019). Attenuation of doxorubicin-induced cardiotoxicity in a human in vitro cardiac model by the induction of the NRF-2 pathway. *Biomed Pharmacother, 112*, 108637. doi:10.1016/j.biopha.2019.108637

Tseliou, E., Pollan, S., Malliaras, K., Terrovitis, J., Sun, B., Galang, G., . . . Marbán, E. (2013). Allogeneic Cardiospheres Safely Boost Cardiac Function and Attenuate Adverse Remodeling After Myocardial Infarction in Immunologically Mismatched Rat Strains. *Journal of the American College of Cardiology, 61*(10), 1108-1119. doi:https://doi.org/10.1016/j.jacc.2012.10.052

Tung, Y. C., Hsiao, A. Y., Allen, S. G., Torisawa, Y. S., Ho, M., & Takayama, S. (2011). High-throughput 3D spheroid culture and drug testing using a 384 hanging drop array. *Analyst, 136*(3), 473-478. doi:10.1039/c0an00609b

Vadivelu, R. K., Kamble, H., Shiddiky, M. J. A., & Nguyen, N.-T. (2017). Microfluidic Technology for the Generation of Cell Spheroids and Their Applications. *Micromachines, 8*(4), 94. doi:10.3390/mi8040094

Visone, R., Ugolini, G. S., Vinarsky, V., Penati, M., Redaelli, A., Forte, G., & Rasponi, M. (2019). A Simple Vacuum-Based Microfluidic Technique to Establish High-Throughput Organs-On-Chip and 3D Cell Cultures at the Microscale. *Advanced Materials Technologies, 4*(1), 1800319. doi:10.1002/admt.201800319

Wobus, A. M., Wallukat, G., & Hescheler, J. (1991). Pluripotent mouse embryonic stem cells are able to differentiate into cardiomyocytes expressing chronotropic responses to adrenergic and cholinergic agents and Ca2+ channel blockers. *Differentiation, 48*(3), 173-182.

Wu, P. H., Giri, A., Sun, S. X., & Wirtz, D. (2014). Three-dimensional cell migration does not follow a random walk. *Proc Natl Acad Sci U S A, 111*(11), 3949-3954. doi:10.1073/pnas.1318967111

Yang, B., Lui, C., Yeung, E., Matsushita, H., Jeyaram, A., Pitaktong, I., . . . Hibino, N. (2019). A net mold-based method of biomaterial-free three-dimensional cardiac tissue creation. *Tissue Eng Part C Methods, 25*(4), 243-252. doi:10.1089/ten.TEC.2019.0003

Yechiel, E., & Barenholz, Y. (1986). Cultured heart cell reaggregates: a model for studying relationships between aging and lipid composition. *Biochim Biophys Acta, 859*(1), 105-109. doi:10.1016/0005-2736(86)90323-8

Yee, K., Malliaras, K., Kanazawa, H., Tseliou, E., Cheng, K., Luthringer, D. J., . . . Marbán, E. (2014). Allogeneic cardiospheres delivered via percutaneous transendocardial injection increase viable myocardium, decrease scar size, and attenuate cardiac dilatation in porcine ischemic cardiomyopathy. *PloS one, 9*(12), e113805-e113805. doi:10.1371/journal.pone.0113805

Yoshioka, N., & Dowdy, S. F. (2017). Enhanced generation of iPSCs from older adult human cells by a synthetic five-factor self-replicative RNA. *PLoS One, 12*(7), e0182018. doi:10.1371/journal.pone.0182018

Yoshioka, N., Gros, E., Li, H. R., Kumar, S., Deacon, D. C., Maron, C., . . . Dowdy, S. F. (2013). Efficient generation of human iPSCs by a synthetic self-replicative RNA. *Cell Stem Cell, 13*(2), 246-254. doi:10.1016/j.stem.2013.06.001

Zhao, H., Chen, Y., Shao, L., Xie, M., Nie, J., Qiu, J., . . . He, Y. (2018). Airflow-Assisted 3D Bioprinting of Human Heterogeneous Microspheroidal Organoids with Microfluidic Nozzle. *Small, 14*(39), e1802630. doi:10.1002/smll.201802630

Zhao, Y., Rafatian, N., Feric, N. T., Cox, B. J., Aschar-Sobbi, R., Wang, E. Y., . . . Radisic, M. (2019). A Platform for Generation of Chamber-Specific Cardiac Tissues and Disease Modeling. *Cell, 176*(4), 913-927.e918. doi:https://doi.org/10.1016/j.cell.2018.11.042

Zimmermann, W. H., Schneiderbanger, K., Schubert, P., Didie, M., Munzel, F., Heubach, J. F., . . . Eschenhagen, T. (2002). Tissue engineering of a differentiated cardiac muscle construct. *Circ Res, 90*(2), 223-230.

1.5 – Closing remarks to Part 1

The three literature reviews conducted within this section examined the current challenges for the field of myocardial regeneration (1.2), presented a snapshot of preclinical approaches to patch-based myocardial repair strategies (1.3) and explored cardiac spheroids in terms of current methods of generation and applications of these microtissues to date (1.4).

The challenges identified in our surgical narrative review (1.2) included the known challenges of how to bioengineer patches with a hierarchical vascular tree and how to promote contractile function (with patches integrating and contracting with host tissue). It also uncovered critical considerations to do with the practical aspects of translating these patches to the clinic. Specifically, how to transplant them, which might need methods of transplantation other than via open traditional surgery. For the purposes of this thesis, this sowed the seeds which led to the invention of surgical minimally invasive robotic transplantation instruments (3.1 and 3.2).

Further exploring the question of how to create an optimal environment for patches to integrate with host tissue, our narrative review (1.2) uncovered a surgical proposal to reinforce patches by sandwiching them between host epicardium and the omentum. This had not been fully explored before, so when we ran our systematic scoping review (1.3) for a snapshot of the literature, we added the criterion that studies returned by our search terms had to use a pedicled omental flap to reinforce the various bioengineered patches employed by the studies we captured in our search. For the first time, we collated studies which reinforced their patches with the omentum, still attached to its original blood supply (the gastroepiploic artery). We found that omentum support seemed to benefit patch-based repair strategies. A future direction of the work contained in this thesis is to perform our *in vivo* experiment detailed in Chapter 2.4 (for which we used a mouse model of MI) in a large animal model (sheep or pig). For that future study, based on our systematic scoping review, it would be beneficial to secure transplanted patches under a pedicled omental flap (rather than the pericardium).

Also borne out of Chapter 1.2 (where we identified current challenges for the field), we identified that the mechanisms underlying the reproducible benefit of epicardial patch transplantation are not understood. In fact, it might be that inducing and/or modulating host acute inflammation is one of the main mechanisms by which this strategy seems to work. This is critical, because it calls into question whether direct cell replenishment, mechanical reinforcement, or even vascularisation and contractility are not completely aligned with why patches seem to work. If it turns out that inflammation is desirable, it also calls into question the strategy of using patient-specific induced pluripotent stem cell (iPSC)-derived cells. Patient-specific patches could be generated by reprogramming cells (such as from a skin biopsy) into iPSCs and then stimulating them to become, for example, cardiomyocytes. In theory, patches could be generated which were an exact immunocompatible match to the patient from whom the original skin sample was taken. This sounds appealing, with no need for immune suppression to prevent patch rejection, but if inflammation is actually a desirable outcome of patch contact with underlying host tissue, then this whole strategy is called into question. This is especially important when the relative difficulty of protocols to generate such a patient-specific cardiac patch is taken into account. If a synthetic material can achieve the same result because the mechanism is induction of underlying inflammation, then pursuit of patient-specific patches may be the wrong approach. Having uncovered these complex considerations for the field, we took steps to provide some clues about the underlying mechanism, such as performing immune cell analysis of tissue samples by flow cytometry (Chapter 2.4, Figure 6), transcriptome (mRNA) analysis (2.4, Figure 7) and ensuring we had robust control groups for our *in vivo* experiment to include a control treatment group with hydrogel patches without cells (2.4).

Finally, we performed a thorough evaluation of vascularised cardiac spheroids written as a book chapter (1.4). We hypothesised that 3D bioprinted heart patches would promote myocardial function after MI, and within this we utilised VCS within our patches. This novel approach aimed to maximse the success of our patches by pre-culturing cardiac cells in 3D (rather than merely suspending them in hydrogel as "free" cells). Therefore, it was important to fully understand what these VCS are, how they are generated and what applications they have been used for previously. Our chapter revealed a very diverse range of methods to generate spheroids, of which hanging drop cultures was one technique (and the one we selected for our experiments contained in the rest of this thesis). We also found a diverse range of applications, including disease modelling and high-throughput testing of drug effects in 3D (as opposed to monolayer).

Overall, this thesis introduction contains three useful articles which provide an essential understanding on which the rest of the thesis is based. Each of the articles in the introduction (1.2, 1.3, 1.4) consolidated knowledge which had not previously been presented in review form in the biomedical literature. In particular, the cardiac surgeon's perspective for bioengineering heart patches was emphasised, including the need for mechanistic understanding and practical considerations for translatability to the operating theatre. The findings of these introductory review articles therefore shaped the thesis and its aims significantly, perhaps most notably with the addition of Part 3 (surgical instruments to transplant patches). The surgical instrument inventions had not been considered at the outset of the project (the original aims were to be addressed in full by the three chapters of Part 2). This filled a particular gap which had not been addressed, of how to transplant patches in future. Therefore, our aims by which we planned to evaluate our hypothesis were refined as:

Aim 1 – to optimise heart patches for cardiac transplantation.

Aim 2 – to evaluate host cardiac functional and structural outcomes *in vivo* in mice modelling MI.

Aim 3 – to invent robotic minimally invasive surgical instruments to transplant patches to the heart.

PART 2 – HEART PATCHES FOR MYOCARDIAL REGENERATION

2.1 – Introduction and relevance to Part 2

To evaluate our hypothesis that 3D bioprinted heart patches would improve cardiac function after MI, we began with Aim 1:

To optimise heart patches for transplantation.

The *ex vivo* work to fully evaluate and optimise patches intended to maximise the chances of success of the patches. This work forms the basis of Chapter 2.2.

We performed an analysis primarily of the following characteristics of patches:

- Printability (which can be thought of as the "ease" with which patches can be 3D bioprinted)
- Durability (how long the patches last for in culture before disintegration begins and therefore when the optimal moment to transplant patches is)
- Contractility (do the patches allow for cardiomyocytes to make connections and become contractile as a whole)
- Vascularisation (can endothelial cells form vasculature within patches)

We found that printability could easily be assessed by bioprinting a grid and analysing how well the method was able to preserve the grid pattern. We found that the optimal time to transplant before disintegration was by about 14 days, patches were able to become contractile (they started to "beat" by about 14 days as well) and endothelial cells "self-organised" into primitive networks within patches. We added novel data about hydrogel composition and compared 3D bioprinting systems themselves. As a result of this ex vivo optimisation, aim 1 was achieved and patches were optimised for transplantation.

The other critical component of successful transplantation is, of course, the surgical transplantation method. We published our surgical patch transplant method and detailed it in Chapter 2.3. We selected a mouse model, which is unusual as it is smaller than other models, but we proved that it can be used (2.3 and 2.4). This opens up the model for future studies and it has distinct advantages in terms of feasibility and high throughput testing where multiple repeats are necessary. Our video method (2.3) provides the full step-by-step reproducible method and materials list for patch transplantation in mice modelling MI. This completely satisfied our Aim 1 by ensuring the surgical procedure was optimised alongside the patches themselves.

Moving on to Aim 2 (to evaluate host cardiac functional and structural outcomes *in vivo* in mice modelling MI), we addressed this in full with Chapter 2.4 (the in vivo study with systematic analyses of the outcomes of transplanting patches in mice with MI). The multiple analyses of this study provide data on 1) functional outcomes using echocardiography; 2) Electrical activity outcomes using 64-electrode isochondral electrical mapping; 3) Structural analysis including the infarct sizes for each experimental group on histology; 4) WBC analyses to look for inflammation-based mechanistic insights using flow cytometry and 5) mRNA analyses to look for transcriptomic mechanistic insights of changes in the mRNA gene expression of each of our experimental groups. We also analysed patches themselves and the effect of the method on mice in terms of mortality. As some studies have included sham control groups of n=1 (Wang et al., 2021), we were careful to fully evaluate the effect of a sham procedure and found that the procedure itself (heart surgery in mice without MI or treatment) could

result in significant variability in functional outcomes. We were also therefore able to compared treatment groups to “healthy” (i.e. non-infarcted) mice and this led to the interesting finding that the transcriptomic profile of our VCS group was similar to sham which was not the case in other treatment groups. We took care to include a hydrogel only (without cells) patch treatment group so that conclusions could be drawn about the role of foreign patch material as opposed to cells themselves. We also used a control group for freely suspended cells (not in spheroids) so that we could speculate about the beneficial effect of pre-culturing cells as 3D microtissues before using them to bioprint patches. Overall, the experiment contained in Chapter 2.4 presents a very detailed spectrum of analyses. In addressing our Aim 2, this chapter (2.4) satisfies both the functional and structural analysis components critical to evaluating the performance of patches *in vivo*.

2.2 – Printability, durability, contractility and vascular network formation in 3D bioprinted cardiac endothelial cells using alginate-gelatin hydrogels

Summary:

The *in vitro* research presented in this article was published in *Frontiers in Bioengineering and Biotechnology*. The article represents the optimisation work to optimise patches for the *in vivo* applications detailed later in this thesis. The article has an emphasis on printability (which can be thought of as the overall "ease" of bioprinting a patch) and durability (answering the question of how durable patches are in culture and when the optimal moment is to transplant them before they lose their integrity). Given that "printability" is difficult to quantify, we invented a simple, novel way to compare printability parameters between different hydrogels (counting the preservation of squares in a grid). It was not previously known whether the bioprinting system itself would influence printability or durability outcomes so we tested three different 3D bioprinting systems and found that there was no significant difference. For durability, we determined the optimum moment to transplant was between day 7 and 14 in culture (when patches started to show contractile activity but before they started to disintegrate). For a commercial partner, ROKIT (Seoul, South Korea), we tested their fibroblast-derived extracellular matrix hydrogel (AlloECM) and found that it could not be mixed with alginate-gelatin (in fact, in every case it caused complete disintegration of patches within 24 hours). The highlight of this paper is our 3D rendering video of a self-organised endothelial cell network (visualised using Imaris software from confocal micrographic data). We showed that endothelial cells "self-organised" into endothelial cell networks when allowed to culture in an incubator for up to 28 days.

frontiers in Bioengineering and Biotechnology

ORIGINAL RESEARCH
published: 26 February 2021
doi: 10.3389/fbioe.2021.636257

Printability, Durability, Contractility and Vascular Network Formation in 3D Bioprinted Cardiac Endothelial Cells Using Alginate–Gelatin Hydrogels

*Christopher David Roche[1,2], Poonam Sharma[1,2,3], Anthony Wayne Ashton[1], Chris Jackson[1], Meilang Xue[1] and Carmine Gentile[1,2]**

[1] Northern Clinical School, Faculty of Medicine and Health, The University of Sydney, Sydney, NSW, Australia, [2] School of Biomedical Engineering, Faculty of Engineering and IT, University of Technology Sydney, Sydney, NSW, Australia, [3] Faculty of Health and Medicine, The University of Newcastle, Callaghan, NSW, Australia

Background: 3D bioprinting cardiac patches for epicardial transplantation are a promising approach for myocardial regeneration. Challenges remain such as quantifying printability, determining the ideal moment to transplant, and promoting vascularisation within bioprinted patches. We aimed to evaluate 3D bioprinted cardiac patches for printability, durability in culture, cell viability, and endothelial cell structural self-organisation into networks.

Methods: We evaluated 3D-bioprinted double-layer patches using alginate/gelatine (AlgGel) hydrogels and three extrusion bioprinters (REGEMAT3D, INVIVO, BIO X). Bioink contained either neonatal mouse cardiac cell spheroids or free (not-in-spheroid) human coronary artery endothelial cells with fibroblasts, mixed with AlgGel. To test the effects on durability, some patches were bioprinted as a single layer only, cultured under minimal movement conditions or had added fibroblast-derived extracellular matrix hydrogel (AlloECM). Controls included acellular AlgGel and gelatin methacryloyl (GELMA) patches.

Results: Printability was similar across bioprinters. For AlgGel compared to GELMA: resolutions were similar (200–700 μm line diameters), printing accuracy was 45 and 25%, respectively (AlgGel was 1.7x more accurate; $p < 0.05$), and shape fidelity was 92% (AlgGel) and 96% (GELMA); $p = 0.36$. For durability, AlgGel patch median survival in culture was 14 days (IQR:10–27) overall which was not significantly affected by bioprinting system or cellular content in patches. We identified three factors which reduced durability in culture: (1) bioprinting one layer depth patches (instead of two layers); (2) movement disturbance to patches in media; and (3) the addition of AlloECM to AlgGel. Cells were viable after bioprinting followed by 28 days in culture, and all BIO X-bioprinted mouse cardiac cell spheroid patches presented contractile activity starting between day 7 and 13 after bioprinting. At day 28, endothelial cells in hydrogel displayed organisation into endothelial network-like structures.

Conclusion: AlgGel-based 3D bioprinted heart patches permit cardiomyocyte contractility and endothelial cell structural self-organisation. After bioprinting, a period of 2 weeks maturation in culture prior to transplantation may be optimal, allowing for a

OPEN ACCESS

Edited by:
João Conde,
New University of Lisbon, Portugal

Reviewed by:
PaYaM ZarrinTaj,
Oklahoma State University,
United States
Heungsoo Shin,
Hanyang University, South Korea

***Correspondence:**
Carmine Gentile
carmine.gentile@uts.edu.au

Specialty section:
This article was submitted to Biomaterials, a section of the journal Frontiers in Bioengineering and Biotechnology

Received: 01 December 2020
Accepted: 01 February 2021
Published: 26 February 2021

Citation:
Roche CD, Sharma P, Ashton AW, Jackson C, Xue M and Gentile C (2021) Printability, Durability, Contractility and Vascular Network Formation in 3D Bioprinted Cardiac Endothelial Cells Using Alginate–Gelatin Hydrogels. Front. Bioeng. Biotechnol. 9:636257. doi: 10.3389/fbioe.2021.636257

degree of tissue maturation but before many patches start to lose integrity. We quantify AlgGel printability and present novel factors which reduce AlgGel patch durability (layer number, movement, and the addition of AlloECM) and factors which had minimal effect on durability (bioprinting system and cellular patch content).

Keywords: 3D bioprinting, spheroids, hydrogel, bioink, durability, printability, alginate, gelatin

INTRODUCTION

The latest developments in three-dimensional (3D) bioprinting technology have led to the hope that viable 3D bioprinted cardiac tissues could be generated to promote myocardial regeneration (Noor et al., 2019; Roche et al., 2020). Extrusion 3D bioprinters have been widely used as a versatile tool to deposit different cells as 'bio-inks' to generate complex 3D tissues, including cardiac tissues (Zhang et al., 2016; Ong et al., 2017a; Maiullari et al., 2018; Noor et al., 2019). This technology promises a safe, precise, automatable and cost-effective method to generate myocardial tissue (Noor et al., 2019; Roche et al., 2020). Extrusion 3D-bioprinters using cell-permissive pressures can extrude myocardial cells without prohibiting their ability to live, mature and function in a physiological environment (Blaeser et al., 2016). These 3D bioprinters extrude bioinks which can be made from hydrogels (Cattelan et al., 2020; Roche et al., 2020).

The bioink formulation is critical to determine printability (a function of the bioink's rheological properties which determines how it interacts with the bioprinting process) which is important for bioprinting without damaging the end bioprinted product (Cattelan et al., 2020; Gillispie et al., 2020). After bioprinting, the tissue can be cultured to allow for a period of tissue maturation before transplantation (Roche and Gentile, 2020). During this post-printing phase, the bioink can promote tissue maturation, with durability in culture being an important characteristic to predict hydrogel disintegration (Bishop et al., 2017; Roche and Gentile, 2020), although the optimal moment to transplant after a period in culture has not previously been confirmed. During this phase, cardiomyocyte contractility should be permitted and endothelial cells within the bioprinted tissue should be permitted to organise into networks, as one of the major challenges in 3D bioprinting of cardiac tissues is the fabrication of a hierarchical vascular system within tissues (Gentile, 2016; Ong et al., 2017b; Polonchuk et al., 2017; Cui et al., 2019; Polley et al., 2020; Roche et al., 2020; Xu et al., 2020).

Here, we present a promising approach to generate 3D bioprinted cardiac patches presenting a structural endothelial cell network using alginate/gelatin (AlgGel) hydrogels – a mix of alginate (to provide an ionically cross-linkable structure for cellular patches) and gelatin (to adapt the alginate for extrusion 3D bioprinting, control rheological properties by varying the gelatin concentration and generate a bioactive hybrid hydrogel). The versatility of AlgGel hydrogels is established

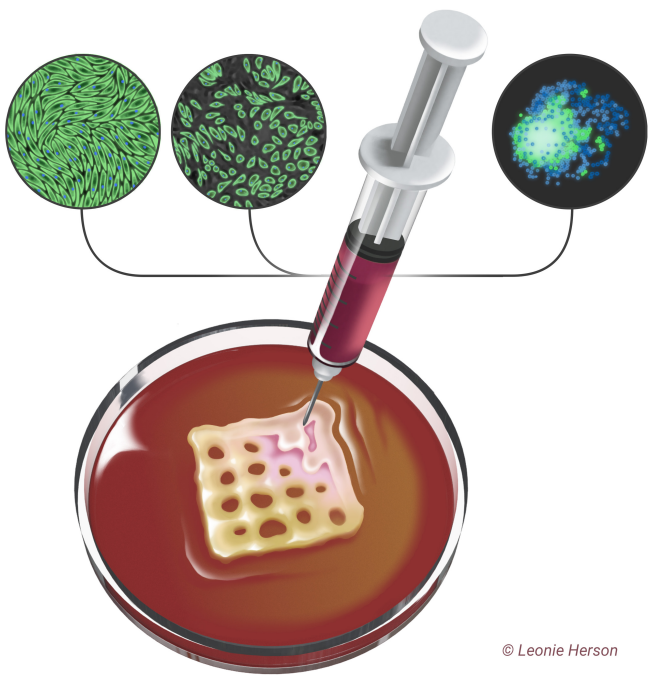

GRAPHICAL ABSTRACT |

(Mancha Sánchez et al., 2020), balancing printability against durability characteristics in culture, whilst also permitting cardiomyocyte contractility and endothelial cell network formation. The extent to which vascular networks are able to self-assemble within patches is closely linked to several other characteristics: 1) printability (for instance, with poor printability, control of patch morphology is undermined); 2) durability (if patches disintegrate too quickly in culture then there would be no patch to host a vascular network); 3) cell viability (since survival of cells, including endothelial and other cell types, is critical); and 4) contractility must be permitted (patches which inhibit contractility of cardiomyocytes will be less suitable for co-culture with contractile cells) (Roche et al., 2020).

We hypothesised that 3D bioprinted endothelial cells can self-organise into structural vascular networks using our approach.

In testing this hypothesis, we aimed to demonstrate that even a low starting density of endothelial cells will self-organise into structural networks within 3D bioprinted patches. In this study we report on printability, durability, cell viability and endothelial cell network formation for 3D bioprinted endothelial cells in AlgGel hydrogels. Our study aims at providing new insights which may overcome common challenges in the field of bioprinting of cardiac tissues for *in vitro* and *in vivo* applications (Roche et al., 2020). The major finding of our study is that the bioprinted patches generated by using our approach present endothelial cell networks, durable structure and contractile function between 14 and 28 days in culture. Our findings have the potential to directly translate *in vitro* testing of bioprinted cardiac patches for *in vivo* applications for cardiac regeneration (Roche and Gentile, 2020).

MATERIALS AND METHODS

All procedures described in this experiment were approved by the Animal Ethics Committee at the Northern Sydney Local Health District (project number RESP17/55; 20/04/2017). Full methodological details are included in the **Supplementary Materials**.

Cultures of Human Coronary Artery Endothelial Cells With Fibroblasts

Human coronary artery endothelial cells (HCAECs) (Sigma-Aldrich, MO, United States) were cultured in MesoEndo Growth Medium (Cell Applications, San Diego, CA, United States). Human dermal fibroblasts (HDFs) (Sigma-Aldrich, MO, United States) were cultured in Dulbecco's Modified Eagle Medium (DMEM, Sigma-Aldrich, St Louis, MO, United States) with added 10% (v/v) FBS + 1% (v/v) pen/strep + 1% (v/v) L-glutamine. Cells were used for bioprinting between passage four and five.

Vascularised Cardiac Spheroid Formation From Mouse Cardiac Cells

Mouse hearts were isolated from neonatal C57Bl/6 mice (1–5 days old), diced into 0.1–0.2 mm pieces and enzymatically digested with the Miltenyi Biotec (Bergisch Gladbach, Germany) neonatal heart dissociation kit according to the manufacturer's instructions. Isolated cells (cardiac cell types present in a whole heart, including myocytes, endothelial cells, and fibroblasts) were suspended in DMEM + 10% (v/v) FBS + 1% (v/v) pen/strep + 1% (v/v) L-glutamine. VCSs were generated by coculturing ∼4000 mouse cardiac cells (immediately after their isolation) in 15 μl hanging drop cultures containing DMEM + 10% (v/v) FBS + 1% (v/v) pen/strep + 1% (v/v) L-glutamine, using Perfecta 3D® 384-well hanging drop plates (3D Biomatrix, Ann Arbor, MI, United States). Spheroids were allowed to form for up to five days in hanging drops in a humidified incubator at 37°C with 20% (v/v) O_2 and 5% (v/v) CO_2. Additional complete DMEM (7 μl) was added to each hanging drop on day three. VCSs were collected and the resulting spheroid suspension was centrifuged at 300 g for 5 mins in a 50 ml Falcon tube. The resulting VCS pellet was ready for direct mixing with hydrogel to create bioink.

Hydrogel Preparation

To prepare the alginate and gelatin (AlgGel) hydrogel 4 mg alginate and 8 mg gelatin powder was sterilised under UV light for 30 min, solubilised at 50°C in 100 ml DMEM + 10% (v/v) FBS + 1% (v/v) pen/strep + 1% (v/v) L-glut. The mixture was then either stored at 4°C or used for bioink immediately after. AlloECM hydrogel (AlloECM®, ROKIT, Seoul, South Korea) was prepared by adding AlloECM powder to AlgGel hydrogel at 5 and 30 mg/ml. The AlloECM-AlgGel was resuspended and mixed thoroughly in a Falcon tube at room temperature, warmed to 37°C in a water bath and then was used immediately for bioprinting. Gelatin-methacryloyl (GelMA) 10% w/v + lithium phenyl-2,4,6-trimethylbenzoylphosphinate (LAP) 0.25% (w/v) in HEPES buffer in light-blocking pneumatic 3 ml syringes was purchased (product no. IK305202, CELLINK Life Sciences, Boston, MA, United States) for use without cells as a printability and durability control hydrogel.

Generation of Bioinks

To create bioinks for bioprinting, hydrogels were added to pellets of either mouse cardiac cell spheroids or a mixture of HCAECs and HDFs (2:1), obtained as described above. 1.5 ml prewarmed (37°C) hydrogel was added to the cell pellet by pipette, of which 0.5 ml typically produced six 10 mm^2 patches. Each patch contained either ∼20,000 HCAECS and ∼10,000 HDFs, or ∼160,000 mouse cardiac cells (∼40 spheroids/patch). The hydrogel was resuspended until the cell pellet disappeared to ensure incorporation of most of the cells. All procedures were performed under a biological safety cabinet for the REGEMAT3D bioprinter. For the *INVIVO* and BIO X bioprinters (which have their own UV steriliser and hepafilter) this was performed within the bioprinting chamber itself.

3D Bioprinting

Bioprinting was performed as fully described in the **Supplementary Materials** (including preparation, parameter setting and bioprinting processes for the three bioprinters). AlgGel was ionically crosslinked by adding $CaCl_2$ after bioprinting of all the patches in one six-well plate. GelMA

was photo-crosslinked immediately after each patch layer was bioprinted by UV light photocuring.

Printability Assessments

Printability was measured in terms of resolution, printing accuracy, shape fidelity (after 28 days in culture) and extrudability for grid pattern bioprinted patches. Resolution was assessed as the width of deposited bioink gridlines (at day one – after crosslinking immediately after bioprinting); printing accuracy was measured as the number of empty squares between bioink gridlines in the grid pattern at day one (a perfect grid should have 16 empty squares between gridlines of bioink); shape fidelity was measured as the number of empty squares remaining with time in culture at day 28; and extrudability outcome observations were (1) whether the nozzle dripped hydrogel between the bioprinting of patches (yes/no) and (2) the average number of times the nozzle was blocked requiring the nozzle to be changed per six patches bioprinted (in series one after the other). To isolate hydrogel printability outcomes for AlgGel, it was compared to GelMA using the BIO X and bioprinting with hydrogel only without cells.

Durability Measurement

To assess survival of patches in culture, patches were monitored daily for macroscopic disintegration for up to 28 days. Culture medium was replaced every 3–4 days and the date of patch disintegration was recorded and time to disintegration (durability) analysed. To evaluate the effects of layer number on patch printability eight single-layer thickness (0.2 mm depth) acellular AlgGels were printed as controls (without cells). To evaluate the effect of minimising movement, 13 AlgGel HCAEC + HDF patches were generated and cultured under minimisation of movement conditions (slow media replacement with 1000 μl narrow-bore non-automated pipette every 7–10 days with no transfer to a microscope for observations) and these were left in culture until the first two patches in the set of 13 disintegrated. To evaluate the addition of exogenous AlloECM hydrogel to the AlgGel, 23 AlloECM + AlgGel patches were printed at low and high concentration of AlloECM. In addition, 13 acellular gelatin-methacryloyl (GelMA) patches were produced as an extended durability control as GelMA is more durable in culture.

Cell Viability Assays, Imaging and Analysis

To assess cell survival, we evaluated cell viability in bioprinted patches after 28 days in culture by staining them with calcein-AM, ethidium homodimer (Live/Dead Assay, Invitrogen, Carlsbad, CA, United States) and Hoechst stain, used to identify live, dead and total cells (nuclei), respectively. Patches in media with stains added were incubated at 37°C for 1 h. After fresh media replacement, patches within the plate were moved to a microscope for automatic fluorescence imaging by several automated microscopic methods (using an M7000 or EVOS Fl AUTO 1 (ThermoFisher, MA, United States), Nikon Ti (Nikon, Tokyo, Japan), or IN Cell Analyzer (GE Life Sciences, IL, United States) to obtain images of the entire patches. Quantification of stained cells was performed by random grid sampling and computer-based estimation using FIJI (ImageJ) software.

Patch Contractile Activity Evaluation

To observe contractile activity, patches were monitored by video light microscopy for intrinsic oscillations. When contractile oscillations were observed, phase contrast microscopy video recordings were obtained using an Olympus CKX53 microscope (Olympus, Tokyo, Japan), with the beating patch contrasted with non-contractile hydrogel in the same conditions. To count the rate of beating activity, videos were played in slow motion and the average rate taken from multiple samples.

3D Bioprinted Cell Staining, Imaging and Analysis

To evaluate endothelial cell organisation into structural networks, we stained bioprinted patches with antibodies against CD31 to identify any structural endothelial cell network-like formation after 28 days in culture. After 28 days HCAEC + HDF-containing and mouse VCS patches were first fixed and then stained using antibody against human/mouse CD31 and Hoechst stain for endothelial cells and nuclei, respectively (see **Supplementary Materials** for full protocol). They were imaged by light microscopy and with a confocal microscope (LSM 800, Zeiss, Oberkochen, Germany). Images were analysed with ImageJ (NIH, Bethesda, United States). For 3D rendering analysis, confocal images were processed by Imaris v7.6 (Oxford Instruments, Zurich, Switzerland).

Statistical Analysis

Results were analysed using PRISM (GraphPad, San Diego, CA, United States). Hypothesis testing for categorical data was performed using the chi-square test. Hypothesis testing for continuous data was performed using the two-tailed Mann–Whitney U test or the Kruskal–Wallis test for a difference between two or any of three non-parametric data groups, respectively. Descriptive statistics (Kaplan–Meier survival/durability data) were tested using pairwise Log-rank (Mantel Cox) tests.

RESULTS

Patch Printability

To evaluate printability outcomes such as resolution, printing accuracy, shape fidelity and extrudability, 5 × 5 line grid patches were bioprinted instead of patches completely filled with bioink, so that these printability measures could be assessed. Patches were bioprinted with a geometry of 10 × 10 × 0.4 mm (length x width x depth) as shown in **Figure 1**. For all three bioprinters, printability outcomes (resolution, printing accuracy, shape fidelity and extrudability) were similar. For AlgGel hydrogel patches, resolution was similar compared to GelMA; printing accuracy was higher for AlgGel with 78/176

(45%) of AlgGel empty internal squares in the grid pattern preserved at day one compared to 53/208 (25%) for GelMA ($p < 0.05$; χ^2 test; $n = 384$); shape fidelity after 28 days in culture was only different if it included the increased print accuracy for AlgGel on day one, with 72/176 (41%) of squares remaining preserved at day 28 for AlgGel and 51/208 (25%) for GelMA ($p < 0.05$; χ^2 test; $n = 384$). However, correcting for differences in print accuracy on day one, the 28-day shape fidelity rate was 72/78 (92%) for AlgGel and 51/53 (96%) for GelMA ($p = 0.36$; χ^2 test; $n = 131$); for extrudability, AlgGel dripped hydrogel from the nozzle and GelMA did not and AlgGel had zero nozzle blockages per six patches compared to one per six patches for GelMA (AlgGel tended toward more flow than input software instructions and GelMA tended toward less flow). Overall, no significant difference in printability was observed between bioprinters but AlgGel had a 1.7x higher printing accuracy, presented some dripping from the nozzle and had no nozzle blockages compared to GelMA hydrogel.

Patch Durability in Culture

To assess patch survival in culture conditions following bioprinting, patches were cultured in media at 37°C for up to 28 days to evaluate durability in the post-printing, pre-transplantation phase (**Figure 2**). The different bioprinting system used had little effect on the overall durability of the resulting AlgGel patches (**Figures 2E,F**). Overall, median (and IQR) for time in days to disintegration (durability) of AlgGel-based patches in media in six-well plates was 10 (3–19) with patches printed by the REGEMAT3D, 14 (13.5–18) with the *INVIVO,* and 14 (10–28) with the BIO X ($p = 0.93$; Kruskal–Wallis test for a difference in any of the three groups). The cellular patch content (mouse VCS, free (not in spheroid) HCAECs + HDFs or acellular hydrogel alone) also had little effect on patch durability ($p = 0.17$; Kruskal–Wallis test) (**Figure 2**). Kaplan–Meier survival curves suggested that the addition of cells compared to hydrogel on its own might reduce the number of bioprinting runs (sessions producing a set of patches) where all patches in that run survived to 28 days (**Figures 2A–C**). However, survival analyses revealed no strong pattern for durability between different cellular contents within the AlgGel patches.

As the bioprinting system and cellular content had minimal effect on patch durability, pooled analysis of all AlgGel patches was performed and median durability overall was 14 days (interquartile range (IQR) 10-27; $n = 59$; $p < 0.05$) (**Figure 2D**), whereas 13/13 GelMA control patches were intact at the end of 28 days ($p < 0.05$). AlgGel acellular patches with one layer were less durable (median survival 3 days; IQR 2.5–4 days; $n = 8$; $p < 0.05$) than two-layer AlgGel acellular patches (median survival 28 days; IQR 19–28; $n = 20$; $p < 0.05$) (**Figure 2D**). The minimisation of movement protocol allowed AlgGel patches to be cultured until day 66 before the end point of 2/13 of these patches losing their integrity (unsuitable for transplantation) was reached. The addition of AlloECM to AlgGel reduced the durability of patches: whilst AlloECM + AlgGel patches retained their structure after bioprinting, 23/23 patches disintegrated in < 1 day (**Figures 2D,G**). This was regardless of the AlloECM concentration in the AlgGel hydrogel (5 or 30 mg/ml), either in the presence or absence of cellular content (**Figures 2A–C**). Overall, factors which reduced patch durability in culture were: bioprinting patches with only one layer of depth, movement disturbance such as during media changes and transfer to a microscopy platform and the addition of AlloECM. Factors which had negligible impact on durability in culture were the bioprinting system used and the cellular content.

Cell Viability

To evaluate cell survival within patches at 28 days, our analysis of epifluorescence microscopy images at low magnification showed viable cells surrounded by hydrogel components of the patches which were variably autofluorescent (**Figure 3**). By random grid sampling, estimated live cell density was ∼80 cells/mm^2/layer (∼16,000 cells per patch) which is a viability rate of ∼53% from the ∼30,000 cells per patch on initial bioprinting. We measured a live/dead ratio equal ∼2.3 at 28 days for these human cells. Viability in mouse mixed cardiac cell (VCS) patches (**Figure 4**) could not be as reliably quantified because many patch-embedded cells were in 3D spheroids. Using a software-based analysis of less autofluorescent confocal microscopy images we measured a live:dead cell ratio of 9:1 for mouse VCSs. VCS diameter was ∼150 μm at 28 days in culture as shown in **Figure 4**. This did not change from day one (*data not shown*), confirming also the fact that VCSs maintained their shape in culture. Overall, our method was associated with viable cells in patches, even after bioprinting and 28 days in culture.

Patch Contractility

To assess whether patches were able to permit contractility of cardiomyocytes, throughout the 28 day experiments all mouse VCS-containing patches were evaluated under a light microscope for contractile activity (**Supplementary Video 1**). Five patches started to display irregular contractile activity on day seven, two on day 10 and one on day 13. Despite six out of eight patches breaking into fragments over the course of the 28 days, all eight patches (or fragments) still showed some contractile activity at the experiment end at day 28. The average rate of (non-fragmented) patch contractions was 258 beats/min (range 230–288) and the rate did not change with time in culture. **Supplementary Video 1** shows VCS patch contractility in real-time and the patch floating in media can be seen oscillating compared to adjacent static areas of non-contractile hydrogel on the well floor. Altogether, the contractility observed in our neonatal mouse VCS-AlgGel patches suggests that there is no barrier in principle to generating contractile cardiac tissue using cardiac spheroids in AlgGel hydrogel (**Supplementary Video 1**).

Patch Endothelial Cell Network Structural Organisation

To assess CD31$^+$ endothelial cells' ability to self-organise into structural networks, we observed for network formation in VCS-containing patches and patches with freely suspended HCAECs

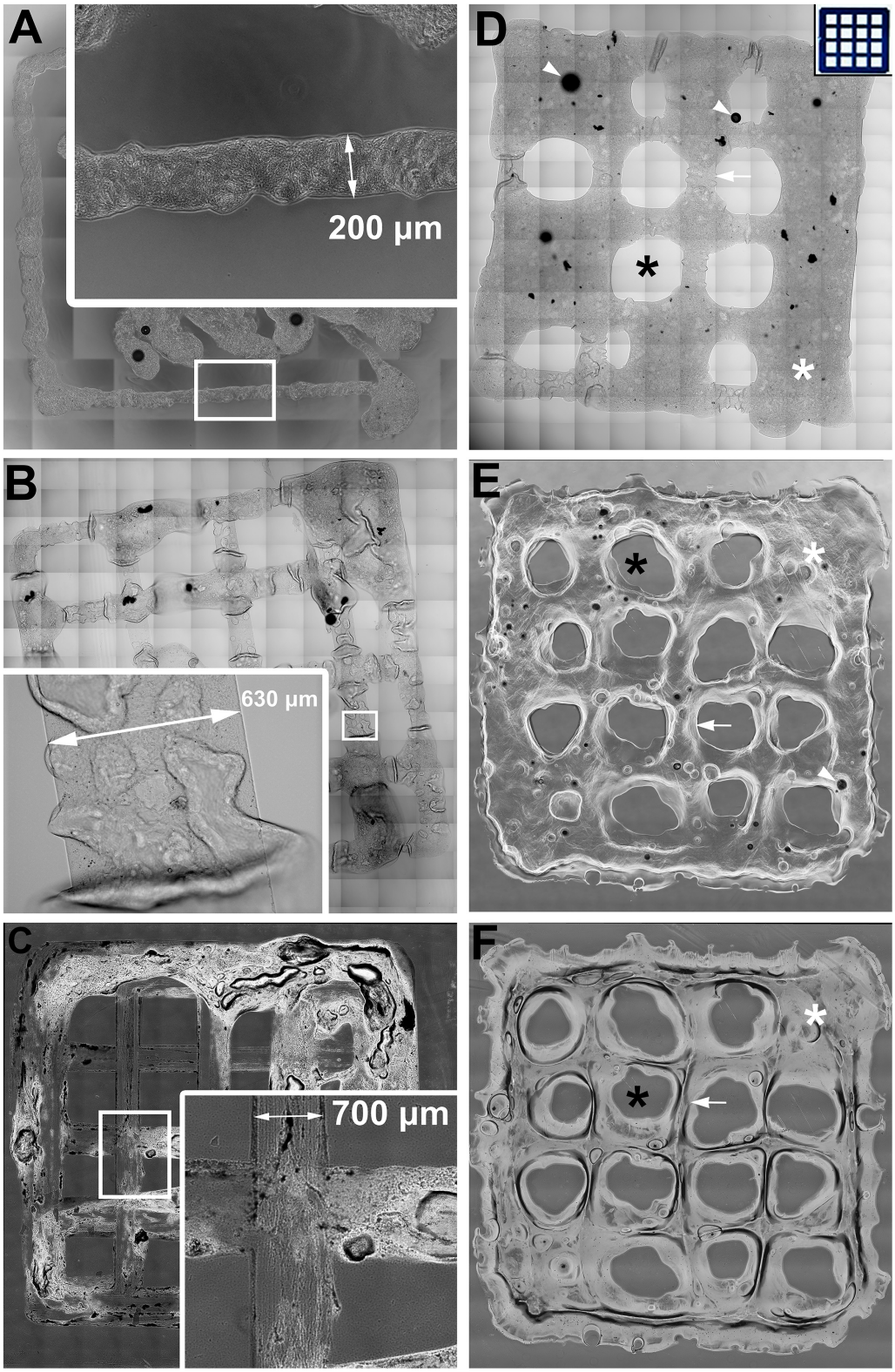

FIGURE 1 | Assessing printability for extrusion 3D bioprinting with AlgGel hydrogels and GelMA. **(A–C)** Representative images of 10 mm^2 AlgGel patches 3D bioprinted using three different bioprinters: a custom-made REGEMAT3D **(A)**, the ROKIT *INVIVO* **(B)**, and the CELLINK BIO X **(C)**. The resolution (line width) of the bioprinted grid patches was between 200 and 700 µm. Printing accuracy of AlgGel **(D)** and GelMA **(E)** was measured as the number of empty squares preserved

(Continued)

FIGURE 1 | Continued
(black asterisks) between lines of bioink (white arrow) compared to the blueprint instructions input into the software on day one **(D)** inset panel). Hydrogel filled seven of the intended 16 empty spaces in **(D)**, whereas in **(E)** two were filled (white asterisks): an example of a printing accuracy of 56 and 88% for these individually displayed representative patches, respectively. The day one GelMA patch in **(E)** is shown after 28 days in culture in **(F)**, still with two spaces filled (a shape fidelity of 100% for this displayed representative patch by this measure). The black dots (white arrowheads) in **(D)** and **(E)** are air bubbles. Scale bars not shown (all patches 1 cm^2). Overall in the complete sample (from which these displayed representative patches are taken), printing accuracy was higher for AlgGel with 78/176 (45%) of AlgGel empty internal squares in the grid pattern preserved at day one compared to 53/208 (25%) for GelMA ($p < 0.05$; $\chi 2$ test; $n = 384$); shape fidelity after 28 days in culture was only different if it included the increased print accuracy for AlgGel on day one, with 72/176 (41%) of squares remaining preserved at day 28 for AlgGel and 51/208 (25%) for GelMA ($p < 0.05$; χ^2 test; $n = 384$). However, correcting for differences in print accuracy on day one, the 28-day shape fidelity rate was 72/78 (92%) for AlgGel and 51/53 (96%) for GelMA ($p = 0.36$; χ^2 test; $n = 131$).

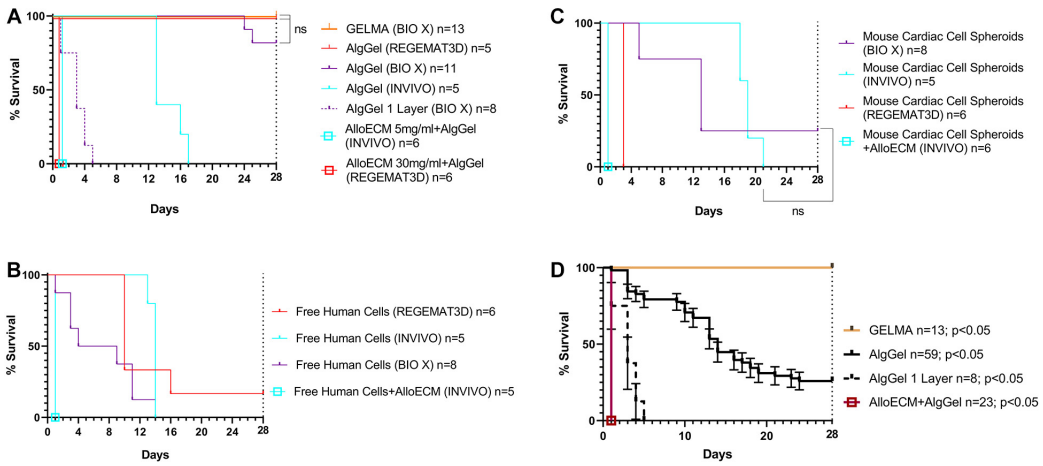

FIGURE 2 | Durability assessments for 3D bioprinted patches in cell culture medium up to 28 days. **(A–C)** Survival analyses grouped by different patch cellular content, either hydrogel without cells **(A)**, with HCAECs and HDFs **(B)** or mouse cardiac cell in VCSs **(C)**. All curves are statistically significant compared to adjacent curves unless marked by "ns" and a black linking line connecting two or more similar (non-significant) curves; $p < 0.05$ Log-rank (Mantel-Cox) test of each line compared pairwise to each other line on the survival curve. In **(A)** identical curves are moved off centre to prevent complete line overlap (applies to AlloECM and GelMA curves). Each curve represents one print run of a series of patches bioprinted one after the other from the same batch of hydrogel ($n = 5$–13 per group). As cellular content had negligible influence on patch durability, pooled analysis of all patches is shown in **(D)**. Overall, these results show that survival was similar whether patches contained AlgGel alone or with cells **(A–C)**. They also show that AlgGel had a median survival of 14 days in culture overall **(D)**, which was reduced by bioprinting single layer patches instead of standard thickness (double layer) or the addition of AlloECM (fibroblast-derived extracellular matrix hydrogel). Compared to GelMA (which is more durable in culture) AlgGel presented a median survival showing that it is likely to need transplanting sooner (at 14 days in culture), because leaving patches to culture for 28 days risks many patches fragmenting and becoming unsuitable for transplantation.

with HDFs, stained for $CD31^+$ cells. For VCS patches, our confocal analysis showed that some $CD31^+$ mouse cardiac endothelial cells in VCS remained in spheroids even after bioprinting and 28 days in culture (**Figure 4D**). The median length of $CD31^+$ linear human endothelial cell structures was 149 μm (IQR 91–225 μm), median width was 46 μm (IQR 29–80 μm) and $CD31^+$ endothelial cell covered area in the hydrogel was ∼2.7%. For these patches (which contained VCS), the $CD31^+$ endothelial cells did not present extensive endothelial cell organisation into networks (**Figure 4**), despite some of the cells moving out of their spheroids (**Figure 4D**), consistent with observations in a previous study (Fleming et al., 2010). Some migrating $CD31^+$ mouse cardiac endothelial cells (or clusters of these cells) were observed within the bioprinted patch outside of spheroids, suggesting that at day 28 patches contained a mixture of cells which had migrated from their spheroids into the hydrogel, cell clusters which had moved away from their initial spheroid and cells which had remained in the same spheroids present at the initial bioprinting (**Figure 4**).

Conversely, $CD31^+$ free (not in spheroid) HCAECs started to organise into structures resembling endothelial cell networks (**Figures 5**, **6** and **Supplementary Video 2**). The median length of $CD31^+$ linear human endothelial cell structures was 88 μm (IQR 62–114 μm), median width was 37 μm (IQR 29–59 μm) and $CD31^+$ endothelial cell covered area in the hydrogel was ∼2.1%. 3D rendering structural analysis revealed a lumen-like space between endothelial surfaces with endothelial cells having the appearance of branched structures (**Figure 6** and **Supplementary Video 2**). Taken together, these findings suggest that (1) AlgGel hydrogels combined with this method permit the structural self-organisation of endothelial cells within bioprinted patches even without additional interventions such as supplementation with angiogenic growth factors and (2) endothelial cells in spheroids with no additional angiogenic factors do not fully migrate out into the surrounding hydrogel for as significant a structural organisation into networks to occur – instead the endothelial cells form an irregular distribution across the patch (**Figure 4**) and some remain in spheroids (**Figure 4D**).

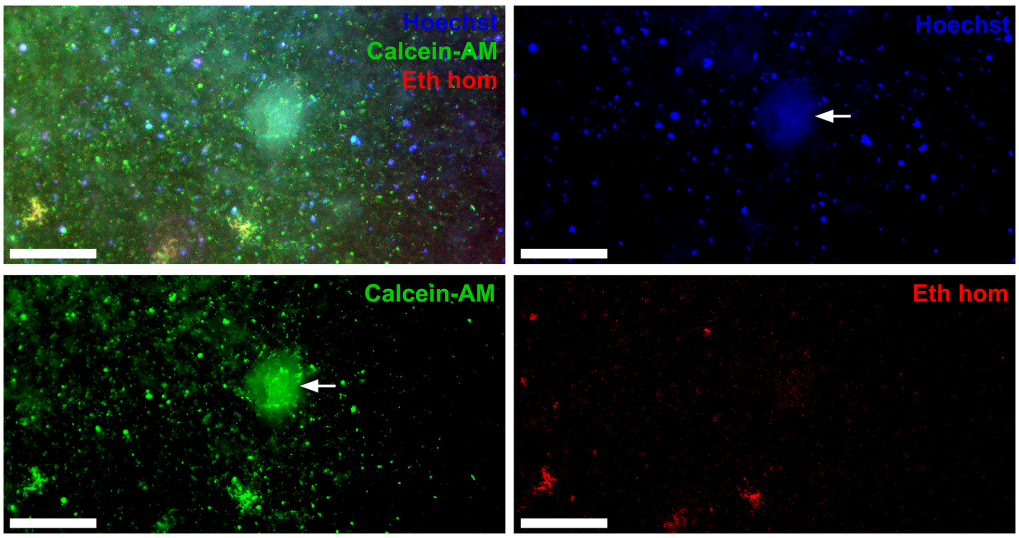

FIGURE 3 | Bioprinted HCAECs and HDFs in AlgGel hydrogel are viable at 28 days. HCAEC + HDFs within a patch 3D bioprinted with the REGEMAT3D shown after 28 days in culture. This patch was stained with Hoechst (blue—nuclei), calcein-AM (green—live cell cytoplasm), ethidium homodimer (red—dead cell nuclei). Despite hydrogel autofluorescence (white arrow), the patch shows live cells (green), and nuclei (blue) at low magnification throughout this representative segment of patch. The live/dead ratio was ~2.3 at 28 days in culture. Magnification bar = 500 μm.

DISCUSSION

3D bioprinting is appealing for biomedical engineering as it can be used to produce uniform tissues, is scalable and automatable (Roche et al., 2020). It is also adaptable for use with different biomaterials and cell types, including iPSC-derived cardiac cells given their potential use for heart regeneration (Roche et al., 2020). Our study using alginate 4% (w/v)/gelatin 8% (w/v) hydrogels and cardiac cells for 3D bioprinting of patches presents a promising approach for cardiac bioengineering. Specifically, supporting our hypothesis, our 3D bioprinted patches showed that it is possible for endothelial cells to self-organise into a structural network. Other studies have previously used differing approaches to describe advances in endothelial cell network assembly (Ong et al., 2017b; Cui et al., 2019; Polley et al., 2020; Xu et al., 2020). We have added to this a 3D rendering of micrographic data that shows endothelial cells self-organised into a structural network with a lumen-like space with our method (**Supplementary Video 2**).

Additionally, as printability and durability are important determinants of whether the patch survives to allow for cells to organise within it, we identified the printability/durability impacts of several factors (bioprinting system, cellular patch content, number of layers of patch depth, minimisation of movement, addition of AlloECM) which had not previously been assessed. As printability can be measured in terms of resolution (e.g., extruded bioink line width), printing accuracy (the degree to which bioprinted constructs match the intended construct set by the blueprint input into the software), shape fidelity (the ability of bioprinted constructs to maintain shape after deposition) and extrudability (the ease of bioink extrusion/flow) (Fisch et al., 2020; Gillispie et al., 2020), we used 5× 5 gridline patterns instead of patches completely filled with bioink to assess these outcome measures. For the first time in direct comparison, we quantified that printing accuracy was 1.7x higher for AlgGel compared to GelMA with our method which was likely related to GelMA's less predictable extrudability (we quantified that GelMA complete nozzle blockages occurred on average once every six patches compared to no blockages for AlgGel). For durability, macroscopic disintegration (durability) was defined as patch integrity being unacceptable for transplantation of a whole patch – for example, using our surgical patch transplantation method in a murine model of myocardial infarction (Roche and Gentile, 2020) – as this is a durability indicator of practical relevance to the surgeon transplanting patches for *in vivo* models. As printability and durability are critical for generating patches which are useable for transplantation, we thoroughly evaluated these characteristics. GelMA was used as a durable control as it is an established alternative to AlgGel for cardiac patch bioprinting which is highly durable in culture (Koti et al., 2019). Other studies have numerically described detailed rheological characteristics, including (not limited to) storage modulus, viscosity and extrusion pressures for similar hydrogels (Mondal et al., 2019). Our study provides data on highly practical printability measures (such as print accuracy) to inform hydrogel-related choices for patch culture and subsequent transplantation.

As the effect of the bioprinting systems themselves on our outcome measures was not previously compared, optimal bioprinting conditions with AlgGel hydrogels were tested with three different extrusion bioprinters: two screw-driven extrusion systems (a custom made REGEMAT3D model and the commercially available Rokit *INVIVO*) and one using pneumatic extrusion (a CELLINK BIOX bioprinter)

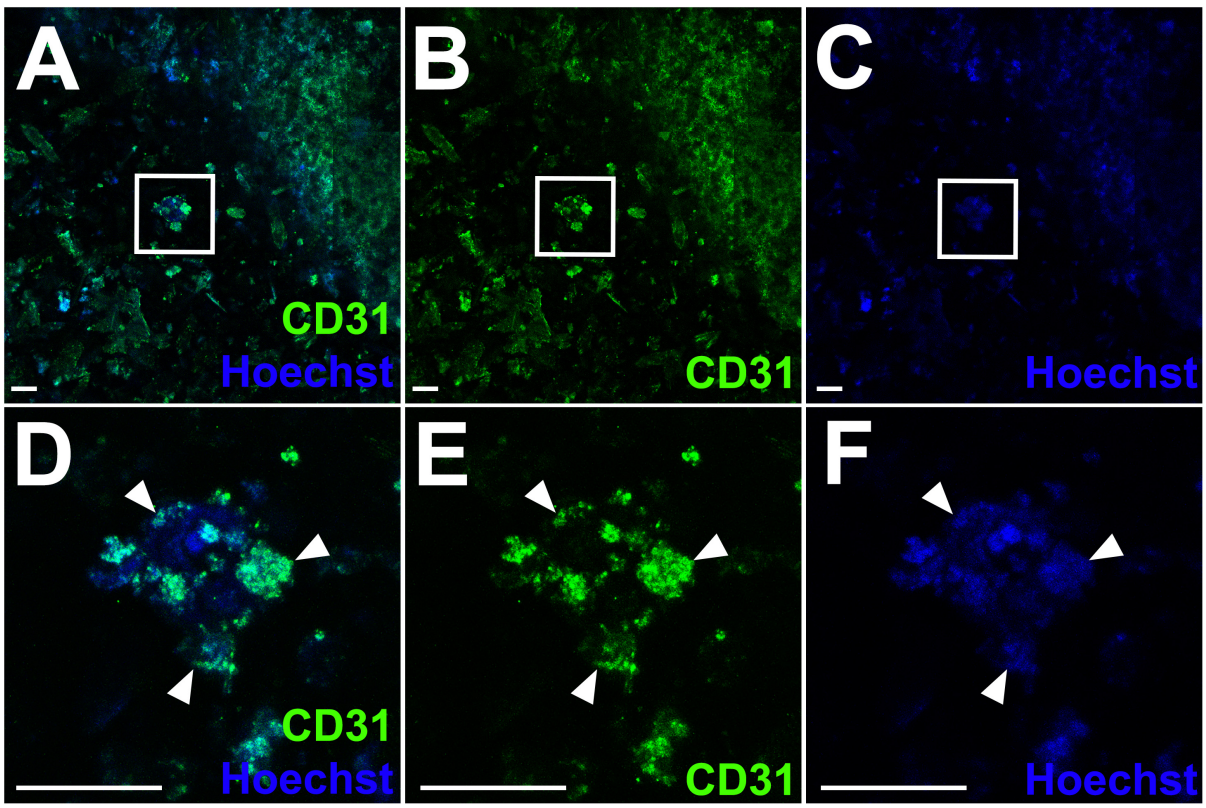

FIGURE 4 | CD31-positive endothelial cells within a patch containing mouse cardiac spheroids. **(A–F)** Laser scanning confocal microscopy (LSCM) images of a BIO X-bioprinted AlgGel patch containing neonatal mouse cardiac spheroids stained for cell nuclei (blue) and $CD31^+$ endothelial cells (green). Scale bars **(A–C)** = 100 μm. **(A)** Merged channel image showing $CD31^+$ cells across a representative segment of patch and a spheroid still intact after bioprinting followed by 28 days in culture (inset panel). **(B)** and **(C)** show CD31 stain and Hoechst stain (nuclei), respectively. **(D)** Magnified image of the spheroid (white arrowheads) highlighted in panel **(A)**. CD31 stain and Hoechst (nuclei) are shown in **(E)** and **(F)**, respectively. Scale bars **(D–F)** = 100 μm.

(**Supplementary Figure 1**). We found that 10 × 10 × 0.4 mm patches – sized for *in vivo* rodent cardiac models (Roche and Gentile, 2020) – can be 3D bioprinted with any system with minimal difference to printability (resolution, printing accuracy, shape fidelity and extrudability) or durability in culture. No matter which system was in use, important parameters influencing the printability of a bioprinted series of patches would have included distance between the bioprinting nozzle tip and the six-well plate surface as well as ambient temperature and hydrogel batch-to-batch variability (see **Supplementary Materials**). Overall, our results suggest that optimising bioprinting parameters was key to the printability and long durability of patches as opposed to the bioprinting platform used (for example, by optimisation pre-testing to determine the ideal flow rate, nozzle speed and temperature settings which were different for each system to work optimally with our hydrogels). It is known that bioprinting parameters and the concentration of AlgGel hydrogels are established determinants of printability and durability (Mancha Sánchez et al., 2020); our study supports this and also adds the finding that the bioprinting system itself was not a strong influencing factor.

We also compared different hydrogel compositions for durable patches that readily retained their macrostructural shape in culture conditions (**Figure 2**). AlgGel hydrogels are a suitable choice for experiments that allow time for a degree of tissue maturation in the post-printing phase before the hydrogel disintegrates (Bociaga et al., 2019). By combining our durability data with our time to observation of patch contractility data (contractility was observed to begin between day seven and 13), we are able to propose that transplantation of patches for an *in vivo* model may be optimal just before 14 days in culture. Other studies have reported related durability measures, for instance degradation rate as % weight loss of patches in culture up to 14 days (Bociaga et al., 2019). However, ours is the first to report a more clinically relevant durability measure based on usefulness of the patch for its intended purpose – surgical transplantation with an established method for *in vivo* testing (Roche and Gentile, 2020). Furthermore, we report comprehensive durability data with survival beyond 14 days and present data on three previously unevaluated determinants of durability: layer number (patch depth), minimising movement of the patches and the addition of an exogenous factor (AlloECM). AlloECM is a fibroblast-derived extracellular matrix hydrogel used to mimic properties of the extracellular matrix. We found AlloECM could be added to AlgGel bioprinted patches with no change to printability or patch morphology on day one (when

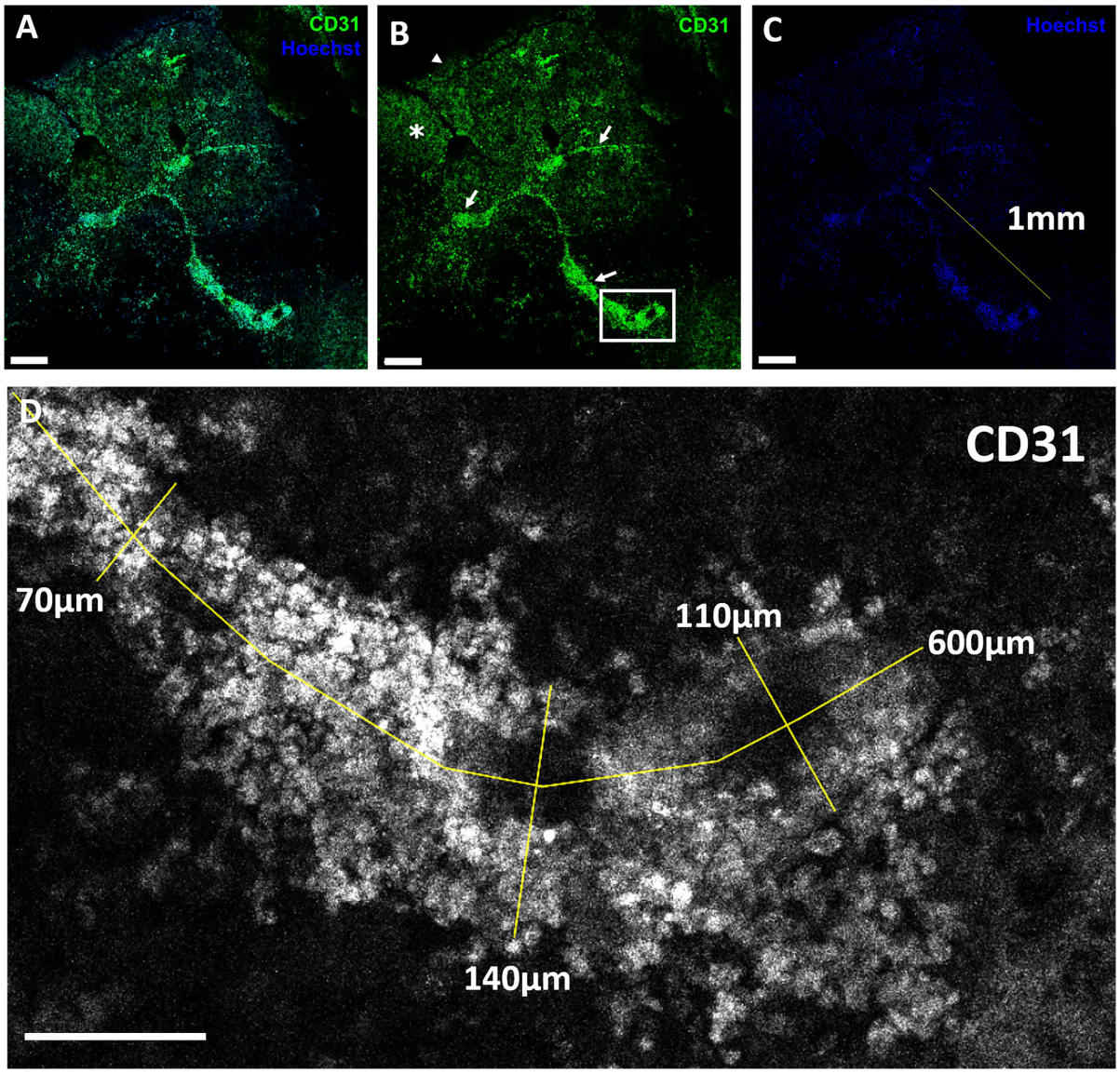

FIGURE 5 | CD31-positive endothelial cell organisation within a 3D bioprinted patch containing HCAECs and HDFs. **(A–C)**. Collapsed Z-stacks of confocal images of a 3D bioprinted AlgGel patch stained with antibodies against CD31 (green) and Hoechst stain (blue). **(A)** Merged channel image of CD31$^+$ endothelial cells (green) and nuclei (blue) within a patch fragment. **(B)** CD31$^+$ endothelial cells (white arrowhead shows border of hydrogel fragment and white asterisk shows hydrogel containing CD31$^+$ cells). A small T-shaped formation of endothelial cells is starting to organise, with small 1 mm branch-like formations starting to form (white arrows). **(C)** The cell nuclei show the same branched organisation which maps to the CD31$^+$ endothelial cells in **(B)**. Magnification bars **(A–C)** = 200 µm. **(D)** Magnified black and white image taken from inset panel in **(B)** shows CD31$^+$ endothelial cells with measurements (yellow lines, measurements indicated on image; scale bar 100 µm) and this structure is shown in more detail in the 3D rendering shown in **Figure 6** and **Supplementary Video 2**.

bioprinted). However, they all disintegrated by the next day. Unlike the acellular AlgGel patches which gradually broke into smaller pieces over time but left significant pieces of patch in the well (**Supplementary Figure 2**), the AlloECM-AlgGel patches were completely disintegrated into pieces of residual hydrogel less than ∼1 mm in diameter. This is the first time durability data have been reported for AlloECM mixed in with AlgGel patches and the finding may have been due to incompatibility between AlloECM and AlgGel hydrogel, including overall pH changes or interference with the ionic crosslinking method used. Conversely, the addition of different cell types within a patch could also alter the microenvironment and therefore affect durability but our data showed there was no major durability difference depending on cell type when we evaluated human and mouse cells in free and spheroid formation, respectively (**Figure 2**). Overall, we determined that bioprinting platform and cellular content are not strong determinants of durability whereas layer number, minimisation of movement in culture media and

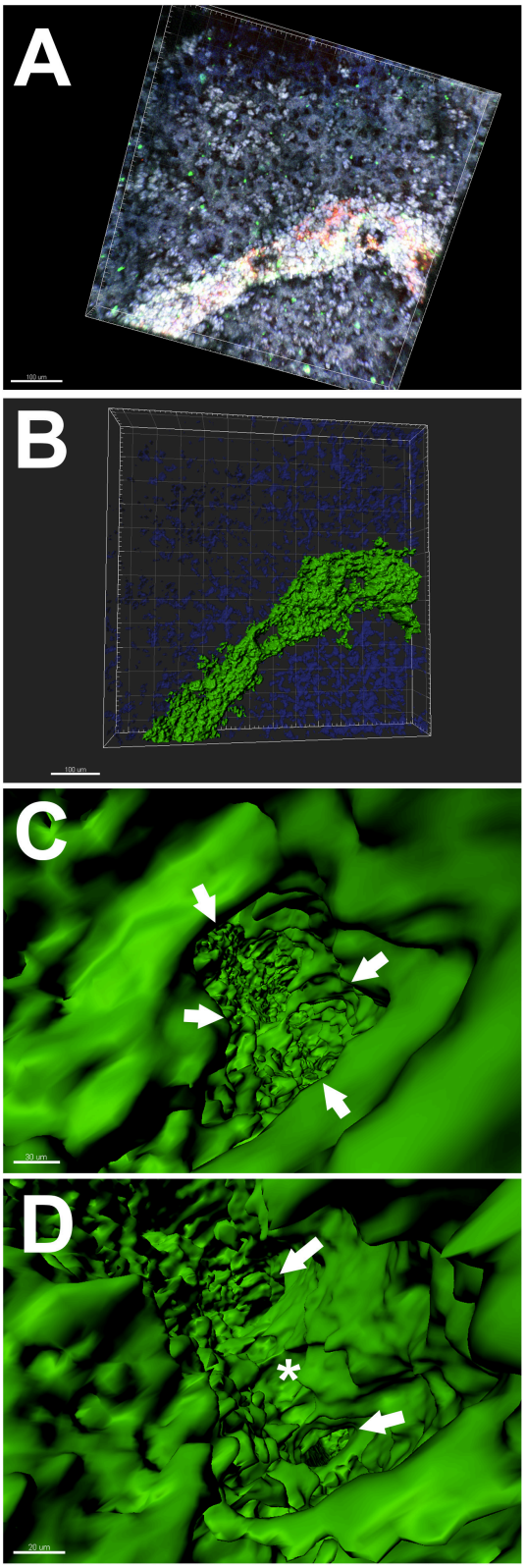

FIGURE 6 | Lumen evaluation of CD31^{+} endothelial cells within a 3D bioprinted patch generated with alginate 4%/gelatin 8% hydrogel. **(A–D)** 3D *(Continued)*

FIGURE 6 | rendering analysis using Imaris software of a 3D bioprinted patch stained with antibodies against CD31 (green) and Hoechst stain (blue). **(A)** and **(B)** 3D rendering of the endothelial structure shown previously (in **Figure 5**). Scale bars 100 μm. **(C)** and **(D)** Higher magnification images depicting the inside of the structural lumen formed by endothelial cells within a 3D bioprinted patch. **(C)** Arrows indicate the inner (luminal) surface of the walls (green). Scale bar 30 μm. **(D)** The star indicates a pillar joining two opposing endothelial surfaces where the lumen branches into two smaller lumens (arrows). Scale bar 20 μm. For a full view of the 3D rendering analysis of the same lumen formed within the 3D bioprinted patch please see **Supplementary Video 2**.

the addition of an exogenous factor (AlloECM) were strong determinants of durability.

For the cellular component of patches, we bioprinted some patches with VCS which are microtissue aggregates of mixed cardiac cell types. VCS cultures can be readily adapted for other cell types such as stem cell-derived cells and are generated using a scaffold-free, self-sustainable approach that allows self-assembly and organisation of cells in 3D (Gentile, 2016). Our evaluation of cell viability at 28 days after bioprinting demonstrated that over time both VCS bioink and bioink with freely suspended endothelial cells and fibroblasts could be cultured in bioprinted hydrogel patches (**Figures 3** and **4**). Accurate and automated quantification of viability for cells embedded in autofluorescent hydrogel patches in 3D is challenging (Noor et al., 2019). Nevertheless, viability of freely suspended cells in bioprinted patches (**Figure 3**) was estimated at approximately 53–61% at day 28, comparable with previous reports from other studies using extrusion bioprinting of 40–80% (Murphy and Atala, 2014; Fisch et al., 2020). For VCS patches, live cell area/total cell area was estimated at ∼72% with a favourable ratio of live to dead cells (9:1). The inability to accurately quantify live cells in 3D spheroids embedded in a 3D patch limits interpretation of this result without further studies. Future studies would benefit from measuring cell viability in 3D in a more automated way, for instance with automated large specimen, serial confocal microscopy techniques aimed at reducing hydrogel autofluorescence artefact. Nonetheless, throughout our study, cells were viable in AlgGel hydrogels.

All BIO X patches containing mouse VCSs presented contractile activity between day seven and 13 and the contractility was transmitted across the patch (**Supplementary Video 1**). We reported that the average rate for these patches was 288 beats/min. Other studies have reported a beating rate of approximately 180 beats/min for isolated neonatal mouse cardiomyocytes in 2D culture (Ehler et al., 2013) and 500 beats/min for live adult mice *in vivo* (Mahmoud et al., 2015). For these VCS patches, our confocal images of cells migrating from the VCS into the hydrogel (**Figure 4**) suggested that at day 28 patches contained both intact VCSs and clusters of cells which had migrated into the hydrogel. The combined presence of cell clusters migrating away from VCSs into the hydrogel and those remaining within VCSs may have been responsible for the generalised contractility observed in these patches

(**Supplementary Video 1**). This might explain why patches did not beat until between one and two weeks after bioprinting, allowing time for some cells to migrate from spheroids and make connections across the patch. Our observed contractile activity stopped and re-started with quiescent non-contractile periods of a few days between. This seemed to be related to disturbing the patches, for example when changing culture medium, which also seemed to be a major factor in promoting macroscopic patch disintegration as well. Nonetheless, patches (or fragments of patches) always resumed contractile activity (all remained contractile on day 28). We were unable to reliably measure the electrochemical discharge which causes cardiomyocyte contraction using our contractility-measuring and pacing system because the patches stopped contracting during the transport to the system platform. This was probably also due to movement disturbance from the transport itself and for this reason our contractility analysis was limited to observance of contractions on video microscopy. Future workflows should minimise patch movement as much as possible, including bioprinting directly onto a surface suitable for electrocardiographic recording and pacing without patch transportation.

Bioengineering of heart tissues requires a vascular network for optimal cell survival and function (Fleming et al., 2010; Roche et al., 2020; Wang et al., 2020) and our observations of stained endothelial cells showed that mouse VCSs did not organise into endothelial network structures to the same extent as freely suspended HCAECs with HDFs (**Figures 4–6** and **Supplementary Video 2**). The endothelial network formation shown in Video 2 is structurally comparable to those reported in some other studies (Noor et al., 2019; Roche et al., 2020), which is noteworthy given our relatively low starting density of endothelial cells (∼2500 cells/mm^3). One recent study (which reported on endothelial cells derived from induced pluripotent stem cells) reported a density of ∼15000 cells/mm^3 (Noor et al., 2019), so even with our HCAEC density being six-fold less, a structural network started to form. The first clinical trial for epicardial-transplanted patch repair in humans found that a functional benefit may be conferred to the failing heart even with a low starting density of stem cell derived cardiovascular progenitor cells (410/mm^3) in large (20 cm^2) patches (Menasché et al., 2018). Our study supports the notion that significant cell growth and self-organisation can occur in patches from a low starting cell density. For future studies, which may use human stem cell-derived cardiac cells or spheroids, additional factors such as vascular endothelial growth factor (VEGF) could be added to promote endothelial cell organisation and cell migration out of spheroids. Alternatively, a mixture of 'free' stem cell-derived endothelial cells and cardiac spheroids could be used. For freely suspended endothelial cells and fibroblasts, we used a ratio of 2:1, respectively. Whilst optimal ratios for various cells in spheroid co-culture have been reported (Noguchi et al., 2016; Polonchuk et al., 2017), the optimal ratio of freely suspended HCAECS and HDFs in AlgGel is not known. The physiological ratio of endothelial cells:fibroblasts in the heart is not universally agreed, but the currently accepted ratio is 4:1 (Pinto et al., 2016; Zhou and Pu William, 2016). In our patches, we doubled the number of fibroblasts relative to endothelial cells (to increase their nourishing/supportive influence) but did not equalise the ratio in case they interfered with endothelial cell self-assembly – as they have previously been shown to interfere with the functioning of other cell types (cardiomyocytes) in equal ratio co-culture (Ong et al., 2017b). Future studies will be needed to determine the optimal ratio of endothelial cells to fibroblasts when freely suspended in hydrogel patches.

Future studies will also be needed to functionally test our self-assembled endothelial cell network. If endothelial cell self-assembly into networks is shown to be a successful approach, it is likely to have advantages over other approaches (such as fabricating artificial moulds and lining them with endothelial cells). Specifically, vascular cells which self-organise following physiological signalling in permissive hydrogel may organise into a hierarchical network of different sized vessels and present a more physiological network without exogenous scaffold material. In summary, both the overall approach and the detailed evaluations in this study pave the way for future studies aimed at myocardial regeneration using cardiac patches.

CONCLUSION

This study provides data of high practical relevance to inform bioengineering workflows focused on optimising cardiac patches prior to transplantation. Specifically, we have shown that 3D bioprinted cardiac cells are viable in alginate/gelatin hydrogels for at least 28 days in culture, allowing endothelial cells to self-organise into a network and for patch contractility. Bioprinted cardiac patches in optimised conditions may develop/mature according to physiological signals in the pre-transplant phase even without being significantly coaxed or controlled by additional interventions. Taking into account patch durability, we conclude that an optimal moment to transplant patches after a period of maturation is just before 14 days in culture.

DATA AVAILABILITY STATEMENT

The datasets presented in this study can be found in online repositories. The names of the repository/repositories and accession number(s) can be found below: Zenodo (CERN, Geneva, Switzerland) repository doi: 10.5281/zenodo.4299230.

ETHICS STATEMENT

The animal study was reviewed and approved by the Animal Ethics Committee at the Northern Sydney Local Health District (project number RESP17/55; 20/04/2017).

AUTHOR CONTRIBUTIONS

CR contributed to the conceptualisation, data generation, data curation, data analysis, data visualisation, funding acquisition, investigation, methodology, resources, validation, project administration, writing (original draft), manuscript review,

and editing. PS cultured and supplied the mouse cardiac cell spheroids used in these experiments. AA was responsible for the supervision, writing (review), and editing. CJ and MX were responsible for the supervision, manuscript review, and editing. CG contributed to the conceptualisation, data generation, data curation, data analysis, data visualisation, funding acquisition, methodology, project administration, supervision, manuscript review, and editing. All authors contributed to the article and approved the submitted version.

FUNDING

This work was supported by a Heart Research Australia Ph.D. Scholarship (grant number 2019-02), a Sir John Loewenthal Scholarship 2019 (University of Sydney), the Le Gros Legacy Fund New Zealand (grant number PhD012019), the UTS Seed Funding, a University of Sydney Kick-Start Grant, a University of Sydney Chancellor's Doctoral Incentive Programme Grant, a Catholic Archdiocese of Sydney 2019 Grant for Adult Stem Cell Research, and a Sydney Medical School Foundation Cardiothoracic Surgery Research Grant.

ACKNOWLEDGMENTS

The authors thank Louise Cole and Chris Evenhuis and acknowledge the use of the equipment in the Microbial Imaging Facility at the i3 Institute in the Faculty of Science, University of Technology Sydney (UTS). The authors also thank Leonie Herson for her work in the design and generation of the central image.

SUPPLEMENTARY MATERIAL

The Supplementary Material for this article can be found online at: https://www.frontiersin.org/articles/10.3389/fbioe.2021.636257/full#supplementary-material

Supplementary Figure 1 | 3D bioprinting platforms used: a custom-made REGEMAT3D model (left column), the ROKIT *INVIVO* (middle column) and the CELLINK BIO X (right column). Hardware **(A–C)** and software **(D–F)** are shown for these three extrusion-based 3D bioprinting systems. The REGEMAT3D customised **(D)** and *INVIVO* 'Creator K' **(E)** software were both accessed on a laptop computer connected to the bioprinter by USB cable and the BIO X software **(F)** was entirely inbuilt on the bioprinter touchscreen.

Supplementary Figure 2 | 3D bioprinted patch fragmentation. Representative phase images of an alginate 4%/gelatin 8% patch on day one **(A)** that was fragmented in culture and became unsuitable for transplantation by day 28 **(B)**.

Supplementary Video 1 | Beating cardiac patches containing mouse vascularised cardiac spheroids in alginate/gelatin hydrogel. The patches shown are oscillating in media with an average rate of 258 beats/min, consistent with mouse cardiac cells. Oscillating patches in media are compared with non-contractile elements such as hydrogel in the well and in the video appendices the appearances of non-contractile patches are shown with and without extrinsic movement applied to the microscopy apparatus.

Supplementary Video 2 | Three-dimensional rendering of CD31 + endothelial network-like structure within an alginate/gelatin patch containing HCAECs and HDFs. The structure shown has a lumen space and branches. These confluent CD31 + endothelial cells (shown in green) self-assembled into this structure over 28 days in culture following extrusion 3D bioprinting.

REFERENCES

Bishop, E. S., Mostafa, S., Pakvasa, M., Luu, H. H., Lee, M. J., Wolf, J. M., et al. (2017). 3-D bioprinting technologies in tissue engineering and regenerative medicine: current and future trends. *Genes Dis.* 4, 185–195. doi: 10.1016/j.gendis.2017.10.002

Blaeser, A., Duarte Campos, D. F., Puster, U., Richtering, W., Stevens, M. M., and Fischer, H. (2016). Controlling shear stress in 3D bioprinting is a key factor to balance printing resolution and stem cell integrity. *Adv. Healthc Mater.* 5, 326–333. doi: 10.1002/adhm.201500677

Bociaga, D., Bartniak, M., Grabarczyk, J., and Przybyszewska, K. (2019). Sodium alginate/gelatine hydrogels for direct bioprinting-the effect of composition selection and applied solvents on the bioink properties. *Materials* 12:2669. doi: 10.3390/ma12172669

Cattelan, G., Guerrero Gerbolés, A., Foresti, R., Pramstaller, P. P., Rossini, A., Miragoli, M., et al. (2020). Alginate formulations: current developments in the race for hydrogel-based cardiac regeneration. *Front. Bioeng. Biotechnol.* 8:414. doi: 10.3389/fbioe.2020.00414

Cui, H., Zhu, W., Huang, Y., Liu, C., Yu, Z. X., Nowicki, M., et al. (2019). In vitro and in vivo evaluation of 3D bioprinted small-diameter vasculature with smooth muscle and endothelium. *Biofabrication* 12:015004. doi: 10.1088/1758-5090/ab402c

Ehler, E., Moore-Morris, T., and Lange, S. (2013). Isolation and culture of neonatal mouse cardiomyocytes. *J. Vis. Exp.* 50154. doi: 10.3791/50154

Fisch, P., Holub, M., and Zenobi-Wong, M. (2020). Improved accuracy and precision of bioprinting through progressive cavity pump-controlled extrusion. *bioRxiv* [preprint] doi: 10.1101/2020.01.23.915868

Fleming, P. A., Argraves, W. S., Gentile, C., Neagu, A., Forgacs, G., and Drake, C. J. (2010). Fusion of uniluminal vascular spheroids: a model for assembly of blood vessels. *Dev. Dyn.* 239, 398–406. doi: 10.1002/dvdy.22161

Gentile, C. (2016). Filling the gaps between the in vivo and in vitro microenvironment: engineering of spheroids for stem cell technology. *Curr. Stem. Cell Res. Ther.* 11, 652–665.

Gillispie, G., Prim, P., Copus, J., Fisher, J., Mikos, A. G., Yoo, J. J., et al. (2020). Assessment methodologies for extrusion-based bioink printability. *Biofabrication* 12:022003. doi: 10.1088/1758-5090/ab6f0d

Koti, P., Muselimyan, N., Mirdamadi, E., Asfour, H., and Sarvazyan, N. A. (2019). Use of GelMA for 3D printing of cardiac myocytes and fibroblasts. *J. 3D Print. Med.* 3, 11–22. doi: 10.2217/3dp-2018-2017

Mahmoud, A. I., O'Meara, C. C., Gemberling, M., Zhao, L., Bryant, D. M., Zheng, R., et al. (2015). Nerves regulate cardiomyocyte proliferation and heart regeneration. *Dev. Cell* 34, 387–399. doi: 10.1016/j.devcel.2015.06.017

Maiullari, F., Costantini, M., Milan, M., Pace, V., Chirivi, M., Maiullari, S., et al. (2018). A multi-cellular 3D bioprinting approach for vascularized heart tissue engineering based on HUVECs and iPSC-derived cardiomyocytes. *Sci. Rep.* 8:13532. doi: 10.1038/s41598-018-31848-x

Mancha Sánchez, E., Gómez-Blanco, J. C., López Nieto, E., Casado, J. G., Macías-García, A., Díaz Díez, M. A., et al. (2020). Hydrogels for bioprinting: a systematic review of hydrogels synthesis, bioprinting parameters, and bioprinted structures behavior. *Front. Bioeng. Biotechnol.* 8:776. doi: 10.3389/fbioe.2020.00776

Menasché, P., Vanneaux, V., Hagege, A., Bel, A., Cholley, B., Parouchev, A., et al. (2018). Transplantation of human embryonic stem cell-derived cardiovascular progenitors for severe ischemic left ventricular dysfunction. *J. Am. Coll. Cardiol.* 71, 429–438. doi: 10.1016/j.jacc.2017.11.047

Mondal, A., Gebeyehu, A., Miranda, M., Bahadur, D., Patel, N., Ramakrishnan, S., et al. (2019). Characterization and printability of sodium alginate -gelatin hydrogel for bioprinting NSCLC co-culture. *Sci. Rep.* 9:19914. doi: 10.1038/s41598-019-55034-55039

Murphy, S. V., and Atala, A. (2014). 3D bioprinting of tissues and organs. *Nat. Biotechnol.* 32, 773–785. doi: 10.1038/nbt.2958

Noguchi, R., Nakayama, K., Itoh, M., Kamohara, K., Furukawa, K., Oyama, J., et al. (2016). Development of a three-dimensional pre-vascularized scaffold-free contractile cardiac patch for treating heart disease. *J. Heart Lung. Trans.* 35, 137–145. doi: 10.1016/j.healun.2015.06.001

Noor, N., Shapira, A., Edri, R., Gal, I., Wertheim, L., and Dvir, T. (2019). 3D printing of personalized thick and perfusable cardiac patches and hearts. *Adv. Sci.* 6:1900344. doi: 10.1002/advs.201900344

Ong, C. S., Fukunishi, T., Nashed, A., Blazeski, A., Zhang, H., Hardy, S., et al. (2017a). Creation of cardiac tissue exhibiting mechanical integration of spheroids using 3D bioprinting. *J. Vis. Exp.* 55438. doi: 10.3791/55438

Ong, C. S., Fukunishi, T., Zhang, H., Huang, C. Y., Nashed, A., Blazeski, A., et al. (2017b). Biomaterial-free three-dimensional bioprinting of cardiac tissue using human induced pluripotent stem cell derived cardiomyocytes. *Sci. Rep.* 7:4566. doi: 10.1038/s41598-017-05018-4

Pinto, A. R., Ilinykh, A., Ivey, M. J., Kuwabara, J. T., D'Antoni, M. L., Debuque, R., et al. (2016). Revisiting cardiac cellular composition. *Circ. Res.* 118, 400–409. doi: 10.1161/circresaha.115.307778

Polley, C., Kussauer, S., David, R., Barkow, P., Mau, R., and Seitz, H. (2020). Printing of vessels for small functional tissues-A preliminary study. *Curr. Direct. Biomed. Eng.* 6:20203121. doi: 10.1515/cdbme-2020-3121

Polonchuk, L., Chabria, M., Badi, L., Hoflack, J. C., Figtree, G., Davies, M. J., et al. (2017). Cardiac spheroids as promising in vitro models to study the human heart microenvironment. *Sci. Rep.* 7:7005. doi: 10.1038/s41598-017-06385-6388

Roche, C. D., Brereton, R. J. L., Ashton, A. W., Jackson, C., and Gentile, C. (2020). Current challenges in three-dimensional bioprinting heart tissues for cardiac surgery. *Eur. J. Cardiothorac. Surg.* 58, 500–510. doi: 10.1093/ejcts/ezaa093

Roche, C., and Gentile, C. (2020). Transplantation of a 3D bioprinted patch in a murine model of myocardial infarction. *J. Vis. Exp.* e61675. doi: 10.3791/61675

Wang, H., Roche, C., and Gentile, C. (2020). Omentum support for cardiac regeneration in ischaemic cardiomyopathy models: a systematic scoping review. *Eur. J. Cardiothorac. Surg.* 58, 1118–1129. doi: 10.1093/ejcts/ezaa205

Xu, L., Varkey, M., Jorgensen, A., Ju, J., Jin, Q., Park, J. H., et al. (2020). Bioprinting small diameter blood vessel constructs with an endothelial and smooth muscle cell bilayer in a single step. *Biofabrication* 12:045012. doi: 10.1088/1758-5090/aba2b6

Zhang, Y. S., Arneri, A., Bersini, S., Shin, S. R., Zhu, K., Goli-Malekabadi, Z., et al. (2016). Bioprinting 3D microfibrous scaffolds for engineering endothelialized myocardium and heart-on-a-chip. *Biomaterials* 110, 45–59. doi: 10.1016/j.biomaterials.2016.09.003

Zhou, P., and Pu William, T. (2016). Recounting cardiac cellular composition. *Circ. Res.* 118, 368–370. doi: 10.1161/CIRCRESAHA.116.308139

Conflict of Interest: The authors declare that the research was conducted in the absence of any commercial or financial relationships that could be construed as a potential conflict of interest.

SUPPLEMENTARY FIGURES AND LEGENDS

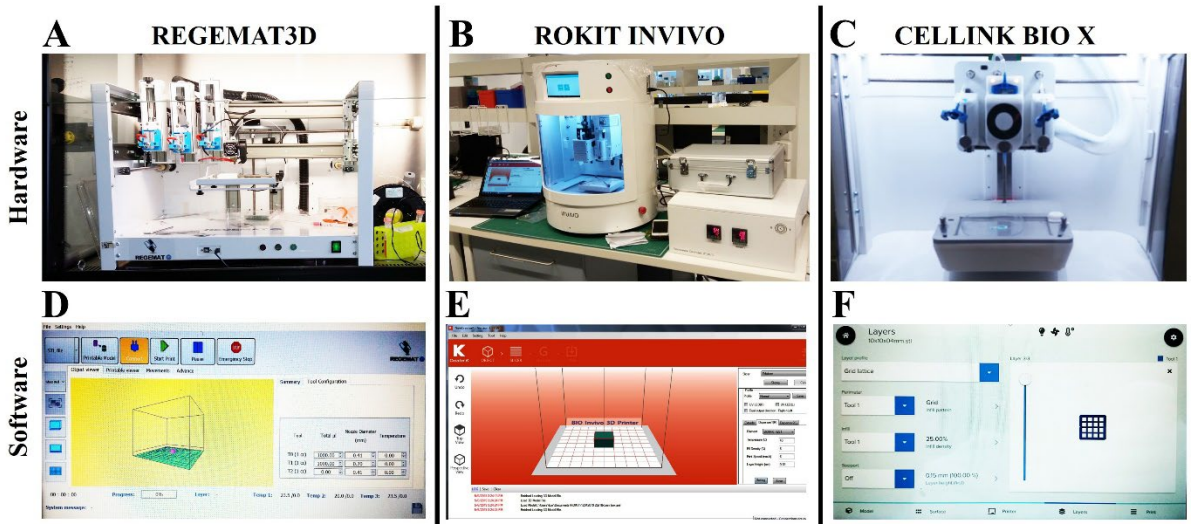

Supplementary Figure 1. 3D bioprinting platforms used: a custom-made REGEMAT3D model (left column), the ROKIT INVIVO (middle column) and the CELLINK BIO X (right column). Hardware (**A-C**) and software (**D-F**) are shown for these three extrusion-based 3D bioprinting systems. The REGEMAT3D customised (**D**) and INVIVO 'Creator K' (**E**) software were both accessed on a laptop computer connected to the bioprinter by USB cable and the BIO X software (**F**) was entirely inbuilt on the bioprinter touchscreen.

Supplementary Figure 2

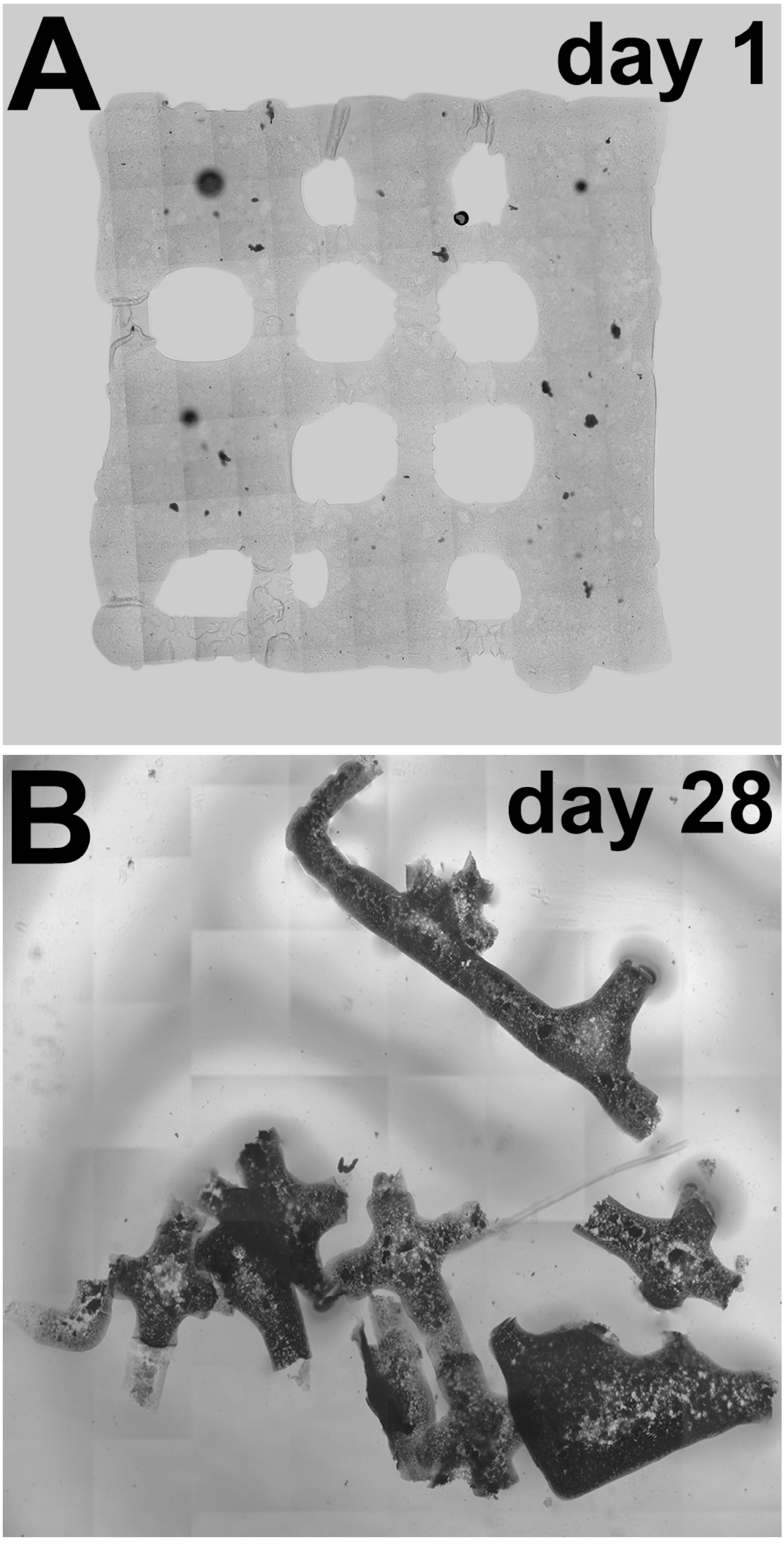

Supplementary Figure 2. 3D bioprinted patch fragmentation. Representative phase images of an alginate 4%/gelatin 8% patch on day one (A) that was fragmented in culture and became unsuitable for transplantation by day 28 (B).

SUPPLEMENTARY MATERIALS

I. Detailed Bioprinting System Preparation and Parameter Setting Methods

Preparation of the 3D Bioprinters

Preparation of the REGEMAT3D. The REGEMAT3D (REGEMAT3D, Granada, Spain) custom-made screw-driven extrusion 3D bioprinter was turned on within a biological safety cabinet pre-sterilised with a germicidal UV lamp. A standard Luer-Lok 3ml syringe was filled with MilliQ water and connected to a Teflon-lined nozzle (200 µm lumen diameter). This is the same nozzle supplied for use with the ROKIT INVIVO bioprinter. The syringe and nozzle were placed, nozzle-down, in 70% (v/v) ethanol and left under a UV lamp for 30 minutes. The syringe was removed and MilliQ water forcibly expelled to clear the nozzle aperture. The syringe was secured in place in the bioprinting mechanism. The bioprinter was calibrated using the REGEMAT3D software platform (full details of all software steps and input parameters available from authors on request).

Preparation of the INVIVO. The inbuilt UV lamps and hepafilter of the INVIVO (ROKIT, Seoul, South Korea) commercially-available screw-driven 3D bioprinter allowed for its use on a standard laboratory bench. A 10 ml Leur-Lok syringe was filled with MilliQ water and a Teflon-lined nozzle (200 µm lumen diameter, ROKIT) attached. The syringe and nozzle were placed, nozzle-down, in 70% (v/v) ethanol and left under the UV lamps for 30 mins. The syringe was removed and MilliQ water forcibly expelled to clear the nozzle aperture. The syringe with nozzle and plunger was secured in place in the bioprinting mechanism. The nozzle was calibrated to the printing bed and floor of six well plates using the automated touchpad screen and the software (Creator K), with printing parameters loaded accordingly on a connected laptop computer. Parameters were kept the same throughout all subsequent print runs (key parameters described below, full data available from authors on request). The printer hardware components were set to keep the ambient temperature of the bioprinter chamber between 27.5-28.0°C throughout printing (bed temperature to 37°C; syringe chamber to 39°C). If ambient temperature in the bioprinter chamber exceeded 28°C the chamber was temporarily vented by opening the front panel.

Preparation of the BIO X. The inbuilt UV lamps and hepafilter of the BIO X (CELLINK Life Sciences, Boston, MA, USA) commercially-available pneumatically-driven extrusion 3D bioprinter enabled use on a standard laboratory bench. For AlgGel patches, a 3 ml BIO X syringe was filled with MilliQ water and a CELLINK 25-gauge conical polypropylene nozzle (250 µm inner diameter) attached. The syringe and nozzle were placed, nozzle-down, in 70% (v/v) ethanol and left under the UV lamps for 30 mins. The syringe was removed and MilliQ water forcibly expelled to clear the nozzle aperture. The syringe with nozzle was placed in the

rightmost (leftmost from operator's perspective) of the three chambers of the bioprinting mechanism (print head 1 which was chosen for the print run). The nozzle was calibrated manually to the floor of six-well plates using the automated touchpad screen. The printer components were set to the same temperatures as the INVIVO (37°C for the bed and 39°C for the chamber). The ambient temperature was measured using a standard thermometer (although this was less important for the BIO X because print flow rate could be altered during the print run to compensate for ambient temperature-related differences in flow). For ease of transfer of hydrogel to syringe the pneumatic bung between the pneumatic mechanism and the hydrogel was not used (pneumatic force was transmitted directly through air in the syringe to the hydrogel pool at the lowest part of the syringe and in the nozzle). The printing parameters were programmed using the step-by-step touchscreen on the printer (key parameters described below, full data available on request). Initial parameter setting was matched to the INVIVO although for the BIO X, adjustments to flow rate and nozzle travel speed were made during the print runs to create optimal patches based on real-time moment-to-moment operator judgement.

For the gelatin-methacryloyl (GelMA) durability control patches, pre-made light-blocking syringes of 10% w/v + LAP 0.25% in HEPES buffer were purchased (product no. IK305202, CELLINK Life Sciences, Boston, MA, USA) and used without cells. Unlike the AlgGel, these syringes were ready-made and so were loaded directly into the BIO X bioprinter by removing the bung and connecting the syringe chamber to the pneumatic mechanism. For fibroblast-derived extracellular matrix hydrogel (AlloECM®, ROKIT, Seoul, South Korea), 30 mg AlloECM powder was custom-ordered directly from ROKIT, who generated it in a work-intensive proprietary protocol and supplied it for this experiment (the effect of combining AlloECM with AlgGel in our methodology was previously unknown).

Loading the Bioink. To transfer the AlgGel-based bioinks to the bioprinting syringes for all bioprinters, the empty syringe chambers without bung or plunger were removed from the bioprinting mechanism by hand. To facilitate transfer of cells in AlgGel, the BIO X syringe's pneumatic bung was discarded whereas for the REGEMAT3D and INVIVO the syringe plungers were removed and placed head up on the floor of the bioprinter. The syringe chamber was held horizontally, the bioink pipetted into the chamber and syringe plunger replaced (INVIVO and REGEMAT3D). To prevent downward pre-extrusion of hydrogel, the syringe was inverted (nozzle upwards) and plunger advanced to the 1 ml (REGEMAT3D) or 5 ml (INVIVO) position to remove void space in the syringe. The BIO X 3 ml syringe did not require handling of a plunger as syringe chambers connected directly to the pneumatic mechanism and AlgGel did not flow out of the nozzle before bioprinting started. For all bioprinters, the syringes were re-secured, nozzle down, into the bioprinter mechanism. For the INVIVO, re-calibration in the z axis was performed at this point to achieve perfect contact between the nozzle and the six-well plate surface. For the BIO X, re-calibration was not required, calibration was always preserved despite removal, filling and return of the syringe to the bioprinting. The

REGEMAT3D required micro-adjustments during bioprinting, by the operator manually twisting the screw-driven extrusion mechanism to increase the flow rate as needed or by manually lifting the plate to make contact with the nozzle.

Parameter Setting and Extrusion Bioprinting Process

AlgGel Bioprinting. For all bioprinters printing was initiated using previously tested parameters as a GCODE or STL file which had been optimised during preliminary tests. These were not changed for within a bioprinting run. Briefly, patch size was set at 10x10x0.4 mm with two 0.2 ml layers in the z axis and a five-line grid pattern (REGEMAT3D lines were diagonally oriented, INVIVO and BIO X were orthogonally oriented). The bioink flow rate was set at 2 mm/s (REGEMAT3D), 7mm/s (INVIVO) and 6 mm/s (BIO X – initial rate which was changed in real time depending on operator-judged printing outcomes). The grid infill / solidity percentage for the patches was set to produce square grids with five lines of bioink deposited in the x and y axes (**Figure 1, 2** and **Suppl Figure 2**). The infill percentage was set at 6% (INVIVO) and 25% (BIO X) and the equivalent measure of pore size was set at 0.6 mm for the REGEMAT3D. Differences were due to each bioprinter having different software and hardware. Parameters were interlinked, for example, changing the nozzle type on the BIO X software and leaving all other parameters the same changed the appearance of the grid. The travel speed of the REGEMAT3D nozzle across the plate in the x-y axis was 50 mm/sec, for the INVIVO it was 3 mm/s and for the BIO X it was 6 mm/s (for the BIO this was the initial speed which was changed in real time depending on printing outcomes). These were some of the parameters determined at preliminary testing to achieve successful and similar grid-pattern patches, for example, reducing the high speed of the REGEMAT3D resulted in suboptimal bioprinting outcomes. The grid pattern was not always perfectly achieved due to hydrogel lateral flow expansion (non-perfect shape fidelity) after extrusion before crosslinking. For the INVIVO the print bed was designed to optimally hold a four-well square 10 x 10 cm plate and the printer nozzle returned to starting position between each patch being printed; therefore the six well plate we used (which was not square) was manually repositioned before printing the next patch in one of the wells. For all bioprinters we continued until the bioink was depleted or the desired number of successful patches were printed (our range was 4-13 successfully bioprinted patches per bioprinting run and we concluded a bioprinting run after a minimum of one, maximum of three six well plates were used). For six patches 0.5 ml bioink was sufficient if no wastage such as pre-extrusion flow occurred. For the BIO X, recalibration was not necessary as it bioprinted a run of six patches one after the other without interruption and had a one-click recommencement function after changeover of six-well plates (with the same parameters preserved). The BIO X allowed for real-time adjustments during the bioprinting to the nozzle speed and the extrusion pressure which the other bioprinters did not.

GelMA Bioprinting (with the BIO X). For the GELMA durability controls, premade GelMA syringes (as described above) were initiated with the slowest settings possible of 1 mm/s print speed and 1 kPa extrusion pressure which were immediately titrated up by the operator once printing began. The flow rate was continuously titrated according to the output seen at the tip of the nozzle to obtain the optimal patch fidelity to a 5 x 5 line two-layer 10 x 10 x 0.4 mm orthogonal grid structure during the print. Significant increases in pressure by the operator were required during the print runs in frequent 2 kPa increments up to ~150 kPa by the end of the bioprinting run of 13 patches. Occasionally, the syringe would block and stop extruding, then due to pressure accumulation, all the GelMA would be expelled and flood the well. At this point the bioprinting was stopped, a new syringe and nozzle at room temperature was loaded and the printing was restarted from the next empty well. The lithium phenyl-2,4,6-trimethylbenzoylphosphinate (LAP) photo-initiator in the GelMA pre-made hydrogel syringes is crosslinked by ultra-violet (UV)-light (instead of ionically by $CaCl_2$ - the crosslinking method for AlgGel), so the inbuilt UV curing lights were used to crosslink the patches. These were set to 15 seconds at 100% intensity of 365 nm UV light delivered at the end of each layer being printed at a height of 3 cm between the UV light source and the patch below it. The modular UV curing lights were used rather than the photocuring tool head which did not come as standard with the BIO X unit. After completion of one six-well plate of bioprinted patches, the patches were covered in 3 ml of media per well, the lid was replaced on the plate and it was transferred to the incubator following the same protocol as for AlgGel acellular patches from then on.

II. Protocols for Fixation, Labelling and Imaging Analysis of Cells

Fixation and Immunolabelling of Patches for CD31+ Confocal Imaging. Following 28 days in culture, bioprinted patches were fixed and stained as follows, with movement/agitation of patches minimised throughout. Patches in six well plates had media aspirated and $CaCl_2$ (2% w/v in PBS) added to the well. This was left for 20 minutes at room temperature. For the fixative solution, we mixed 10% (w/v) formalin in neutral buffer (1.2 ml), acetic acid (0.6 ml) and 96% (v/v) ethanol in water (10.2 ml), under a fume hood (final concentrations 1% (w/v) formalin + 9% (v/v) neutral buffer + 5% (v/v) acetic acid + 81.6% (v/v) ethanol + 3.4% (v/v) water). After 20 minutes, the 2% (w/v) $CaCl_2$ was aspirated and replaced with the fixative solution described above at room temperature for three hours. Then, the fixative was aspirated and the patch rinsed in PBSA (PBS containing 0.01% sodium azide) for 10 minutes per wash three times. To minimise disintegration, patches were rinsed with 2% (w/v) $CaCl_2$ in between PBSA washes. Patches were permeabilised in PBSA containing 0.2% Triton X-100 for 20 minutes at room temperature, then blocked in 3% bovine serum albumin (BSA) in PBSA (w/v; Blocking Solution) for 30 minutes at room temperature. For human cells, mouse anti human primary antibodies against CD31 (product no. 555446. BD Pharmingen™,

NJ, USA) were added diluted in Blocking Solution (antibody concentration 50 µl/ml) and incubated in the dark at 4°C overnight. Patches were then washed three times (10 minutes each wash) at room temperature in PBSA with $CaCl_2$ rinsing in between each wash. Secondary antibodies (Alexa Fluor® 647 AffiniPure Donkey Anti-Mouse; 715-605-151. Jackson Immunoresearch Laboratories PA, USA) were diluted in blocking solution (7 µl secondary antibody in 1000 µl Blocking Solution). Hoechst stain was added to the same solution (1 drop per 1 ml). This solution was pipetted onto the patch and left for 1.5 hours at room temperature. For mouse cells we fixed and immunolabelled using the same procedures described above except the primary antibody was rat anti-mouse CD31 (553370. BD Pharmingen™, NJ, USA) and secondary antibody was donkey anti-rat (Alexa Fluor® 647 AffiniPure; 712-605-153. Jackson Immunoresearch Laboratories PA, USA). At the end of secondary antibody and Hoechst staining, mouse and human cultures were then washed 3 x 10 minutes in PBSA at room temperature. Patches were mounted onto a microscope glass slide, preserving the 3D depth by adding glass spacers on the side of the patches, the mounting media (VectaShield®, Vector Laboratories, Burlingame, CA, USA), then a coverslip on top and sealing the prepared slide with a film forming polymer (nail varnish) applied to all edges.

Post-processing for Visualisation of Microscopic Images. Levels were thresholded with brightness and contrast adjusted in Adobe Photoshop.

Quantification methods. For random grid sampling with manual counting of cells, the number of cells per 500 μm^2 of one layer of patch was manually counted over ten random areas of patch and the average was used to estimate live cell density for one layer which was doubled to account for the two layer depth of the patch. For software-based estimation of live and dead cells, FIJI (ImageJ) software was used to analyse the particles from a thresholded black and white binary image for each of the colour channels, green, red and blue. The total area covered by pixels for the green channel (live cells) or the red channel (dead cells) was divided by the blue channel area (total nuclei) to obtain the estimated ratios of live and dead cells. For length and width measurements of CD31+ endothelial cells within a patch, 20 random measurements were taken of linear CD31+ endothelial cell structures using Adobe Photoshop software and the median and interquartile ranges calculated.

III. Supplementary Discussion Points:

Additional Considerations for Bioprinting System Optimisation

Maintaining Optimal Nozzle-plate Contact. The BIO X allowed for continuous printing into six-well plates after one calibration without losing contact with the plate surface. The INVIVO, which has a 10 x 10 cm printing bed which would fit a four-well plate or a petri dish, required manual rotation of the six-well plate to align the next well to receive the next patch to be printed. This could alter the plate-nozzle distance sufficiently to have a marked effect on the resulting patch. The nozzle-plate distance could become too wide and therefore more hydrogel needed to be extruded before contact with the plate was made. If it was too narrow, the Teflon tip of the nozzle would be squashed into the plate and mechanically disrupt the print layers in the Z axis. In the latter case, the printing of the second layer in the Z axis could be severely disturbed as the height of each of our layers was 0.2 mm and if the nozzle was too deep for the first layer, it would not raise far enough to be clear for the second layer and therefore the Teflon would run through and damage the integrity of the first layer.

Temperature and Realtime Adjustments. The BIO X allowed for real time adjustments of flow rate based on the operator's judgement of how well the bioink was flowing on any given print run to compensate for temperature-related changes in flow. The BIO X also allowed temperature control of the print bed and the syringe-holder but not the ambient temperature in the printing chamber which was not displayed. The INVIVO also does not allow for direct ambient temperature control of the chamber but does display the ambient temperature. Both these bioprinters allowed for control of the temperature of the bioprinting bed and the syringe chambers of the bioprinting mechanism. We found these two temperature settings could be set up initially to achieve predictable warming or cooling of the ambient temperature. Venting the chamber by opening the front panel was used if ambient temperature went above and the optimal temperature which we found to be 28°C for our hydrogel/method. Micro-adjustments could be made during the printing, such as turning down the temperature of the bed once printing begins (as far as zero degrees) so that the patches hit the cold surface of the six-well plate and the hydrogel is less likely to lose its structure. The REGEMAT3D did not allow for any temperature controls. For all three bioprinters, parameters such as flow rates of the bioink out of the nozzle or speed of movement of the nozzle across the plate were set to achieve precise control of the patch morphology (**Figure 1** and **2**). However, an increase or decrease in ambient temperature by even 0.5°C could result in the next patch being markedly different despite all other parameters being the same: too cold and the hydrogel became more viscous and less hydrogel was extruded, too warm and it became less viscous and more hydrogel was extruded.

Overall, the bioprinting parameters (and especially temperature) determined the quality of the patches at baseline on day zero. Some were controllable (such as input software parameters) and others were not

controllable (such as humidity or batch-batch hydrogel variability). These parameters seemed to be the major determinant of patch durability. Variation in uncontrollable parameters may explain the variation in durability between patches over the 28 day period despite keeping all controllable parameters the same. Each bioprinter introduced different levels of parameter variation: the BIO X was fully automated (preserving controllable parameters, for example by continuous printing without interruption of patches in six-well plates and one-touch restarting for the print process with existing parameters). However, it also allowed for changes of bioprinting parameters (such as flow rate) in real time during a live print. This allowed the operator to compensate for variability at the time of bioprinting. The INVIVO was similarly automated although printing occurred one patch at a time with the printer performing a re-homing (calibration) cycle before the next patch. As the print bed was designed for a four-well (square) 10 x 10 cm plate, six-well plates had to be manually rotated into position between each patch print, introducing some variability in parameters (such as nozzle-plate distance). The custom-made REGEMAT3D required the operator to insert hands into the print space and make manual adjustments to flow rate and bioprinter bed height throughout the bioprinting process, introducing the most uncontrollable parameter variability of the three bioprinters. Nonetheless, the overall durability of patches was not found to be significantly different between the three bioprinting systems.

2.3 – Transplantation of a 3D bioprinted patch in a murine model of myocardial infarction

Summary:

Our surgical method was published as a video article in the Journal of Visualized Experiments (JoVE). The article contains a video demonstrating how to perform the method along with the step-by-step written method and complete list of equipment. The discussion section comments on the advantages and disadvantages of this method whereby patches are transplanted epicardially in mice immediately after left anterior descending (LAD) coronary artery ligation to generate MI. This method was not previously published and most studies opted for slightly larger models such as rats. It is possible that some researchers would have chosen a rat model in the belief that a mouse model would be too small, but we have now shown that the mouse model is suitable if the correct equipment such as magnifying glasses and a microscope are used for the intubation and surgery, respectively. This opens up the option of using mice, allowing for selection of genetically modified mouse strains and generally greater feasibility allowing for higher numbers of repeats and lower costs.

Transplantation of a 3D Bioprinted Patch in a Murine Model of Myocardial Infarction

Christopher D. Roche[1,2,3,4], **Carmine Gentile**[1,2,3]

[1] The University of Sydney [2] University of Technology Sydney (UTS) [3] The Royal North Shore Hospital [4] University Hospital of Wales

Corresponding Author

Carmine Gentile
Carmine.Gentile@uts.edu.au

Citation

Roche, C.D., Gentile, C. Transplantation of a 3D Bioprinted Patch in a Murine Model of Myocardial Infarction. *J. Vis. Exp.* (163), e61675, doi:10.3791/61675 (2020).

Date Published

September 26, 2020

DOI

10.3791/61675

URL

jove.com/video/61675

Abstract

Testing regenerative properties of 3D bioprinted cardiac patches in vivo using murine models of heart failure via permanent left anterior descending (LAD) ligation is a challenging procedure and has a high mortality rate due to its nature. We developed a method to consistently transplant bioprinted patches of cells and hydrogels onto the epicardium of an infarcted mouse heart to test their regenerative properties in a robust and feasible way. First, a deeply anesthetized mouse is carefully intubated and ventilated. Following left lateral thoracotomy (surgical opening of the chest), the exposed LAD is permanently ligated and the bioprinted patch transplanted onto the epicardium. The mouse quickly recovers from the procedure after chest closure. The advantages of this robust and quick approach include a predicted 28-day mortality rate of up to 30% (lower than the 44% reported by other studies using a similar model of permanent LAD ligation in mice). Moreover, the approach described in this protocol is versatile and could be adapted to test bioprinted patches using different cell types or hydrogels where high numbers of animals are needed to optimally power studies. Overall, we present this as an advantageous approach which may change preclinical testing in future studies for the field of cardiac regeneration and tissue engineering.

Introduction

A heart transplant is the gold standard treatment for patients with end-stage heart failure but there is a shortage of donor organs. It requires immune system suppression to prevent graft rejection and the one-year mortality rate is 15% worldwide[1]. Therefore, there is a longstanding incentive to regenerate the myocardium in preclinical animal models with a view to translating to human trials[2,3,4,5,6,7,8,9]. Recent advances in 3D bioprinting of stem cells or stem cell-derived cardiac cells have gained attention as a promising approach to regenerate the myocardium[2,3,9,10,11,12].

The first human safety trials applying patches to regenerate the heart have been reported, with autologous bone marrow mononuclear cells suspended in collagen or embryonic stem cell-derived cardiac progenitor cells in fibrin, transplanted to the epicardium[7,8,13]. However, for a more precise, scalable, automatable and reproducible method, 3D

bioprinting of optimized hydrogel patches to be applied to the epicardial surface of the heart is a promising approach to regenerate the myocardium for patients who would otherwise need a heart transplant[2, 10, 11, 12].

Before translation to human trials can occur, preclinical animal studies are needed. Preclinical in vivo models pursuing regeneration of the myocardium have been reported in pigs[5], sheep[14], rats[6] and mice[4]. A common model of myocardial infarction (MI) in mice uses permanent ligation of the left anterior descending (LAD) coronary artery[15, 16]. Among the different strains of mice used, permanent LAD ligation in C57BL6 mice has an acceptable survival rate and typically presents consistent remodeling and cardiac changes after MI[16]. In rodent models, several approaches have been described where cardiac tissue has been applied to the heart in pursuit of effective regeneration of damaged myocardium[4, 6, 17]. While large animals still represent a more clinically relevant model to test cardiac regenerative properties[5, 14], the versatility and feasibility of the mouse model lends itself to this fast-moving area of study. This may avoid some of the pitfalls typical of large animal studies, including (but not limited to): 1) high animal mortality (unless diagonal coronary arteries are ligated leading to unpredictable segmental infarcts[14], or the distal end of the LAD is occluded followed by reperfusion instead of permanent ligation[5]); 2) ethical issues with the relatively increased harm caused by large animal protocols compared to mice[18]; 3) increased cost and/or feasibility issues, for instance the relative unavailability of large animal equipment such as MRI scanners[14]. It is also important to consider that given the extensive duration and commitment typical of large animal studies, they have the potential to become outdated before they are finished, especially with the rapid developments typical of this field. For instance, it is only recently that the critical role played by inflammatory cells and mediators in regulating cardiac regeneration has emerged[19, 20]. Furthermore, the critical role of preclinical studies, such as small animal models, has been highlighted by a Lancet Commission as an essential step to gain robust knowledge before moving to human trials[21].

To facilitate progress in understanding mechanisms and optimizing conditions for patch-based cardiac regeneration approaches in vivo, we present a novel approach describing a 'scoop and drape' method to apply a 3D bioprinted alginate/gelatine hydrogel patch to the surface of infarcted hearts in C57BL6 mice. The aim of this approach is to provide a versatile in vivo model to test 3D bioprinted patches that are likely to be feasible in broad research contexts for the rapidly-evolving field of cardiac regeneration[2]. This method could be adapted to test patches generated by non-bioprinting methods, different hydrogels and autologous or allogenic stem cell-derived cells within patches in vivo. However, detailed consideration of bioprinting, hydrogels or cell types is beyond the scope of this study which focuses on the surgical transplantation method.

The advantages of the protocol include that the myocardial infarction and application of a bioprinted patch are performed in one surgical procedure that can be performed quickly, with readily-available, cost effective laboratory tools and with a relatively low mortality rate. It also typically allows for a higher number of animals than large animal models in a smaller space, which permits robust comparison of multiple experimental groups, particularly useful for multiple group comparison in vivo. On the other hand, this protocol has the disadvantages that: 1) the mouse model is more distant from human heart size, anatomy and physiology than in large animal models and it does not directly translate into humans;

2) the murine LAD branches proximally, with significant variability between individual mice, which leads to infarct size variability (a problem shared with large animal models); 3) the patch must be applied over the whole anterior heart surface, which is less precise than applying over a specific infarct area; and 4) the patch is applied immediately at the time of MI (for human use it is likely to be more clinically useful to develop a patch for application to the chronically infarcted failing heart months following the initial MI[14]).

Nonetheless, if chosen appropriately according to the hypothesis being tested, this protocol can provide critical in vivo data quickly, with high n numbers, in a way that is consistent with the materials, budget and expertise available in most laboratories. Compared to large animal models, it is an in vivo model that is versatile enough to adapt to emerging 3D bioprinting technologies (for example by the relative ease of performing pilot studies to test feasibility and safety before moving to larger animal models). It would be well-suited for researchers who want to generate in vivo data efficiently and inexpensively, perhaps running multiple comparisons of 3D bioprinted patches with different bioprinting parameters, cells or hydrogels in the patches. It would be especially useful for testing the interactions of different mixtures of stem cells and stem cell-derived cells with hydrogels in vivo without excess wastage of expensive cell lineages or other materials that might occur if using large scale patches. Using a mouse model would also facilitate testing of patches containing species-compatible mouse-derived cell and stem cell lineages or human-derived cells where uniform mice with a specific immune deficiency are desirable. Additionally, testing in genetically modified mouse strains could allow researchers to isolate the effects of specific genes on signaling pathways and in specific cell types relevant to cardiovascular disease, which would not currently be possible in a large animal model.

Protocol

All procedures described in this experiment were approved by the Animal Ethics Committee at the Northern Sydney Local Health District, NSW, Australia (project number RESP17/55).

1. Anesthesia and intubation

NOTE: Turn on and set up the stereomicroscope, the heat pad (covered with an absorbant sheet) and ventilator system.

1. Clean gloves, the surgical area, and the tools with 70% ethanol.
2. Weigh the mouse to calculate the dosage of anesthesia injected by the intraperitoneal route (ketamine 40 mg/kg, xylazine 5 mg/kg, atropine 0.15 mg/kg) and give the injection.
3. Once the mouse reaches a deep plane of anesthesia, shave the ventral left side of the thorax with a trimmer.
4. Place the mouse in a chamber containing 2% isoflurane (ensuring adequate extraction ventilation in the room).
   NOTE: The relatively low dose of ketamine/xylazine injection together with 2% isoflurane inhalation reduces the risk of mouse death while allowing optimal intubation without waking the mouse up.
5. Place the mouse supine and restrain it from its upper incisor teeth with a 3.0 suture taped to the bench, as shown in the video. Confirm sedation by performing a toe pinch. Position a high-intensity illuminator above the mouse neck so that the oropharynx can be visualized.
   NOTE: Alternatively, the mouse can be placed on the stand from the intubation kit (e.g., Kent Mouse Intubation

Kit) with an elastic band secured under the top incisors to hold the mouth open to identify the trachea.

6. Use a curved spatula to open the jaw and another pair of spatulas/blunt forceps to lift the tongue gently out of the way. Be sure to intubate while positioned at or slightly below eye-level with the body of the mouse.
7. Visualize the opening and closing of the vocal cords. When open, insert the 20 G plastic catheter supplied with the intubation kit.
8. Carefully transfer the intubated mouse to an operating surface equipped with a heating pad. Connect the mouse to the ventilator (e.g., MouseVent) that automatically sets the target volume based on mouse weight.
9. Deliver 1.5-2% isoflurane with oxygen (which is automatically regulated by the ventilator: ensure there is a connection from an oxygen cylinder to the automatic ventilator at 1-2 L/min flow rate to the ventilator). Verify the intubation by checking for bilateral chest rise. Verify anesthesia by performing a toe pinch.
10. Apply opthalmic ointment (e.g., Puralube Vet Opthalmic Ointment) to both eyes to prevent them from drying out.

2. Preparing the surgical field

1. Secure the intubation tube with tape at the connecting site between the ventilator and the breathing tube/catheter.
2. Cut a longer piece of tape and secure its left front foot to the operating surface in a slightly elevated position. Also tape down the other extremities.
3. Clean the chest with sterile 70% isopropanol and povidone iodine solution, cleaning in a circular motion moving from center to periphery.
4. Verify anesthesia once more with a toe pinch.
5. Administer 0.08 mg/kg Temvet (buprenorphine) in 0.1 mL of 0.9% saline via subcutaneous injection.

3. Left lateral thoracotomy

1. Use fine-tip forceps to gently lift the skin at a point approximately 5 mm to the left of the prominent xiphoid cartilage. Use surgical scissors to create a superomedial incision in the skin from this point upwards and towards the midline, to the level of the manubrium.
2. Use curved forceps to gently separate the skin and muscle layers. Open the muscle layer, following the skin incision.
3. Identify and make an incision in the third intercostal space, following the natural angle of the ribcage.
4. Use a retractor to gently spread apart the 3rd and 4th ribs.
5. Gently remove the thin pericardium with forceps.
6. If the LAD is not visualized, gently push the left auricle (see **Supplementary Figure 1**) upwards and locate the coronary arteries underneath.

4. Left anterior descending (LAD) permanent coronary artery ligation

1. Cut a ~3 mm long 3-0 silk suture and put this reinforcing 3-0 silk suture piece on top of the LAD in the same direction as the LAD (as shown in the video at time point 02:12 – 02:20).
2. Identify the LAD and pass a 7-0 silk suture under the LAD. If the LAD is not clearly visualized, insert the needle 1 mm inferior and medial to the inferiormost point reached by the tip of the left auricle during dynamic movement of the heart.

   NOTE: This structure is a lighter color red to the ventricular chambers of the heart but darker than the

adjacent lung and is best visualized in the video at time point 01:54 – 01:55 where it is visible just inferior to the superior arm of the retractor, superior to the left lung (see **Supplementary Figure 1** for annotated video still image).

3. Complete two throws with the 7-0 silk suture and close it tightly passing on top of the supportive 3-0 silk suture to secure the LAD. If the ligation is successful, the anterior ventricular area distal from the ligature will blanch.
4. Complete the knot with a third throw in the opposite direction to secure it, ensuring no upward traction force is transmitted to the suture. Additional throws are not required to reduce the risk of damage to the myocardium or LAD by suture cutting through.

5. Transplantation of the bioprinted patch onto the epicardium

1. Carefully move the bioprinted patch from a six well plate to the infarct area by using the sterile inside surface of an opened surgical scalpel packet.
2. Carefully position the bioprinted patch onto the anterior epicardial surface, where it should cover the whole surface and drape over the inferior and lateral edges, covering the left ventricle and the infarct zone (blanched area).
3. Gently close and remove the retractor without directing sharp edges towards the heart.
4. Use 6-0 prolene sutures in a simple interrupted pattern to close the ribcage and the muscle layers.
5. With the Sigh Breath function while closing the chest with the 6-0 prolene sutures, inflate the lungs to remove excess air in the pleural cavity, which would otherwise become trapped in the chest cavity and result in a pneumothorax.
6. Ensure that the chest is tightly sealed.
7. Decrease the isoflurane to 1.0%. Close the skin with 6-0 prolene sutures in a simple interrupted pattern. Turn the isoflurane vaporizer off.

6. Mouse recovery

1. Topically apply 2 mg/mL bupivacaine in 0.9% saline to the incision. Administer also: i) Antisedan (atipamezole) 1 mg/kg; ii) Lasix (furosemide) 8 mg/kg; iii) 600 µL of 0.9% saline solution via a subcutaneous injection.
   NOTE: Antisedan is to reverse the anesthetic more rapidly; furosemide is to offload excess fluid due to cardiac output compromise and additional fluid administered with drug injections.
2. Monitor the mouse and wait until independent breathing is observed to remove the mouse from the intubation tube.
3. When the mouse demonstrates an adequate bilateral breathing rate and depth and responds to a toe pinch, place the mouse in a clean recovery cage placed on a heat pad.
4. Provide the mouse with moist food (moistened for chewability), a water bottle and nutrient/hydrating gel. Monitor for an exaggerated breathing effort, excessive bleeding, or other potentially life-threatening complications.
5. For the next three days, administer 0.08 mg/kg Temvet (buprenorphine) in 0.1 mL of 0.9% saline via subcutaneous or intraperitoneal injection, twice daily, then once daily up to the fifth day following the procedure.
6. House mice in pairs separated by cage dividers to prevent isolation whilst preventing fighting behaviors. Monitor mice at least daily until the end of the experiments (28

days) with close attention to their wellbeing and increased frequency of monitoring if there are any concerns.

Representative Results

At transplantation, the viscosity of the patch at room temperature (without additional crosslinker being applied) allowed it to 'drape' over the contours of the heart (**Figure 1**) and move dynamically with the cardiac cycle. After the surgery, we left the patches for 28 days in vivo as studies have found this to be a suitable time period allowing for patch effects on host cardiac function[3,4] (although it has been reported that full functional effects may not be seen until three months after transplantation)[22]. The photograph of a patch shown in situ on a mouse heart in **Figure 1** was taken immediately after application, showing the ability of the patch to drape over the heart at transplantation. This representative result shows that the hydrogel allows for the patch to mold to the contours of the heart and where excessive tension occurred the hydrogel was able to split as shown by the bare (hydrogel-free) triangular area in **Figure 1** (indicated by a black star in the image). Survival data (Kaplan-Meier survival curves) are shown in **Figure 2** compared to mice undergoing a sham procedure (passage of a needle and suture under the LAD without ligation followed by closure of the mouse chest).

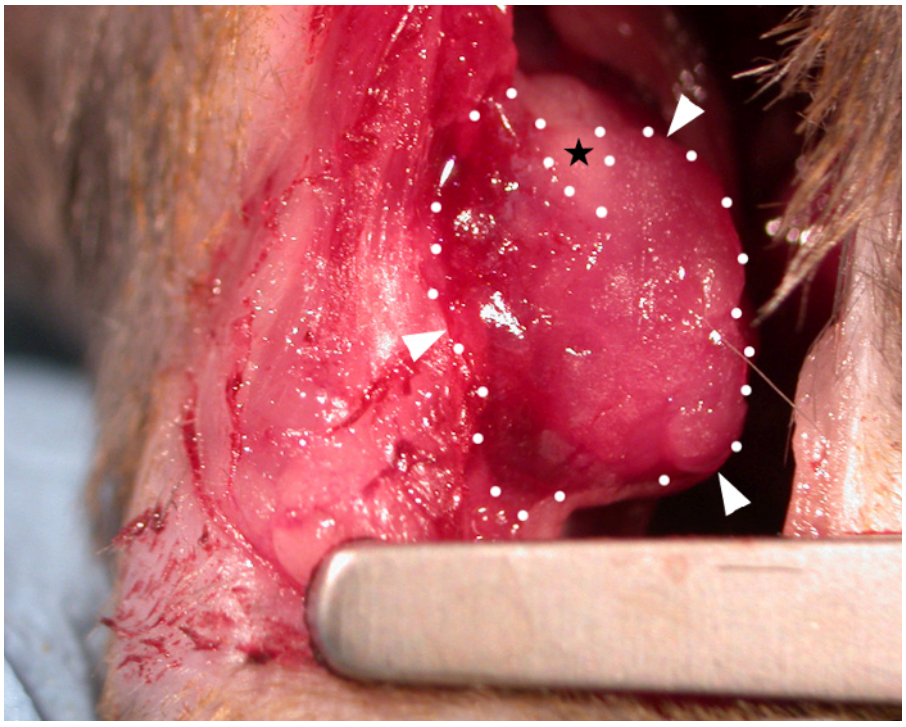

Figure 1: A bioprinted cardiac patch applied onto the epicardium of a C57BL6 mouse heart. A 10 mm x 10 mm x 0.4 mm bioprinted patch (immediately after transplantation) containing hydrogel (alginate 4% (w/v)/gelatine 8% (w/v) in media) is shown draped over the infarcted area and adhering to the epicardial surface (white arrowheads and dotted lines = border of the patch). The patch viscosity allows it to mold to the contours of the heart and where excessive tension occurred at the superior aspect the patch has split to make a triangular bare area not covered by hydrogel (black star). Please click here to view a larger version of this figure.

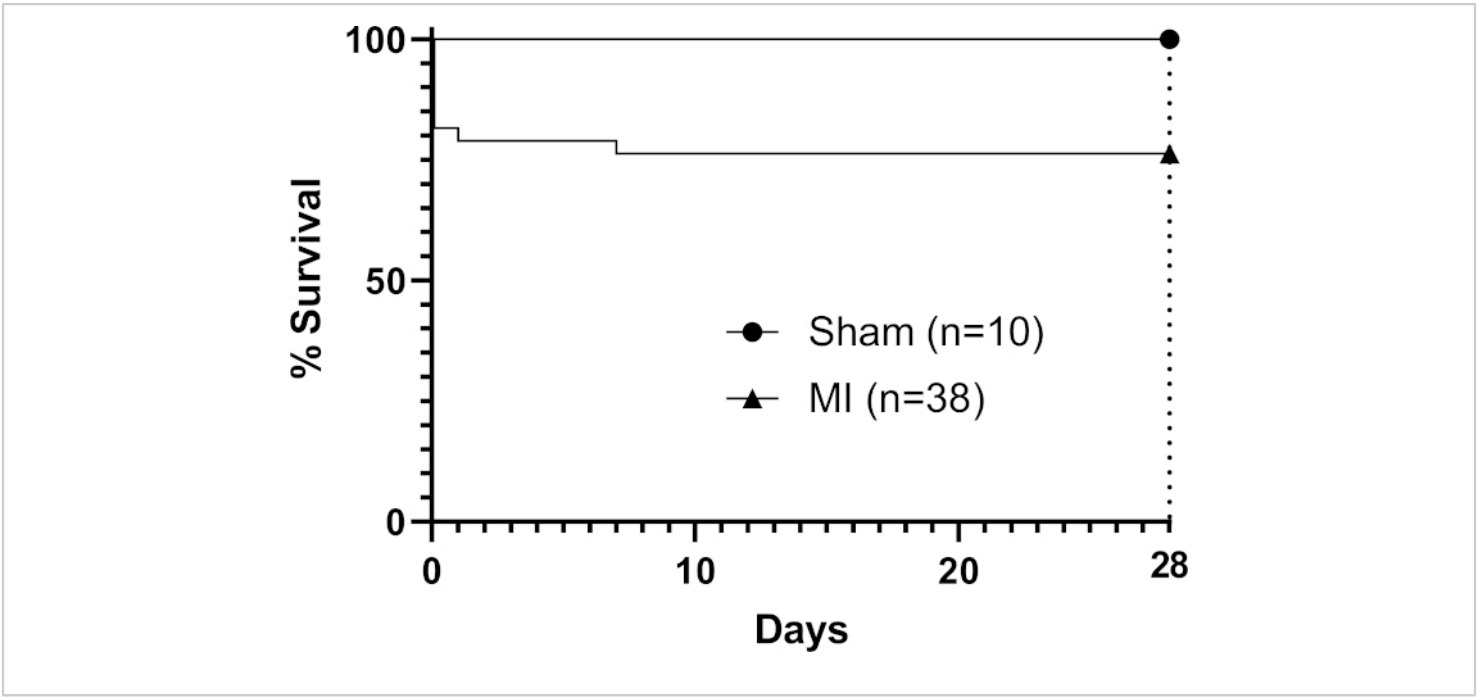

Figure 2: Kaplan-Meier survival analysis through 28 days post-MI. Nine mice in the procedural group died (n=38) to give an overall mortality rate of 24%. Please click here to view a larger version of this figure.

Supplementary Figure 1: Video still image (video time point 01:54 – 01:55) showing the left auricle (left atrial appendage). The arrow points to the inferomedial tip of the left auricle which is visible as a triangular structure at the superior left edge of the heart. In case the LAD is not clearly visualized, the tip of the left auricle can be used as a landmark for needle entry to pass a suture under the LAD. The entry point is 1 mm inferior and medial to the inferiormost point the tip of the left auricle reaches during dynamic movements of the heart (black arrow shows inferomedial tip of the left auricle). Please click here to download this figure.

Discussion

The method facilitates the operator to efficiently transplant a bioprinted patch by applying it to the epicardial surface of an infarcted mouse heart following permanent LAD ligation. In this feasibility-focused method, we are able to perform this procedure on eight mice per working day (including preparation of the room before and afterwards). A bioprinting run producing eight 1 cm^2 patches in wells of six-well plates takes 2-3 hours (including preparation time before and after). We used the sterile inside of a surgical scalpel packet as the scoop for our patch, which is readily accessible and generally adds minimal cost, utilizing the natural adhesive properties of the alginate/gelatine hydrogel patch to drape the patch across the anterior infarcted surface of the heart. In our experience, the protocol for LAD ligation in mice is operator dependent and a lower mortality rate at 28 days can be achieved with experienced operators specialized in one model. Van den Borne et al.[16] reported that C57BL6 mice present a 44% mortality following permanent LAD ligation at 28 days without the application of a patch, which is higher than the upper limit of 30% that we observed with the method.

The intubation step is critical and in-and-of-itself can be a source of mortality for mice unless performed by a skilled operator. It is made difficult due to the tiny size of the trachea, which is why magnifying glasses are worn by the operator for this step. We use injected ketamine/xylazine as well as inhaled isofluorane for induction of anesthetic so that the mouse is deeply anesthetized at relatively low doses of each drug. Therefore, there is no risk for the mouse to wake up during this intubation step but the high mortality associated with high single-drug doses is avoided. Atropine was also given to counteract side effects such as bradycardia and hypersalivation. The use of a spotlight applied to the throat externally lights up the trachea internally so it is more visible and the vocal cords must be visualized opening and closing with the mouse's respiratory rate (usually ~120 breaths per minute). It is critical to position the mouse perfectly (which is why a hard surface is preferred rather than a warming mat underneath the mouse for this step) with the two incisor teeth held by a looped thread and the tongue retracted extremely gently with blunt forceps/pair of spatulas to open the mouth and visualize the trachea. Once the intubation is completed, the operator must be careful not to dislodge the tube in the transfer from the intubation area to the operating bed (which does have a heat mat underneath it to prevent hypothermia). When connecting the breathing tube to the ventilator apparatus, it is critical to stabilize the tube with one hand and connect the ventilator circuit with the other, so that there is minimal movement of the breathing tube such as pushing it more deeply into the trachea when connecting the ventilator segment of the tubing.

In this study, we used alginate 4% (w/v)/gelatine 8% (w/v) in Dulbecco's Modified Eagle Medium (DMEM). Alginate/gelatine hydrogels are known for their biocompatibility, low cost and biomechanical properties making them useful for 3D tissue engineering strategies[23]. These hydrogels can be crosslinked by mild gelation by adding calcium ions, which allows for viscosity to be altered. After bioprinting, we applied calcium chloride ($CaCl_2$) 2% (w/v) in phosphate-buffered saline (PBS) onto patches and then cultured them in DMEM in six well plates for 7-14 days before transplanting them. This was the optimal window after patches containing cardiac cells started to beat in culture but before patches started to disintegrate. Whilst $CaCl_2$ could be added regularly throughout the post-bioprinting phase to reduce patch disintegration, we found that the intrinsic viscosity of the hydrogel was sufficient for patches to maintain their structure up to transplantation with only one initial dose of $CaCl_2$.

The method allowed for successful transplantation without sutures (which may damage the heart) or glue (which may block the interface between the patch and the heart). Future studies may confirm the hypothesis that sutureless and glueless transplantation does not negatively impact engraftment in mice as it is critical that the patch does not slip off the heart or interfere with the lungs. Other studies assessing engraftment of patches in permanent LAD ligation models with patch-based repair[3] have measured engrafted area (mm^2) remaining with time[24], the grafted patch thickness (μm) remining with time[25], quantification of transplanted cells by polymerase chain reaction (PCR)[26] or bioluminescence photon emission flux of labelled live donor cells (a measure of photons emitted per second which can quantify labelled grafted cells surviving in living animals over time)[27]. Future studies may use these methods to further evaluate whether sutureless and glueless transplantation affects patch engraftment (as well as structural and functional effects on the host myocardium). Nonetheless, macroscopically after 28 days in vivo in our immunocompetent mice, the anterior mediastinum

presented variable fibrinous material and adhesions. The mechanism of patch-based cardiac regeneration may be from stimulation of host macrophage inflammatory responses[19] or secreted immunological factors[20] rather than numerical cell replenishment. If inflammation plays a positive role, the presence of foreign hydrogel material may be beneficial. Alternatively, to reduce the presence of foreign material it may be beneficial if the hydrogel component disintegrates over time. In fact, some approaches use biomaterials which support cells initially and then disintegrate, leaving only tissue[28,29]. Future studies to fully analyze patch engraftment and better understand the mechanisms behind patch-based cardiac regeneration may lead to optimized experimental designs before translation to human trials[2].

Overall, this protocol is likely to be widely feasible and also suited to testing multiple groups of 3D bioprinted patches, for instance with different cellular contents. Future directions for this method include the bioprinting of patches containing advanced hydrogels not previously tested in vivo or testing the effects of different autologous or allogenic stem cell-derived cells, for optimization before proceeding to large animal models.

Disclosures

None.

FUNDING STATEMENT:

Christopher D. Roche was supported by a Sir John Loewenthal Scholarship 2019 (University of Sydney), the Le Gros Legacy Fund New Zealand (PhD012019) and a Heart Research Australia PhD Scholarship (2019-02). Carmine Gentile was supported by a University of Sydney Kick-Start Grant, University of Sydney Chancellor's Doctoral Incentive Programme Grant, UTS Seed Funding, Catholic Archdiocese of Sydney Grant for Adult Stem Cell Research and a Sydney Medical School Foudation Cardiothoracic Surgery Research Grant.

Acknowledgments

With thanks to Natalie Johnston for the recording of the non-surgical footage and all video editing.

References

1. Lund, L. H. et al. The registry of the International Society for Heart and Lung Transplantation: thirty-fourth adult heart transplantation report-2017; focus theme: allograft ischemic time. *Journal of Heart and Lung Transplantation.* **36** (10), 1037-1046 (2017).
2. Roche, C. D., Brereton, R. J. L., Ashton, A. W., Jackson, C., Gentile, C. Current challenges in three-dimensional bioprinting heart tissues for cardiac surgery. *European Journal of Cardio-Thoracic Surgery.* **58** (3), 500-510 (2020).
3. Wang, H., Roche, C.D., Gentile, C. Omentum support for cardiac regeneration in ischaemic cardiomyopathy models: a systematic scoping review. *European Journal of Cardio-Thoracic Surgery.* ezaa205. Epub ahead of print (2020).
4. Mattapally, S. et al. Spheroids of cardiomyocytes derived from human-induced pluripotent stem cells improve recovery from myocardial injury in mice. *American Journal of Physiology-Heart and Circulatory Physiology.* **315** (2), H327-h339 (2018).
5. Gao, L. et al. Large cardiac muscle patches engineered from human induced-pluripotent stem cell-derived cardiac cells improve recovery from myocardial infarction in swine. *Circulation.* **137** (16), 1712-1730 (2018).

6. Yang, B. et al. A net mold-based method of biomaterial-free three-dimensional cardiac tissue creation. *Tissue Engineering Methods (Part C).* **25** (4), 243-252 (2019).
7. Menasché, P. et al. Human embryonic stem cell-derived cardiac progenitors for severe heart failure treatment: first clinical case report. *European Heart Journal.* **36** (30), 2011-2017 (2015).
8. Menasché, P. et al. Transplantation of human embryonic stem cell-derived cardiovascular progenitors for severe ischemic left ventricular dysfunction. *Journal of the American College of Cardiology.* **71** (4), 429-438 (2018).
9. Beyersdorf, F. Three-dimensional bioprinting: new horizon for cardiac surgery. *European Journal of Cardio-Thoracic Surgery.* **46** (3), 339-341 (2014).
10. Noor, N. et al. 3D printing of personalized thick and perfusable cardiac patches and hearts. *Advanced Science.* **6** (11), 1900344 (2019).
11. Maiullari, F. et al. A multi-cellular 3D bioprinting approach for vascularized heart tissue engineering based on HUVECs and iPSC-derived cardiomyocytes. *Scientific Reports.* **8** (1), 13532 (2018).
12. Zhang, Y. S. et al. Bioprinting 3D microfibrous scaffolds for engineering endothelialized myocardium and heart-on-a-chip. *Biomaterials.* **110** 45-59 (2016).
13. Chachques, J. C. et al. Myocardial assistance by grafting a new bioartificial upgraded myocardium (MAGNUM clinical trial): one year follow-up. *Cell Transplant.* **16** (9), 927-934 (2007).
14. Chachques, J. C. et al. Elastomeric cardiopatch scaffold for myocardial repair and ventricular support. *European Journal of Cardio-Thoracic Surgery.* **57** (3), 545-555 (2020).
15. Reichert, K. et al. Murine left anterior descending (LAD) coronary artery ligation: an improved and simplified model for myocardial infarction. *Journal of Visualized Experiments.* (122) (2017).
16. van den Borne, S. W. M. et al. Mouse strain determines the outcome of wound healing after myocardial infarction. *Cardiovascular Research.* **84** (2), 273-282 (2009).
17. Noguchi, R. et al. Development of a three-dimensional pre-vascularized scaffold-free contractile cardiac patch for treating heart disease. *Journal of Heart and Lung Transplantation.* **35** (1), 137-145 (2016).
18. Walker, R. L., Eggel, M. From mice to monkeys? Beyond orthodox approaches to the ethics of animal model choice. *Animals.* **10** (1), 77 (2020).
19. Vagnozzi, R. J. et al. An acute immune response underlies the benefit of cardiac stem-cell therapy. *Nature.* **577**, 405-409 (2019).
20. Waters, R. et al. Stem cell-inspired secretome-rich injectable hydrogel to repair injured cardiac tissue. *Acta Biomaterialia.* (69), 95-106 (2018).
21. Cossu, G. et al. Lancet Commission: stem cells and regenerative medicine. *Lancet.* **391** (10123), 883-910 (2018).
22. Kawamura, M. et al. Enhanced therapeutic effects of human iPS cell derived-cardiomyocyte by combined cell-sheets with omental flap technique in porcine ischemic cardiomyopathy model. *Scientific Reports.* **7** (1), 8824 (2017).
23. Lee, K. Y., Mooney, D. J. Alginate: properties and biomedical applications. *Progress in Polymer Science.* **37** (1), 106-126 (2012).

24. Kainuma, S. et al. Cell-sheet therapy with omentopexy promotes arteriogenesis and improves coronary circulation physiology in failing heart. *Molecular Therapy.* **23** (2), 374-386 (2015).

25. Suzuki, R. et al. Omentopexy enhances graft function in myocardial cell sheet transplantation. *Biochemical and Biophysical Research Communications.* **387** (2), 353-359 (2009).

26. Zhou, Q., Zhou, J.Y., Zheng, Z., Zhang, H., Hu, S.S. A novel vascularized patch enhances cell survival and modifies ventricular remodeling in a rat myocardial infarction model. *Journal of Thoracic and Cardiovascular Surgery.* **140** (6), 1388-1396.e1383 (2010).

27. Lilyanna, S. et al. Cord lining-mesenchymal stem cells graft supplemented with an omental flap induces myocardial revascularization and ameliorates cardiac dysfunction in a rat model of chronic ischemic heart failure. *Tissue Engineering (Part A).* **19** (11-12), 1303-1315 (2013).

28. Miller, J. S. et al. Rapid casting of patterned vascular networks for perfusable engineered three-dimensional tissues. *Nature Materials.* **11** (9), 768-774 (2012).

29. Zhang, B. et al. Biodegradable scaffold with built-in vasculature for organ-on-a-chip engineering and direct surgical anastomosis. *Nature Materials.* **15** (6), 669-678 (2016).

Materials List for

Transplantation of a 3D Bioprinted Patch in a Murine Model of Myocardial Infarction

Christopher D. Roche[1,2,3,4], **Carmine Gentile**[1,2,3]

[1]The University of Sydney [2]University of Technology Sydney (UTS) [3]The Royal North Shore Hospital [4]University Hospital of Wales

Corresponding Author

Carmine Gentile

Carmine.Gentile@uts.edu.au

Citation

Roche, C.D., Gentile, C. Transplantation of a 3D Bioprinted Patch in a Murine Model of Myocardial Infarction. *J. Vis. Exp.* (), e61675, doi:10.3791/61675 (2020).

Date Published

September 26, 2020

DOI

10.3791/61675

URL

jove.com/video/61675

Materials

Name	Company	Catalog Number	Comments
3-0 non-absorbable black braided treated silk	Ethicon	232G	
6-0, 24” (60 cm) Prolene (polypropylene) suture, blue monofilament	Ethicon	8805H	
7-0, 18” (45 cm) silk black braided	Ethicon	768G	
Adjustable stereo microscope with 6.4x magnification	Olympus	SZ 3060 STU1	
Anitisedan (atipamezole)	Zoetis	N/A	
Atropine sulphate 0.6 mg, 1 mL vials, 10 pack	Symbion Pharmacy Services	ATRO S I2	
Bupivacaine, 20 mL, 5 vials	Baxter Heathcare	BUPI I C01	
Temvet (buprenorphine), 300 µg/mL, 10 mL bottle	Troy Laboratories	TEMV I 10	
Curved-tip forceps	Kent Scientific	INS650915-4	Iris dressing forceps, 10 cm-long curved dressing forceps; 0.8 mm serrated tips; stainless steel.
Dissecting scissors for cutting muscle/skin	Kent Scientific	INS600393-G	Dissecting scissors, straight, 10 cm long
Endotracheal intubation kit	Kent Scientific	ETI-MSE	Including intubation catheter/tube (20 G), fibre-optic light source and dental spatula
Fine scissors	Kent Scientific	INS600124	McPherson-Vannas micro scissors, 8 cm long, straight, 0.1 mm tips, 5 mm blades; stainless steel.
Lasix (furosemide) 20 mg, 2 mL, 5 pack	Sigma Company	LASI A 1	
Heat pad for animal recovery post-op	Passwell	PAD	Passwell Cosy Heat Pad for Animals - 26cm x 36cm; 10 Watts; Soft PVC Cover
Ketamine 100 mg, 50 mL	CEVA Animal Heath	KETA I 1	
Needle holder	Kent Scientific	INS600137	Castroviejo needle holder, serrated, 14 cm long, 1.2 mm jaws with lock

PhysioSuite with MouseVent G500 automatic ventilator	Kent Scientific	PS-MVG	
Puralube Vet Opthalmic Ointment (sterile occular lubricant)	Dechra	17033-211-38	
Self-retaining toothed mouse retractor	Kent Scientific	INS600240	ALM serrated self-retaining retractor, 7 cm long
Straight forceps	Kent Scientific	INS650908-4	Super fine dressing forceps, 12.5 cm Long, serrated tips, 0.35 x 0.10 mm; stainless steel.
Surgical magnifying glasses	Kent Scientific	SL-001	
VetFlo vaporizer	Kent Scientific	VetFlo-1205S-M	
Xylazine 100 mg, 50 mL	Randlab	XYLA I R01	

2.4 – 3D bioprinted alginate-gelatin hydrogel patches containing cardiac spheroids recover heart function in mice modelling myocardial infarction

Summary:

This article is currently under review with *Acta Biomateralia* and contains the complete method, results and discussion for an *in vivo* study using patches similar to the ones optimised in Chapter 2.1 and the surgical transplantation method detailed in Chapter 2.2. The study aimed to evaluate the hypothesis that cardiac function would be improved after MI with epicardial transplantation of 3D bioprinted patches containing VCS in alginate-gelatin bioink. The mixed cardiac cells used were induced pluripotent stem cell-derived cardiomyocytes (iCMs), human coronary artery endothelial cells (HCAECs) and cardiac fibroblasts (CFs). VCS bioink was compared to similar bioink with those cells freely suspended in the hydrogel (not in spheroids) as well as hydrogel on its own (with no cells). We found a significant increase in left ventricular ejection fraction (LVEF%) with the VCS-containing patches by day 28 post MI. We also found lesser increases when the cells were suspended freely and even with hydrogel without cells. To look for mechanistic insights, we also performed electrical mapping analyses in collaboration with our industry partner MappingLab (Oxford, UK). Some patches were also incubated *in vitro* and analysed with confocal microscopy and electrical mapping and this showed that the VCS displayed the strongest electrical activity waveforms, supporting the hypothesis that VCS confer an advantage over freely suspended cells and that our patches allow for electrical activity. Using histology we analysed trends between infarct size and cardiac function. It was recently reported that the mechanism underlying the benefits of patch-based regeneration strategies is due to modulation of the host innate immune response. We therefore performed flow cytometry to quantify cell types in heart tissue following patch transplantation and found significant differences in macrophage polarisation and natural killer cells on day 28 post MI. Using mRNA (transcriptome) analysis we explored changes in gene expression within patches and found that the VCS patch treatment group was similar to non-infarcted (sham) mice. This striking finding suggests a return in the transcriptomic profile to the non-infarcted state at day 28, which coincides with the most significant increase in LVEF% (in the VCS treatment group). Overall, this paper adds to the evidence that patch based strategies to regenerate myocardial function after MI are efficacious. It suggests that VCS containing patches were the most efficacious of the three treatments and provides mechanistic insights into why the treatment strategy seems to produce a reproducible improvement after MI.

3D bioprinted alginate-gelatin hydrogel patches containing cardiac spheroids recover heart function in a mouse model of myocardial infarction

Christopher D Roche[1,2,3], Haiyan Lin[3], Yizhou Huang[2,4,5], Charles E de Bock[4,5], Dominik Beck[2], Meilang Xue[3], Carmine Gentile[1,2*]

1 Faculty of Medicine and Health, University of Sydney, Sydney, NSW, Australia

2 Faculty of Engineering and IT, University of Technology Sydney (UTS), Sydney, NSW, Australia

3 Sutton Arthritis Research Laboratory, Kolling Institute, University of Sydney, Sydney, NSW, Australia

4 Children's Cancer Institute, Lowy Cancer Research Centre, UNSW Sydney, Sydney, NSW 2052, Australia.

5 School of Women's and Children's Health, UNSW Sydney, Sydney, NSW 2052, Australia.

*Corresponding author: Department of Biomedical Engineering, Faculty of Engineering and IT, Building 11, 81 Broadway, Ultimo, NSW 2007, Australia. Tel: +61-2-95144502; e-mail: carmine.gentile@uts.edu.au.

Keywords: 3D bioprinted patches, cardiac spheroids, *in vivo* testing, myocardial infarction, heart failure, hydrogels, stem cells,

Abstract

Epicardial transplantation of 3D bioprinted patches represents a promising protective strategy against infarction-induced myocardial damage. We previously showed that 3D bioprinted tissues containing cardiac spheroids (in alginate/gelatin (AlgGel) hydrogels) promoted cell viability/function and endothelial cell tubular self-assembly. Here, we hypothesise that bioprinted cardiac spheroid patches improve cardiac function after myocardial infarction (MI). To determine treatment effects of hydrogel alone or with cells, MI mice were transplanted with: (i) AlgGel acellular patches, (ii) AlgGel with freely suspended cardiac cells, (iii) AlgGel with cardiac spheroids. We included control MI mice (no treatment) and mice undergoing sham surgery. We performed measurements to 28 days including echocardiography, flow cytometry and transcriptomic analyses. Our results measured median baseline (pre-surgery) left ventricular ejection fraction (LVEF%) for all mice at 66%. Post-surgery, LVEF% was 58% for Sham (non-infarcted) and 41% for MI (no treatment) mice. Patch transplantation increased LVEF%: 55% (acellular; p=0.012), 59% (cells; p=0.106), 64% (spheroids; p=0.010). Flow cytometry demonstrated host cardiac tissue immune cell population changes with treatments. RNAseq transcriptomes demonstrated similar gene expression profiles for Sham and mice treated with cardiac spheroid patches. Inflammatory and genetic mechanisms may play important roles in regulating host responses after patch transplantation in infarcted hearts. Future studies are needed to elucidate the possible immune cell and gene expression-related molecular mechanisms underlying these initial findings.

Graphical Abstract

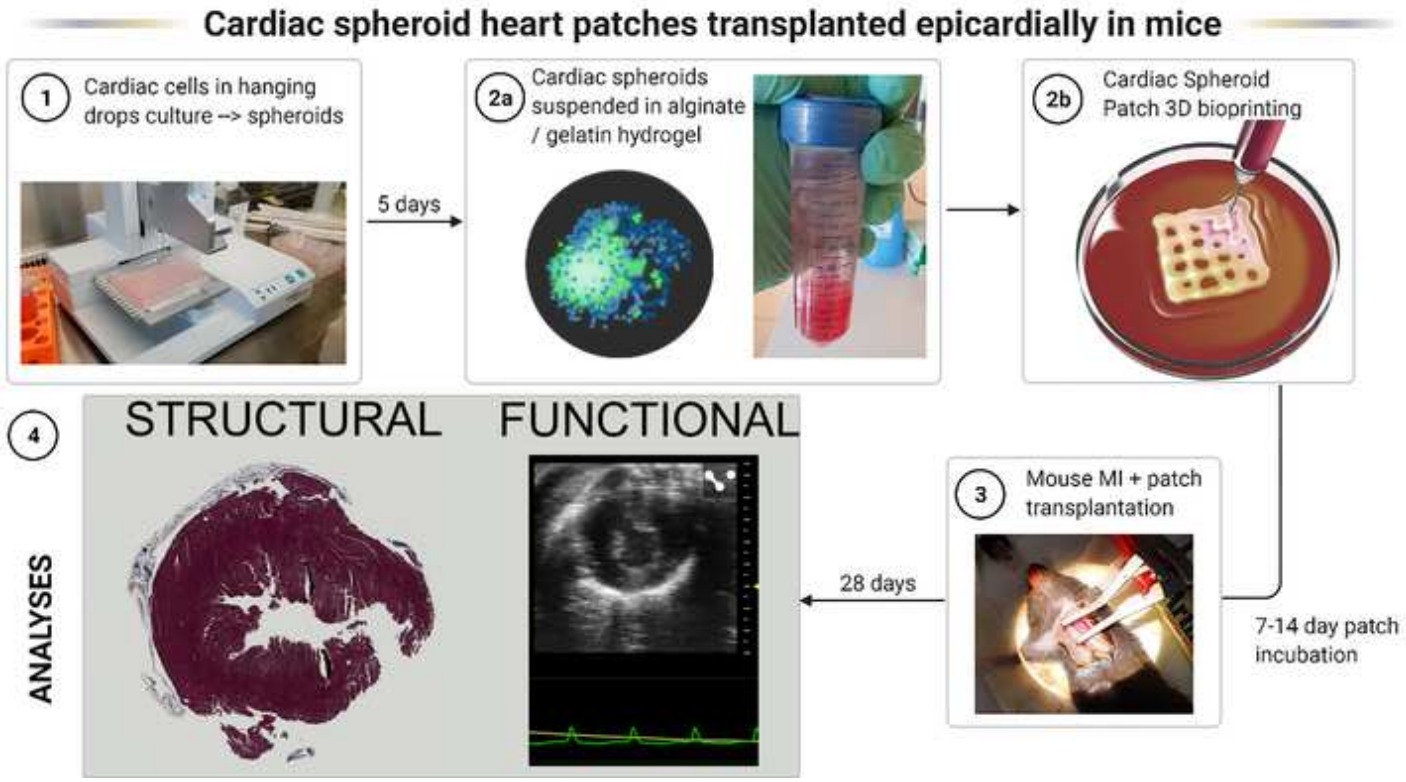

Introduction

Recent advances in 3D bioprinting and cell culture allow fabrication of patches for epicardial transplantation to protect the myocardium [1, 2]. For end-stage heart failure patients there is currently no ideal way to repair damaged heart muscle so that function can be regained, with the gold standard treatment being whole heart allotransplantation [3]. This requires a donor heart to arise (during which time patients may die whilst on a waiting list), major surgery with a significant mortality rate and the need for immunosuppressive drugs for life to reduce the risk of transplant rejection which carry risks of tumour development [4, 5]. This unmet need has driven extensive research into many treatment approaches to restore myocardial function [6], of which one promising approach is 3D bioprinting of heart tissue patches for epicardial transplantation [7].

Whilst this field is progressing to human trials, there remain persistent questions about the mechanism by which epicardial patches benefit cardiac structure and function after myocardial infarction (MI) [8-13]. Recent evidence suggests host inflammation modulation may be a primary mechanism and not, for instance, pursuit of cell number replenishment [14]. Despite recent advances in this field, additional preclinical studies are required to elucidate optimal conditions for heart patch bioengineering [7, 15]. Our laboratory has developed cardiac spheroids containing cell types found in the human heart [7]. Recently were employed as building blocks for the generation of vascularised viable and functional heart tissues [16]. Given their unique features to recapitulate some of the human heart microenvironment, we hypothesise that bioprinted patches containing vascularised cardiac spheroids (VCS) can improve cardiac function in mice with MI.

Herein, we present novel results from epicardial transplantation of 3D bioprinted hydrogel-based patches according to our established protocols in a surgical MI mouse model following permanent left anterior descending (LAD) artery ligation [15]. Our results raise new mechanistic questions and represent an initial search for mechanistic clues rather than an in-depth analysis of one aspect.

We 3D bioprinted patches with alginate/gelatin (AlgGel) and human cardiac fibroblasts (CFs), human coronary artery endothelial cells (HCAECs) and induced pluripotent stem cell-derived cardiomyocytes (iCMs). We examined for differences in cardiac functional and structural outcomes in MI mice receiving patches containing: 1) AlgGel hydrogel alone (MI+PATCH), 2) AlgGel with cardiac cells suspended freely (MI+PATCH CELLS), and 3) AlgGel with VCSs (MI+PATCH SPHEROIDS). Control mice received either a sham procedure (Sham) or LAD ligation without receiving any patch (MI). Finally, flow cytometry, histological and RNAseq analyses of tissues were performed to identify structural, cellular and molecular changes in the different treatment groups.

Materials and Methods

All procedures described in this experiment were approved by the University of Technology Sydney (UTS) Animal Care and Ethics Committee (project number ETH19-4338; 20/04/2017). The method was publicly preregistered before the start of the experiment (https://doi.org/10.17605/OSF.IO/7BQEW). The Vevo LAB echocardiography manual (including equations used for echocardiographic parameter calculations) is available from this article's permanent data repository (https://doi.org/10.5281/zenodo.6198612).

Culture of human cardiac cells. HCAECs (Sigma-Aldrich, MO, United States) were cultured in MesoEndo Growth Medium (Cell Applications, San Diego, CA, United States). CFs (Cell Applications, San Diego, CA, United States) were cultured in Cardiac Fibroblast Growth Medium (Sigma-Aldrich, St Louis, MO, United States). HCAECS and CFs were used for bioprinting at passage three. iCMs (iCell®, FujiFilm Cellular Dynamics, Madison, WI, United States) were cultured according to manufacturer's recommendations in iCell® Cardiomyocytes Maintenance Medium (FujiFilm Cellular Dynamics). In total, ~850,000 cells per 10x10x0.4 mm patch were used (iCMs : HCAECs : CFs, ratio 1 : 1.5 : 2.5).

VCS formation from cardiac cells. Mixed cardiac cells (iCMs : HCAECs : CFs, in the same ratio 1 : 1.5 : 2.5) were suspended in Spheroid Medium (2 : 1 : 1 of the iCell Maintenance Medium, MesoEndo and Cardiac Fibroblast Growth Media, respectively). VCSs were generated by coculturing ~10,000 mixed cardiac cells in 15 µl hanging drop cultures in Spheroid Medium, using Perfecta 3D® 384-well hanging drop plates (3D Biomatrix, Ann Arbor, MI, United States). VCSs were allowed to form for up to five days in hanging drops in a humidified incubator at 37°C with 21% (v/v) O_2 and 5% (v/v) CO_2 following our previous protocol [17]. In total, ~850,000 cells (83 spheroids) per patch were used.

Hydrogel preparation. Hydrogel was prepared according to our previous method optimised for cardiac applications [7]. Briefly, AlgGel powder – 4 mg alginate and 8 mg gelatin – was sterilised under UV light for 30 min then solubilised at 50°C in 100 ml Dulbecco's Modified Eagle Medium (DMEM) + 1% (v/v) pen/strep + 1% (v/v) L-glut.

Bioink generation. To create bioinks for bioprinting, AlgGel was added to pellets of mixed cardiac cells (iCMs, CFs, HCAECs), either as free cells (not in spheroids) or as VCS. Prewarmed (37°C) AlgGel was added to the cell or VCS pellet by pipette, of which 0.5 ml typically produced six 10 mm^2 patches. The AlgGel was resuspended until the cell pellet disappeared to ensure incorporation of most of the cells. All procedures were performed under a biological safety cabinet and within the bioprinter chamber.

Heart patch 3D bioprinting. Bioprinting was performed with a BIO X pneumatically driven extrusion 3D bioprinter (CELLINK Life Sciences, Boston, MA, USA). We used an optimised protocol based on our previous method for 3D bioprinting of AlgGel-based patches [7]. Briefly, a 3 ml BIO X syringe was filled with 70% (v/v) ethanol and a CELLINK 25-gauge conical polypropylene nozzle (250 µm inner diameter) attached. The syringe and nozzle were placed in 70% (v/v) ethanol and the bioprinter sterilised with its built-in UV lights. The syringe was then loaded into the bioprinter and an "empty run" was performed to pneumatically cleanse the syringe and nozzle of ethanol by expelling it using high air flow until completely dry (accepting a theoretical risk of some impact on cell viability for the apparent benefit of a contamination rate of zero in our experiments). The printer components were set to 25°C for the bed and 39°C for the pneumatic syringe chamber. For ease of transfer of hydrogel to syringe, the pneumatic bung between the pneumatic mechanism and the hydrogel was not used (pneumatic force was transmitted directly through air in the syringe to the hydrogel pool at the lowest part of the syringe and in the nozzle). Adjustments to flow rate and nozzle travel speed were made during the print runs to create optimal patches based on real-time moment-to-moment operator judgement. Patch size was set at 10 x 10 x 0.6 mm with three 0.2 mm layers in the z axis. The grid infill / solidity percentage for the patches was set at 25%. AlgGel was ionically crosslinked on an ice block by adding $CaCl_2$ after bioprinting of all the patches in one six-well plate. Then, we cultured patches up to the moment of transplantation (after one and before three weeks of time in culture) based on our previous study determining the optimum moment for transplant [7].

In vitro heart patch analyses (confocal microscopy, 3D rendering and multiple electrode array). Patches were incubated *in vitro* for 28 days and analysed. These patches were stained for nuclei, cardiomyocytes, fibroblasts and endothelial cells (Hoechst stain and antibodies against cTNT, vimentin and CD31/PECAM, respectively) as previously described [18]. Patches were imaged with a Leica Stellaris confocal microscope (Leica Microsystems, Wetzlar, Germany) and 3D rendering analyses were generated using IMARIS visualisation software (Oxford Instruments, Abingdon, Oxfordshire, UK). Some patches were placed on a multiple electrode array (MEA) platform (Mappinglab, Oxford, UK) to confirm the presence of electrical activity.

Murine MI with heart patch transplantation. We transplanted patches to the epicardial surface of mouse hearts using an optimised protocol based on our previous surgical method [15]. Briefly, male 9-10 week old (mature) B and T cell-depleted B6.Rag1 mice (Australian BioResources, Moss Vale,

NSW, Australia) were randomly assigned by an independent facility manager and had their baseline echocardiography. The surgery was performed by one researcher (CG). Anaesthesia was performed by one researcher (CR) with mixed anaesthesia of intraperitoneal ketamine (40 mg/kg) and xylazine (5 mg/kg) plus inhaled isoflurane (5 L/min induction, 0-2 L/min maintenance). Mice were intubated and ventilated then left thoracotomy was performed to gain surgical access to the heart. Mice were assigned to experimental groups by an ethical semi-randomised approach (an ethics-driven approach where randomisation may be altered to reduce the risk of mouse death and where experimental group numbers are added to according to mortality rates with the objective of using the lowest number of mice overall) – in accordance with best ethical practice to reduce mouse numbers in experimental groups for procedures where mortality rates are inherently very high (up to ~50%). The five experimental groups were: 1) Sham surgery (suture passed around the left anterior descending artery (LAD) and tied loosely without occluding the artery); 2) MI by permanent LAD ligation (MI); 3) MI followed by immediate transplantation of a hydrogel (AlgGel) patch without cells (MI+PATCH); 4) MI plus AlgGel patch with freely suspended mixed cardiac (iCM, CF, HCAEC) cells (MI+PATCH CELLS); and 5) MI plus AlgGel patch with mixed cardiac cell VCS (MI+PATCH SPHEROIDS). In the postoperative period, mice were given twice daily subcutaneous buprenorphine injections (0.08 mg/kg) for the first three days after surgery and cared for following standard postoperative protocols for four weeks.

Cardiac functional analyses

Echocardiography. All mice were imaged using a Vevo 3100 Preclinical Imaging System (FUJIFILM VisualSonics, Toronto, Canada) at baseline, midpoint (day 14) and endpoint (day 28). Echocardiography was performed by one fully trained researcher (CR), with mice under isoflurane anaesthesia via a nose cone (5 L/min induction followed by 2 L/min maintenance). Mice were placed supine on a warming platform and B and M mode echo data were obtained for parasternal long axis and short axis views. Long axis data were analysed using the AutoLV (automatic artificial intelligence-based analysis) function by one researcher (CR) and validity confirmed independently (blind) by a VisualSonics data specialist (FUJIFILM Visualsonics, Toronto, Canada).

Electrical mapping. Electrical mapping was performed by trained researchers (CR and CG) using an EMS64-USB-1003 Electrical Mapping System and EMapRecord/Scope software (MappingLab, Oxford, UK). Electrical activity mapping data were obtained by placement of a probe onto the epicardial surface or patch in the open chest at surgery. Data were obtained at timepoints: baseline (pre-MI); immediately after LAD ligation (post-MI); immediately after patch transplantation (post-PATCH); and at the end of experiment at day 28 (END). Independent data validation, analyses and processing were performed by a MappingLab data specialist (Yatong Li) and a high inclusion threshold for data quality was used.

Structural analyses. At 28 days post procedure, mice were euthanised and 1 mm heart tissue transverse (axial) slices of the left ventricle (distal to the LAD ligation) were obtained for structural analyses (histology, flow cytometry and mRNA analysis).

Histological tissue analyses. Histology (H&E, PicroSirius Red, Masson's Trichrome) was performed on 4 µm transverse heart tissue sections. Slides were digitalised and infarct size calculated by the midline infarct arc length method [19]. Measurement and analyses were performed blind followed by unblinding at the stage of processing data for visualisation. Mice that died before day 28 had post-mortem performed and samples sent for independent (blind) histological analysis (Cerberus Sciences, Melbourne, Australia).

Cell quantification by flow cytometry. Flow cytometry was performed on heart tissue using a BD LSRFortessa™ flow cytometer and data analysed by BD FACSDiva software (BD Biosciences, Franklin Lakes, NJ, United States) – full list of antibodies used for staining in the **Supplementary Materials**. Samples were taken and processed immediately based on our previously reported protocol [20]. Briefly, tissue samples were chopped into small pieces and subjected to Liberase™ (Roche Diagnostics, NSW, Australia) digestion. Liberated cells were incubated with a cocktail of

primary antibodies for 45 minutes at room temperature before processing through the cell cytometer. Flow cytometry data were analysed as relative numbers (no comparison of absolute numbers was performed for batches processed on different occasions).

RNAseq analyses. Cardiac apex samples were processed for mRNA transcriptomic analysis according to the protocol of a commercially available mRNA isolation kit (RNeasy Fibrous Tissue Mini Kit, Qiagen, Cat no. 74704, Hilden, Germany). Total RNA from cardiac apical cells was isolated (phenol– 17 chloroform separation of TRIzol LS) and purified according to the manufacturer's instructions (see the **Supplementary Materials** for the protocol). RNA quality assessment, library preparation, and sequencing were performed by BGI Genomics (Hong Kong, China) using DNBSEQ™ sequencing technology and an Agilent 2100 Bioanalyzer (see the **Supplementary Materials** for full RNA sample data including RNA Integrity Number (RIN) per sample). Samples were independently processed by BGI (Batch no. INSP21000010163). Raw sequencing reads were filtered for adapters – reads in which more than 10% of bases were unknown and reads in which more than 50% of bases were low quality (base quality < 20). The resultant high-quality reads were aligned to the mouse genome (mm10) using the software STAR (Spliced Transcripts Alignment to a Reference) [21] with standard parameters. We mapped an average of 26,346,213 reads per sample achieving an average alignment rate was 98.78%. Gene expression levels were quantified using the tool featureCounts [22]. Expression levels were normalized using the software package DeSeq2 [23] in the R statistical analysis software [24]. Genome-wide expression profiles were analysed using principal component analysis (PCA). Hierarchical clustering with average linkage and Euclidean distance was performed using Partek Genomics Suite® (Partek®, St Louis, MO, USA).

Statistical analyses. Results were analysed using PRISM (GraphPad, San Diego, CA, United States). Stepwise hypothesis testing for continuous data was performed using two-tailed Mann–Whitney U tests with Bonferroni correction or Kruskal-Wallis tests (for a difference in more than two groups). Hypothesis testing of categorical data was performed with two-tailed Fisher's exact contingency testing. Kaplan-Meier survival curve hypothesis testing was performed using the Log-rank (Mantel-Cox) test.

Results

Bioprinted VCS patches present stable and functional spheroids at 28 days. Our analysis of 3D bioprinted patches at 28 days post incubation demonstrated the presence of VCS (stained with antibodies for iCMs (cTNT), CFs (vimentin) and HCAECs (CD31), **Figure 1 and Videos 1, 2 and 3**). Our analysis also demonstrated that HCAECs self-assembled into networks, both within and outside of spheroids (**Figure 1 and Video 2**). Overall, our analyses of cell structures in patches *in vitro* provided evidence that cells within our AlgGel patches formed endothelial cell networks, consistent with our previous reports [7, 17]. We detected electrical signals within our patches supporting a degree of electrical activity at 28 days (**Suppl. Figure 1**). This is consistent with our previous report of cardiomyocyte activity in patches incubated *in vitro* over 28 days [7].

Transplantation of patches containing VCS protected against MI-induced reduction in cardiac function. Results for our primary functional outcome (LVEF%) are shown in **Figure 2**. The increased LVEF% with treatment was consistent with our secondary analyses of other functional echocardiographic parameters (**Suppl. Figure 2**). The increased LVEF% of the MI+PATCH SPHEROID group was consistent with that group's favourable electrical activity profile (**Figure 3, 5 and Suppl. Figure 1**).

Median baseline (before surgery) LVEF% from all mice (survivors and non-survivors) was 66% (IQR 61-70; n=51) with a similar mean±SD (65±8). Baseline characteristics and 28-day mortality rates were similar between groups with overall mouse survival at 56% (**Suppl. Figure 3**).

Patches containing VCS increased the median LVEF% from 41% to 64% compared to control infarcted mice at 28 days (**Figure 2**). On pairwise hypothesis testing between groups, LVEF% for

the MI group (LAD ligation and no patch) had a statistically significant difference compared to all groups except for MI+PATCH CELLS (**Figure 2**). There was no statistically significant difference between treatment groups (MI+PATCH, MI+PATCH CELLS, MI+PATCH SPHEROIDS) or between each treatment group and Sham (Sham day 28 median LVEF% = 58 (IQR 57-72; n=7)). Overall, the median LVEF% was increased from 41% for MI (IQR 37-48; n=7) to: 55% (IQR 51-59; n=7), 59% (IQR 48-60; n=5) and 64% (IQR 58-67; n=5) with MI+PATCH, MI+PATCH CELLS or MI+PATCH SPHEROIDS, respectively.

These results show a trend back towards 'baseline' LVEF% values with any of the three patch groups. Whilst MI+PATCH SPHEROIDS presented the largest increase in LVEF% (compared to MI), even patches without cells presented an absolute value increase of 15%. With such an increase in the MI+PATCH control group, the study did not detect a statistically significant difference between patches with spheroids (absolute value increase 23%) and patches with no cells at all.

Transplantation of VCS-containing patches did not have significant effects on conduction velocity. To evaluate electrical activity modulation, conduction velocity (CV) was analysed using 64-electrode electrical maps (**Figure 3)**. There was a drop in the mean CV between the Sham and MI group at the time of surgery. No difference was detected between any of the day 28 CVs (p=0.86 (n=20); Kruskal-Wallis test) (**Figure 3**). Comparison of CVs for immediately post-MI against day 28 was not statistically significant for any group where LAD ligation was performed (respective day 28 medians (mm/ms) were: 0.56 (MI), 0.69 (MI+PATCH), 0.82 (MI+PATCH+CELLS) and 0.56 (MI+PATCH+SPHEROIDS); p=0.21 (n=42) Kruskal-Wallis test) (**Figure 3**). Overall, LAD ligation (MI) seemed to decrease conduction velocity to 68-75% of its normal value (at the time it was performed) and this change persisted until day 28.

Infarct size trended downwards in mice receiving VCS containing patches compared to MI. Transplantation of patches containing cardiac spheroids showed a trend towards smaller infarct sizes (**Figure 4**). Some mice presented regional infarctions and different infarction patterns on histology (**Suppl. Figure 4**). There was a trend towards decreasing infarct size moving through treatment groups from MI to MI+PATCH, MI+PATCH CELLS and then to MI+PATCH SPHEROIDS (**Figure 4**). Reducing infarct size was strongly correlated with increasing LVEF% for the MI group, weakly correlated for the MI+PATCH group and not correlated for the MI+PATCH SPHEROIDS group (R squared values, 66%, 15% and 0.3%, respectively) (**Figure 4E**). Infarct patterns were variable (**Figure 4A-C and Suppl. Figure 4**), with mice showing varying infarct region appearances. Variable infarction pattern was also reported by our independent post-mortem histological analysis of mice that died in the postoperative period (see the **Data Repository** https://doi.org/10.5281/zenodo.6198612 - doi pending publication). In some mice, patch fragments were still visible on histology at day 28 (**Suppl. Figure 5**). In some mice, regional infarctions were not detected, consistent with independent post-mortem analysis of mice that died before day 28 (Cerberus Sciences). In that post-mortem analysis, infarctions were observed in focal segments (including regional infarcts only affecting the cardiac apex) and overall infarct size showed a highly variable range of ~20-70% (see the data repository).

Integrative analysis of CV and LVEF%. We next sought to investigate potential mechanisms underlying the variability of treatment responses within each group. We analysed coefficients of determination (R squared expressed as a %) for the relationship of CV (electrical mapping) to the LVEF% (**Figure 5**). Additionally, we performed representative side-by-side analysis of the electrical map at day one (immediately after LAD ligation), electrical map at day 28, and LVEF% progression (baseline – midpoint – endpoint) for individual mice. Electrical maps on day one (**Figure 5C, F, I, L**) were similar to a baseline (pre-LAD ligation) map (**Figure 5A**). The MI+PATCH CELLS representative mouse was the only mouse in this analysis which showed no improvement in LVEF% from day 14 (midpoint) to day 28 (endpoint) – the other mice (sham, MI+PATCH and MI+PATCH SPHEROIDS) all showed a V-shaped LVEF% progression, with a drop at midpoint and recovery at endpoint (**Figure 5**). Sham group mice (needle and suture passed under the LAD and

tied loosely without occlusion) also showed variability in LVEF% (**Figure 5B**) and mean CV (**Suppl Figure 6**) despite having no infarction – representing the impact of the cardiac surgical model itself.

Tissue immune cell analysis by flow cytometry. Recent reports suggested that mechanisms regulating myocardial regeneration by using cells/materials in contact with the host heart may be dependent on the innate immune response in the host [14, 25, 26]. Therefore, we performed host (mouse) tissue immune cell population analyses in heart tissues isolated at day 28 using flow cytometry and quantified the absolute immune cell count for each group (**Figure 6**).

For macrophages, we demonstrated a trend towards reversal of the M1:M2 macrophage ratio from 3.4:1 (sham) to 1:4 (MI), accompanied by a partial return towards sham values with each of our three treatment groups (**Figure 6A**). Despite the M1:M2 ratio being a dichotomous simplification of a complex continuum [25], our results demonstrate that the addition of the patch can play a role on macrophage activity. The ratio of neutrophils to monocytes favoured a monocyte dominance only for the MI+PATCH SPHEROIDS group (compared to all other groups, including sham) (**Figure 6B**). For all groups, there were proportional changes in tissue monocytes and tissue macrophages compared to all other live singlet immune cells (**Figure 6C-D**).

For natural killer cells (NKs) there was a reduction in the number of these cells in all treatment groups compared to MI (**Figure 6E**). The same analysis demonstrated an increase in the proportion of haematopoietic stem cells (HSCs) within all treatment groups compared to MI and Sham, with the greatest increase seen in the MI+PATCH SPHEROIDS group (**Figure 6F**).

For WBC:Macrophage ratio and M1:M2 ratio compared directly against infarct size (**Suppl. Figure 7C**) and LVEF% (**Suppl. Figure 7A**) there was no strong correlation. To support our results, we additionally performed a secondary continuous (not categorical) data comparison of median values per group and the results of this are shown in **Supplementary Figure 8**. Overall, our results demonstrated changes in host immune cell numbers on day 28, suggesting that host immune system modulation may be an important mechanism underlying the benefits of epicardial patch transplantation for MI.

The transcriptomic profile for the spheroid group was similar to Sham (non infarcted). Whole mouse transcriptomes were profiled in triplicates for samples from five groups MI, MI+PATCH, MI+PATCH CELLS, MI+PATCH SPHEROIDS, and Sham. PCA of mouse transcriptomes identified samples segregating into three visual clusters including cluster 1 with samples from MI as well as MI+PATCH (“Patch”), cluster 2 with samples from MI+PATCH CELLS (“Cells”), and cluster 3 with samples from MI+PATCH SPHEROIDS (“Spheroids”) as well as Sham (**Figure 7A**). Cluster 3 also contained an outlier from the group of “Cells” (sample number 50). Differential gene expression analysis comparing all sample groups identified 462 transcripts that were significantly different between groups (p-value 0.05 and fc > |1.5|; **Supplementary Tables S1-10**). Hierarchical clustering of these transcripts confirmed the clustering previously observed by principal component analysis (**Figure 7B**). We found that there were no differentially expressed transcripts when samples of the Sham and Spheroids groups were compared, suggesting that these cells were indeed molecularly similar.

To determine the molecular responses of MI cells treated with VCS, we further interrogated the expression of 97 transcripts differentially expressed between samples in these two groups (**Supplementary Table S3**). Hierarchical cluster analysis of these transcripts showed that exposure of MI cells to Spheroids led to dominant molecular repression of gene expression (**Figure 7C**, 79 genes down and 18 genes up). The same gene expression program was also recapitulated in samples from Sham (that is, the spheroid-treated group and the non-infarcted sham group were molecularly similar).

When interrogated for biological pathways, we found that these genes showed a clear enrichment for functions associated with Cardiovascular System Development and Function as well as Cellular Development, Growth, Proliferation, Assembly and Organization (**Figure 7D**, top panel, **Supplementary Table S11**).

Within the subset of pathways associated with Cardiovascular System Development and Function the repression of the genes ASPH, ATP2A2, KCNJ11, MYL4, MYL7, RYR2 and CLU were strongly associated with the regulation of contraction of the heart, cardiac contractility, and contraction of cardiac muscles (**Figure 7D**, bottom panel, **Supplementary Table S12**). Enrichment analysis for canonical pathways highlighted relevant pathways associated with beta adrenergic signalling and dilated cardiomyopathy (**Supplementary Figures 9, 10 and 11**).

Discussion

Our study adds to the evidence that epicardial patches protect the myocardium after MI. Moreover, our "return-to-baseline" cardiac functional results (**Figure 2**) are promising. This study represents a broad multiple-analysis search for new mechanistic clues not previously uncovered. Our initial analyses bring up an interesting mechanistic proposition: namely, that stimulating host immune cells (**Figure 6**) by subjecting them to contact with foreign material could account for some (but not all) of the cardiac functional benefit we observed. The rest of the benefit may be influenced by gene expression changes (**Figure 7**). This might explain why only our most successful (spheroid) treatment group "reversed" the transcriptomic profile for MI mice (to resemble non-infarcted (sham) mice by day 28). For this study we focused on *in vivo* outcomes since we had performed *in vitro* bioink analyses in our previous studies [7, 17]. Further discussion points are made in the Supplementary Materials.

For cardiac function, our results suggest that a *clinically* significant rise in LVEF% (an absolute value gain of approximately 20% and even a return towards baseline) can be achieved by patch transplantation in mice modelling acute MI. This adds further evidence to other reports that this treatment strategy is effective [6, 27-29]. The full mechanism remains unknown but our results do not refute the proposition that the mechanism may be associated with stimulating a host innate immune system response; suggested by Vagnozzi et al (2019) with a myocardial injection-ischaemia/reperfusion injury model [14]. Our findings (especially that hydrogel with no cells has some effect) are consistent with human trials reporting potential improvements in function even with a limited cell density in patches transplanted to the epicardium [12]. In our study, we have reported that even without cells, hydrogel alone transplanted to the epicardium (in the acute phase of MI) raised the LVEF% from 41% to 55% (**Figure 2**). Some might interpret this to mean that all of our treatment groups (cells or not) reversed a heart failure state to an acceptable (non-heart failure) state. Interpreted in this way, our results may not support the hypothesis that cell spheroids offer a *clinically* significant advantage over our other treatments. Similarly, the small (statistically non-significant) potential difference between our spheroid group (~64% median LVEF%) and freely suspended cells group (~59%) would represent only an absolute increase of ~5% on top of the ~20% observed compared to MI without treatment (~41%).

Nonetheless, we showed a trend towards incremental increases in LVEF% with the addition of cells and then cell spheroids compared to AlgGel patches without cells (**Figure 2**). Mechanistically, if underlying host immune-genetic modulation is important (**Figure 6 and 7**), this raises an interesting consideration. Specifically, it calls into question whether cell number replenishment strategies – or even the goals of host-patch vascular network anastomoses (**Figure 1 and Video 3**) and electrical activity integration (**Figure 3, 5 and Suppl. Figure 1**) – would be fully aligned with the underlying mechanistic processes conferring myocardial protection. To proceed with human trials [8, 10, 12] without understanding mechanisms may subject patients to treatments which are not aligned with the underlying reason why they work [30]. Better understanding of the mechanisms regulating optimal prognosis in heart failure patients receiving a bioprinted patch is critical in this field (already subject to ethical concerns about suboptimal media-hyped treatments [31-33]). Without better understanding of these mechanisms, there is a risk of unnecessary patient harm, wasted research resources and time [1, 30, 33].

In this context, we therefore cast a broad net to search for mechanistic insights. We analysed electrical maps and performed individual mouse sequential echocardiography (baseline

– midpoint – endpoint) to identify progression in LVEF% changes (**Figure 2A**). We found that relationships between electrical mapping results, infarct size and LVEF% were not straightforward, with variability in these measures due to the procedure itself (as shown by high variability in our Sham group) as well as the inherent variability of these recordings – LVEF% is known to be highly variable, depending on heart rate, preload and afterload. It is worth noting that our day 28 analyses are based on survivors (**Suppl Figure 3**), which introduces an attrition bias for mice with good collaterals or with smaller infarcts. The variability inherent to infarct size, CV and LVEF% is a limitation of all animal studies in the cardiac regeneration field. Future studies should factor this in when calculating numbers to adequately power studies including removal of anomalous results, high variation in results and multiple statistical comparisons.

To explore the role of immune cells in host cardiac tissue, we tested for the presence of different immune cell numbers using flow cytometry (**Figure 6**). We demonstrated a trend towards a reversal of the ratio of so-called M1:M2 macrophages in our MI group compared to other groups (**Figure 6A**). The M1:M2 ratio is a simplification, for example, it presents a complicated continuum as a dichotomy [25, 34]. Nonetheless, 'classically activated' M1 macrophages have been associated with phagocytosis, elimination of tumour cells and pathogen killing, whereas 'alternatively activated' M2 macrophages have been described as profibrotic inducers of fibrosis [34]. Some have stated that M1 may exacerbate ischaemic injury whereas M2 macrophages are associated with cardioprotective effects [35], whereas others have moved away from describing macrophages in terms of M1/M2 [25, 34]. Despite limitations, our findings suggest changes in macrophages with treatment groups applied after MI (all treatment groups trended towards a re-reversal of the ratio back towards an increased proportion of M1 compared to M2 macrophages). Our results might suggest that increased M1 (phagocytotic) activity compared to M2 (fibrotic) activity is important, but the results were not statistically significant due to low cell numbers in the MI group – studying depleted macrophages in the established infarct zone is a known challenge. Our use of RAG1 mice suggests B or T cell-driven mechanisms are less important (RAG1 mice do not have mature B or T cells). Despite limitations in flow cytometry (such as batch variability), these findings complement more extensive immune cell analyses [14] and support recent understanding that innate immune system behaviour and characterisation is complex [34, 36]. These data will need to be followed up with future dedicated studies, including full immunohistochemistry analysis for spatially resolved assessment of the effects of different treatments.

Our transcriptomic analyses demonstrated that mice in the MI+PATCH SPHEROIDS group presented transcriptomic profiles similar to non-infarcted sham mice. We found that there were no differentially expressed transcripts when samples of the sham and spheroids groups were compared, suggesting that these cells were molecularly similar. RNAseq aims at broad comparison and identification of molecular avenues for detailed follow-up studies. Nonetheless, we identified interesting changes in gene expression, such as for myosin light-chain 4 (MYL4) and 7 (MYL7) which were similar for both MI vs MI+PATCH SPHEROIDS and MI vs Sham (a log2FoldChange of approximately 5, **Supplementary Table S3 and S4**, respectively). Loss of MYL4 function may cause progressive atrial cardiomyopathy [37] and downregulation of MYL7 is implicated in myocardial structural abnormalities and cardiac hypertrophy [38]. For acellular (hydrogel only) compared to SPHEROID patch treatment, enrichment analyses for canonical pathways highlighted genes associated with beta adrenergic signalling and dilated cardiomyopathy (**Supplementary Figures 9, 10 and 11**). Further detail on cardiovascular genes and their associations is in **Supplementary Tables S11 and S12**. For the first time (to our knowledge), our mRNA analysis has pointed to underlying host gene expression modulation as an important potential mechanism for future studies to evaluate fully.

Our functional data (LVEF%) also showed a return to sham (non-infarcted) values for the MI+PATCH SPHEROIDS group (**Figure 2**). Taken together, this supports the hypothesis that treatment with VCS patches enacted beneficial changes on underlying host gene expression. It needs to be emphasised that without splitting the VCS microtissue into its component cells and testing each as a control group, it cannot be ruled out that only one of the cell lines contained in the microtissue is contributing to these results. However, VCSs are a specific entity, in-and-of-

themselves, and to "split" this entity into its component cells (e.g. a control group for "spheroids" made only of 3D cultured CFs) would arguably not be warranted. It may be warranted as part of a larger future study testing multiple bioinks (and our feasibility-focused mouse patch transplantation protocol is suited to high-throughput testing of different bioinks). VCS patch treatment enriched for genes associated with regulation of cardiac functions (contractility) and cell growth and development. The near-complete return to a transcriptomic profile resembling sham mice was not seen in the other experimental treatment groups (MI +PATCH or MI+PATCH CELLS). Along with our immune cell analysis (flow cytometry) we can therefore speculate that the incremental gain in cardiac function seen between groups (patch only, freely suspended cells or cells pre-cultured as spheroids) could be due to a "dual" mechanism along with stimulation of host inflammation. That is, stimulation of host inflammatory cells provided *some* of the "uplift" in LVEF% (accounting for the partial uplift observed with acellular hydrogel material placed onto the heart) which was then *increased further* by a genetic mechanism (with some effect from freely suspended cells, but the strongest effect only coming through for the cardiac spheroids group). In other words, modulation of host immune cells boosted heart function half-way but to get the maximal improvement required genetic changes. This hypothesis would require testing by a dedicated future study (beyond our descriptive/ phenotypic analyses whereby it has first been proposed here). For some reason, genetic changes seemed only fully able to happen with the spheroid group (freely suspended cells only seemed to induce some modifications and did not induce the full "back to baseline" mRNA changes). Given the high variance in our datapoints (individual mice) in the MI+PATCH CELLS group (**Figure 2B and Figure 4D**) confounding factors are possible for that group (such as patch non-adherence to the heart, missing a regional infarction on sampling or small infarct generation at LAD ligation). However, our electrical mapping data supported that the spheroid group had a favourable electrical profile (**Figure 5 and Suppl Figure 1**), which is also consistent with the genetic changes we report in the spheroid group (**Figure 7**). More study is needed to fully elucidate these mechanisms.

Despite having directly compared single cells versus spheroid containing patches in an animal MI model, we identified limitations in our study. A limitation is that patches were transplanted to the heart immediately after LAD ligation, whereas for human patients the treatment need is for chronic heart failure to restore myocardial function. This is more of a "protection" rather than a regenerative treatment for established heart failure. At the same time, whilst many studies run up to 28 days, some have reported functional outcomes which only emerge later (8 weeks or more) [6]. Furthermore, our study in mice is not directly translatable to human trials without a large animal trial which would more closely resemble human surgery. In our model, it is also possible that difficult-to-quantify variables may influence outcomes, such as the extent to which a patch successfully attaches and interacts with the host heart tissue underneath. We also did not analyse all immune cells, and other cell types such as mast cells may have important roles to play [39]. Systems such as the nervous [40] and lymphatic system [41] may also be important and this is the focus of other studies [42]. Further considerations related to the mouse MI model are discussed in the **Supplementary Materials**.

Overall, our results hint at the mechanistic complexities underlying patch-based myocardial repair. The future directions for this study remain mechanistic: a dedicated study should examine our proposal that host immune responses and gene expression changes each account for part of the cardiac functional benefit we observed.

Conclusions

Our findings show a significant improvement in cardiac function by epicardial transplantation of AlgGel patches containing spheroids in mice modelling MI. We found no strong evidence for a clinically or statistically significant difference whether transplanting hydrogel patches alone (even without cells) or patches containing cardiac cells (iCMs, CFs, ECs). Nonetheless, the trend seemed towards an incremental improvement with cells and then another incremental improvement with cell spheroids in patches. Gene expression changes for the spheroid group may explain why this group apparently returned the strongest functional improvement. Even hydrogel alone (without cells) raised the LVEF% from 41% to 55%, adding to evidence that direct cardiac cell number replenishment may not be a mechanism by which cardiac function is improved (in epicardial patch-based myocardial regeneration strategies). This broad-based multiple analysis study provides new directions of inquiry (for specific immune cells and/or gene expression) for future studies that had not previously been considered. Dedicated preclinical studies are needed to examine specific mechanisms in full and answer the question why epicardial patch transplantation improves cardiac function.

Acknowledgements. With thanks to Diego C Fajardo of The Children's Cancer Institute, Lowy Cancer Research Centre, UNSW, Australia, for his guidance in the processing of mRNA samples. With thanks to Cerberus Sciences (for independent post-mortem histology analysis), FUJIFILM VisualSonics (for echocardiography training and independent data quality validation) and Yatong Li of MappingLab (for electrical mapping training, independent data analysis, processing, validation and visualisation), and CELLINK Life Sciences (for 3D bioprinter training). With thanks to Louise Cole, i3 Institute, Sydney, for use of the equipment in the Microbial Imaging Facility at the i3 Institute in the Faculty of Science, University of Technology Sydney (UTS). With thanks to Cathy Gory (UTS) for assistance with histological specimen preparation. Graphical abstract created with the assistance of Biorender.com.

Data Availability Statement

The datasets associated with this experiment are available in the **Supplementary Materials** and the permanent data repository (https://doi.org/10.5281/zenodo.6198612 - doi pending publication). Raw confocal microscopy data for Figure 1 runs to >500GB and is therefore available from a specialist computer in the data visualisation suite at the i3 Institute (Level 7, Building 4), Faculty of Science, University of Technology Sydney (UTS) (*via* request to CG). Data associated with electrical mapping is available *via* Yatong Li at MappingLab. Complete exported (PDF) flow cytometry data is in the data repository and the raw data (BD FACSDiva) is on a computer attached to the BD LSRFortessa™ flow cytometer at the Kolling Institute, Level 11, University of Sydney (*via* request to MX). Data associated with Figure 7 (gene expression) are available *via* DB.

Contribution Statement

CR: Conceptualization; Data acquisition; Data processing; Data curation; Formal analysis; Funding acquisition; Project administration; Visualization; Validation; Writing—original draft; Writing—review and editing. HL: Data generation for Figure 6); Data curation; Supervision; YH: Writing—review and editing; CdB: advice on mRNA data processing; Formal analysis; Visualisation; Supervision; Writing—review and editing. DB: (especially transcriptomic data) Data processing; Data curation; Formal analysis; Validation; Supervision; Writing— review and editing. MX: (especially flow cytometry data) Data acquisition; Data processing; Data curation; Visualisation; Supervision; Writing— review and editing. CG: Conceptualization; Data acquisition; Data processing; Data curation; Visualisation; Funding acquisition; Project administration; Visualization; Supervision; Writing—review and editing; All authors contributed to the article and approved the submitted version. Primary Guarantors (overall and data acquisition): CG and CR. Guarantors (specific): YL (electrical mapping data processing and visualisation); MX (flow cytometry data visualisation); DB (mRNA data visualisation).

Declaration of No Competing Interest

The authors declare no conflict of interest. They have no competing financial interests or personal relationships that could have appeared to influence the work reported in this paper.

Figure Legends

Figure 1. Cardiac spheroids (A-D) and freely suspended cardiac cells (E-H) with endothelial cell networks present at 28 days in 3D bioprinted patches. (A) Overview of a 3D rendered region of a cardiac spheroid patch stained with antibodies for cardiomyocytes (red, cTNT), endothelial cells (blue, CD31) and fibroblasts (green, vimentin). **(A)** shows the overlay, whereas (**B)** and (**C)** show the cardiomyocyte and the endothelial cell population, respectively. (**D**) is a side closeup view of a spheroid from (**A**). Arrows point at spheroids within the patch. Images taken from **Video 1**. **Figure 1.** (**E-H**) 3D rendering analyses of bioprinted patches containing cardiac cells (not in spheroid conformation) at 28 days that were stained with antibodies for cardiomyocytes (red, cTNT), endothelial cells (blue, CD31) and fibroblasts (green, vimentin), respectively. Arrows in (**A**) and (**B**) indicate the extensive endothelial cell network formed within the patch. (**C-D**) Single cells are observed in certain areas of the patch in the periphery, indicating absence of complete maturation in these areas. Images taken from **Video 2** (**A and B**) and **Video 3** (**C and D**). Full-length videos are in the data repository. Due to the resources required to obtain 3D large-sample multichannel images for cell patches, no imaging of acellular (hydrogel only) patches were taken. Scale bars = 150 μm.

Figure 2. Patch transplantation protects against MI-induced reduction in cardiac function. (**A**) Sequential LVEF% values for each experimental group taken at baseline (before surgery), midpoint (14 days after surgery) and endpoint (28 days after surgery). For each group, individual lines on the graph show individual mice. Variability in the LVEF% was observed in individual mice as shown by high variability in endpoint values for sham mice and high variability in baseline values in all groups. Compared to MI, all three treatment groups trended towards higher LVEF% values at both midpoint and endpoint. (**B**) Median LVEF% for each treatment group at day 28 shows a trend towards increasing improvements in LVEF%. (**C**) Median LVEF% per group at baseline, midpoint and endpoint; For other functional outcome measures (fractional shortening and cardiac output) see **Suppl Figure 2**. p values Error bars show interquartile range; p values calculated with pairwise Mann-Whitney U tests.

Figure 3. No treatment rescued mean CV by day 28 following LAD ligation. Left anterior descending artery (LAD) ligation immediately reduced the median conduction velocity (CV) compared to pre-MI (baseline) values (taken immediately before LAD ligation). The statistically significant difference between pre-MI (baseline) values and post LAD ligation values (on day zero) seemed to persist up to day 28 (that is, there was no evidence of a return in CV back towards baseline values detected at this level of statistical power). In fact, the trend in the MI group was for the CV to fall further by day 28 in parallel with falling cardiac function (see also **Figure 2**). Overall, reduction in CV was seen with LAD ligation and there was no evidence of recovery by day 28. Error bars show quartile range, p values were calculated using stepwise Mann-Whitney U tests (Bonferroni-corrected level of significance is p=0.0083 for six stepwise calculations against pre-MI baseline values and p=0.010 for five stepwise calculations against values taken immediately post-LAD ligation). Only high quality 64 electrode electrical mapping readings were used in this analysis and where there was any question about the quality of individual readings that reading was not used.

Figure 4. In mice surviving up to 28 days, the strong correlation between infarct size and LVEF% in the MI group was reduced for the MI+PATCH group and reduced further for the MI+PATCH SPHEROIDS group. (**A-C**) Infarction (collagen) staining with Picrosirius Red (PSR) for a mouse in the MI group (**A**), MI+PATCH group (**B**) and MI+PATCH SPHEROIDS group (**C**) shows that i**nfarct patterns were variable (black arrows point to infarcted area stained with PSR)**. (**D**) Shows infarct size (infarcted LV / Total LV) across groups. Median LVEF% for each group is plotted as a blue line (values on the right Y axis). There was a trend towards a lower infarct size between the MI group and the interventional groups (MI+PATCH, MI+PATCH CELLS, MI+PATCH SPHEROIDS) but the result was not statistically significant. (**E**) Shows coefficients of determination (R squared) values for the LVEF% plotted against the infarct area (sham not shown as no LAD ligation was performed and infarct size was zero in all cases). The moderately strong

correlation between LVEF% and infarct size in the MI group (66%) was disrupted in treatment groups MI+PATCH (15%) or MI+PATCH SPHEROIDS (0.3%). Points on graph represent individual mice (median infarct size from multiple repeat measurements of different histological sections; error bars show IQR) and goodness of fit (R squared) to trend lines is expressed as a percentage. Only mice with infarct size >0 were used for this analysis (for chart including infarct area = zero see **Suppl Figure 4**)

Figure 5. Electrical remodelling of the infarcted LV may be an important mechanism contributing to improved LVEF%. (**A**) Representative image of a baseline (pre-MI) 64-electrode array electrical map (isochronal activation map) of the anterior cardiac surface. The isochronal (AT) map represents the sequential event of depolarisation. It is constructed with relative values to the earliest activation time from 64 channels. The deep red colour means the earliest activation site. More red colours on a map means fast CVs. AT map from post LAD ligation readings (**C, F, I, L**) show that the normal pathway for conductive activation is mainly blocked (red meets blue, the loss of colour gradient) in the MI area (in blue). This gradient (seen in the baseline (pre-ligation) map in **A**) is not fully recovered after all of treatments (**G, J, M**) possibly due to the formation of scar tissues.(**B**) Day 28 mean LVEF% (n=1 repeat reading per mouse from best echocardiographic trace of up to 7 sequentially acquired traces) plotted against mean CV (n=4 repeat readings per mouse) (error bars=SD; only upper bar shown). Sham group values show wide variation in LVEF% on day 28 even with only a sham procedure (see also **Figure 2A**). Wide error bars show variability in CV readings. The MI+PATCH SPHEROID group seemed to trend towards increasing overall mean CV with increasing LVEF%. (**C-E**) For a mouse underdoing a sham procedure AT maps on day one at surgery (**C**) and day 28 (**D**) were similar. (**E**) Shows the corresponding baseline (day one before surgery), midpoint (day 14 after surgery) and endpoint (day 28) LVEF% for the same sham group mouse. (**F-H**) For a mouse undergoing MI +PATCH transplantation electrical maps on day one post-LAD ligation (**F**) and day 28 (**G**) show loss of colour gradient and a white area where no signal was detected. (**I-K**) Electrical maps for this MI+PATCH CELLS mouse (with a cellular patch transplanted) shows partial recovery of the electrical map. The day 28 electrical map (**J**) showed a greater area of blue squares (slow CV) and more abrupt transition between fast (red) and slow (blue) areas when compared to day one for that mouse (**I**). The corresponding LVEF% (**K**) was similar compared to other groups with a decrease at the midpoint and partial recovery by the endpoint. (**L-N**) For a mouse in the MI+PATCH SPHEROIDS group, electrical maps (**L-M**) showed partial recovery of gradient. The corresponding LVEF% showed a steep uptick between midpoint and endpoint (**N**).

Figure 6. Immune cell analysis at 28 days post-surgery suggests significant changes in inflammatory cell populations in heart tissue across experimental groups. (**A**) Macrophage analysis for experimental groups with M1 macrophage to M2 macrophage ratios (total sum M1 and M2 numbers for the whole experimental group were compared due to low numbers of events in individual mice in some groups. Absolute numbers for M1:M2 / all immune cells in total were: 17:5 / 229180 [SHAM]; 1:4 / 43147 [MI]; 13:5 / 153252 [MI+PATCH]; 28:23 / 555858 [MI+ PATCH CELLS]; 218:115 / 67448 [MI+PATCH SPHEROIDS]). Compared to sham, data show a trend towards a reversal of the M1:M2 ratio for MI which then trends towards a return to sham (not infarcted) values with any treatment (MI+PATCH, MI+PATCH CELLS or MI+PATCH SPHEROIDS. (**B**) Neutrophil:Monocyte whole group ratios show the spheroid group reversed the ratio seen in all other groups (to favour monocytes relative to neutrophils). (**C-F**) Proportion of monocytes (**C**), neutrophils (**D**), NK cells (**E**) and HSC (**F**) show significant changes in cell proportions on day 28 post surgery. Overall, these initial data point to immune cell changes warranting further dedicated analysis. Despite limitations of flow cytometry, the data suggest differences between groups and also that some modification of immune cell activity occurs whether epicardial patches contain no cells (MI+PATCH), freely suspended iPSC-CMs, iCFs, ECs (MI+PATCH CELLS) or the same cells suspended in hydrogel as spheroids (MI+PATCH SPHEROIDS). Bars show group total sum crude ratios (**A-B**), medians $x10^3$ (**C-D**) or $x10^4$ (**E-F**); error bars (**C-F**) show upper limit interquartile range.

Figure 7. The transcriptomic profile of MI+PATCH SPHEROID mice is similar to Sham mice (without MI). (**A**) Principal component analysis of whole transcriptome expression levels. (**B**)

Heatmap of gene expression for all transcripts differential gene expressed between MI, Patch, Cells, Spheroids, and Sham (**C**) Heatmap of gene expression for all transcripts differential gene expressed between MI and Spheroids (**D**) Enrichment analysis for genes differentially expressed between MI and Spheroids. Diseases and Biological Functions (top panel) and Cardiovascular System Development and Functions (bottom panel).

Video Legends

Video 1. Visualisation of confocal micrographic data showing cellular structure of a patch (3D rendering). This abbreviated video shows a slice (taken through the middle) of a cellular patch populated with human iCMs (red, cTNT), CFs (green, vimentin) and HCAECs (blue, CD31) on day 28 of incubation.

Video 2. Visualisation of confocal micrographic data showing cellular structure of a patch (3D rendering). This abbreviated video shows a slice (taken through the middle) of a cellular patch which has formed endothelial cell networks (blue, CD31) with supporting fibroblasts (green, vimentin).

Video 3. Visualisation of confocal micrographic data showing cellular structure of a patch (3D rendering). This abbreviated video shows a slice (taken through the middle) of a cardiac spheroid patch which shows vascularised cardiac spheroids (VCS) still intact at day 28 of incubation. There are also cardiomyocytes (red, cTNT), endothelial cells (blue, CD31) and fibroblasts (green, vimentin) which have migrated out of spheroids and spread across the patch. Endothelial cell networks are visible both within the spheroids and outside them.

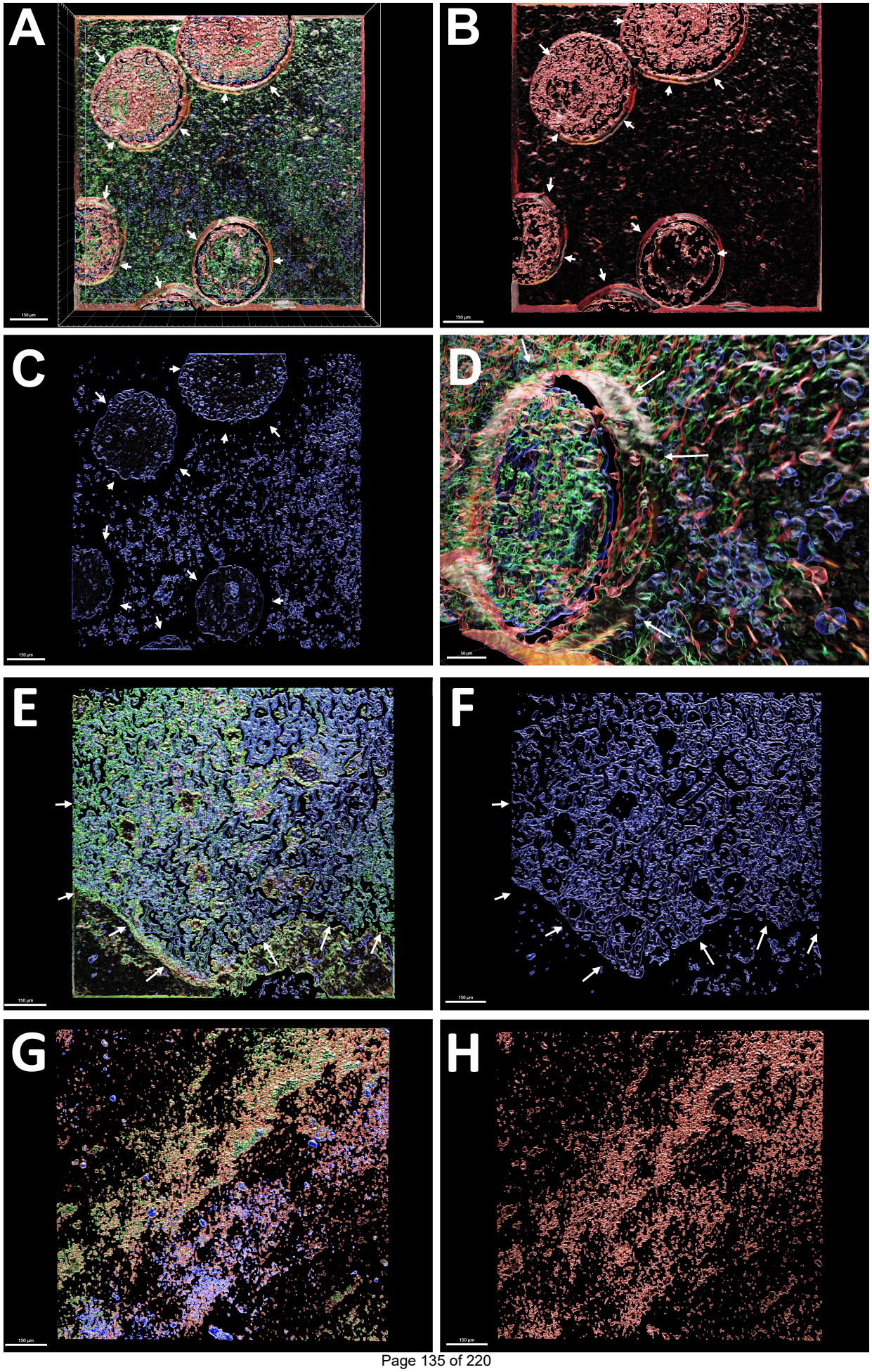

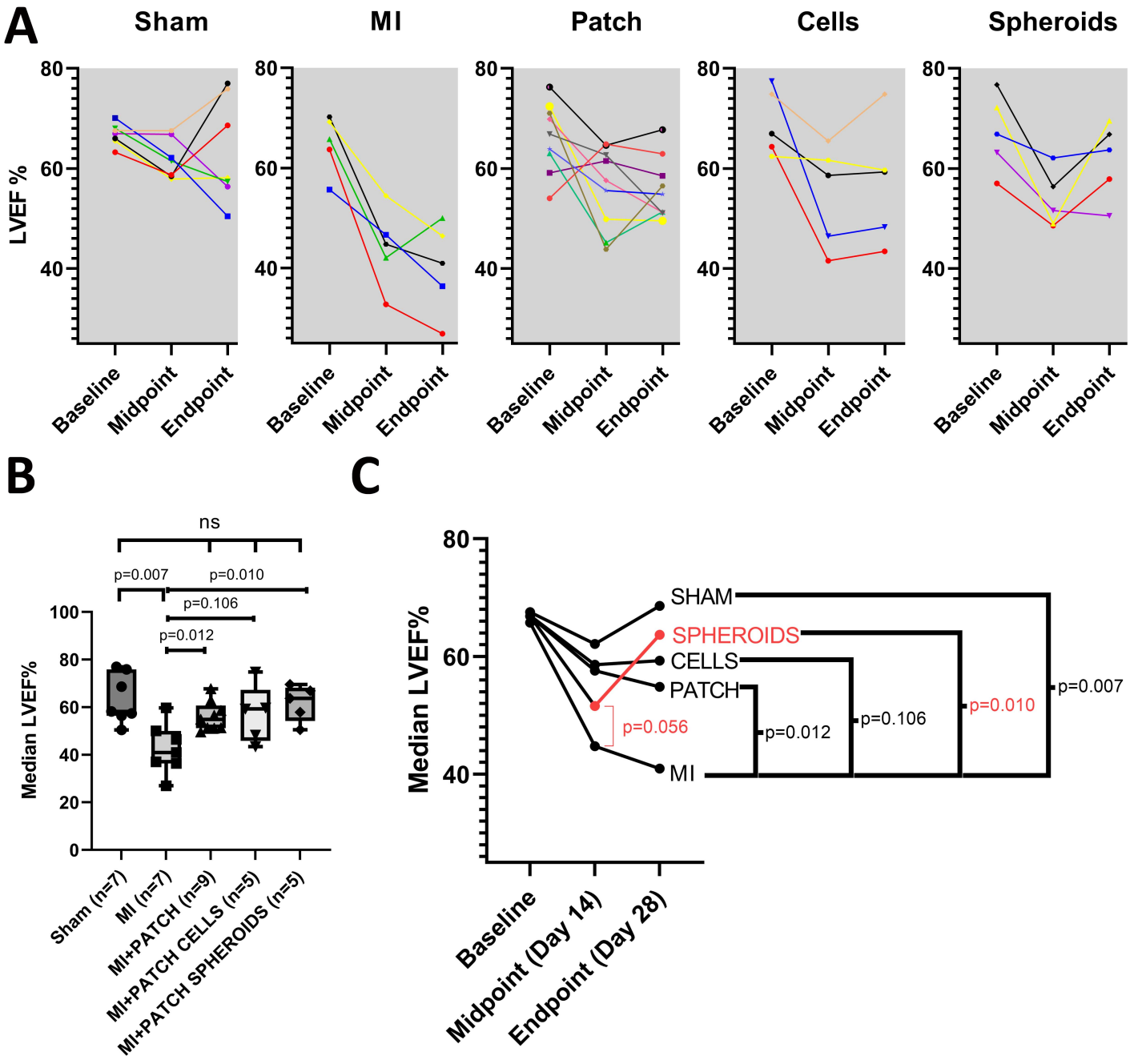

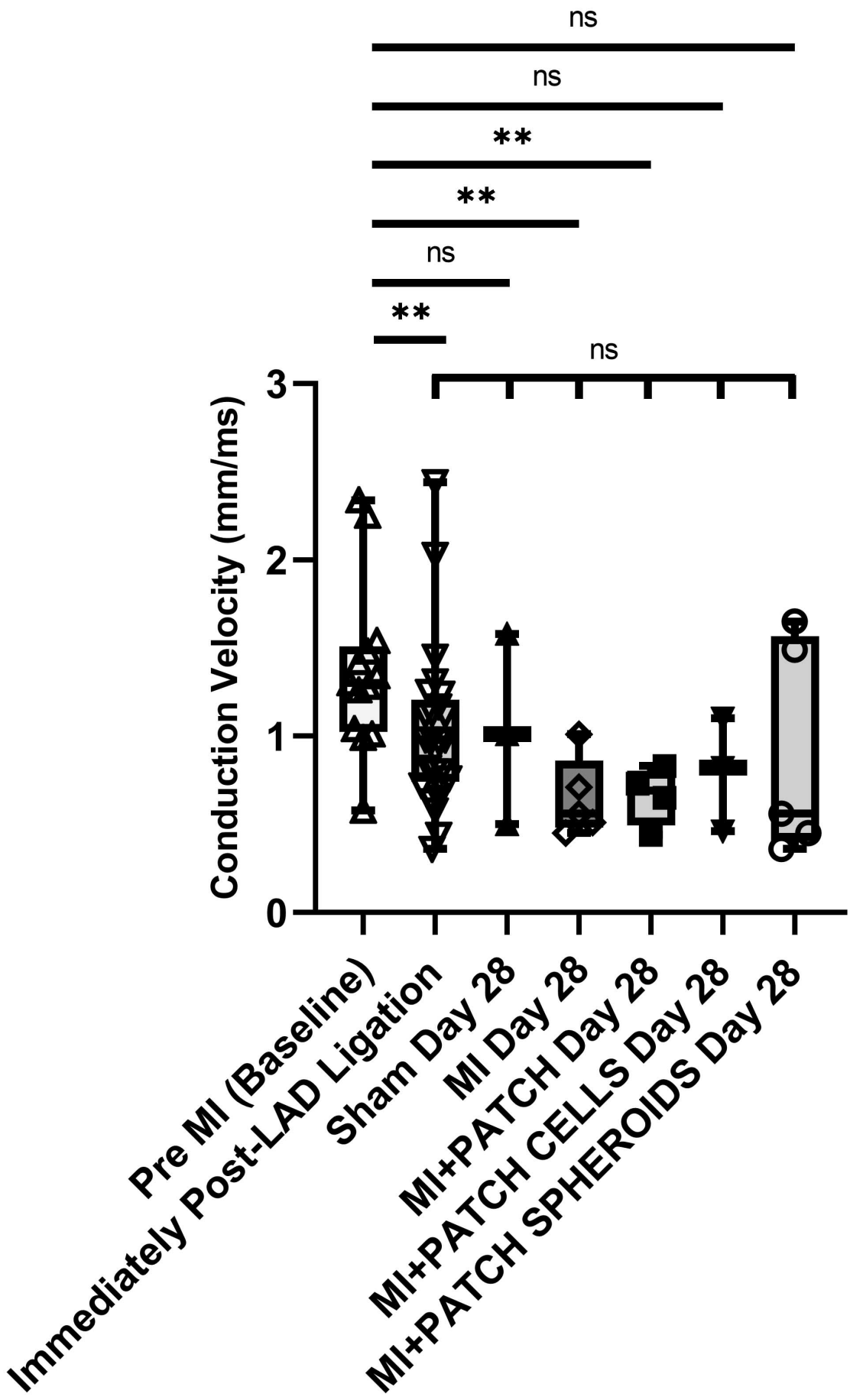

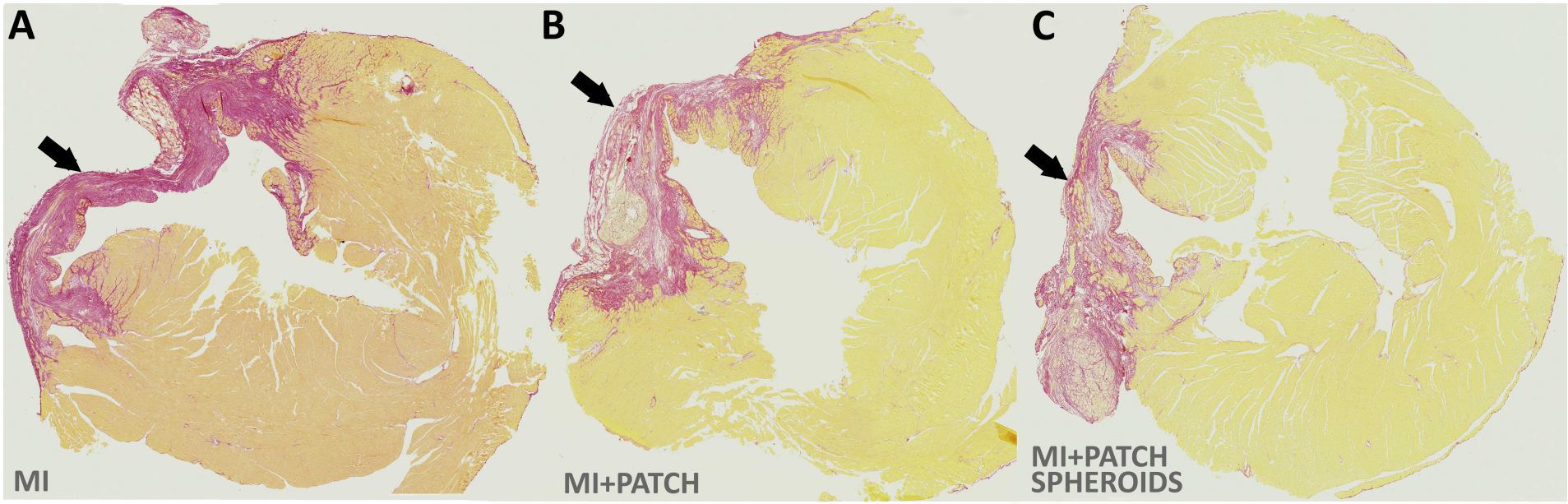

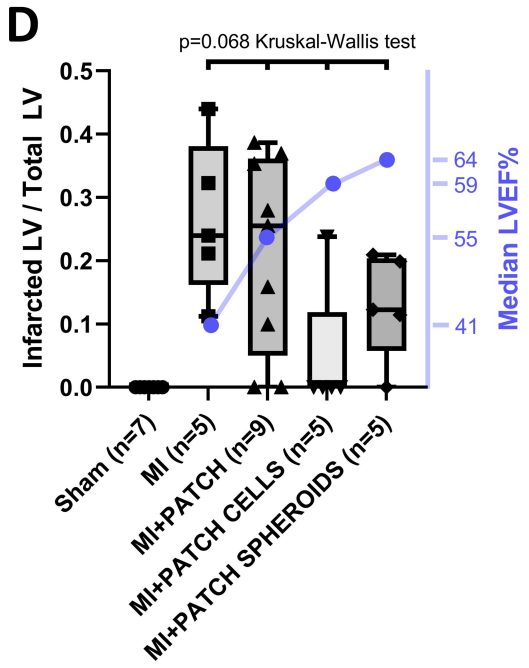

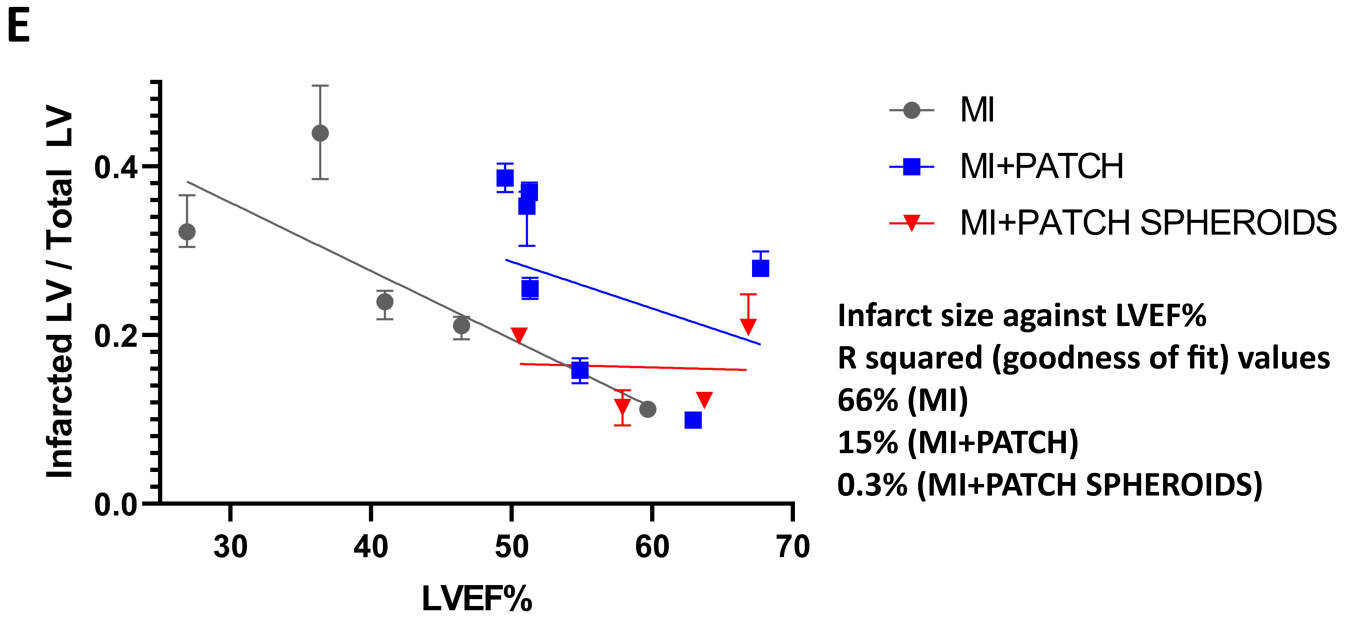

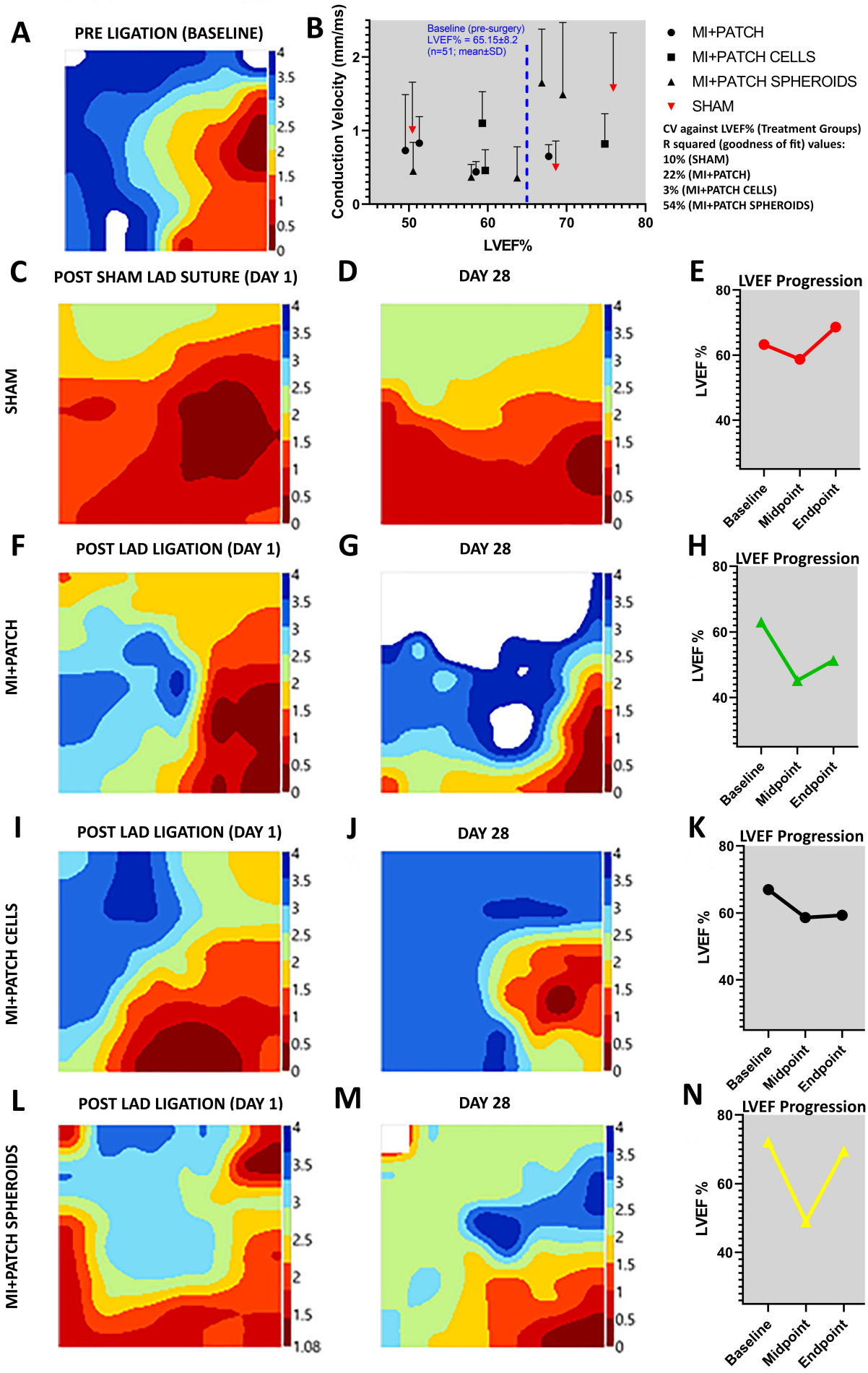

Click here to access/download;Figure(s);Figure 6 Flow Cytometry_New_New2_REVISED_FLAT.tif

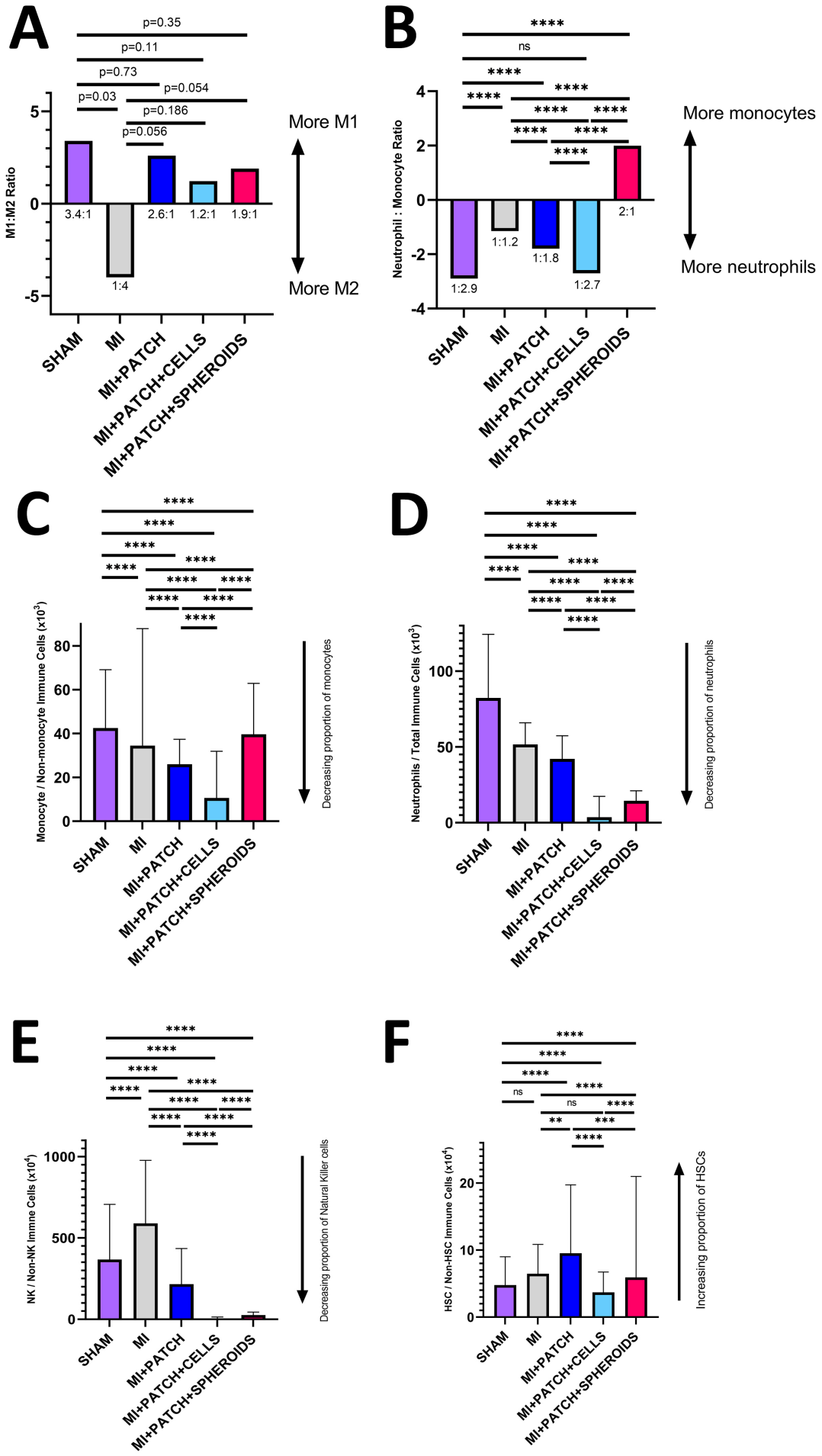

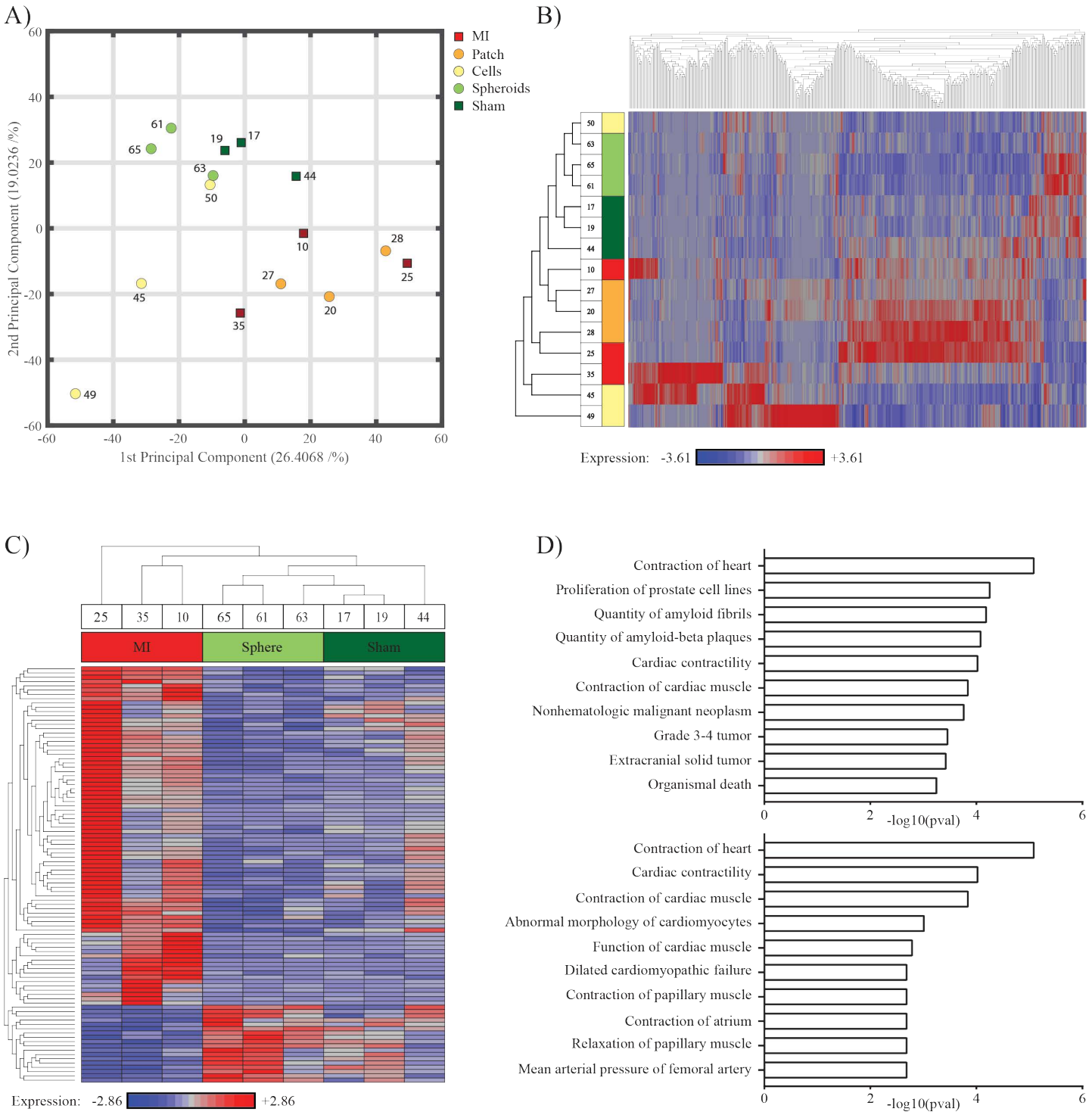

Click here to access/download
e-component
Video 1.mp4

Alterative link: https://youtu.be/ArgQtwc3rdQ

Click here to access/download
e-component
Video 2.mp4

Alternative link: https://youtu.be/FATRxwPn9Pg

Click here to access/download
e-component
Video 3.mp4

Alternative link: https://youtu.be/J_qXIiAJsGQ

References

[1] C.D. Roche, R.J.L. Brereton, A.W. Ashton, C. Jackson, C. Gentile, Current challenges in three-dimensional bioprinting heart tissues for cardiac surgery, Eur J Cardiothorac Surg 58(3) (2020) 500-510.

[2] L. Wang, V. Serpooshan, J. Zhang, Engineering human cardiac muscle patch constructs for prevention of post-infarction LV remodeling, Frontiers in cardiovascular medicine 8(111) (2021).

[3] G.A. MacGowan, D.S. Crossland, A. Hasan, S. Schueler, Considerations for patients awaiting heart transplantation—insights from the UK experience, J Thorac Dis 7(3) (2015) 527-31.

[4] C.D. Roche, J.S. Dobson, S.K. Williams, M. Quante, J. Popoola, J.W.M. Chow, Malignant and noninvasive skin tumours in renal transplant recipients, Dermatol Res Prac 2014 (2014) 409058.

[5] L.H. Lund, K.K. Khush, W.S. Cherikh, S. Goldfarb, A.Y. Kucheryavaya, B.J. Levvey, B. Meiser, J.W. Rossano, D.C. Chambers, R.D. Yusen, J. Stehlik, The registry of the International Society for Heart and Lung Transplantation: thirty-fourth adult heart transplantation report-2017; focus theme: allograft ischemic time, J Heart Lung Transplant 36(10) (2017) 1037-1046.

[6] H. Wang, C.D. Roche, C. Gentile, Omentum support for cardiac regeneration in ischaemic cardiomyopathy models: a systematic scoping review, Eur J Cardiothorac Surg 58(6) (2020) 1118-1129.

[7] C.D. Roche, P. Sharma, A.W. Ashton, C. Jackson, M. Xue, C. Gentile, Printability, durability, contractility and vascular network formation in 3D bioprinted cardiac endothelial cells using alginate-gelatin hydrogels, Front Bioeng Biotechnol 9 (2021) e636257.

[8] J.C. Chachques, J.C. Trainini, N. Lago, O.H. Masoli, J.L. Barisani, M. Cortes-Morichetti, O. Schussler, A. Carpentier, Myocardial assistance by grafting a new bioartificial upgraded myocardium (MAGNUM clinical trial): one year follow-up, Cell Transplant 16(9) (2007) 927-34.

[9] Y. Sawa, S. Miyagawa, T. Sakaguchi, T. Fujita, A. Matsuyama, A. Saito, T. Shimizu, T. Okano, Tissue engineered myoblast sheets improved cardiac function sufficiently to discontinue LVAS in a patient with DCM: report of a case, Surg Today 42(2) (2012) 181-4.

[10] Y. Sawa, Y. Yoshikawa, K. Toda, S. Fukushima, K. Yamazaki, M. Ono, Y. Sakata, N. Hagiwara, K. Kinugawa, S. Miyagawa, Safety and efficacy of autologous skeletal myoblast sheets (TCD-51073) for the treatment of severe chronic heart failure due to ischemic heart disease, Circ J 79(5) (2015) 991-999.

[11] P. Menasché, V. Vanneaux, A. Hagege, A. Bel, B. Cholley, I. Cacciapuoti, A. Parouchev, N. Benhamouda, G. Tachdjian, L. Tosca, J.H. Trouvin, J.R. Fabreguettes, V. Bellamy, R. Guillemain, C. Suberbielle Boissel, E. Tartour, M. Desnos, J. Larghero, Human embryonic stem cell-derived cardiac progenitors for severe heart failure treatment: first clinical case report, Eur Heart J 36(30) (2015) 2011-7.

[12] P. Menasché, V. Vanneaux, A. Hagege, A. Bel, B. Cholley, A. Parouchev, I. Cacciapuoti, R. Al-Daccak, N. Benhamouda, H. Blons, O. Agbulut, L. Tosca, J.H. Trouvin, J.R. Fabreguettes, V. Bellamy, D. Charron, E. Tartour, G. Tachdjian, M. Desnos, J. Larghero, Transplantation of human embryonic stem cell-derived cardiovascular progenitors for severe ischemic left ventricular dysfunction, J Am Coll Cardiol 71(4) (2018) 429-438.

[13] Y. Yoshikawa, S. Miyagawa, K. Toda, A. Saito, Y. Sakata, Y. Sawa, Myocardial regenerative therapy using a scaffold-free skeletal-muscle-derived cell sheet in patients with dilated cardiomyopathy even under a left ventricular assist device: a safety and feasibility study, Surg Today 48(2) (2018) 200-210.

[14] R.J. Vagnozzi, M. Maillet, M.A. Sargent, H. Khalil, A.K. Johansen, J.A. Schwanekamp, A.J. York, V. Huang, M. Nahrendorf, S. Sadayappan, J.D. Molkentin, An acute immune response underlies the benefit of cardiac stem-cell therapy, Nature (2019).

[15] C.D. Roche, C. Gentile, Transplantation of a 3D bioprinted patch in a murine model of myocardial infarction, J Vis Exp (2020) e61675.

[16] L. Polonchuk, M. Chabria, L. Badi, J.C. Hoflack, G. Figtree, M.J. Davies, C. Gentile, Cardiac spheroids as promising in vitro models to study the human heart microenvironment, Sci Rep 7(1) (2017) 7005.

[17] L. Polonchuk, L. Surija, M.H. Lee, P. Sharma, C. Liu Chung Ming, F. Richter, E. Ben-Sefer, M.A. Rad, H. Mahmodi Sheikh Sarmast, W.A. Shamery, H.A. Tran, L. Vettori, F. Haeusermann, E.C. Filipe, J. Rnjak-Kovacina, T. Cox, J. Tipper, I. Kabakova, C. Gentile, Towards engineering heart tissues from bioprinted cardiac spheroids, Biofabrication 13(4) (2021) 045009.

[18] P. Sharma, C. Liu Chung Ming, X. Wang, L.A. Bienvenu, D. Beck, G. Figtree, A. Boyle, C. Gentile, Biofabrication of advanced in vitro 3D models to study ischaemic and doxorubicin-induced myocardial damage, Biofabrication 14(2) (2022) 025003.

[19] J. Takagawa, Y. Zhang, M.L. Wong, R.E. Sievers, N.K. Kapasi, Y. Wang, Y. Yeghiazarians, R.J. Lee, W. Grossman, M.L. Springer, Myocardial infarct size measurement in the mouse chronic infarction model:

comparison of area- and length-based approaches, Journal of Applied Physiology 102(6) (2007) 2104-2111.
[20] M. Xue, H. Lin, H.P.H. Liang, K. McKelvey, R. Zhao, L. March, C. Jackson, Deficiency of protease-activated receptor (PAR) 1 and PAR2 exacerbates collagen-induced arthritis in mice via differing mechanisms, Rheumatology (Oxford) (2020).
[21] A. Dobin, C.A. Davis, F. Schlesinger, J. Drenkow, C. Zaleski, S. Jha, P. Batut, M. Chaisson, T.R. Gingeras, STAR: ultrafast universal RNA-seq aligner, Bioinformatics 29(1) (2013) 15-21.
[22] Y. Liao, G.K. Smyth, W. Shi, featureCounts: an efficient general purpose program for assigning sequence reads to genomic features, Bioinformatics 30(7) (2014) 923-930.
[23] M.I. Love, W. Huber, S. Anders, Moderated estimation of fold change and dispersion for RNA-seq data with DESeq2, Genome Biology 15(12) (2014) 550.
[24] RCoreTeam, R: a language and environment for statistical computing, R Foundation for Statistical Computing, Vienna, Austria. https://www.R-project.org/.
[25] A.J. Whitehead, A.J. Engler, Regenerative cross talk between cardiac cells and macrophages, Am J Physiol Heart Circ Physiol 320(6) (2021) H2211-h2221.
[26] Y. Li, H. Li, J. Pei, S. Hu, Y. Nie, Transplantation of murine neonatal cardiac macrophage improves adult cardiac repair, Cell Mol Immunol 18(2) (2021) 492-494.
[27] L. Wang, Y. Liu, G. Ye, Y. He, B. Li, Y. Guan, B. Gong, K. Mequanint, M.M.Q. Xing, X. Qiu, Injectable and conductive cardiac patches repair infarcted myocardium in rats and minipigs, Nat Biomed Eng (2021).
[28] L. Gao, Z.R. Gregorich, W. Zhu, S. Mattapally, Y. Oduk, X. Lou, R. Kannappan, A.V. Borovjagin, G.P. Walcott, A.E. Pollard, V.G. Fast, X. Hu, S.G. Lloyd, Y. Ge, J. Zhang, Large cardiac muscle patches engineered from human induced-pluripotent stem cell-derived cardiac cells improve recovery from myocardial infarction in swine, Circulation 137(16) (2018) 1712-1730.
[29] S. Mattapally, W. Zhu, V.G. Fast, L. Gao, C. Worley, R. Kannappan, A.V. Borovjagin, J. Zhang, Spheroids of cardiomyocytes derived from human-induced pluripotent stem cells improve recovery from myocardial injury in mice, Am J Physiol Heart Circ Physiol 315(2) (2018) H327-h339.
[30] C. Roche, G. Iyer, M. Nguyen, S. Mabroora, A. Dome, K. Sakr, P. R., L. V., C. Wilson, C. Gentile, Cardiac patch transplantation instruments for robotic minimally invasive cardiac surgery: initial proof-of-concept designs and surgery in a porcine cadaver [preprint], Front Robot AI (2021).
[31] F. Gilbert, J.N.M. Viana, C.D. O'Connell, S. Dodds, Enthusiastic portrayal of 3D bioprinting in the media: ethical side effects, Bioethics 32(2) (2018) 94-102.
[32] F. Gilbert, C.D. O'Connell, T. Mladenovska, S. Dodds, Print me an organ? Ethical and regulatory issues emerging from 3D bioprinting in medicine, Sci Eng Ethics 24(1) (2018) 73-91.
[33] G. Cossu, M. Birchall, T. Brown, P. De Coppi, E. Culme-Seymour, S. Gibbon, J. Hitchcock, C. Mason, J. Montgomery, S. Morris, F. Muntoni, D. Napier, N. Owji, A. Prasad, J. Round, P. Saprai, J. Stilgoe, A. Thrasher, J. Wilson, Lancet Commission: stem cells and regenerative medicine, Lancet 391(10123) (2018) 883-910.
[34] P. Ruytinx, P. Proost, J. Van Damme, S. Struyf, Chemokine-induced macrophage polarization in inflammatory conditions, Front Immunol 9(1930) (2018).
[35] J.C. Chachques, C. Gardin, N. Lila, L. Ferroni, V. Migonney, C. Falentin-Daudre, F. Zanotti, M. Trentini, G. Brunello, T. Rocca, V. Gasbarro, B. Zavan, Elastomeric cardiowrap scaffolds functionalized with mesenchymal stem cells-derived exosomes induce a positive modulation in the inflammatory and wound healing response of mesenchymal stem cell and macrophage, Biomedicines 9(7) (2021).
[36] S. Alvarez-Argote, C.C. O'Meara, The evolving roles of cardiac macrophages in homeostasis, regeneration, and repair, Int J Mol Sci 22(15) (2021).
[37] W. Peng, M. Li, H. Li, K. Tang, J. Zhuang, J. Zhang, J. Xiao, H. Jiang, D. Li, Y. Yu, P.C. Sham, S. Nattel, Y. Xu, Dysfunction of myosin light-chain 4 (MYL4) leads to heritable atrial cardiomyopathy with electrical, contractile, and structural components: evidence from genetically-engineered rats, J Am Heart Assoc 6(11) (2017) e007030.
[38] J. Sun, X. Guo, P. Yu, J. Liang, Z. Mo, M. Zhang, L. Yang, X. Huang, B. Hu, J. Liu, Y. Ouyang, M. He, Vasorin deficiency leads to cardiac hypertrophy by targeting MYL7 in young mice, J Cell Mol Med 26(1) (2022) 88-98.
[39] S.A. Legere, I.D. Haidl, J.F. Légaré, J.S. Marshall, Mast cells in cardiac fibrosis: New insights suggest opportunities for intervention, Front Immunol 10(MAR) (2019).

[40] R. Gong, Z. Jiang, N. Zagidullin, T. Liu, B. Cai, Regulation of cardiomyocyte fate plasticity: a key strategy for cardiac regeneration, Signal Transduct Target Ther 6(1) (2021) 31.
[41] K. Klaourakis, J.M. Vieira, P.R. Riley, The evolving cardiac lymphatic vasculature in development, repair and regeneration, Nature reviews. Cardiology 18(5) (2021) 368-379.
[42] M. Su, Z. Luo, J. Yu, R. Zhang, J. Wang, C. Huang, W. Li, W. Yuan, H. Zhang, G. Cai, S. Shen, Effects of fastigial nucleus electrostimulation on cardiac nerve regeneration, neurotransmitter release, and malignant arrhythmia inducibility in a post-infarction rat model, Eur J Neurosci (2021).

Supplementary Figures 1-11

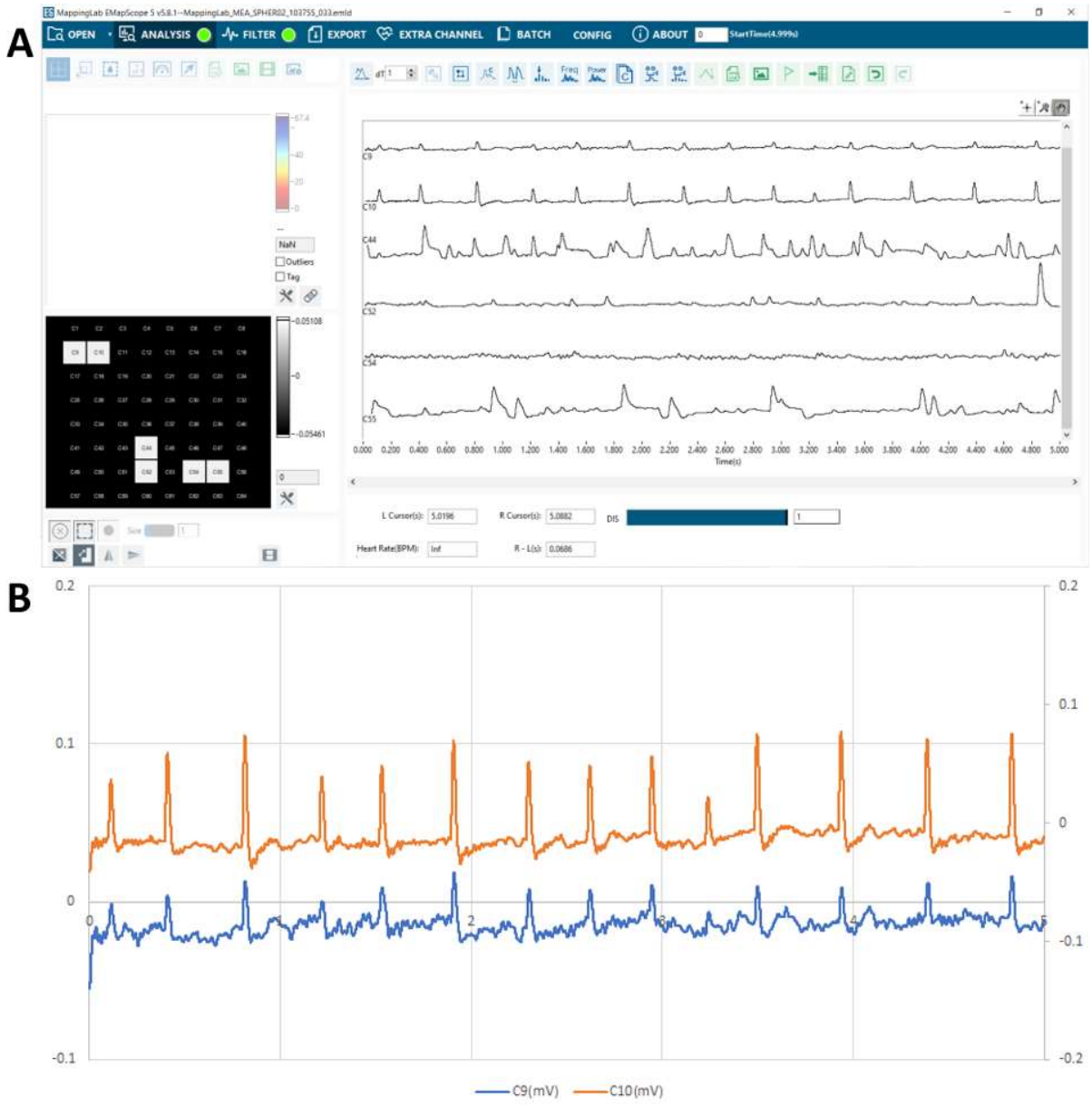

Supplementary Figure 1. Ex vivo detection of electrical activity confirmed electrically active cells after 28 days of patch incubation. (**A**) The raw data shows that electrical activity is present in gel containing human cardiac spheroids. (**B**) Shows processed data (independently confirmed electrical activity). The neighbouring channels Ch9 and Ch10 both had typical electrograms of field potentials with the same rhythmic waveforms, meaning the depolarisation wavefront from iCM rich spheroids can be propagated. Patches with cells (not in spheroids) had weaker electrical activities in comparison of spheroids (data not shown) confirming that both types of bioink are viable.

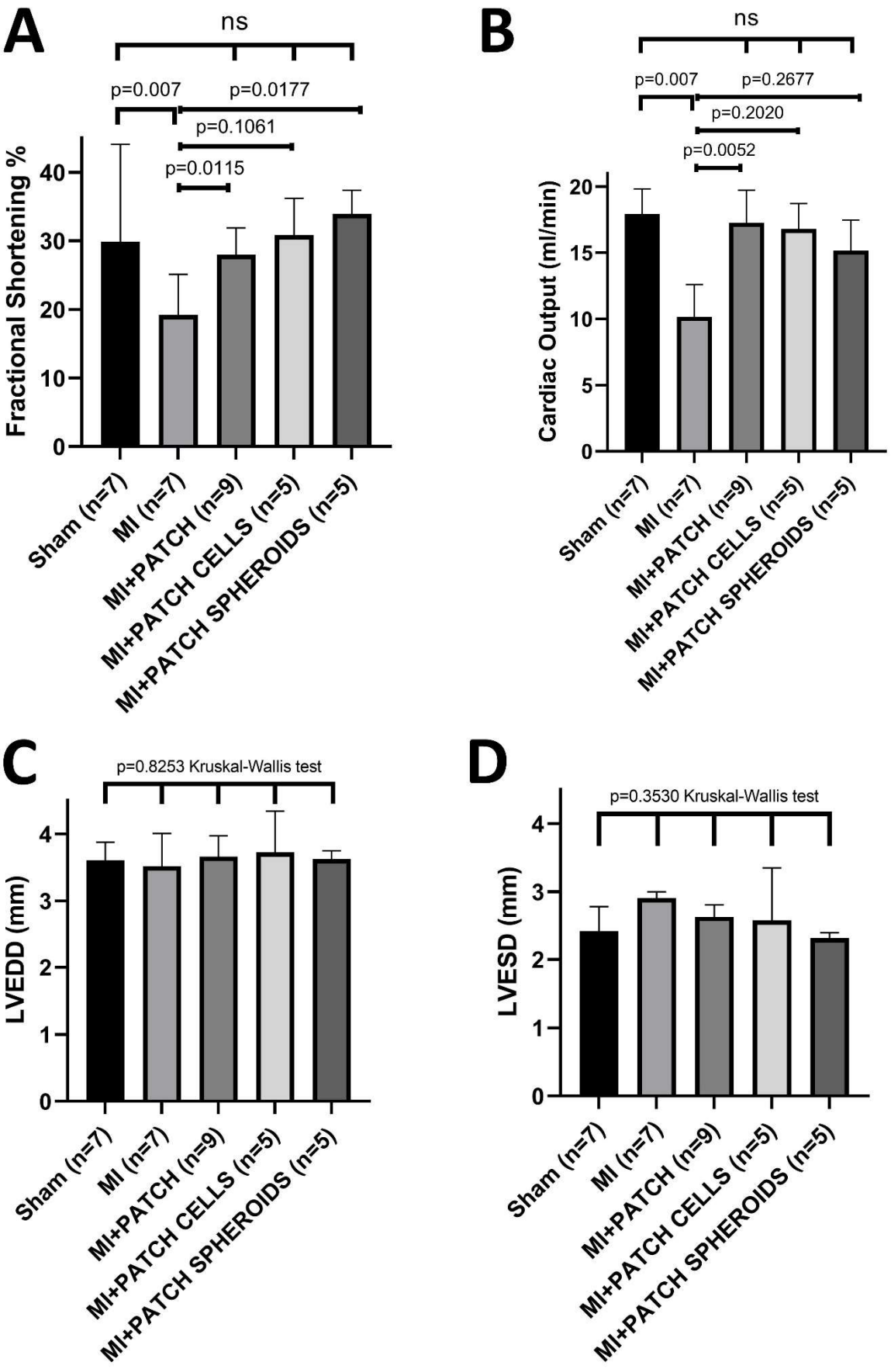
A
ns
p=0.007
p=0.0177
p=0.1061
p=0.0115
Fractional Shortening %
0
10
20
30
40
Sham (n=7)
MI (n=7)
MI+PATCH (n=9)
MI+PATCH CELLS (n=5)
MI+PATCH SPHEROIDS (n=5)
B
ns
p=0.007
p=0.2677
p=0.2020
p=0.0052
Cardiac Output (ml/min)
0
5
10
15
20
Sham (n=7)
MI (n=7)
MI+PATCH (n=9)
MI+PATCH CELLS (n=5)
MI+PATCH SPHEROIDS (n=5)
C
p=0.8253 Kruskal-Wallis test
LVEDD (mm)
0
1
2
3
4
Sham (n=7)
MI (n=7)
MI+PATCH (n=9)
MI+PATCH CELLS (n=5)
MI+PATCH SPHEROIDS (n=5)
D
p=0.3530 Kruskal-Wallis test
LVESD (mm)
0
1
2
3
4
Sham (n=7)
MI (n=7)
MI+PATCH (n=9)
MI+PATCH CELLS (n=5)
MI+PATCH SPHEROIDS (n=5)

Supplementary Figure 2. Evaluation of cardiac functional outcome measures other than the LVEF%. (**A-D**) Cardiac functional analyses using the same method as was performed for the LVEF% in **Figure 2B** but with alternative outcome measures. (**A**) Fractional shortening % (FS) analysis returns similar results to LVEF%. FS measures % change in left ventricular diameter during systole and correlates with LVEF% unless there are abnormalities in ventricular geometry, activation (including bundle branch blocks) or regional areas (regional differences in contractile function may be missed). Accepted normal FS values on M-mode echocardiography are >25%. (**B**) Cardiac output (CO) showed similar results to LVEF% (**Figure 2B**) but the interval between median CO for MI group mice and MI+PATCH CELLS or MI+PATCH SPHEROIDS was reduced and consequently p values for groups having cellular patch transplantation compared to MI were higher. (**C-D**) Left ventricular end diastolic (LVEDD) and systolic (LVESD) diameters were the same in all groups. No difference was observed for sham mice (no MI or treatment) compared to MI mice (LAD ligation without treatment) which is not concordant with the other functional outcome measures (**A-B**), suggesting that LVEDD and LVESD alone may not be useful as outcome measures in mouse models of MI. Baseline median(IQR) values (n=51): FS=34.8(32.0-38.3); CO=14.5(10.3-16.8); LVEDD=3.3(2.8-3.6); LVESD=2.0(1.8-2.4).

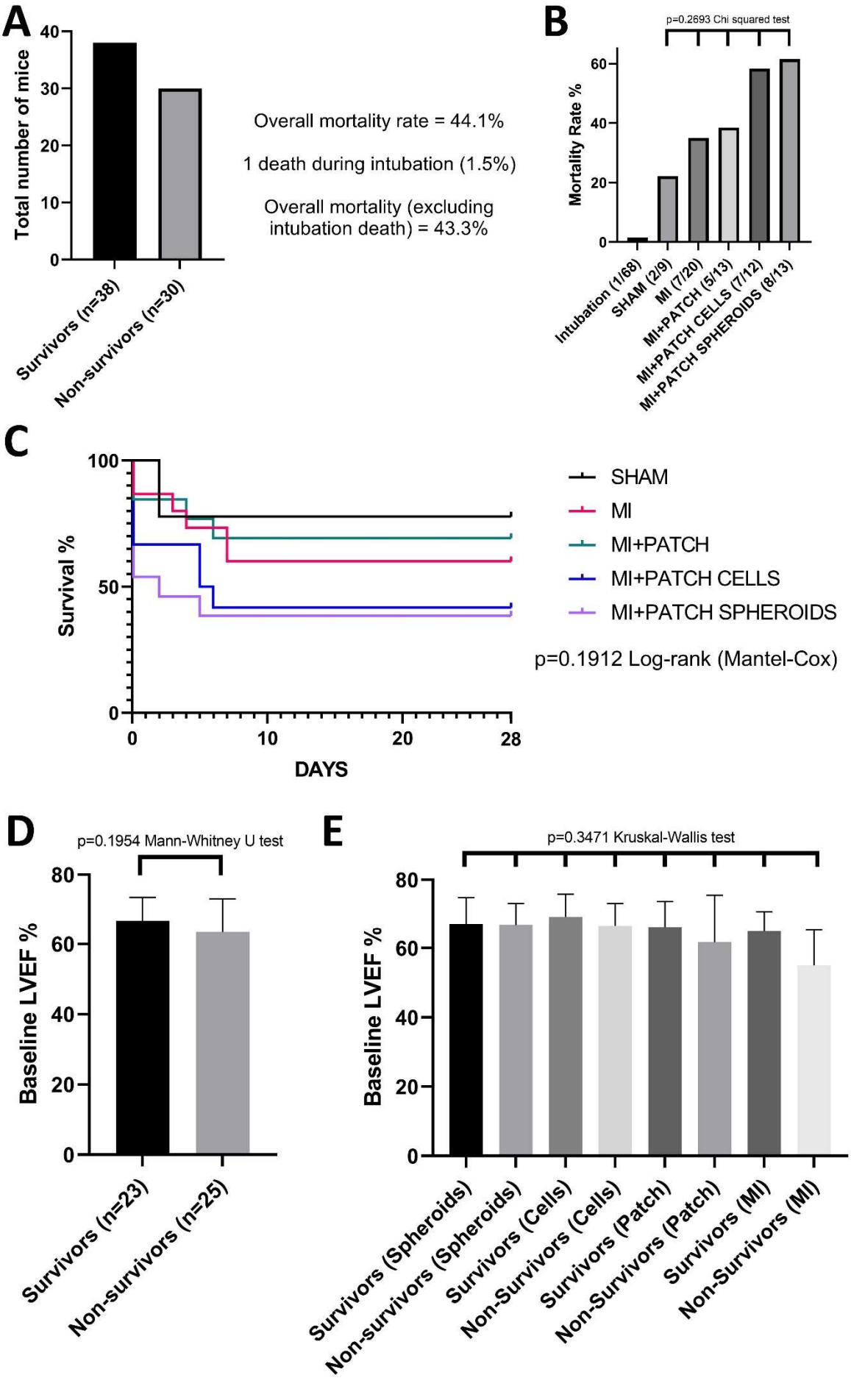
A
Total number of mice
40
30
20
10
0
Survivors (n=38)
Non-survivors (n=30)
Overall mortality rate = 44.1%
1 death during intubation (1.5%)
Overall mortality (excluding intubation death) = 43.3%
B
p=0.2693 Chi squared test
Mortality Rate %
60
40
20
0
Intubation (1/68)
SHAM (2/9)
MI (7/20)
MI+PATCH (5/13)
MI+PATCH CELLS (7/12)
MI+PATCH SPHEROIDS (8/13)
C
Survival %
100
50
0
0
10
20
28
DAYS
SHAM
MI
MI+PATCH
MI+PATCH CELLS
MI+PATCH SPHEROIDS
p=0.1912 Log-rank (Mantel-Cox)
D
p=0.1954 Mann-Whitney U test
Baseline LVEF %
80
60
40
20
0
Survivors (n=23)
Non-survivors (n=25)
E
p=0.3471 Kruskal-Wallis test
Baseline LVEF %
80
60
40
20
0
Survivors (Spheroids)
Non-survivors (Spheroids)
Survivors (Cells)
Non-Survivors (Cells)
Survivors (Patch)
Non-Survivors (Patch)
Survivors (MI)
Non-Survivors (MI)

Supplementary Figure 3. Mortality data and baseline LVEF% characteristics. (**A-B**) Mortality rates overall (**A**) and by experimental group (**B**) including all mice (+1 mouse that died during intubation and +10 mice in the MI group which were part of our pilot study to establish that our mortality rate for B6.RAG1 mice (immune suppressed C57Bl6 without mature B or T cells) did not exceed an accepted literature rate for non-immune suppressed C57Bl6 mice of 44%(1). (**C**) Kaplan-Meier survival analysis for each experimental group showed a trend towards increased mortality in the groups with patches containing cells (MI+PATCH CELLS and MI+PATCH+SPHEROIDS) but not in the group with patches containing hydrogel only without cells (MI+PATCH), but the Log-rank (Mantel-Cox) test result was not significant. No strong statistically significant difference was shown in mortality in our experimental groups. (**D-E**) For the MI control group compared to our three treatment groups, median baseline cardiac function (LVEF%) was not significantly different in survivors (up to day 28) compared with non-survivors that died before reaching day 28 (error bars show interquartile range; analysis excludes sham mice, pilot MI group mice and the mouse that died during intubation).

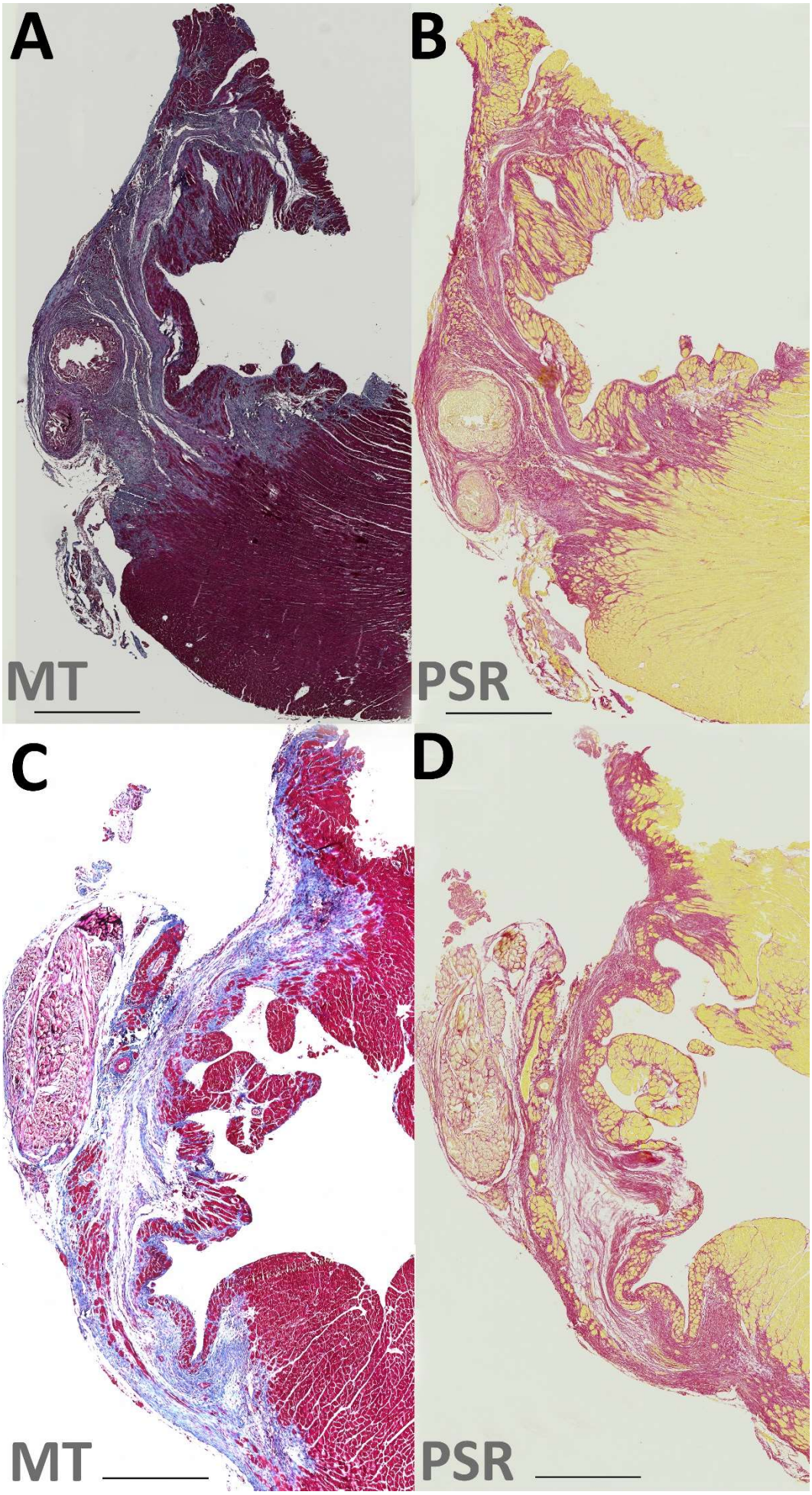
A
B
MT
PSR
C
D
MT
PSR

Supplementary Figure 4. Patterns of infarction were variable and may have influenced cardiac function in ways not accounted for by the infarct size measurement alone. (**A-B**) Staining with Masson's Trichrome (**A**) and Picrosirius Red (**B**) for a mouse in the MI group with infarct size of 32%. (**C-D**) shows histology from a mouse in the MI+PATCH group with a similar infarct size (35%) with severe loss of cell architecture and localised wall-thinning. Mice with similar absolute infarct sizes might have had different LVEF% effects, for example due to different patterns of infarction. Scale bars = 500 μm

Supplementary Figure 5. A patch remnant captured on histology still adherent to the mouse heart on day 28 post surgery. (A-C) shows a patch in situ on the epicardial surface at day 28 with H&E (**A**), Picrosirius Red (**B**) and Masson's Trichrome (**C**) staining, respectively. This mouse had no detected underlying infarction. Reasons for undetected infarction include the mouse having a minimal infarction generated at the time of surgery, or the sample not capturing a small or focal infarction (especially if the infarction was apical – we sampled the midzone). Nonetheless, taken together with the trend towards treatment groups presenting an improved LVEF% and lower infarct size, it is possible that infarct size was smaller due to the treatment itself and therefore less likely to be detected on histology (our sampling method took multiple slices for multiple analyses rather than the whole heart for histology alone). Scale bars = 500 μm. Raw data for these images (.CZI files) are available in the data repository.

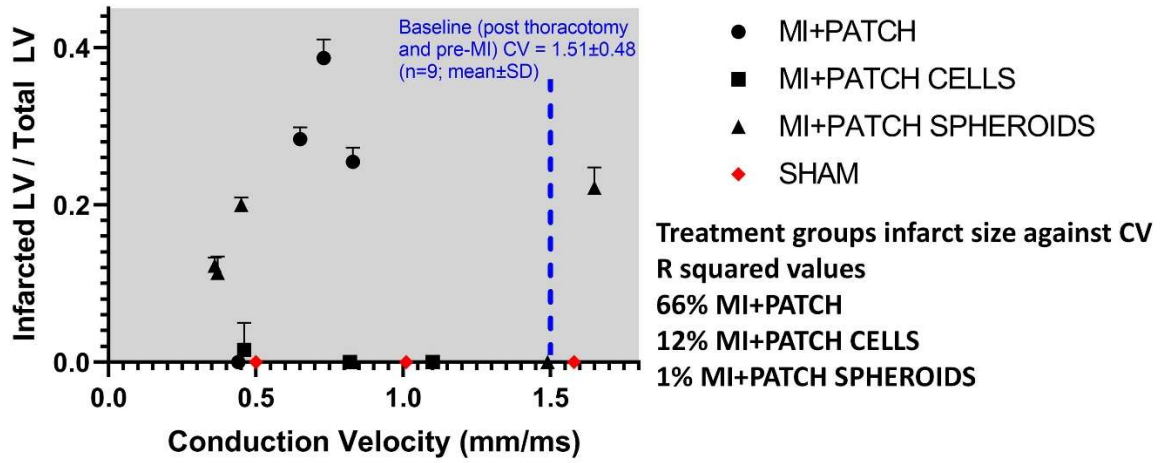

Supplementary Figure 6. Day 28 mean CV (n=4 repeat readings per mouse) plotted against mean infarct size values (error bars=SD (only upper bar shown); up to 6 repeats per mouse) in treatment groups and the sham group. Sham group (infarct area = zero) CV values vary widely and even sham group mice could present low mean conduction velocity readings (red diamonds). Most mice dropped their conduction velocity on day 28 compared to baseline (pre-MI). Coefficients of determination (R squared) were similar to values for infarct size plotted against LVEF%. The strong correlation in the MI group was reduced to a weak

correlation with a patch treatment (12%) and reduced further to no correlation (1%) with the spheroid group.

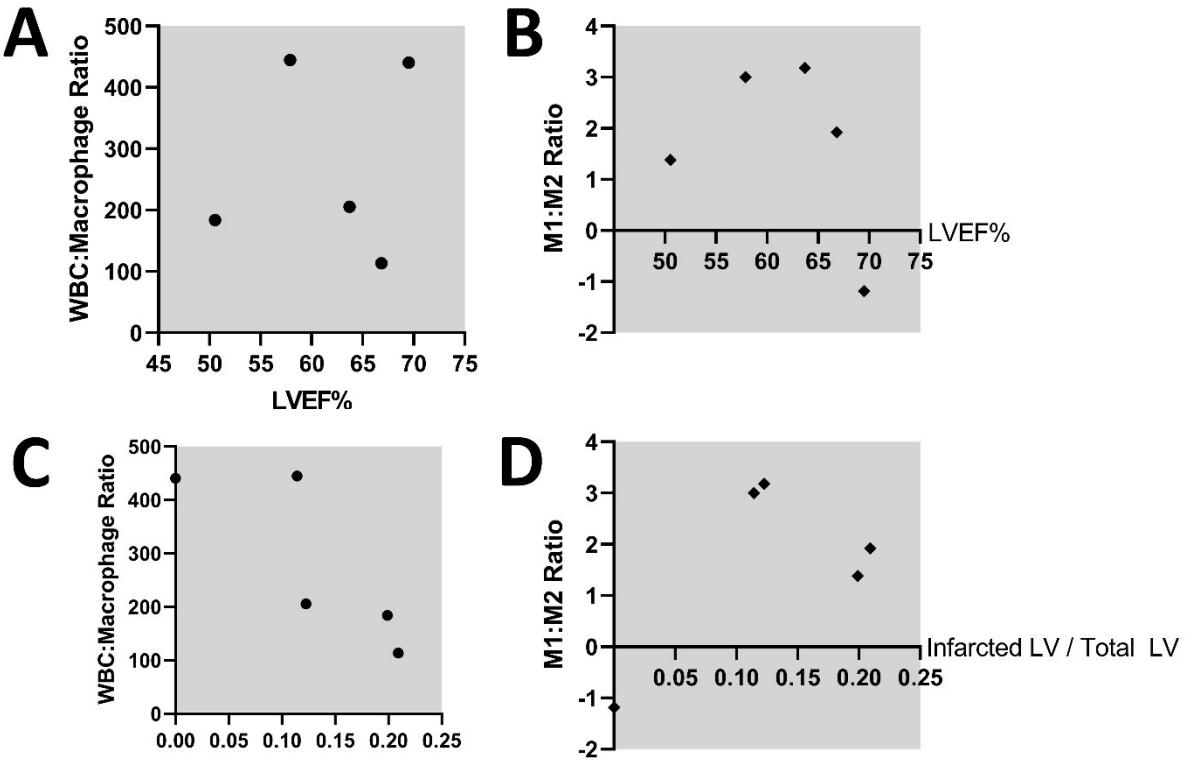

Supplementary Figure 7. No strong trends were identified between macrophages plotted against infarct size or LVEF% for mice in the spheroid group. (**A-D**) For the 5 mice surviving to day 28 in the MI+PATCH SPHEROIDS group, no strong correlation was seen between either M1:M2 ratio or total WBC:Macrophage ratio plotted against LVEF% (**A=B**) or infarct size (**C-D**).

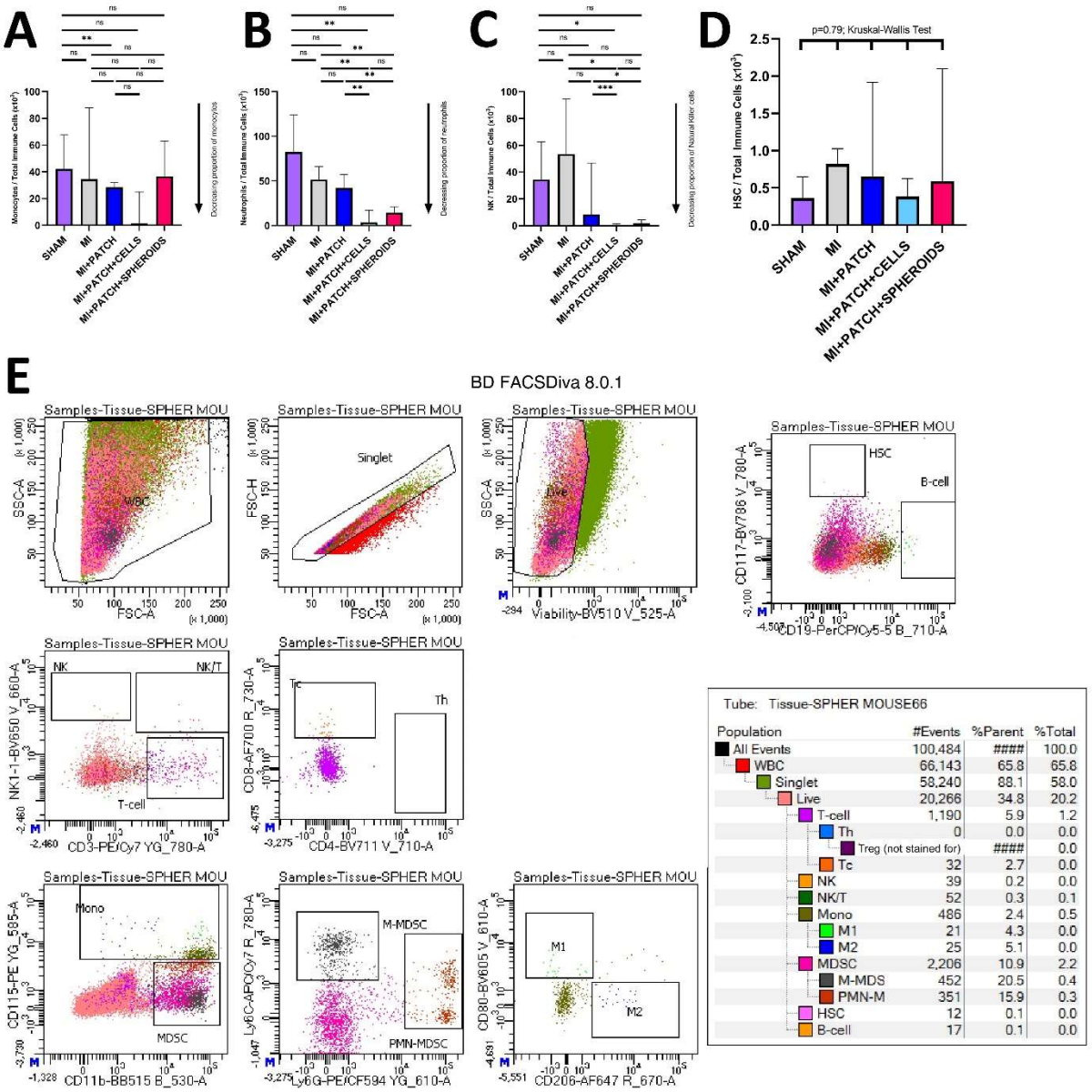

Supplementary Figure 8. Supplementary analysis of flow cytometry data for tissue immune cells. (**A-D**) Secondary analysis of the categorical (type of cell) data presented in **Figure 6** with the data processed here as continuous data (number of cells). Despite this method of assessing the data returning more statistically insignificant results, the results support our contention that changes occurred in host (mouse) tissue immune cells on day 28 post surgery. Bars show medians x10^3 (error bars show inter-quartile ranges). (**E**) The full flow cytometry immune cell profile for the heart tissue of the mouse showing the greatest drop and recovery in LVEF% in our experiment. This shows an M1:M2 ratio of approximately 1:1. This is the same mouse for which data were presented in **Figure 3P-S**. This mouse had electrical mapping readings on day one (**Figure 5L**) and day 28 (**Figure 5M**) which showed a change towards higher maximum conduction velocities (CVs) and a V-shaped LVEF% progression (**Figure 5N**) from baseline to midpoint (14 days) to endpoint (28 days).

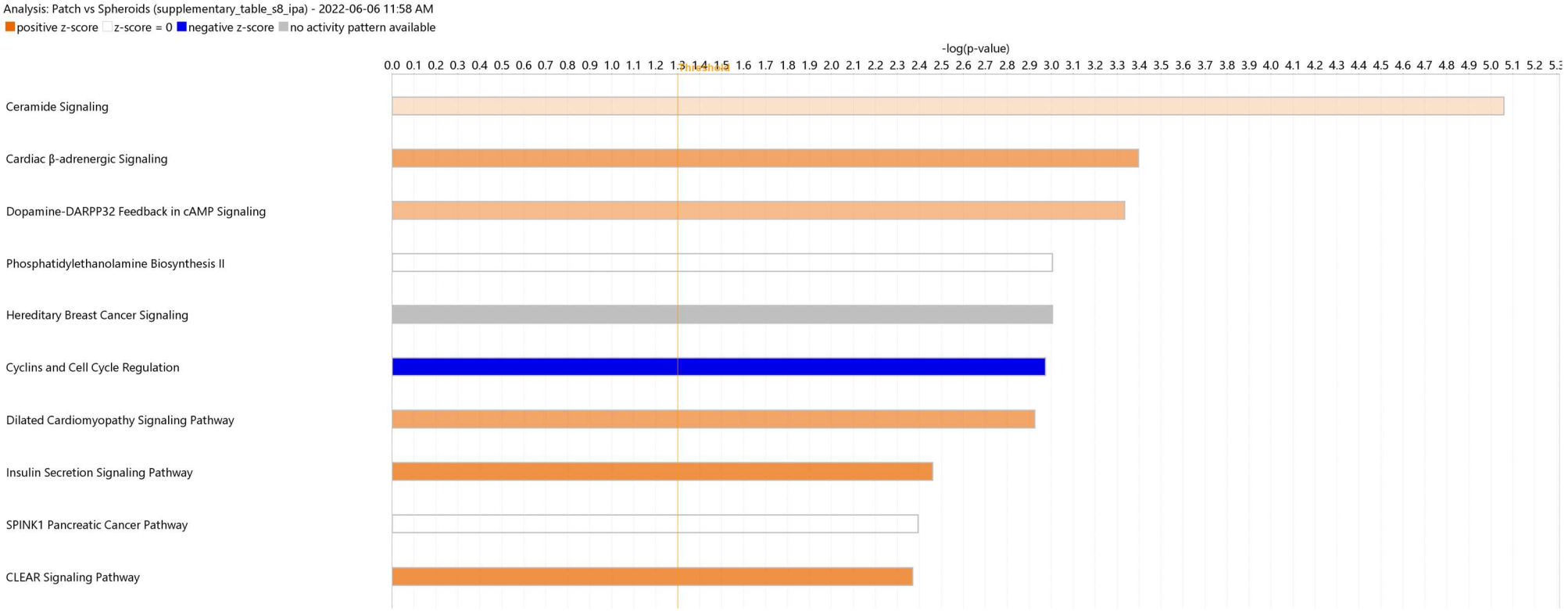

Supplementary Figure 9. Enrichment for Canonical Pathways. Analysis compares hydrogel (acellular) patch treatment with spheroid patches and shows upregulation of genes associated with the labelled canonical pathways. Gene expression associated with cardiac beta-adrenergic signaling (regulating heart rate and contractility) was upregulated. Of note, gene expression associated with dilated cardiomyopathy signalling was also upregulated in the spheroid group (see **Supplementary Figure 10**).

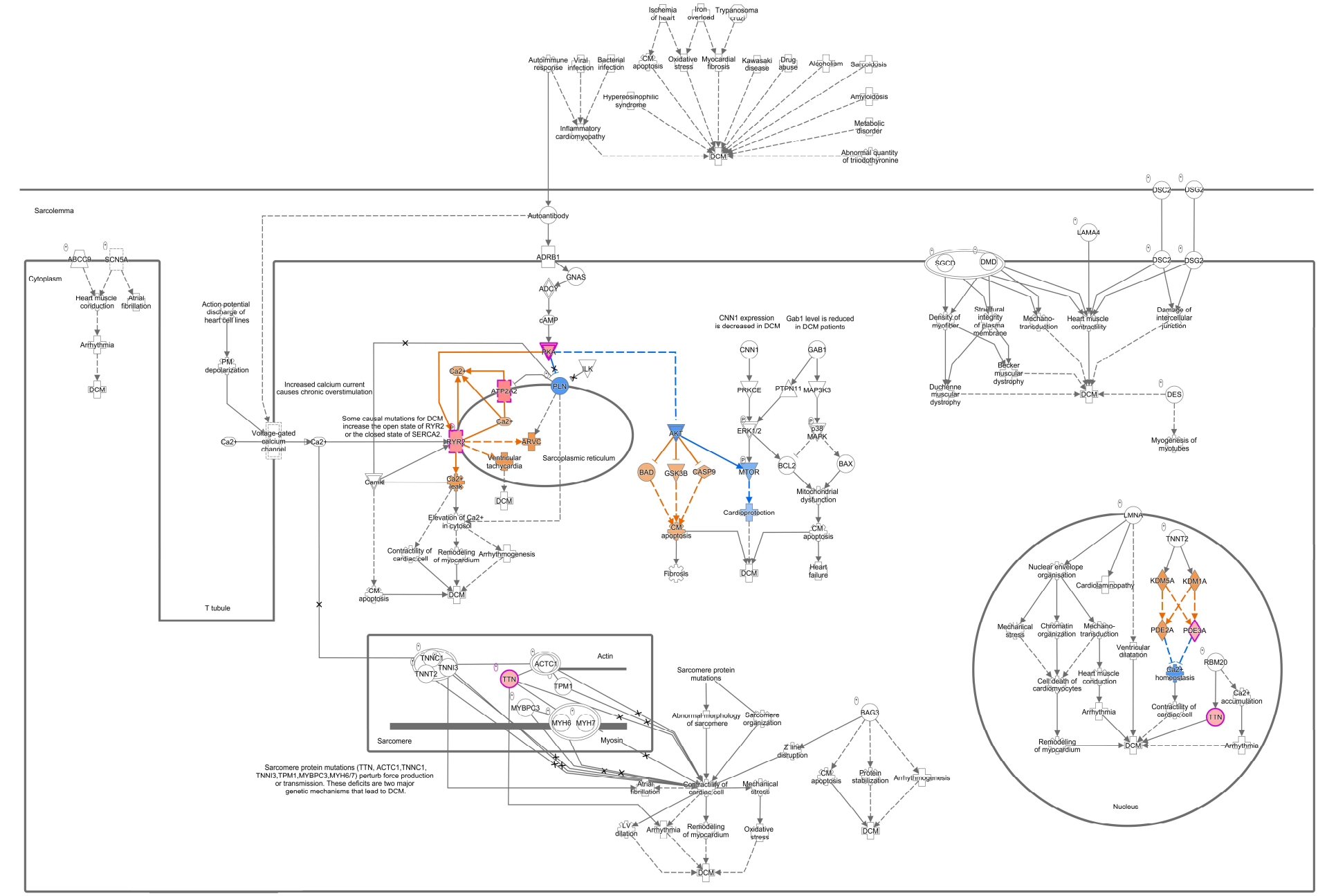

Supplementary Figure 10. Dilated Cardiomyopathy Signalling pathway. Upregulated gene expression in the spheroid group compared to hydrogel (acellular) patch treatment was associated with multiple genes known to be associated with dilated cardiomyopathy. Overall, genetic changes induced in the spheroid treatment group may have altered molecular events within the myocardium such as calcium signalling, remodelling and apoptosis.

Categories	Functions	Diseases or Functions Annotation	p-value	Molecules
Cardiovascular Disease Cardiovascular System Development and Function Organ Morphology Organismal Development Organismal Injury and Abnormalities Skeletal and Muscular Disorders Hereditary Disorder Hematological System Development and Function Skeletal and Muscular System Development and Function Tissue Morphology Cellular Function and Maintenance Cellular Assembly and Organization,Cellular Development,,Cellular Growth and Proliferation,Embryonic Development Cell Morphology,, Dermatological Diseases and Conditions	enlargement	Enlargement of heart	0.00000171	ACSL1,APOE,ATP2A2,CAST,COL3A1,CTSB,CTSD,DOT1L,DSP,IL6ST,KCNJ11,LDB3,NPR3,PFKFB1,PPP2CA,RYR2,TTN,USP18
	dilated cardiomyopathy	*Dilated cardiomyopathy*	*0.00000937*	*ACSL1,APOE,ATP2A2,CAST,COL3A1,DSP,LDB3,NPR3,PPP2CA,RYR2,TTN,USP18*
	abnormal morphology	Abnormal morphology of heart	0.000016	ACSL1,APOE,ATP2A2,CAST,CCND3,COL3A1,CTSB,CTSD,DOT1L,DSP,IL6ST,KCNJ11,LDB3,NPR3,PFKFB1,PPP2CA,RYR2,TTN,USP18
	abnormal morphology	Abnormal morphology of cardiovascular system	0.0000331	ACSL1,APOE,ATP2A2,CAST,CCND3,COL3A1,CTSB,CTSD,DOT1L,DSP,IL6ST,KCNJ11,LDB3,NPR3,PAM,PFKFB1,PPP2CA,RYR2,TTN,USP18
	familial dilated cardiomyopathy with left ventricular noncompaction	Familial dilated cardiomyopathy with left ventricular noncompaction	0.0000841	LDB3,RYR2
	diastolic pressure	Diastolic pressure	0.000141	APOE,ATP2A2,DOT1L,NPR3,TTN
	quantity	Quantity of fibrous layer of blood vessel	0.000168	APOE,MMP12
	dilated cardiomyopathy 1A	Dilated cardiomyopathy 1A	0.000275	DSP,LDB3,TTN
	enlargement	Enlargement of left ventricle	0.000413	APOE,ATP2A2,KCNJ11,LDB3,RYR2,TTN
	function	Function of cardiac muscle	0.000442	APOE,ATP2A2,PFKFB1,RYR2,SPHK1,TTN,USP18
	abnormal morphology	Abnormal morphology of left ventricle	0.00048	APOE,ATP2A2,LDB3,RYR2,TTN
	morphology	Morphology of left ventricle	0.000531	APOE,ATP2A2,IL6ST,KCNJ11,LDB3,RYR2,TTN
	familial primary dilated cardiomyopathy	Familial primary dilated cardiomyopathy	0.000565	DSP,LDB3,RYR2,TTN
	abnormal morphology	Abnormal morphology of heart ventricle	0.000721	APOE,ATP2A2,CCND3,IL6ST,LDB3,RYR2,TTN
	hypertrophy	Hypertrophy of heart	0.000734	APOE,ATP2A2,CTSB,CTSD,IL6ST,KCNJ11,PFKFB1,RYR2,TTN,USP18
	left ventricular dilation	Left ventricular dilation	0.000806	APOE,ATP2A2,LDB3,RYR2
	dominant dilated cardiomyopathy	Dominant dilated cardiomyopathy	0.000851	DSP,LDB3,TTN
	thickness	Thickness of left ventricle	0.000988	APOE,IL6ST
	mean arterial pressure	Mean arterial pressure	0.00109	APOE,ATP2A2,CD247,COMP,KCNJ11
	abnormal morphology	Abnormal morphology of aorta wall	0.0015	APOE,COL3A1
	function	Function of cardiomyocytes	0.00156	RYR2,SPHK1,TTN
	cardiac contractility	Cardiac contractility	0.00158	APOE,ATP2A2,PFKFB1,PPP2CA,RYR2,TTN
	dilated cardiomyopathy 1S	Dilated cardiomyopathy 1S	0.00179	DSP,TTN
	fractional shortening	Fractional shortening of heart	0.00284	ACSL1,PFKFB1,RYR2
	organization	Organization of sarcomere	0.00284	LDB3,NEURL2,TTN
	vascularization	Vascularization of absolute anatomical region	0.00287	APOE,C3,MMP12,SPHK1,SPHK2
	morphology	Morphology of heart cells	0.0032	ATP2A2,CTSB,CTSD,IL6ST,RYR2,TTN,USP18
	abnormal morphology	Abnormal morphology of ventricular wall	0.0038	APOE,ATP2A2,CCND3,IL6ST
	morphology	Morphology of heart ventricle	0.00382	APOE,ATP2A2,CCND3,IL6ST,KCNJ11,LDB3,RYR2,TTN
	blood pressure	Blood pressure	0.00501	APOE,ATP2A2,CD247,COMP,DOT1L,KCNJ11,NPR3,TTN
	vasculogenesis	Vasculogenesis	0.00522	APOE,ATP2A2,C3,COL3A1,COMP,CTSB,GLMN,IL6ST,MMP12,PAQR3,PDE3A,PIGF,SPHK1,SPHK2,USP18
	abnormal morphology	Abnormal morphology of spiral modiolar artery	0.00532	APOE
	dilated cardiomyopathic failure	Dilated cardiomyopathic failure	0.00532	ATP2A2
	dilated cardiomyopathy with woolly hair and keratoderma	Dilated cardiomyopathy with woolly hair and keratoderma	0.00532	DSP
	dilated cardiomyopathy with woolly hair, keratoderma, and tooth agenesis	Dilated cardiomyopathy with woolly hair, keratoderma, and tooth agenesis	0.00532	DSP
	contraction	Contraction of papillary muscle	0.00532	ATP2A2
	dilated cardiomyopathy 1g	Dilated cardiomyopathy 1g	0.00532	TTN
	dilated cardiomyopathy with left ventricular noncompaction type 1c	Dilated cardiomyopathy with left ventricular noncompaction type 1c	0.00532	LDB3
	density	Density of vasa vasorum	0.00532	APOE
	mean arterial pressure	Mean arterial pressure of femoral artery	0.00532	ATP2A2

Supplementary Figure 11. Enrichment for System Development Functions. Enrichment analysis (hydrogel (acellular) patches compared to spheroid patches) highlighted gene expression changes, especially with genes associated with dilated cardiomyopathy.

Supplementary Material: Supplementary Discussion Points and Data Visualisation Statement

Supplementary Discussion Pertaining to Electrical Mapping:

Taken together, our electrical mapping data (**Figure 3, 5 and Suppl Figure 1**) suggests that with treatment no overall change in CV occurred (**Figure 3**) but that there may have been changes to the electrical map gradient appearances (**Figure 5**). Whilst human cardiomyocytes would not be expected to couple with underlying host (mouse) cardiomyocytes, treatments may have had an effect on host (mouse) electrical mapping profiles (**Figure 5**). **Figure 5** hints that restoration of a non-infarcted gradient pattern may have been important in mice that improved their LVEF% (especially between day 14 and 28). When the gradient effect was blunted in an individual mouse (MI+PATCH CELLS, **Figure 5J**) the 'uptick' in LVEF% between midpoint and endpoint was not observed (**Figure 5K**). Instead, the drop in LVEF% observed between baseline and midpoint (day 14) persisted to the endpoint at day 28 (**Figure 5K**). Conversely, with spheroid patch treatment there was a sharp uptick between day 14 and day 28 (**Figure 5N**) and the corresponding electrical maps (**Figure 5L-M**) showed a partial electrical recovery towards baseline. These individual mouse analyses (**Figure 5**) reflected the whole group median LVEF% progression (**Figure 2C**) where the post day 14 uptick was steepest for the spheroid group (contrast the precipitous drop in the MI group). It is possible that the ability of the heart to compensate for infarcted areas by modulating/increasing CV in non-infarcted areas contributes to improvements in function. This suggests that the success of treatment for any individual mouse may be associated with remodelling (with associated electrical activity modification) and not only raw infarct size. Of note, even a sham procedure (passing a suture underneath the LAD and tying it loosely without ligating the LAD) was associated with changes in the overall CV (**Figure 3** and **5B**) and electrical map appearances (**Figure 5C-D).** This might suggest that even with a small needle passed under the LAD and suture tied without occlusion, the surgery in-and-of itself can affect the conduction system of the murine heart. This might help to explain why sham mice had diverging LVEF% results at the day 14 midpoint and day 28 endpoint (**Figure 2A**).

Supplementary Discussion Pertaining to the Mouse Model:

Different species of mice react differently to LAD ligation(1) and mice within the same experiment have different infarct sizes and patterns, with different effects on myocardial function. It is not known how this relates to human myocardial response to coronary artery blockage. Additionally, we showed that individual mice across all our experimental groups (including sham surgery) can present different cardiac function (LVEF%) progression from baseline to midpoint to endpoint in this protocol. This could reflect intrinsic variability in the LVEF%, some variability factor intrinsic to the protocol itself (such as passing a needle and suture through heart tissue under the LAD), or variability in measurement techniques (such as mouse echocardiography in the presence of adhesions after cardiac surgery).

Another important limitation is that only mice surviving to the end of the experiment contributed to our full set of day 28 analyses. Day 28 values may be influenced by attrition bias due to some mice dying in the operative or postoperative period. Our mortality rate of 44% was exactly the same as the literature rate for non-immune suppressed C57Bl/6 mice having LAD ligation without a patch(1). The choice of male mice was based on a pilot study which determined that female mice and mice with body weight below 22g seemed to have higher mortality and abandonment rates from intubation of smaller tracheas (data not shown). We detected no difference in our protocol (or mortality rate) with immune competent C57Bl/6 mice compared to mature B and T cell deplete RAG1.Bl6 mice (data not shown). Future murine studies must choose their mouse model very carefully (ideally only using male mice with body weight over 22 g) and critical considerations include: 1) more severely immune suppressed mice such as NOD/SCID gamma are not required and so may be unethical; 2) immune

competent BALB/c mice have a reported mortality rate of only 15% with a wall-thinning dominant pattern of ventricular response to MI(1) and these are available as T-cell depleted (BALB/c-Fox1nu) allowing for acceptance of xenografts, so therefore this strain may be preferable; and 3) different mouse strains may show different macrophage responses (C57Bl/6 show easier activation to produce M1 whereas Balb/c tend towards M2 polarisation(2) and there may be tissue specific responses as well(3)) which should be evaluated carefully, especially for dedicated mechanistic studies. Overall, if carefully designed, murine studies for patch transplantation may have a place for mechanistic studies, new treatments and studies where feasibility and high numbers of repeats are important(4).

Supplementary Discussion Pertaining to Statistical Interpretations:

We purposefully chose to run conservative non-parametric, Bonferroni-corrected statistical analyses (that is, we ran hypothesis tests which are more likely to return statistically insignificant results). With our 44% mortality rate (similar to previous reports using *immune competent* C57Bl/6 mice (1)), to adequately power a two-group comparative study for cellular against spheroid patches would need ~85 mice per group (with alpha (type I error probability) of $p<0.05$). To repeat our entire study with five experimental groups and power to detect the differences we presented would require ~125 mice per group (625 in total) with a Bonferroni corrected threshold for significance ($p<0.01$). This would not be ethical to show potential LVEF% differences of ~5% (clinically insignificant). Therefore, the trends we identify herein should be evaluated in this context as a worthwhile next-best alternative. In light of our results, future studies should consider why they would *not* pre-culture their cell populations (in spheroids) before suspending them in patches. In fact, yet another interpretation of our results might be that the spheroid group showed a (Bonferroni-corrected) statistically significant difference compared to MI without treatment ($p=0.010$), whereas the cells (not in spheroid) group did not ($p=0.106$). Altogether, our nuanced results support the use of cardiac spheroids in bioinks rather than no cells or freely suspended cells but further study is warranted.

Supplementary Notes on Data Visualisation for Figures:

Brightness was adjusted for **Figure 1** (+150 using Adobe Photoshop). For histology slides (**Figure 4**, **Suppl. Figure 4 and Suppl. Figure 5**), the grey background (only) was normalised to adjacent background areas polygonal histology images were rectangularised using the Photoshop Clone tool. Images were cropped to fit with adjacent slides. No changes to the underlying data were made and no changes were made to the histological information (background only).

Supplementary Discussion References:

1. van den Borne SWM, van de Schans VAM, Strzelecka AE, Vervoort-Peters HTM, Lijnen PM, Cleutjens JPM, et al. Mouse strain determines the outcome of wound healing after myocardial infarction. Cardiovasc Res. 2009;84(2):273-82.
2. Orecchioni M, Ghosheh Y, Pramod AB, Ley K. Macrophage polarization: different gene signatures in M1(LPS+) vs. classically and M2(LPS–) vs. alternatively activated macrophages. Front Immunol. 2019;10(1084).
3. Bleul T, Zhuang X, Hildebrand A, Lange C, Böhringer D, Schlunck G, et al. Different innate immune responses in BALB/c and C57BL/6 strains following corneal transplantation. Journal of Innate Immunity. 2021;13(1):49-59.
4. Roche CD, Gentile C. Transplantation of a 3D bioprinted patch in a murine model of myocardial infarction. J Vis Exp. 2020:e61675.

2.5 – Closing remarks to Part 2

The three articles which make up Part 2 have successfully addressed Aim 1 (optimisation of patches) and Aim 2 (evaluation of functional and structural results). Taken together, these chapters represent a robust method to generate heart patches *in vitro*, transplant them in a surgical model in mice and then evaluate their effects *in vivo*.

Chapter 2.2 represents a detailed process of optimisation of these patches. Many new insights are presented and several questions for the field are answered, with perhaps the most relevant being the optimum moment to transplant patches before they start to disintegrate in culture. We found that week 2 was optimal, after allowing a short period for cells to organise and start beating but not long enough that patches lose their integrity and become unsuitable. In keeping with the surgical flavour of our approach, we reported useful, feasible outcome measures (as opposed to less accessible numerical ones). For example, we simply defined the moment of disintegration was the moment that a surgeon could not use the patch for transplantation. For printability, we used a simple grid pattern and assessed known printability outcome measures such as shape fidelity simply by how many of the squares were preserved in the "finished product" of the patches once they had been bioprinted and cultured. For patch contractility, we recorded when patches started to beat under video light microscopy, which is an accessible and reproducible method of determining that patches are contractile. Also, the negative findings of this chapter are useful, specifically that there was no difference in 3D bioprinting system used, even comparing current market-leading 3D bioprinting systems to an old custom-made model. We found that specialised hydrogel supplements such as fibroblast-derived extracellular matrix hydrogel (AlloECM) could not be added directly to alginate/gelatin (AlgGel) patches and that mixing them caused rapid and complete disintegration of patches. Arguably the most eye-catching finding of this chapter (2.2) is the 3D rendering video reconstruction of endothelial cells in networks which had "self-organised" into tubes over 28 days within patches. Our video "tour" of one of these tubes showed a lumen-like space. This provides evidence that allowing self-organisation of cells might be an appropriate strategy (rather than more controlling strategies to place cells where the user wants them).

Since patches would not be optimised unless they can be shown to work with their surgical transplantation protocol, we published the video method for this in full (2.3). This was the first time this method has been published with the complete methodological details with the intention that it be made fully reproducible for others. The mouse MI model we published has significant advantages, for instance (compared to large animal models) it allows for greater feasibility, generally higher numbers of repeats, lower cost, less physical space, initial testing of untested biomaterials or patches with optimal control groups, testing of expensive patches which need to be small and potentially the use of genetically modified mice. This video method publication has the potential to allow for extensive mechanism-focused studies, which is critical before advancing to large animal and human trials.

Our *in vivo* study (2.4) is the key results chapter of this thesis and the sole chapter addressing Aim 2 (the *in vivo* effect of patches on functional and structural outcomes). We purposefully designed this experiment to take full advantage of the mouse model, specifically with our relatively extensive analyses of results (sequential cardiac functional readings, electrical mapping data, histology, flow cytometry and mRNA transcriptomic analyses). Whilst obtaining a full spectrum of outcome measures was resource intensive, the mouse model's relative feasibility permitted for this. We were also able

to select RAG1 mice with no mature B or T cells, which effectively rules out those cells from being involved in our results. Limitations included a high mortality rate of 44% (which introduces a survivor bias) and high variability inherent to the model (as shown by variability in results for the sham group – a significant finding in-and-of-itself). We also had to trade off the need to take multiple axial heart slices (distal to the LAD ligation) for multiple analysis with the risk of missing of infarct on histological slices. Due to taking multiple heart tissue slices (mRNA at the apex, flow cytometry at the mid-LV and histology taken last nearest to the ligation), we probably missed some infarct sizes on histology, shown especially in the MI+PATCH CELLS experimental group (Chapter 2.4, Figure 4). Nonetheless, our results are strong, with a return to baseline leap in cardiac function for our treatment groups (MI+PATCH SPHEROIDS). Our negative treatment control (MI+PATCH) had no cells and even with this patch there was an improvement in LVEF%, suggesting that the cells did not contribute to the whole effect. Stikingly, our mRNA analysis showed that the spheroid group returned its transcriptomic profile to one resembling the sham (non-infarcted mice). Synthesising these two results, it is tempting to speculate that the hydrogel (foreign material) induced inflammation modulation and his gave a partial response in terms of improved LVEF%. To reach the full protective effect (the rest of the improvement in LVEF% seen with CELLS or SPHEOIDS group mice), it seems as if gene expression changes are required. If true, this would represent a very significant finding. A dedicated future study should seek to answer the question of whether host inflammation modulation boost cardiac function “half-way” and then genetic modulation boosts it all the way “back to baseline”.

PART 3 – ROBOTIC MINIMALLY INVASIVE PATCH TRANSPLANTATION INSTRUMENTS

3.1 – Introduction and relevance to Part 3

The inventions which make up Part 3 of this thesis were developed in response to the finding from our preparatory literature reviews (1.2 and 1.3) that previous studies had all worked towards a model of open surgical transplantation. If patch-based myocardial repair is to become a fully translatable technology for the befit of heart failure patients, it may need to be deliverable by minimally invasive and/or robotic surgery in future. In 2021, other research groups published studies reporting minimally invasive methods to transplant patches to the heart surface for the first time (Wang et al., 2021; Zhu et al., 2021). Concurrently, our group was the first to pioneer *robotic* minimally invasive approaches (Chapter 3.2 and 3.3). In our multidisciplinary team bringing together cardiac surgery expertise, bioengineering knowledge and mechanical and mechatronic engineering, we invented surgical instruments for this purpose.

Our first chapter (3.2) presents the "world first" brief report which contains our preliminary work from inception of the original idea to development of our first instrument design and initial part prototyping for that design. The instrument is a complex robotic "hand" device designed to connect to a robotic control unit (arm). It is capable of extensive manipulation with multiple degrees of freedom (as shown by our *in silico* video demonstration (**Chapter 3.2, Suppl. Video 1**). Our prototyping attempt resulted in many learning points which were taken forward to the next phase, not least that the instrument would need to be enlarged and simplified. Nonetheless, the brief report itself is noteworthy in that it became the first time anyone had published even the approach let alone a design and initial prototyping to start moving towards proof-of-concept testing.

The proof-of-concept article (3.3) took the work presented in Chapter 3.2 forwards to the next stage. Designs were much more extensively developed, with three instruments designed in detail and then one of these chosen for full prototyping and use in a pig cadaver model of surgery. The work is early stage, and we reported it in the style of the initial attempt for the whole approach (including our failed first attempt (Chapter 3.3, Figure 8) and our successful second attempt (Chapter 3.3, Figure 9).

Both of these articles/chapters successfully addressed Aim 3 of this thesis (to invent robotic minimally invasive surgical instruments to transplant patches to the heart). They represent an original contribution of innovative work which was a direct answer to a question raised in the literature reviews which form the Introduction (Part 1) of this thesis.

3.2 – A world first surgical instrument for minimally invasive robotically-enabled transplantation of heart patches for myocardial regeneration: a brief research report

Summary:

This brief research report article was published in Frontiers in Surgery. It represents the initial stage of development for robotic minimally invasive surgical instruments to transplant patches similar to those detailed in Part 2 of this thesis. This project developed out of the realisation that all published approaches to epicardial patch transplantation involved traditional open surgical incisions such as median sternotomies. This could limit the translatability of patches since by the time patches are ready for clinical use, they may need to be transplanted by minimally invasive robotic approaches. In the same year (2021) as we published our work on this, others published the first reports of minimally invasive (non-robotic) methods of patch transplantation. Our brief research report and the more extensive proof-of-concept testing of the following chapter (3.2) represent the first time anyone has presented robotic minimally invasive patch transplantation.

frontiers in Surgery

BRIEF RESEARCH REPORT
published: 06 October 2021
doi: 10.3389/fsurg.2021.653328

A World-First Surgical Instrument for Minimally Invasive Robotically-Enabled Transplantation of Heart Patches for Myocardial Regeneration: A Brief Research Report

Christopher David Roche[1,2,3*†], *Yiran Zhou*[4†], *Liang Zhao*[4‡] *and Carmine Gentile*[1,2‡]

[1] Northern Clinical School of Medicine, University of Sydney, Sydney, NSW, Australia, [2] School of Biomedical Engineering, Faculty of Engineering and IT, University of Technology Sydney, Sydney, NSW, Australia, [3] Department of Cardiothoracic Surgery, University Hospital of Wales, Cardiff, United Kingdom, [4] School of Mechanical and Mechatronic Engineering, Faculty of Engineering and IT, University of Technology Sydney, Sydney, NSW, Australia

OPEN ACCESS

Edited by:
Zhilian Yue,
University of Wollongong, Australia

Reviewed by:
Esko Kankuri,
University of Helsinki, Finland
ZQ Zhang,
University of Leeds, United Kingdom

***Correspondence:**
Christopher David Roche
croche@doctors.org.uk

†*These authors share first authorship*

‡*These authors share last authorship*

Specialty section:
This article was submitted to Visceral Surgery, a section of the journal Frontiers in Surgery

Received: *14 January 2021*
Accepted: *02 September 2021*
Published: *06 October 2021*

Citation:
Roche CD, Zhou Y, Zhao L and Gentile C (2021) A World-First Surgical Instrument for Minimally Invasive Robotically-Enabled Transplantation of Heart Patches for Myocardial Regeneration: A Brief Research Report. Front. Surg. 8:653328. doi: 10.3389/fsurg.2021.653328

Background: Patch-based approaches to regenerating damaged myocardium include epicardial surgical transplantation of heart patches. By the time this therapy is ready for widespread clinical use, it may be important that patches can be delivered via minimally invasive and robotic surgical approaches. This brief research report describes a world-first minimally invasive patch transplantation surgical device design enabled for human operation, master-slave, and fully automated robotic control.

Method: Over a 12-month period (2019–20) in our multidisciplinary team we designed a surgical instrument to transplant heart patches to the epicardial surface. The device was designed for use via uni-portal or multi-portal Video-Assisted Thorascopic Surgery (VATS). For preliminary feasibility and sizing, we used a 3D printer to produce parts of a flexible resin model from a computer-aided design (CAD) software platform in preparation for more robust high-resolution metal manufacturing.

Results: The instrument was designed as a sheath containing foldable arms, <2 cm in diameter when infolded to fit minimally invasive thoracic ports. The total length was 35 cm. When the arms were projected from the sheath, three moveable mechanical arms at the distal end were designed to hold a patch. Features included: a rotational head allowing for the arms to be angled in real time, a surface with micro-attachment points for patches and a releasing mechanism to release the patch.

Conclusion: This brief research report represents a first step on a potential pathway towards minimally invasive robotic epicardial patch transplantation. For full feasibility testing, future proof-of-concept studies, and efficacy trials will be needed.

Keywords: instrumentation, regeneration, thorascopic surgery, myocardial patch, automation, keyhole, chest

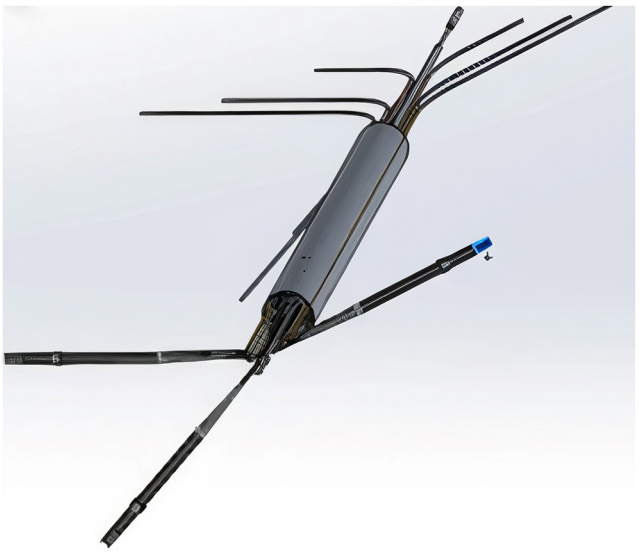

GRAPHICAL ABSTRACT |

INTRODUCTION

Since the first reports of robotic minimally invasive cardiac surgery (1), there has been increasing attention given to the role of minimally invasive robotics in cardiothoracic surgery (2–6). Meanwhile, tissue engineers have been making gains toward regenerating the myocardium (7–9). The first human trials of patches containing biomaterials/cells applied to the epicardial surface to regenerate the heart have been reported with promising results (10–14). Moreover, increasingly accessible techniques such as 3D bioprinting (one approach to generating heart tissue patches) promise scalability, reproducibility, and highly refined control over the characteristics of the patch to be grafted (7). However, many approaches to regenerate the myocardium surgically using patches applied to the epicardial surface have worked toward a model of open surgery via median sternotomy (8). There is an unanswered but pressing question whether surgical patch-based repair of the heart will need to be delivered by minimally invasive and/or robotic surgery by the time it reaches widespread clinical use (7). Additionally, for heart failure patients who may not be fit for a heart transplant or major surgery but who may tolerate a less invasive keyhole procedure (15), this solution may open up a therapeutic avenue for them.

Our team therefore conceptualised and designed a novel surgical instrument to deliver heart tissue patches to the epicardium. Our multidisciplinary team included a cardiothoracic surgeon, a bioengineer and two specialists in robotics, mechanical engineering, and mechatronics. To our knowledge, the early-stage design we present is a world-first with no similar design existing. This descriptive brief research report represents the initial step on a potentially significant pathway to pivot the field away from its focus on traditional open surgery.

METHOD

Design Process, Objectives, Reasoning

The design process was initiated with several discussions amongst the team to determine the objectives, requirements, and feasibility of the idea. An initial outline of the design was sketched with attention to the ergonomics at human surgery, the size and material requirements for thoracic insertion and manipulation of the instrument within the chest cavity, the shape requirements to ensure suitability for human cardiothoracic anatomy, the mechanism to allow for an operator to manoeuvre the instrument using handles outside the chest cavity at the proximal (external) end of the instrument and the ability for the device to be controlled in future by both master-slave robotics and fully automated robotics.

Using SOLIDWORKS® (Dassault Systèmes SOLIDWORKS Corp, Waltham, MA, USA) computer aided design (CAD) software, the instrument blueprint was created and revised several times to ensure it was optimised. At this stage, attention was given to the points of attachment for patches onto the instrument and the details of how the patch would fold into the instrument when retracted and then be spread out for deployment when expanded (without damaging the patch). Another challenge was the releasing mechanism for the patch to release it from the instrument. It was decided that tiny attachment nodules/hooks would be placed at the distal ends of the manoeuvrable arms and at the apex of the pyramid created by the three arms converging. When the arms are expanded (outfolded) this stretches out the patch between the metal arms. This has the effect that when outstretched the patch itself would move away from the apex and fold out to form the base of a pyramid.

The patches will be made from alginate 4%/gelatin 8% in cell culture medium, which is a hydrogel that becomes fluid at temperatures over ∼28°C and is more solid at lower temperatures. It can be crosslinked ionically by adding calcium chloride (2% w/v in phosphate buffered saline) which increases the strength of the material. A similar hydrogel with a modified molecular structure, gelatin methacryloyl (GelMA), can be used in a similar way to alginate/gelatin but is more robust when it is crosslinked which is done by UV light photocuring. Therefore, we created the instrument design to include areas for attachment nodules/hooks which would be attached to areas within the patch containing small rings of GelMA at the corners and the centre. These reinforced patch ring-corners would be attached to the arms distally. In the folded position, the patch centre will be similarly attached to the instrument platform where the proximal ends of the three arms converge (the apex of the pyramid formed by the arms). When opening the arms (pitch rotational movement) this will pull the patch away from the platform where the proximal ends of the arms converge as it unfolds and expands to become the outstretched base of the pyramid. Next, to release the three patch corners from the apex, the instrument arms can be moved laterally (yaw rotational movement). To ensure that release happens first at the apex/central connection the strength of the GelMA ring will be modified by using fewer layers so that this connection releases first (before the GelMA ring connection to the distal tips of the arms). In case of failure to release by

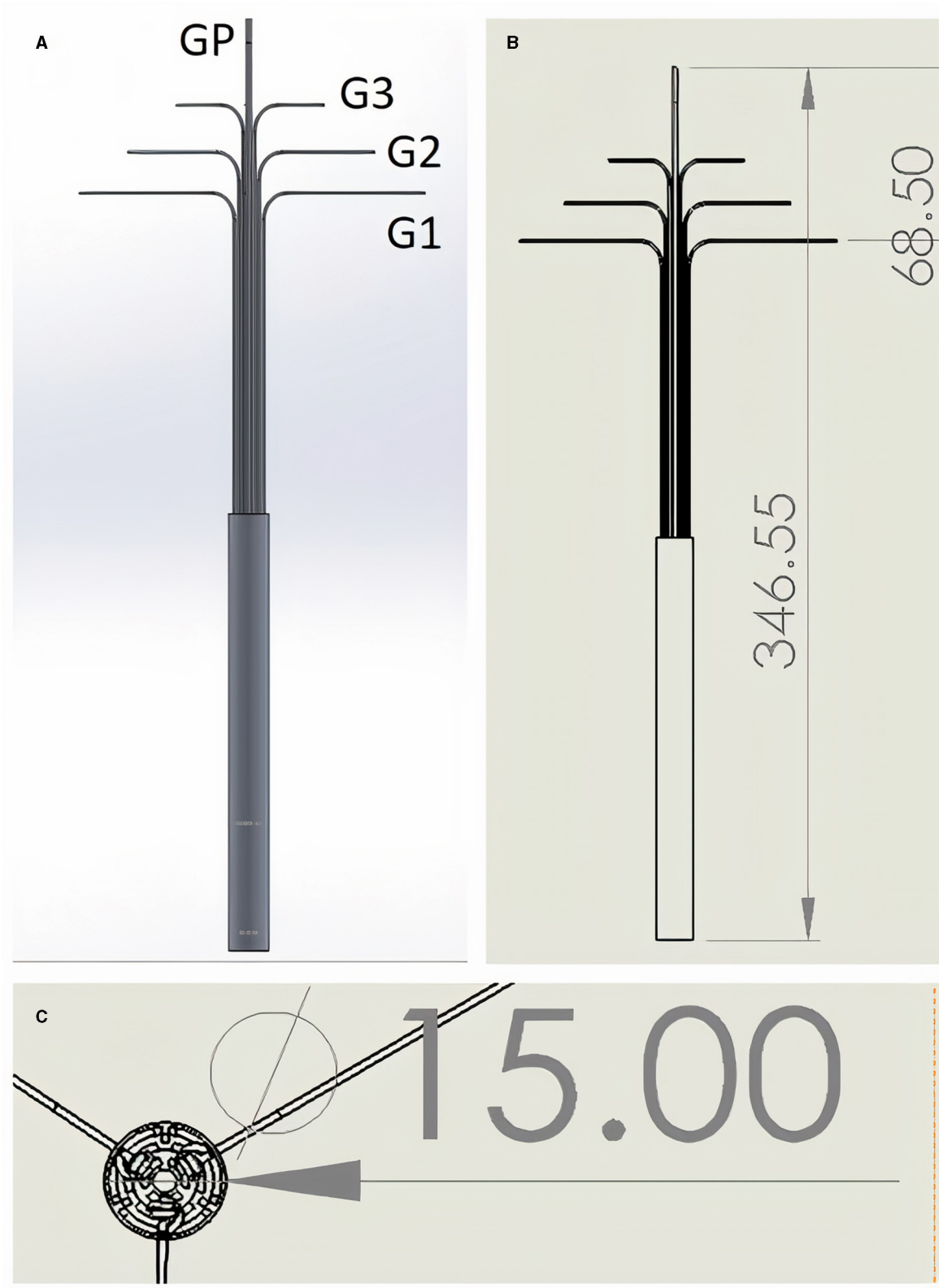

FIGURE 1 | (A,B) Lateral view. One single Grip (GP) controls forward protrusion and backwards retraction of the instrument. Grips G1–G3 are triplicate (only two of each are visible in the 2D lateral view images shown), and control each of the three distal arms to which they are attached (distal arms not visible - infolded and covered by sheath). G3 Grips control the curvature of the patch, G2 the rotation angle of the arm, and G1 the deployment angle of the arm. **(C)** "Top down" view showing triplicate arrangement of Grips when in line with each other and opened with 120 degree angles between each set of three Grips. Grips exit the cylindrical instrument body which has diameter of 15 mm. All measurements in mm. See **Supplementary Video 1** for dynamic demonstration *in silico*.

this mechanism, the platforms with the hook/nodule attachments can be moved in a sliding movement distally away from the instrument body, theoretically releasing them by breaking the GelMA rings.

The head has a rotational mechanism (role rotational movement) which allows for the rotation of the patch through 360 degrees. One arm is able to be made shorter than the other two during patch deployment. This means that by opening that arm past 90 degrees to the main instrument body whilst shortening it, the patch should be able to open and face any lateral direction (similar to the triangle that can be made with the extended index and middle finger to the thumb in opposition). This gives the instrument three degrees of rotational movement in addition to the three degrees of translational movement in the X, Y, and Z axis which are achieved by movements at the entry into the chest (similar to moving a pencil pinched lightly between the thumb and index finger). Additional to these six degrees of freedom, each arm is capable of pitch and yaw rotation individually. The shortenable arm has the additional benefit of being openable in a confined space, for example, if facing the surface of the heart when opening, so that its excursionary movement can be completed without damaging surrounding structures. Overall, these movements will allow for the patch to be expanded in the hemithorax and then rotated to face the surface of the heart at the correct angle.

One surgical approach for the operation of this instrument is via standard left-sided anterolateral multiportal video-assisted thorascopic surgery (VATS)—similar to a left lower lobectomy approach but with the left lung deflated via endobronchial intubation and single lung ventilation of the right lung. The pericardium would need to be partly opened to gain access to the epicardial surface. In particular, for a chronic ischaemic cardiomyopathy heart failure patient or after myocardial infarction (MI), the target area may be the anterolateral surface of the heart over the left ventricle. With the rotational head and the releasing mechanism, it should be possible to manoeuvre the patch and apply it to the epicardium on most surfaces reachable without moving the heart: a minimally invasive VATS transplantation of a regenerative cardiac patch.

Following these discussions and revisions aimed at optimising the instrument design we 3D printed a version of the instrument to assess for size and identify learning points. This "sizing and learning" print was in preparation for the full metal prototyping which will use 17-4 Ph Stainless Steel (SAE Type 630 stainless steel—hardened stainless steel containing ∼15% chromium, 5% nickel, 5% copper).

RESULTS

Early-Stage Design Outcomes

The device has nine Grips plus one push-out Grip (**Figure 1**, **Supplementary Video 1**). Each arm has three Grips (**Figure 1A**, Labels G1, G2, and G3). The top Grip (G3) controls the attachment platforms and therefore the curvature of the patch (it also acts as a releasing mechanism if attachment platforms are moved beyond the maximal boundary of the outfolded patch), the middle Grip (G2) controls the rotation angle of the arm, and the bottom Grip (G1) controls the deployment angle of the arm. The push out Grip (GP) protracts or retracts the arms from their sheath. **Supplementary Figure 1** shows a frontal and trimetric view of the mechanism with the sheath removed.

The designed length of the instrument was 35 cm and cylinder diameter was 1.5 cm (**Figures 1B,C**). Each arm was 60 mm, thus the maximum size of a triangular outfolded patch would be ∼18 cm^2. The tips of each arm are 11.2 cm apart while opened at 90 degrees to the body of the instrument. The smallest parts in our instrument were the joints which are cylindrical type joins (which act like screws connecting two linked pieces) and these were 1 mm diameter and 1 mm height.

Special features of the instrument included a space between the arms when infolded where the folded patch could be stored prior to deployment (**Figure 2**). The patch could therefore be inserted into the chest within the mechanism (and covered by the outer sheath) without damaging it during insertion. Control over each of the three arms was achieved by three separate mechanisms connecting the arms to the Grips at the proximal end of the device (**Supplementary Figure 2**).

The arms were designed so that they could be individually rotated, including when the arms are folded out from their closed position. The region conveying rotationary control is shown in **Supplementary Figure 3**. In **Supplementary Figure 3B** the proximal (operator's end) region where the Grips converge is shown.

Along each arm the design includes a moveable attachment platform which can be controlled using Grip number 3 (control pathway highlighted in **Supplementary Figure 2A**). **Supplementary Video 1** shows the releasing mechanism as it moves along one of the three arms. This movement from the distal aspect of an arm to the proximal aspect allows for the attachment platforms to be moved, pulling them away from the patch connections and releasing the patch. These patch connecting platforms are shown in more detail in **Figure 3**.

The attachment platforms will have small hooks (not shown in the figure) where they will be able to attach to rings of a semi-robust crosslinked hydrogel (GelMA) at the corners of the patch. If the releasing mechanism fails to move the hook from the patch and release that corner, the arm could be rotated using the rotationary mechanism shown in **Supplementary Figure 3** to pull the connection away from the patch. To reduce the risk of injury to surrounding structures, the edges of the design are curved and smooth (**Figure 4**).

3D Printing of Sizing and Learning Resin Prototype

Some of the parameters for the 3D printer settings for the sizing and learning prototype are shown in **Supplementary Figure 4**. We used a Stratasys J750^{TM} polyjet multi-material 3D printer (Stratasys, Eden Prairie, MN, USA). The materials used to print the test (sizing and learning) prototype parts were VeroVivid (a translucent colour material) and Agilus (an elastomeric polymer) which cost under £10 GBP ($14 USD). The total cost (excluding hardware purchase) of the sizing and learning print was <£60

FIGURE 2 | (A,B) Close-up angled view **(A)** and complete lateral view **(B)** of the distal end of the instrument (the patient end where the patch would be enclosed). Movements of this compartment are controlled at the other (operator's) end of the instrument by the connected Grips shown in **Figure 1**.

GBP ($83 USD). A comparison of the resin size to the computer-aided design blueprint is shown in **Figure 4**. The printed product underwent a chemical bath (in a solvent named Opteon SF-79, which is used to dissolve the support material for the printed parts) and during this final phase some of the tiny cylinder joints (6 out of 13) were lost.

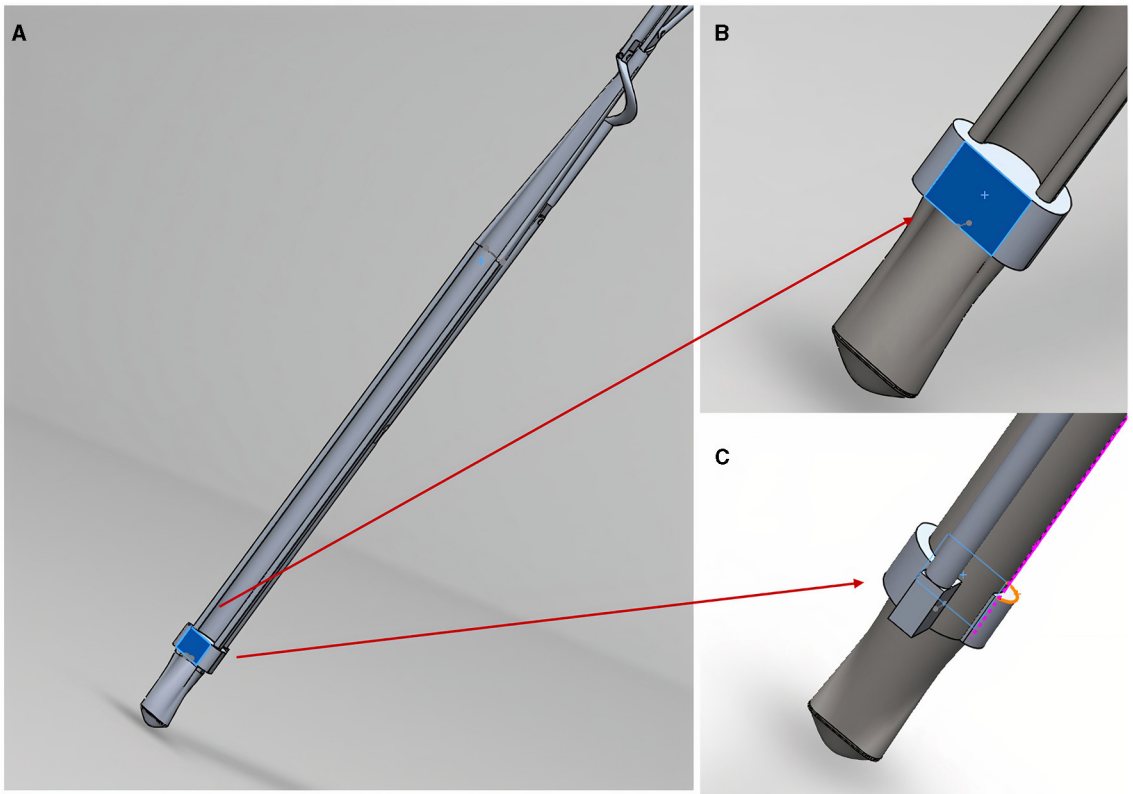

FIGURE 3 | The patch releasing mechanism in close-up. **(A)** Shows an arm patch attachment point/platform (highlighted in blue); **(B)** shows anterior view close-up of the platform where a hook/nodule (not shown) will attach patch corners; **(C)** shows a posterior view of the platform shown in **(B)**.

DISCUSSION

Brief Research Report key Considerations and Unanswered Questions

Our novel surgical instrument design is aimed at minimally invasive approaches to transplant patches for myocardial regeneration and is enabled for future robotic control of the device. Whilst it has not been designed to fit with current commercially available cardiothoracic surgical robots, it has been designed to be ready for robotic control, where the instrument itself would be attached as a forearm to a robotic arm. This was based on the capabilities in our department to build a full robotic arm and the instrument could be used for master-slave or full automation. It is important that any new instrument design is enabled for compatibility to these envisaged future robotic controls.

The sizing and learning resin 3D print gave several insights which will be invaluable for the full prototyping phase from stainless steel. Firstly, it showed us that a major challenge is going to be accounting for the manufacturing machine error with such small parts (our smallest components are 1 mm diameter × 1 mm height cylinder joints). The printer we used has a high resolution (horizontal build layers down to 14 μm) but there is also print error margin of ±150–200 μm (up to 1% of the diameter of our instrument and 20% of our 1 mm cylinder joints). These valuable learning points taught us that the next phase will likely require both a slight enlarging of the instrument and also the use of a very low error manufacturing technique for the stainless steel prototype. Furthermore, each part in the design is a perfect fit and therefore allowed no space for collision volume (the distance away from the molecular centre which may come into contact with adjacent parts). The metal print in future will require micro-adjustments across every part of the design to add ±100 μm space around each part so that there is room for manufacturing machine error in the generation of the stainless steel prototype.

Another consideration is that following the initial fabrication of the instrument it will have to be immersed in the same chemical bath used for the resin sizing and learning print (Opteon SF-79) during which time our tiny joints can still be lost. In fact, during the resin learning print 6 of our 13 joints were lost during the chemical bath. Therefore, we may need to include over 20, adding in extra joints in anticipation that some will be lost during the manufacturing process. Future trials by our group will determine whether these issues can be minimised by increasing the size of the instrument without removing the clinical utility.

We have envisaged the instrument being used for VATS approaches and it should be highly versatile so it can be used with multiple surgical approaches via uniportal (one large "keyhole" in the chest for all instruments) or multiportal (several keyhole incisions) VATS—for example with a left anterolateral approach.

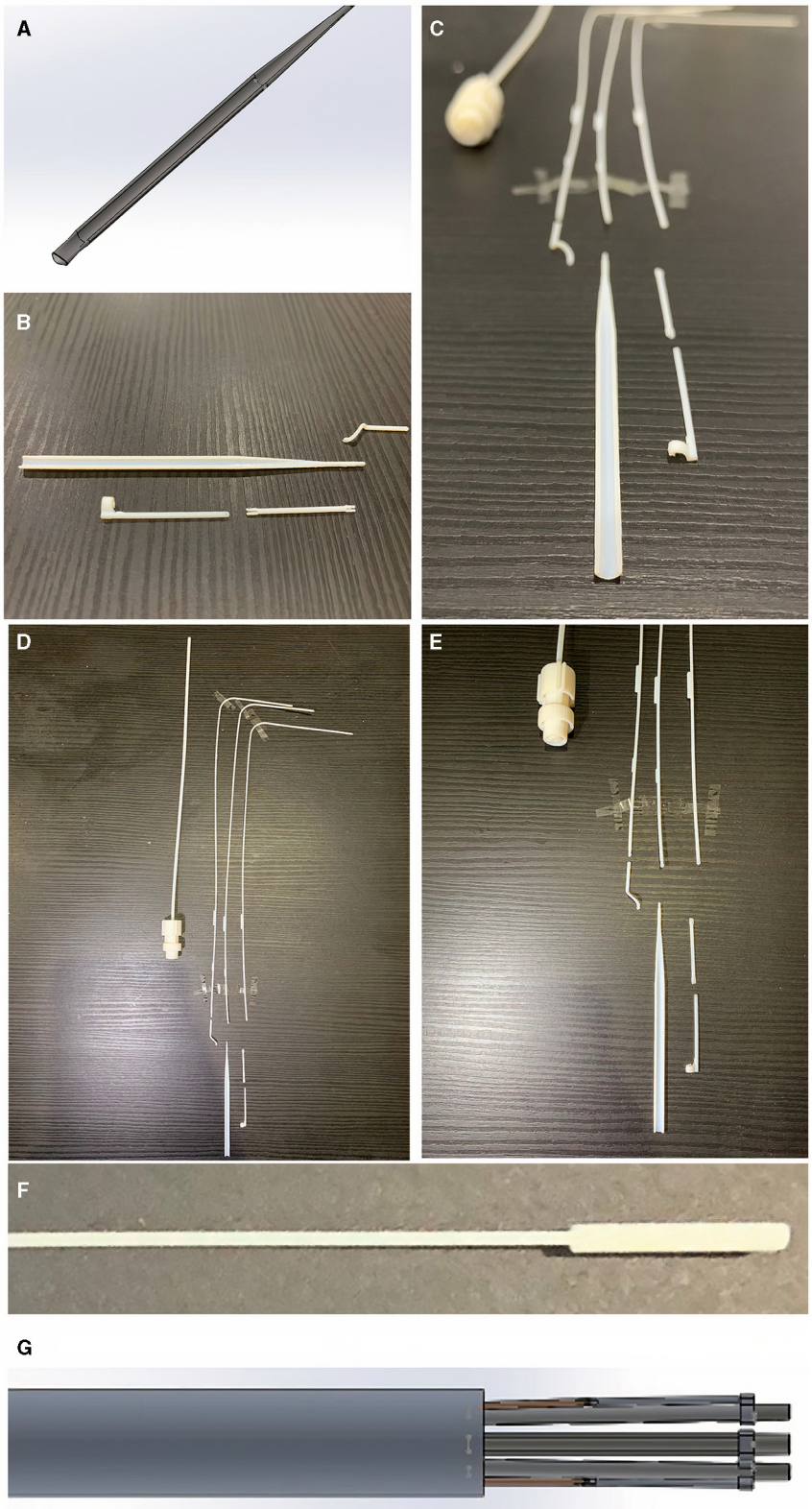

FIGURE 4 | Curved edges of the arm to reduce risk of injury to surrounding structures inside the chest. **(A)** Shows the CAD blueprint for the main component of one of the arms. The photographs in **(B,C)** show the same curved edged arm with surrounding component parts after the sizing and learning resin print (VeroVivid and Agilus). These parts were reproduced with a high degree of accuracy to the blueprint and the surrounding component parts fitted with the main body of the arm. This

(Continued)

FIGURE 4 | suggests these components will be accurately fabricated in the subsequent stainless steel prototype. Photographs in **(D,E)** show component parts outcome of Agilus/VeroVivid resin sizing and learning print. Despite inherent printer error margin, sizes were accurate to the CAD blueprint and appropriate for surgical use. There were limitations to the resolution printable by this method shown by the fusion of resin material at the distal tip in the photograph **(F)** compared to the input CAD image shown in **(G)**. This has shown that subsequent prototyping will require a manufacturing method capable of retaining the detail of small parts within the device.

The exact approach would depend on the target area of the heart (for instance we would probably want to deploy the patch over a specific infarcted or failing area of the left ventricle). This will likely need a wide space and multiple ports to get a good view and manoeuvre into the best position.

The patch itself (see **Supplementary Video 1**) can be customised in many ways with different biomaterials to control the viscosity of the patch and also for different cell types within the patch (16). Many different cells have been tried by researchers in this field, often derived from stem cells (7). Our approach might be able to treat heart failure for patients who would otherwise not be eligible for a transplant (in a less invasive standalone procedure to patch the myocardium rather than replace the whole heart). There are many complex considerations for this, including whether one could generate a patch of patient-specific heart tissue from stem cells reprogrammed from the patient's own skin cells and transplant that (7). Importantly, all approaches to myocardial regeneration with a patch have so far have imagined an open surgical transplantation method which may actually preclude this treatment in many of the heart failure patients it is ultimately intended to benefit.

The therapeutic approach will be different for the acute vs. chronic phase of ischaemic cardiomyopathy and/or MI and initially this instrument has been designed with a view to being applicable in a non-acute situation as a standalone procedure. In the acute phase it may not even be required to transplant cells but just putting a patch as an adjunct to regular treatment which stimulates macrophages and other inflammatory responses may be beneficial for remodelling and cardiac function after MI (17). For this instrument, it is clinically most likely to be useful for chronic heart failure caused by ischaemia or MI. There are many open questions and a large amount of research is focused on regenerating the myocardium (7, 8). The unique selling point of this instrument is that no one has yet presented a solution to the question of how to transplant patches without open surgery. By the time regenerative patches for the myocardium are ready for clinical use they may need to be able to be transplanted by minimally invasive and/or robotic approaches. If patch transplant were to be used as an adjunct in a patient already undergoing another procedure, a minimally invasive method would need to exist because the primary procedure may not be via open surgery. As a standalone treatment for high-risk patients with heart failure who cannot have open surgery, it may be beneficial for them if this can be done by a less invasive approach.

This brief research report represents the first time this approach has been presented (without restriction for anyone to build upon). Whilst it has been developed for cardiac applications, it could even be co-opted for other applications (e.g. abdominopelvic) where diverse minimally invasive robotic approaches are also being developed (5, 6). Its main limitation is that the descriptive work herein is at an early stage. It is likely that future instrument designs will have to be larger, perhaps more fitting for a 5–6 cm incision rather than a 2 cm one. This would also have the potential benefit of bypassing the major challenge of how to infold a patch then outfold it like a net (without crushing it). Specifically, a 5–6 cm diameter instrument could potentially accommodate a non-folded patch large enough to be used without repeated application of small patches. Future studies will be needed to optimise designs, fully prototype them and then assess the actual performance of any prototype in proof-of-concept surgery followed by full *ex-vivo* (cadaver) and *in-vivo* trials. Efficacy will need to be evaluated in terms of transplantation success over repeated applications (with full measurement of parameters such as time to delivery, deployment accuracy in a non-beating and beating heart, patch size, covered epicardial surface area and a full range of quantitative and qualitative analyses—all compared to relevant controls). Then trials will be needed for a functional demonstration of a clinically and statistically significant improvement in cardiac function (including non-inferiority against the alternative approach of traditional open surgery). Whilst this brief report article has focused on a surgical instrument design, significant work will also be needed to show that the patch matrix we propose—alginate 4%/gelatin 8% patches ± cells based on our previous optimisation for cardiac applications (9, 16, 18)—is superior to reference patch materials. Translating these technologies is a lengthy process, which is part of the point: it should happen in parallel to the advancements currently underway in the field of myocardial regeneration, or the field risks unveiling a successful new treatment to a world that might have moved away from traditional open surgery (2, 19), limiting how to actually deliver it.

CONCLUSION

Over 12 months our multidisciplinary team has invented a design for a novel surgical instrument which is at the leading edge of innovation in this field. Findings from our sizing and learning resin print of this instrument have prepared the way for the stainless-steel prototype to be manufactured. This is a world-first achievement which may alter the direction of research for surgical transplantation of patches for myocardial regeneration. This brief research report presents the first step on this pathway, for which further trials will be needed.

DATA AVAILABILITY STATEMENT

The original contributions presented in the study are included in the article/**Supplementary Material**, further inquiries can be directed to the corresponding author/s.

AUTHOR CONTRIBUTIONS

YZ: conceptualization, data curation, formal analysis, investigation, methodology, resources, software, validation, visualization, and writing—review and editing. CR: conceptualisation, data curation, formal analysis, funding acquisition, investigation, methodology, project administration, supervision, validation, writing—original draught, and writing—review and editing. CG and LZ: conceptualisation, data curation, funding acquisition, methodology, project administration, supervision, and writing—review and editing. All authors contributed to the article and approved the submitted version.

FUNDING

CR was supported by a Sir John Loewenthal Scholarship 2019 (University of Sydney), the Le Gros Legacy Fund New Zealand [PhD012019] and a Heart Research Australia Scholarship [PhD2019-02]. CG was supported by a University of Sydney Kick-Start Grant, University of Sydney Chancellor's Doctoral Incentive Programme Grant, a Sydney Medical School Foundation Cardiothoracic Surgery Research Grant, UTS Seed Funding and the Catholic Archdiocese of Sydney Grant for Adult Stem Cell Research (2019).

SUPPLEMENTARY MATERIAL

The Supplementary Material for this article can be found online at: https://www.frontiersin.org/articles/10.3389/fsurg.2021.653328/full#supplementary-material

Supplementary Figure 1 | The instrument with the sheath covering the distal arms removed. Frontal **(A)** and trimetric **(B)** views show the instrument with arms in the infolded position.

Supplementary Figure 2 | Control pathways linking the operator's end to the distal arms. **(A–C)** Highlighted views of the three Grips controlling the distal arms.

Supplementary Figure 3 | Mechanism allowing for adjustment of the rotational angle of the arms. Infolded arms **(A)** can be outfolded to open position and rotated individually by the grips shown in **(B)**. View shown in **(A)** is the distal (patient's end) and **(B)** shows a "top down" view of the proximal (operator's end) of the instrument (looking down onto the Grips).

Supplementary Figure 4 | 3D printing parameters for the resin sizing and learning prototyping of individual parts.

Supplementary Video 1 | Video walkthrough of patch delivery device, including background and mechanistic demonstration from the computer-aided design (CAD).

REFERENCES

1. LaPietra A, Grossi EA, Derivaux CC, Applebaum RM, Hanjis CD, Ribakove GH, et al. Robotic-assisted instruments enhance minimally invasive mitral valve surgery. *Ann Thoracic Surg.* (2000) 70:835–8. doi: 10.1016/S0003-4975(00)01610-6
2. Torregrossa G, Balkhy HH. The role of robotic totally endoscopic coronary artery bypass in the future of coronary artery revascularization. *Eur J Cardiothorac Surg.* (2020) 58:217–20. doi: 10.1093/ejcts/ezaa104
3. Güllü AÜ, Senay S, Ersin E, Demirhisar Ö, Kocyigit M, Alhan C. Feasibility of robotic-assisted atrial septal defect repair in a 6-year-old patient. *Int J Med Robot.* (2021) 17:e2185. doi: 10.1002/rcs.2185
4. McBride K, Steffens D, Stanislaus C, Solomon M, Anderson T, Thanigasalam R, et al. Detailed cost of robotic-assisted surgery in the Australian public health sector: from implementation to a multi-specialty caseload. *BMC Health Serv Res.* (2021) 21:108. doi: 10.1186/s12913-021-06105-z
5. Bai W, Cao Q, Wang P, Chen P, Leng C, Pan T. Modular design of a teleoperated robotic control system for laparoscopic minimally invasive surgery based on ROS and RT-Middleware. *Ind Rob.* (2017) 44:596–608. doi: 10.1108/IR-12-2016-0351
6. Zhou X, Zhang H, Feng M, Zhao J, Fu Y. New remote centre of motion mechanism for robot-assisted minimally invasive surgery. *Biomed Eng Online.* (2018) 17:170. doi: 10.1186/s12938-018-0601-6
7. Roche CD, Brereton RJL, Ashton AW, Jackson C, Gentile C. Current challenges in three-dimensional bioprinting heart tissues for cardiac surgery. *Eur J Cardiothorac Surg.* (2020) 58:500–10. doi: 10.1093/ejcts/ezaa093
8. Wang H, Roche CD, Gentile C. Omentum support for cardiac regeneration in ischaemic cardiomyopathy models: a systematic scoping review. *Eur J Cardiothorac Surg.* (2020) 58:1118–29. doi: 10.1093/ejcts/ezaa205
9. Roche CD, Gentile C. Transplantation of a 3D bioprinted patch in a murine model of myocardial infarction. *J Vis Exp.* (2020) e61675. doi: 10.3791/61675
10. Menasché P, Vanneaux V, Hagege A, Bel A, Cholley B, Cacciapuoti I, et al. Human embryonic stem cell-derived cardiac progenitors for severe heart failure treatment: first clinical case report. *Eur Heart J.* (2015) 36:2011–7. doi: 10.1093/eurheartj/ehv189
11. Menasché P, Vanneaux V, Hagege A, Bel A, Cholley B, Parouchev A, et al. Transplantation of human embryonic stem cell-derived cardiovascular progenitors for severe ischemic left ventricular dysfunction. *J Am Coll Cardiol.* (2018) 71:429–38. doi: 10.1016/j.jacc.2017.11.047
12. Chachques JC, Trainini JC, Lago N, Masoli OH, Barisani JL, Cortes-Morichetti M, et al. Myocardial assistance by grafting a new bioartificial upgraded myocardium (MAGNUM clinical trial): one year follow-up. *Cell Transplant.* (2007) 16:927–34. doi: 10.3727/096368907783338217
13. Sawa Y, Miyagawa S, Sakaguchi T, Fujita T, Matsuyama A, Saito A, et al. Tissue engineered myoblast sheets improved cardiac function sufficiently to discontinue LVAS in a patient with DCM: report of a case. *Surg Today.* (2012) 42:181–4. doi: 10.1007/s00595-011-0106-4
14. Sawa Y, Yoshikawa Y, Toda K, Fukushima S, Yamazaki K, Ono M, et al. Safety and efficacy of autologous skeletal myoblast sheets (TCD-51073) for the treatment of severe chronic heart failure due to ischemic heart disease. *Circ J.* (2015) 79:991–9. doi: 10.1253/circj.CJ-15-0243
15. Moscarelli M, Lorusso R, Abdullahi Y, Varone E, Marotta M, Solinas M, et al. The effect of minimally invasive surgery and sternotomy on physical activity and quality of life. *Heart Lung Circ.* (2021) 30:882–7. doi: 10.1016/j.hlc.2020.09.936
16. Roche CD, Sharma P, Ashton AW, Jackson C, Xue M, Gentile C. Printability, durability, contractility and vascular network formation in 3D bioprinted cardiac endothelial cells using alginate-gelatin hydrogels. *Front Bioeng Biotechnol.* (2021) 9:e636257. doi: 10.31219/osf.io/ct6rk
17. Vagnozzi RJ, Maillet M, Sargent MA, Khalil H, Johansen AK, Schwanekamp JA, et al. An acute immune response underlies the benefit of cardiac stem-cell therapy. *Nature.* (2019) 577:405–9. doi: 10.1101/506626
18. Polonchuk L, Surija L, Lee MH, Sharma P, Liu Chung Ming C, Richter F, et al. Towards engineering heart tissues from bioprinted cardiac spheroids. *Biofabrication.* (2021) 13:045009. doi: 10.1088/1758-5090/ac14ca

19. Leonard JR, Rahouma M, Abouarab AA, Schwann AN, Scuderi G, Lau C, et al. Totally endoscopic coronary artery bypass surgery: a meta-analysis of the current evidence. *Int J Cardiol.* (2018) 261:42–6. doi: 10.1016/j.ijcard.2017.12.071

Conflict of Interest: The authors declare that the research was conducted in the absence of any commercial or financial relationships that could be construed as a potential conflict of interest.

Publisher's Note: All claims expressed in this article are solely those of the authors and do not necessarily represent those of their affiliated organizations, or those of the publisher, the editors and the reviewers. Any product that may be evaluated in this article, or claim that may be made by its manufacturer, is not guaranteed or endorsed by the publisher.

3.3 – Cardiac patch transplantation instruments for robotic minimally invasive cardiac surgery: initial proof-of-concept designs and surgery in a porcine cadaver

Summary:

Building on the initial design and prototyping work from our preliminary brief research report outlined in the previous chapter (3.1), in our multidisciplinary team we produced several more instrument designs. The designs underwent prototyping, simulation of robotic control systems *in silico* and we tested one of our instruments at surgery in a porcine cadaver. Each design had specific objectives and potential advantages and disadvantages which would be influenced by the choice of patch to go with the instrument. We chose one (called the HeartStamp) to take forward to full prototyping and testing in a porcine cadaver. The test was performed manually with movements consistent with robotic control. All instruments were designed to be compatible with robotic control systems of the kind available at the Robotics Institute of the University of Technology Sydney (UTS). We made all of the data from this initial proof-of-concept study publicly available for free for any other research group to build upon. The work was nominated for three prestigious awards and won one of these (see the list of publications, presentations and awards section of this thesis, page 9).

frontiers in Robotics and AI

ORIGINAL RESEARCH
published: 18 January 2022
doi: 10.3389/frobt.2021.714356

Cardiac Patch Transplantation Instruments for Robotic Minimally Invasive Cardiac Surgery: Initial Proof-of-concept Designs and Surgery in a Porcine Cadaver

Christopher D. Roche[1,2,3], Gautam R. Iyer[2], Minh H. Nguyen[2], Sohaima Mabroora[2], Anthony Dome[2], Kareem Sakr[2], Rohan Pawar[2], Vincent Lee[2], Christopher C. Wilson[2] and Carmine Gentile[1,2]*

[1]Northern Clinical School of Medicine, Kolling Institute, University of Sydney, Sydney, NSW, Australia, [2]Faculty of Engineering and IT, University of Technology Sydney (UTS), Sydney, NSW, Australia, [3]Department of Cardiothoracic Surgery, University Hospital of Wales, Cardiff, United Kingdom

OPEN ACCESS

Edited by:
Kaspar Althoefer,
Queen Mary University of London,
United Kingdom

Reviewed by:
Giacinto Barresi,
Italian Institute of Technology (IIT), Italy
Selene Tognarelli,
Sant'Anna School of Advanced Studies, Italy

***Correspondence:**
Christopher D. Roche
croche@doctors.org.uk

Specialty section:
This article was submitted to Biomedical Robotics, a section of the journal Frontiers in Robotics and AI

Received: 25 May 2021
Accepted: 17 November 2021
Published: 18 January 2022

Citation:
Roche CD, Iyer GR, Nguyen MH, Mabroora S, Dome A, Sakr K, Pawar R, Lee V, Wilson CC and Gentile C (2022) Cardiac Patch Transplantation Instruments for Robotic Minimally Invasive Cardiac Surgery: Initial Proof-of-concept Designs and Surgery in a Porcine Cadaver. Front. Robot. AI 8:714356. doi: 10.3389/frobt.2021.714356

Background: Damaged cardiac tissues could potentially be regenerated by transplanting bioengineered cardiac patches to the heart surface. To be fully paradigm-shifting, such patches may need to be transplanted using minimally invasive robotic cardiac surgery (not only traditional open surgery). Here, we present novel robotic designs, initial prototyping and a new surgical operation for instruments to transplant patches *via* robotic minimally invasive heart surgery.

Methods: Robotic surgical instruments and automated control systems were designed, tested with simulation software and prototyped. Surgical proof-of-concept testing was performed on a pig cadaver.

Results: Three robotic instrument designs were developed. The first (called "Claw" for the claw-like patch holder at the tip) operates on a rack and pinion mechanism. The second design ("Shell-Beak") uses adjustable folding plates and rods with a bevel gear mechanism. The third ("HeartStamp") utilizes a stamp platform protruding through an adjustable ring. For the HeartStamp, rods run through a cylindrical structure designed to fit a uniportal Video-Assisted Thoracoscopic Surgery (VATS) surgical port. Designed to work with or without a sterile sheath, the patch is pushed out by the stamp platform as it protrudes. Two instrument robotic control systems were designed, simulated *in silico* and one of these underwent early 'sizing and learning' prototyping as a proof-of-concept. To reflect real surgical conditions, surgery was run "live" and reported exactly (as-it-happened). We successfully picked up, transferred and released a patch onto the heart using the HeartStamp in a pig cadaver model.

Conclusion: These world-first designs, early prototypes and a novel surgical operation pave the way for robotic instruments for automated keyhole patch transplantation to the heart. Our novel approach is presented for others to build upon free from restrictions or

cost—potentially a significant moment in myocardial regeneration surgery which may open a therapeutic avenue for patients unfit for traditional open surgery.

Keywords: robotics, keyhole surgery, minimally invasive (MIS), cardiac surgery, myocardial repair, cardiac patch, thoracic, cardiothoracic

INTRODUCTION

Advances in regenerative medicine have raised the hope of restoring damaged heart muscle (Roche et al., 2020). Approaches include bioengineering patches for transplantation to the heart surface, which may utilize increasingly accessible methods such as 3D bioprinting (Roche et al., 2020; Roche et al., 2021a). Transplantation of patches containing cells and biomaterials to regenerate heart muscle (myocardium) has been performed in animal models (Gao et al., 2018; Roche and Gentile, 2020; Wang et al., 2021) and human trials (Chachques et al., 2007; Sawa et al., 2012; Menasché et al., 2015; Sawa et al., 2015; Menasché et al., 2018). Until recently (Roche et al., 2021b; Wang et al., 2021), open surgical approaches have been investigated (Wang et al., 2020), even though this could exclude heart failure patients unfit for the physiological demands of open chest surgery (but who might be fit enough to undergo a less invasive procedure). Furthermore, if patch-based myocardial repair is to realize its paradigm-shifting therapeutic potential (for example, as a standalone procedure and/or an adjunct for a patient already undergoing surgery for some other reason), it should be compatible with minimally invasive (keyhole) robotic surgical approaches (Roche et al., 2021b). Otherwise, it could be hard to justify a traditional open surgical operation, not least because the risk/benefit threshold may be harder to meet (Trevis et al., 2020). For example, conventional open surgeries, splitting the sternum (median sternotomy) or via the ribcage (thoracotomy), have been associated with a longer initial recovery and higher incidence of overall complications/adverse events than minimally invasive approaches (Lim et al., 2021; Moscarelli et al., 2021).

With the advancement of minimally invasive robotic cardiothoracic surgery (Torregrossa and Balkhy, 2020; Güllü et al., 2021), it is increasingly pertinent to develop feasible, cost-effective, synergistic instrument-control systems (Trevis et al., 2020). Current surgical robots established in clinical use, including da Vinci® Surgical Systems (Intuitive Surgical Inc., Sunnyvale, CA, United States), have shown that a master-slave (semi-automated) robotic system can perform robotic surgery on humans, resulting in new ways to perform challenging cardiac surgery (Güllü et al., 2021) and potentially improving established operations (Torregrossa and Balkhy, 2020). However, robots like the da Vinci are currently expensive—one Sydney hospital recently reported the implementation cost alone for the *da Vinci Xi* was $4.4 million AUD (approximately $3.2 million USD) (McBride et al., 2021)—which may limit widespread implementation (Crew, 2020).

Here, we hypothesize that a feasible minimally invasive robotic approach for transplantation of cardiac patches could be developed without prohibitive costs. To achieve robotic keyhole cardiac patch transplantation, surgical instrument development was accompanied by development of customized control systems. We present world-first cardiac patch transplantation instrument designs, with simulated robotic control systems, along with initial prototyping and a proof-of-concept surgical test in a pig cadaver.

MATERIALS AND METHODS

Full methodological technical details are available in the **Supplementary Materials** and the complete reproducible dataset is freely available from the permanent data repository associated with this manuscript (https://doi.org/10.5281/zenodo.4784952). **Supplementary Material** was uploaded for peer review with the manuscript.

Instrument Design Process and Objective Setting. Three different instruments and two control systems for instruments were created using computer-aided design (CAD) software (SolidWorks, Waltham, MA, United States). Initial instrument designs, named "Claw", "Shell-Beak" and "HeartStamp" after their mechanisms (which resembled, respectively, a claw, a bird's beak closing to form a shell-like compartment, and a stamp for pressing patches onto the heart) were created based on learning from 12 months of preliminary design and resin-based part prototyping (Roche et al., 2021b). Instrument designs had to be able to transplant a hydrogel-based patch via minimally invasive heart surgery and to be capable of robotic control (for master-slave control or full automation). Additionally, designs had to be: 1) safe (made from biocompatible, non-toxic materials without sharp edges); 2) either disposable or sterilisable by autoclaving and/or sterile sheath covering during surgery; 3) the correct size for human use; 4) strong enough to withstand moment forces at the keyhole entry point (between the ribs at the chest wall); 5) feasible for prototyping without needing specialist manufacturing techniques and at a reasonable cost. Additional design objectives were added for specific instruments. For the Claw (2 cm diameter), it was designed to deliver multiple small patches to precise areas of the heart surface one after the other. For the Shell-Beak (2 cm diameter) the objective was to deploy a cardiac patch which is larger than the diameter of the cardiac instrument. For the HeartStamp (5 cm diameter) additional objectives included: 1) sizing—the diameter of the prototype should be 5 cm and the length greater than 30 cm; 2) ease of use—the design must be intuitive enough for a surgeon to be able to use the device with no additional training; and 3) a surgical camera as well as keyhole forceps must be able to fit inside the device to ensure the surgery is minimally invasive. Ideas were formalized using Scamper tables, tree diagrams, CAD and materials lists for prototyping (see the **Supplementary Materials**). The full methodological datasets (including

SolidWorks files and components) are available in the permanent data repository (https://doi.org/10.5281/zenodo.4784952).

Surgical Compatibility. The Claw and Shell-Beak were designed to fit 2 cm diameter keyhole ports in the chest wall (a frequently used diameter for multiple port keyhole surgery). The HeartStamp was designed for a specific cardiothoracic surgical approach: uniportal Video-Assisted Thorascopic Surgery (VATS)—an approach where all keyhole instruments are inserted via one slightly larger (~5 cm) port used in thoracic surgery. The HeartStamp was also designed to be prototyped from readily available materials and compatible with autoclaving and/or sterile sheath covering.

Proof-of-concept Control System Designs and Simulations (in silico). Using SolidWorks and TinkerCAD (San Francisco, CA, United States), two instrument control systems were designed and simulated. Control System 1 was designed for (and applied to) the Claw design instrument to show compatibility with one of the instrument designs (*in silico*). Control System 2 was designed to control nine rods in a 2 cm diameter (keyhole) cylinder, aimed at demonstrating individual rod control for up to nine rods and multiple (greater than 6) degrees of freedom for instrument movements—tailored to our previous preliminary instrument design (Roche et al., 2021b). Systems used either screw-driven rotationary force or push-pull and gear-based mechanisms to control instrument movements and release the patch. Technical details are available in the permanent data repository (https://doi.org/10.5281/zenodo.4784952).

Proof-of-concept 3D Print Prototyping (Control System 2). Control System 2 was prototyped to show proof-of-concept. A Polylactic Acid (PLA) "sizing and learning" prototype was 3D printed (layer resolution 100 µm, PLA filament diameter 1.75 mm, nozzle diameter 0.4 mm) using a MakerBot Replicator+ extrusion 3D printer (MakerBot, New York, NY, United States) followed by manual assembly of parts to show proof-of-concept feasibility. The complete Makerbot STL file instructions sent to the 3D printer are available in the permanent data repository (https://doi.org/10.5281/zenodo.4784952).

Proof-of-concept Prototyping (HeartStamp Instrument). To determine the optimal prototyping method according to our objectives, we engaged in repeated brainstorming sessions and further developed those ideas using the tables, charts and CAD files shown in the **Supplementary Materials**. We purchased basic hardware materials (for the complete list with catalogue numbers, supplier and pricing see dataset at permanent https://doi.org/10.5281/zenodo.4784952) before manually self-assembling them to create the prototype.

Proof-of-concept Surgery. One researcher (CDR) performed the surgery (with the assistance of CG) using standard surgical materials (including a Haight-Finochietto rib retractor, Symmetry Surgical, Nashville TN, United States) and the HeartStamp prototype. A pig cadaver model was used (an anatomically suitable and ethically permissable model chosen because it could fulfil requirements for proof-of-concept testing without any animals being harmed). We used a combination of moulded and 3D bioprinted hydrogel patches—alginate 4% (w/v) / gelatin 8% (w/v) in Dulbecco's Modified Eagle Medium, previously optimized for cardiac applications (Roche and Gentile, 2020; Roche et al., 2021a). All patches were generated the day before the test and stored at 4°C overnight. On arrival, the pig cadaver was laid in the right lateral position, surgical field prepared with drapes and incision sites marked. To maximize utility, two surgical incisions/approaches were attempted one after the other: 1) left antero-lateral (left of the midline from the front of the chest to the side) and 2) left postero-inferolateral (left of the midline, towards the back, lower down and to the side). The anterolateral approach aimed to simulate a minimally invasive (trans)apical approach (left 5th intercostal space, mid-clavicular line) and the postero-inferolateral approach aimed to simulate a type of approach suitable for uniportal VATS. To simulate real surgical conditions, the operations were performed in real time with one attempt each and reported in full. Operations were video recorded/photographed and observed by an independent observer (Technical Operations Manager, Sydney School of Veterinary Sciences) who assisted when required (including abducting the right upper limb so it did not obstruct the surgical field). The operating room ambient temperature was 4°C and the HeartStamp was operated manually by the surgeon with all mechanisms tested by movements which would be feasible when connected to a robotic control system.

RESULTS

Early-Stage Instrument Design Outcomes

Claw Design. The Claw instrument was designed to maintain narrowness of diameter while enclosing a patch in a safe compartment at the distal tip, which would allow the surgeon to manipulate it with no risk of the patch falling off before opening over the target area. The designs achieved a 2 cm diameter while also holding a patch on the transplant platform until the moment of release (**Figure 1**, **Supplementary Figure S1** and **Supplementary Video S1**). To avoid the patch falling or being knocked off the instrument during transplantation to the heart, the head was designed with two claws in the shape of a rounded-base triangle on a cylinder arc or a tapering rectangle with the short edges meeting together (initial designs shown in **Supplementary Figure S2**). The initial designs did not completely enclose the patch compartment, therefore in the final design the infolding panels forming the "claw" part were changed to a cone shape on a circular base (20 mm base diameter and 19.88 mm overall height—complete measurements shown in **Supplementary Figure S1**). The infolding-outfolding mechanism used a ball joint with a rack and pinion (**Supplementary Figure S3** and **Supplementary Videos S1, S2**). The resulting final Claw design (shown in complete form in **Figure 2** and **Supplementary Video S1**) consists of two "claws" at one end (responsible for opening and closing of the instrument) and a plate holder (**Supplementary Figure S4**) with clips to secure the patch during shift in phasing angle (enabling control of the precise position of patch delivery). The plate holder was designed with a diameter of 9.80 mm considering the keyhole surgery incision (**Supplementary Figure S4**).

As observed in **Figure 1**, Controller Rods 1 and 6 are responsible for controlling the open and close action for the

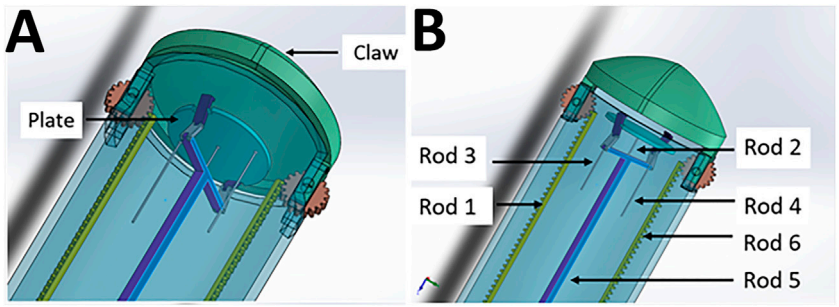

FIGURE 1 | The Claw design in detail. **(A)** The plate (transplantation platform) where the hydrogel patch sits, enclosed by the "claw" to create a safe compartment. **(B)** Controller rods allow opening of the claw (Rod 1 and 6), changing the phasing angle of the plate (Rod 3 and 4), release of the patch securing clips (Rod 5) and protrusion and retraction of the platform (Rod 5 supported by Rod 2). For clarity, Rods 3 and 4 are shown cut short but would actually travel through the instrument to the proximal (control unit) end with the other rods (see also **Figure 6C** which shows the whole length and proximal connections of rods to micro-servo motors).

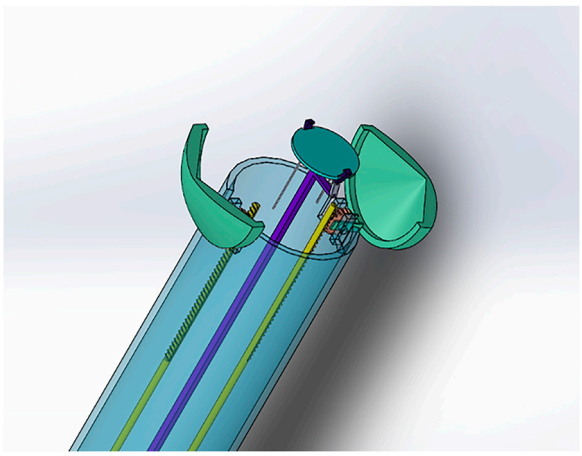

FIGURE 2 | Claw design (open position with plate holder protruding). For secure robotically-enabled transplantation of cardiac patches using minimally invasive heart surgery.

"claw" component of the instrument holding the patch in place. Both the rods work on a rack and pinion system with a gear of 20 teeth (**Supplementary Figure S3** and **Supplementary Video S2**). The gear is in turn connected with the claws, thus allowing movement for opening and closing the instrument (**Supplementary Video S1**). Once the claws are open, Rod 2 facilitates protrusion of the plate holding the patch (the transplantation platform) out of the instrument. Cardiac patches will be placed on the plate and held in position by the clips connected through Rod 5. After the plate is pushed out of the instrument to the desired position, Rods 3 and 4 will be moved in a linear position to change the phasing angle of the plate. This is done to achieve a precise angle to position the patch on the heart (**Supplementary Video S1**). This is facilitated by three joint mechanisms—which we have labelled as *L-link* connected to the plate from one end and attached with *T-link* from the other end through *H-link* (as shown in **Supplementary Figure S5**). Once the position of attachment for the cardiac patch is determined, Rod 5 will move in a linear direction to release open the clip thus releasing the patch from the instrument (*via* a ball joint). Using Rod 2 for support, the patch can be pressed on the required target site (**Supplementary Video S1**).

Shell-Beak Design. To address the potential challenge of transplanting a patch larger than the instrument platform, we designed a second instrument called "Shell-Beak" (**Figure 3**). The design was inspired by the functionality of a bird's beak and simplicity was sought to maximize feasibility. Conceptually, the distal end of the instrument holds an infolded strip of patch, which can be angled during transplantation and pushed out towards the target site. The motion forces would be transmitted with simple push/pull movements of rods surrounded by an encasing cylinder. The patch dispenser has a coin-like base at both ends, in which the patch could have one attachment when infolded to the distal base at the releasing end of the instrument (**Supplementary Figure S6**). The rods and base are connected using ball joints, which gives flexibility to the structure so that is can hold the patch, adjust its facing angle, and push it towards the targeted site during operation. This mechanism is facilitated using a push/pull controller rod arrangement (**Figure 3**). The opening and closing of the beaks were designed using a bevel-gear system. This mechanism converts rotational motion to rotational motion (unlike in the Claw design where linear motion is converted to rotational motion). The angle adjustment platform is responsible for controlling the phasing angle and patch positioning onto the target site. The rotational control of the arm is designed to activate the bevel-gear mechanism to open and close the beak head. An inwardly concave patch holder was conceptualized (**Figure 3**), which would be fabricated from a soft and flexible material and this would sit on top of the patch (with the patch sandwiched between the holder and the distal coin base). The tips of the patch holder would be linked to (or clipped into) the distal tips of the beak, so as to facilitate the instrument holding a patch of eliptical shape of up to ~10 cm in length.

HeartStamp Design. This design (**Figures 4**, **5**) was created to be readily prototyped from standard materials while still

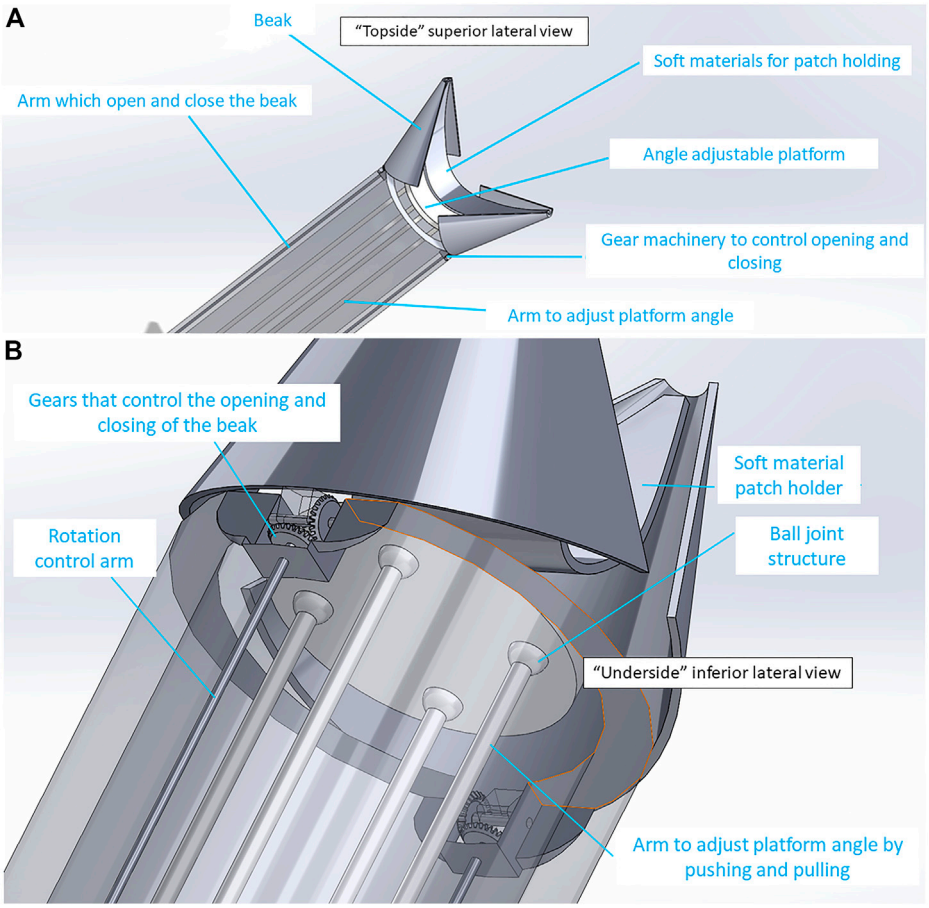

FIGURE 3 | "Shell-Beak" design with flexible patch holder connected to the patch dispenser system. **(A)** "Topside" superior lateral view of the distal (head) of the instrument with partially open beak and flexible patch-holder with space for an infolded patch between the patch-holder and the adjustable platform. **(B)** "Underside" inferior lateral view looking at the base of the patch platform. Ball joints and gear mechanism are shown which allow for changes to the phasing angle of the platform and opening/closing of the beak, respectively.

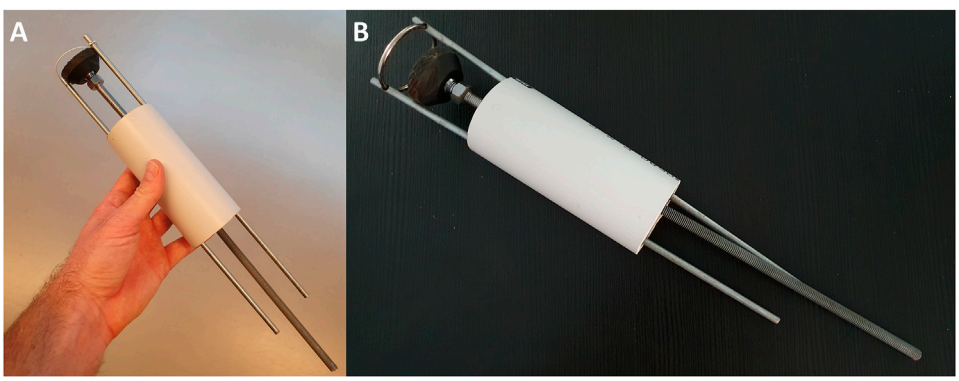

FIGURE 4 | The HeartStamp prototype for cardiac patch transplantation. The HeartStamp is designed to transplant a patch to the surface of the heart via a uniportal VATS incision. The instrument is shown prior to use at surgery with a flexible ring and the operator's hand for scale **(A)** and with a rigid ring after use at surgery **(B)**. Computer-aided design (CAD) images associated with this prototype are shown in **Figure 5**.

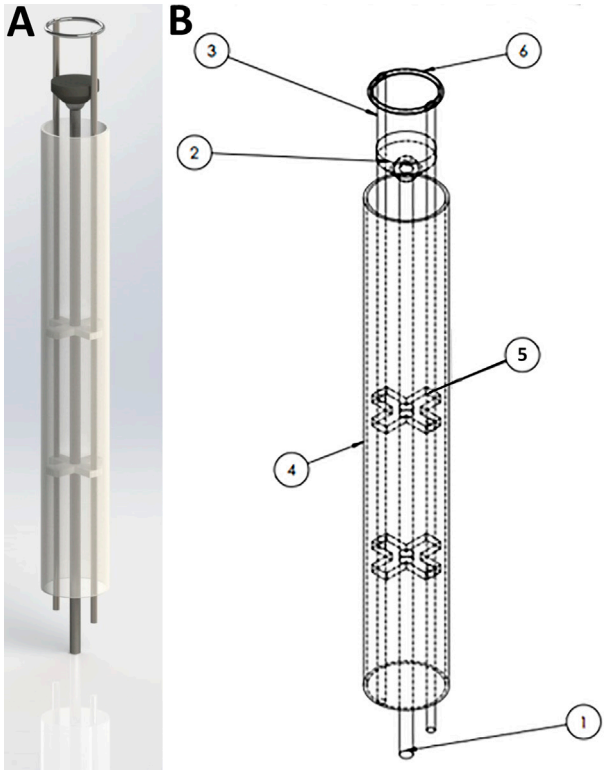

FIGURE 5 | SolidWorks design for the HeartStamp device prototype. 3D rendering of the HeartStamp instrument **(A)** and technical details with labelled parts **(B)**. Item labels: 1) Central Rod (controls the puck); 2) Puck (pushes patch off the ring and onto the heart); 3) Paired Ring Rod (controls the ring angle); 4) Tube (provides protection for components-tube length is modifiable with a long tube shown here whereas a short tube version was used at surgery and shown in **Figure 4**); 5) Paired X-shaped Support (supports the rods); 6) Metal ring (the heart patch is rested on this). The resulting prototype generated from these computer-aided designs is shown in **Figure 4** and the raw data are available in the **Supplementary Materials**.

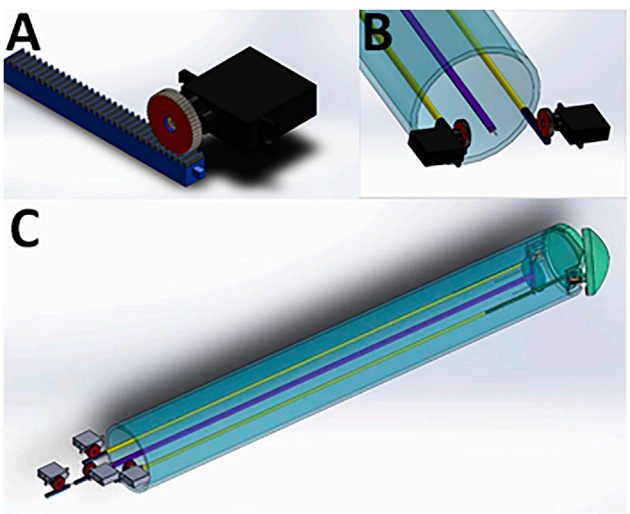

FIGURE 6 | Mounting of micro-servo motors onto the rods of the instrument using the Claw design as an example. **(A)** One micro-servo motor unit attached to a rod. **(B)** The proximal (tail end) of the instrument showing two micro-servo motor units. **(C)** View of the whole instrument, showing four micro-servo motor units and the rods connecting the proximal to the distal end.

satisfying the requirements for robotic minimally invasive patch transplantation. It was designed to fit a control unit with: 1) a central rod protruding and retracting a "stamp"; and 2) two lateral rods attached to a ring which could change the phasing angle of the ring (if one is activated) or extend the longitudinal range of the instrument without changing the ring angle (if both are activated equally). The HeartStamp is a second-generation design and prototype based on a previous design concept called "Umbrella" (**Supplementary Figure S7**) and incorporating elements of the Claw and Shell-Beak. The first-generation (Umbrella) design included a partially-flexible cylinder accommodating independent wires and several joint spaces. A central push platform was used to push the patch onto the heart. For the HeartStamp (**Figures 4**, **5**), the design was optimized for surgery so that the central push mechanism was surrounded by a rigid cylinder able to sit between the ribs in a uniportal VATS entry hole in the chest wall (with or without the use of a retractor to spread the ribs). The push stamp platform (puck) is attached to a central rod travelling through the cylinder to the control unit (or surgeon's hand if being deployed manually). The stamp platform is surrounded by a metal ring with rods at the 12 o'clock and 6 o'clock positions). Both rods travel through the cylinder and can be

FIGURE 7 | A proposed control unit sizing and learning polylactic acid (PLA) prototype. This control unit was prototyped to show preliminary feasibility and identify learning points in preparation for more extensive metal prototyping. It is the complete triplicate prototype for the single subunit (one third) mechanism shown in **Supplementary Video S3**. Each subunit controls three rods and the three subunits are added together in a wheel-and-spoke fashion with 120 degrees between each subunit. The complete control unit was designed to control up to nine rods in a narrow-diameter (2 cm) keyhole surgical instrument such as the one detailed in our preliminary brief research report (Roche et al., 2021b).

protruded and retracted by the control unit, allowing for the phasing angle of the ring to be adjusted. The device is autoclavable and/or compatible with a sterile sheath. If a sheath is used, the stamp platform contacts the sheath and pushes it out, pushing the patch off from its position on the plastic sheath on the opposite side.

Control Systems 1 and 2

We designed two control systems/units and ran *in silico* simulations using CAD software as described below.

Control System 1. To control the Claw, a control system with an Arduino microcontroller and micro-servo motors was designed (Control System 1, **Figure 6** and **Supplementary Video S2**). This was simulated *in silico* (**Supplementary Video S2**), suggesting that the surgeon would be able to control the instrument using a computer console. The control system could be connected to the instrument head using mechanical components from the other end of the system (such as rods passing through a cylindrical tube). The overall dimension for this design was kept to 2 cm maximum diameter, meaning that the instrument could pass through small keyhole ports if a strong material and high-resolution manufacturing technique was used for the small parts. To demonstrate the working of the instrument for simulation purposes, an Arduino microcontroller was coded with micro-servo motors connected to each rod (**Supplementary Video S2**) - simulating *in silico* the working of a linear actuator using micro-servo motors. TinkerCAD was used for this simulation purpose. The connections are outlined in **Supplementary Video S2**. Each micro-servo motor is connected to a potentiometer. The potentiometer acts like a common "regulator" which when rotated in a clockwise direction will move the micro-servo motor, which in turn will result in an individual rod within the instrument moving in linear motion. The control system will be mounted onto the rods as shown in **Figure 6** and **Supplementary Video S2**. On rotating the potentiometer in a clockwise direction, this will result in the rod moving in the forward direction. Similarly, when rotated in an anti-clockwise direction the rod will be retracted. If applied to the Claw design instrument, for example, Potentiometer 1 can be connected to the two micro-servo motors opening the Claw (**Figure 6**), wherein both Rod 1 and Rod 6 will be positioned in a mirror manner. Potentiometer 2 controls Rod 2 to take the cardiac patch securely outside the device. This rod can then be controlled to 360 degrees in any direction to position the patch over the target site. Similarly, Potentiometers 3 and 4 control Rods 3 and 4, respectively, to change the phasing angle of the plate over which the patch sits. Rod 5 controls the releasing of the clips over the plate that secure the patch onto the plate. Linear movement of Rod 5 results in opening and closing of the clip thus leading to release of a cardiac patch on the target site. The potentiometer acts as a joystick with which the surgeon can alter the linear motion of the rods connected to the micro-servo motors. Overall, this approach presents a control system to control the push and pull motion for each rod of an instrument with a similar mechanism to the Claw.

Control System 2. To control more rods, we designed a second control unit based on a different approach capable of controlling nine rods at the same time (Control System 2, **Supplementary Video S3**)—tailored to an early instrument design invented during our previous preliminary work (Roche et al., 2021b). This was designed to provide more degrees of freedom (planes of movement) in a low-diameter (2 cm) keyhole surgical instrument. Thanks to our *in silico* simulation, we tested its rod retraction, protrusion and rotation, where push-pull forces could be applied to nine rods via three U-shaped subunits/connectors (**Supplementary Video S3**). Each subunit connector was designed to move each rod independently and to combine movements to move either two or three rods simultaneously. This subunit is replicated three times in a wheel formation with 120 degrees between each of the three subunits (connected to three rods each) in the resting position. A prototype for this control unit was 3D printed followed by manual assembly of parts to show proof-of-concept feasibility (**Figure 7**).

Proof-of-concept Surgery (Pig Cadaver)

To show surgical feasibility of our approach, we operated on a porcine cadaver for the transplantation of patches using the HeartStamp. The pig had died of unrelated causes and its

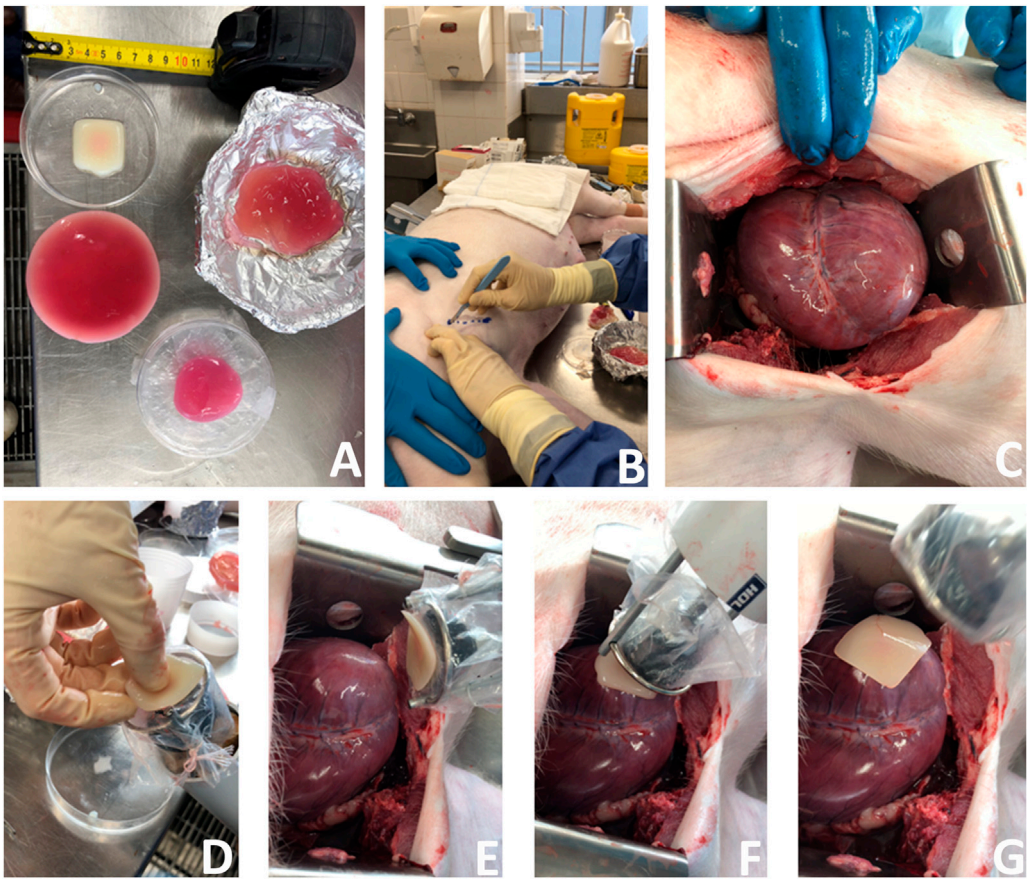

FIGURE 8 | A new surgical operation for epicardial patch transplantation using the HeartStamp—left anterolateral approach with sheath. This surgery was performed once in real time, accepting complications to more closely simulate real surgical conditions (because the heart was enlarged and not accessible using the usual anatomical landmark we had to convert this operation to an open (not keyhole) approach—a complication which happens in human cardiothoracic surgery as well). We chose to continue and report the operation exactly as it happened. **(A)** Patches for cardiac applications were created using alginate/gelatin hydrogel by 3D bioprinting (the white patch) or moulding techniques (pink patches). **(B)** A left anterolateral surgical incision was made in a fresh cadaver of a pig which had recently died of unrelated causes. **(C)** The incision was extended, the chest wall tissues retracted, pericardium cut to expose the heart and the heart manouvred slightly into position. **(D)** The 3D bioprinted patch was manually applied to the plastic sheath at the distal (patient) end of the HeartStamp instrument. **(E)** The HeartStamp was moved into position by the surgeon and the patch remained lightly adherent to the plastic sheath. **(F)** The patch was transplanted to the epicardial surface over the left ventricle. **(G)** The HeartStamp is withdrawn, leaving the patch *in situ* on the epicardium. To complete the operation, the patch was then secured under the pericardium and the chest closed surgically.

cadaver was provided by the University of Sydney Veterinary School (which avoided disposal without utilisation and avoided use of a live animal for testing). To simulate real surgery, each of our surgical approaches was performed once in real time and reported in full.

Surgical Approach 1. We initially tried a minimally invasive left antero-lateral (left of the midline from the front of the chest to the side) approach (**Figure 8**) to mimic that used for access to the heart tip (apex). However, the pig heart was enlarged (due to previously established heart failure) and the incision in the usual anatomical landmark of the 5th intercostal space was too high to visualize the cardiac apex and therefore the incision had to be converted to a larger, open surgical approach (a complication in human cardiothoracic surgery as well). Nonetheless, using this approach we were able to visualize the anterior interventricular (left anterior descending) artery and transplant a patch to the often-infarcted territory supplied by this artery (**Figure 8**). We used a plastic sheath to simulate a sterile surgical instrument sheath and placed a 3D bioprinted alginate/gelatin patch onto the heart surface. The patch adhered to the sheath, even when turned vertically upside down (**Figure 8**; **Supplementary Video S4**). The stamp mechanism was used to push the patch off the plastic onto the heart by protrusion of the stamp (central rod) while stabilising the ring (lateral two rods). The stamp contacted the inner surface of the sheath, pushing it out and the patch was released from the outer surface.

Surgical Approach 2. We made a 6 cm incision aiming for the porcine left 6th intercostal space, posterior axillary line.

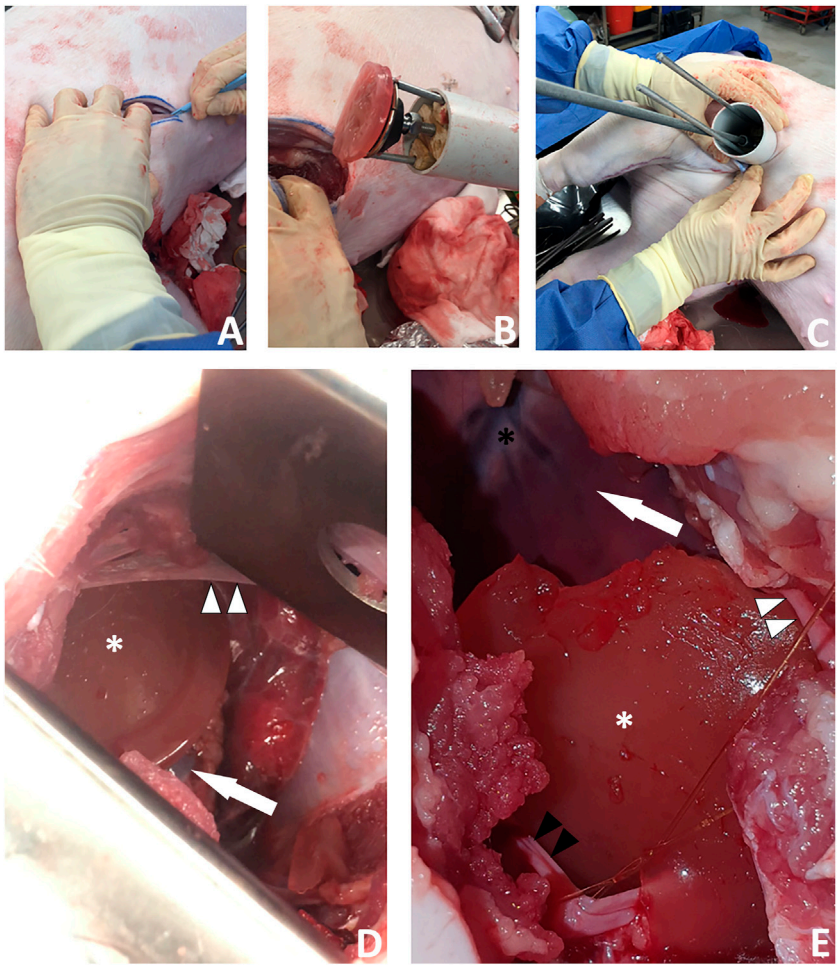

FIGURE 9 | A new surgical operation for epicardial patch transplantation using the HeartStamp—left postero-inferolateral approach without sheath. This surgery was performed once in real time to better simulate real surgical conditions and there were no complications. **(A)** A postero-inferolateral surgical incision was made in a fresh cadaver of a pig which had recently died of unrelated causes. The previously made left antero-lateral incision (the other approach we tested shown in **Figure 8**) is concealed under the surgeon's left hand in the photograph shown in panel **(A)**—higher up and more towards the midline. **(B)** A moulded alginate/gelatin hydrogel patch was picked up by the instrument (without manual application) and is shown here adherent to the ring at the distal (patient) end of the HeartStamp instrument. The black stamp head is seen in retracted position under the patch. The HeartStamp is moved into position by the surgeon. **(C)** The HeartStamp is shown in position, inserted through the incision in the chest wall (the 5 cm diameter HeartStamp cylindrical body fits the 5 cm incision). This entry route is similar (in location and size) to established approaches used for uniportal (one port for all surgical instruments) VATS—a type of keyhole surgery on the chest. The rods are seen from the control (operator) end with the two shorter rods being lateral and connected to the ring (distal end—inside the patient) and the longer rod being central and connected to the stamp. **(D)** For confirmation that the patch was successfully transplanted (as shown in **Supplementary Video S4**), we used a retractor to open the wound and visualize the patch (white asterisk) on the apex of the heart (white arrow). A thin beam of pericardium is seen superiorly (white arrowheads). **(E)** Close-up view of the patch (white asterisk) shown on the heart apex (not shown—concealed by the patch) after we opened the chest fully to examine the patch location. Left/superior pericardial tissue is seen (white arrowheads) and right/inferior pericardium (black arrowheads) is visualized attached to a surgical suture. The heart is seen in the background of the image (white arrow) along with the anterior interventricular (left anterior descending) blood vessels (black asterisk).

We cut through the soft tissues, separated the ribs with a retractor and cut the pericardium over the apex of the heart. We then removed the retractor and used the HeartStamp without a sheath to directly pick up a patch on the operating table (**Supplementary Video S4**). The patch was adherent to the ring and the two protruding ends of the lateral rods which control the ring. The instrument was inserted manually into the chest and operated manually by engaging the stamp protrusion mechanism. The stamp moved forwards and pressed the patch onto the heart surface at the apex (**Figure 9** and **Supplementary Video S4**). We checked the position of the patch afterwards and confirmed it was *in-situ* at its intended location. We then closed the surgical wound, suturing the pericardium back together on top of the patch to secure it in place. All the movements (patch pick-up, patch transfer and patch release onto the heart) were enacted manually by the surgeon and were consistent with those possible using robotic control mechanisms.

DISCUSSION

We have demonstrated early-stage proof-of-concept feasibility for patch transplantation via robotic minimally invasive approaches. We have presented our designs in detail (including those which were not taken forward to prototyping) because each design may have a specific value for certain types of patch. Considerations for the patches themselves are described in detail elsewhere (Roche et al., 2021a), but for example, alginate/gelatin (Roche and Gentile, 2020), fibrin-based (Menasché et al., 2018) or more complex matrices such as methacrylated elastin/gelatin/carbon-nanotube would all have very different properties/shape-memory behaviours (Wang et al., 2021). We have made all of our early-stage proof-of-concept data freely available for others to build upon and further trials will be required (including optimising instruments for certain patch types) for full systematic efficacy analyses. Nonetheless, our proof-of-concept surgical test of one of our prototyped designs (the HeartStamp) represents a world-first and potentially a significant step forward. The novel work presented in this article is the result of a collaborative study bringing together experts in robotics, mechanical engineering, cardiothoracic surgery and biofabrication. We are the first to present both the approach (epicardial heart patch transplantation by robotic minimally invasive cardiothoracic surgery) and instruments (designs and initial prototyping) to achieve this goal.

Our approach overcomes several mechanistic limitations which occurred in our design process. This is illustrated by our 'Claw' and 'Shell-Beak' designs which had a 2 cm diameter to make them compatible with conventional keyhole surgery (that is, three or more 2 cm ports and the surgeon triangulating) as well as uniportal (all instruments in one 5–6 cm hole). For example, with the Claw design we initially encountered the problem that the facing angle might be nonadjustable, meaning it would have to be inserted perpendicular to the contour of the target heart surface (**Supplementary Video S1).** To overcome this, we used a rack and pinion system combined with ball joints which allowed changes to the phasing angle (**Supplementary Video S1**). With this design (**Figures 2**, **6**), the Claw releasing compartment was supported by a combination of linkages and ball joints and the phasing angle could be adjusted to align with the contact contour of the target area. Conversely, for the HeartStamp (**Figures 4**, **5**), we realized that a clamping method to hold down the patch was not needed due to the sticky nature of our alginate/gelatin patches (**Supplementary Video S4**). This finding allowed us to keep a simple design whereby a patch could be pressed on the heart in the desired location (similar to a stamp, a puck was pushed out through a ring to detach the patch off the ring and onto the heart). In this case, the phasing angle could simply be controlled by two independent rods controlling a ring through which the puck presses and this mechanism worked both when covered by a plastic sheath and without a sheath. It remains an open question whether the stickiness of the patch itself could be controlled to avoid adhesions and deformation, and this is especially important for any infold-outfold designs such as the Shell-Beak (**Figure 3**). The flexible patch holder elipse of the Shell-Beak (conceptualized to sit on top of the patch) could potentially assist against patch deformation. Such a patch holder could potentially even be generated at the same time as the patch and used as a patch loading and stabilising mechanism (although this would need further testing and questions would remain such as where the patch holder goes at the moment of transplant). Due to the stickiness of the alginate/gelatin patches, there should be no requirement for a forceful releasing mechanism with any of our systems, provided the plate is made from non-adhesive material (less adhesive to the patch than the heart is). It has been shown that hydrogels can remain in situ in the sub-pericardial space (Zhu et al., 2021) and our patches (which do not retain sutures) are also designed to be secured under the pericardium.

As instruments without control mechanisms would have limited usefulness, we developed control systems to operate instruments robotically. For any control system, at the operator's end (the tail of the instrument), it is crucial to consider appropriate connections of the instrument to the control system. Our Control System 1 demonstrated the working of an instrument for simulation purposes *via* an Arduino microcontroller which was coded with micro-servo motors connected to each rod (**Supplementary Video S2**). The objective was to replicate *in silico* the working of a linear actuator using micro-servo motors (the connections are outlined in **Supplementary Video S2).** While connecting multiple micro-servo motors with Arduino microcontrollers may seem uncomplicated *in silico*, there are potential limitations for its translation to the clinic. For example, if we connect all the servos to Arduino supply pins (outside a computer simulation setting) then they may not work optimally in standard operating theatres because of a lack of current to drive all the motors. When developing a real-time prototype, we would probably have to use a servo driver PCA 9685 and a relay. It should be noted that the Arduino is a first step and future work may include custom PCB boards, voltage rectifiers and/or a field-programmable gate array (FPGA). Nonetheless, in simulation, we successfully used micro-servo motors along with an Arduino UNO to demonstrate this feasible approach.

For Control System 2, our *in silico* proof-of-concept demonstration (**Supplementary Video S3**) and 3D printed prototype of the unit (**Figure 7**) paves the way for full functional prototyping and connection with a robotic mechanism to initiate and cease motion via a software controller. This control system design shows that it may be possible to control a large number of rods despite a tiny space, provided it is made from strong material using high-resolution manufacturing techniques. By altering the 120-degree angles of the spokes, rotation of groups of three adjacent rods at the same time is possible (**Supplementary Video S3**). At the distal face of the control unit (the patient-facing side which would be closest to the patient—where the rods exit the control unit), a gear mechanism is connected to the rods. This gear mechanism is designed to allow rotation of all the rods *en masse*. The combination of movements should allow for a large number (greater than 6) of degrees of freedom. This opens up the possibility of robotic initiation and maintenance of multiple movements simultaneously—well beyond the computational power of a human controlling the instrument manually.

The culminative achievements presented herein are the surgical patch transplantation operations (**Figures 8**, **9** and **Supplementary Video S4**). Of the two surgical approaches we tried, the more successful was *via* a minimally invasive approach using a left postero-inferolateral (left of the midline, towards the back, lower

down and to the side) incision similar (in terms of size and entry point) to that which could be used for certain operations by uniportal VATS—where all keyhole instruments and the camera are inserted through one port (**Figure 9** and **Supplementary Video S4**). We purposefully ran these operations once each in real time and we report them exactly as they happened, including any complications, to better simulate real surgical conditions. These proof-of-concept operations lay the foundations for more extensive trials, during which several limitations will need to be addressed. These include application of the instrument to a robotic control unit so that the manual operation component is removed, *in vivo* testing so that feasibility is demonstrated with a beating heart (although some cardiac surgery is performed on an arrested heart using cardiopulmonary bypass, this technique should be appropriate for beating heart surgery), performance of surgery in a theatre environment which is more closely controlled to resemble that of human surgery, optimising the exact surgical approach and quantifying complication rates over high numbers of repeats, as well as obtaining quantitative data for full analysis to show safety and efficacy.

Our overall objective was to develop a surgical robotic invention using accessible feasibility-focused approaches with low costs (for instance, the HeartStamp unit production cost was less than $100 AUD). Others have used a similar approach (avoiding prohibitively high costs) to develop master-slave systems working on the principle of semi-autonomous control (Bai et al., 2017; Zhou et al., 2018). Fully autonomous systems have also been developed, although human surgeon supervision may still be needed (Shademan et al., 2016). Fully autonomous unsupervised robotic systems for surgery would need to overcome safety concerns (Trevis et al., 2020). For example, it is foreseeable that a component or power malfunction (unsupervised) at a key moment in the surgery could lead to patient harm—after all, human cardiothoracic surgeons do not work alone unsupervised. Nonetheless, to future-proof instruments against technological progress making them redundant, they should ideally be compatible with both master-slave and full automation.

Overall, robotic-assisted keyhole surgery promises remarkable advantages for the cardiothoracic surgeon, especially if it can be done remotely (Torregrossa and Balkhy, 2020). Paradigm-shifting scenarios could be unlocked, such as for emergency robotic operations by remote on patients in geographical locations too distant for transfer; or for rare operations where expert surgeons could perform a higher volume of a niche procedure, doing more cases remotely on a global patient pool. For early proof-of-concept studies such as this one to be translated from the bench to the bedside, future independently developed approaches to robotic cardiac surgery are likely to be important for widespread translation into surgical practice. As bioengineers make progress with patches for myocardial regeneration (Menasché et al., 2018; Wang et al., 2021), it is critical that the method of delivery of patches is considered (Roche et al., 2021b). Otherwise is it possible that bioengineers will unveil a new treatment which is limited by the practical consideration of how to transplant it (Roche et al., 2021b). It is important to re-emphasize that the work herein is early stage, because over-inflation of expectations has been identified as a harmful ethical pitfall in the field of regenerative medicine (Gilbert et al., 2018a; Gilbert et al., 2018b; Cossu et al., 2018). Nonetheless, the early-stage proof-of-concept work herein represents a first step on a pathway to achieving minimally invasive robotic cardiac patch transplantation.

CONCLUSION AND RELEVANCE

For the first time, we have presented a new overall approach to myocardial regeneration—epicardial patch transplantation by minimally invasive robotic surgery. We demonstrated the feasibility of this approach in a surgical operation using a pig cadaver. Our approaches and components are presented freely for others to build upon, without restriction or cost: this has the potential to pivot the field away from its focus on open heart surgery towards a minimally invasive robotic approach—potentially a key step towards clinical translation of myocardial patch transplantation.

DATA AVAILABILITY STATEMENT

The datasets presented in this study can be found in online repositories. The names of the repository/repositories and accession number(s) can be found below: https://doi.org/10.5281/zenodo.4784952 (CERN, Geneva, Switzerland) with additional datasets in the **Supplementary Material** attached to this article. All **Supplementary Materials** were uploaded for peer review with the article.

AUTHOR CONTRIBUTIONS

CR: Conceptualization (overall approach); Conceptualization (instruments); Surgical advice for instrument and control system conceptualization; Conceptualization (surgery); Data Generation; Data curation; Formal analysis; Funding acquisition; Project administration; Visualization; Supervision; Validation; Writing—original draft; Writing—review and editing; performance of surgical operation. GI: Conceptualization (instruments—except HeartStamp); conceptualization (control systems); Data generation; Data curation; Formal analysis; Project administration; Visualization; Supervision; Validation; Writing—original draft; Writing—review and editing; MN: Conceptualization (instruments—except HeartStamp); conceptualization (control systems); Data generation. SM: Conceptualization (instruments—except HeartStamp); conceptualization (control systems); Data generation; Writing—original draft. AD, KS, RP, and VL: Team which conceptualized, designed and prototyped the HeartStamp Instrument. CW: mechanical engineering advice for instruments (except HeartStamp); Project administration; Supervision; Writing— review and editing. CG: Conceptualization (instruments—except HeartStamp); biomedical engineering advice for patches; Funding acquisition; Project administration; Visualization; Supervision; Writing—review and editing; assistance and data generation during surgical operation. Further contribution details (including non-author contributions) are found in the **Supplementary Materials**. All authors contributed to the article and approved the submitted version.

FUNDING

The work herein had no specific grant or funding attached to it. CDR has been generally supported in his research by a Heart Research Australia PhD Scholarship (grant number 2019-02), the Le Gros Legacy Fund New Zealand (grant number PhD012019) and a Paulette Isabel Jones Completion Scholarship 2021 (USYD). CG has been supported by UTS Seed Funding, a University of Sydney Kick-Start Grant, a University of Sydney Chancellor's Doctoral Incentive Programme Grant, a Catholic Archdiocese of Sydney 2019 Grant for Adult Stem Cell Research, and a Sydney Medical School Foundation Cardiothoracic Surgery Research Grant.

ACKNOWLEDGMENTS

The authors would like to acknowledge the non-author contributors to this work (for the full list see the **Supplementary Materials**), ICU Staff Specialist at the Royal North Shore Hospital, colleagues at the Sydney School of Veterinary Science, Faculty of Science at the University of Sydney, peer reviewers and editor. For this work CDR received a confirmed nomination for the Asia/Oceania Young Scientist Award associated with the Biofabrication 2021 conference and Cutlers' Surgical Prize 2022. The work was presented by CDR as winner of a Rising Star Award for outstanding contribution to cardiovascular research (Sydney Cardiovascular Symposium 2021).

SUPPLEMENTARY MATERIAL

The Supplementary Material for this article can be found online at: https://www.frontiersin.org/articles/10.3389/frobt.2021.714356/full#supplementary-material

Supplementary Video S1 | Brief overview of robotic keyhole patch transplantation demonstrated with the "Claw" instrument design.

Supplementary Video S2 | Video walkthrough for *in silico* demonstration of instrument Control System 1 using potentiometers, an Arduino microcontroller and servo motors.

Supplementary Video S3 | Video walkthrough for in silico demonstration of one subunit of Control System 2. The subunit shown is one of three and is tailored to a nine-rod instrument similar to the one we described in our previous preliminary brief research report (Roche et al., 2021b). In the complete control unit the three subunits would be arranged in a wheel-and-spoke formation with 120 degrees between each subunit in the neutral position. The initial 'sizing and learning' prototyping result for the full triplicate control unit is shown in **Figure 7**.

Supplementary Video S4 | Detailed background and video walkthrough for the first-in-kind surgical operation to transplant a patch to the heart using the 'HeartStamp' instrument. Surgery was performed on a fresh pig cadaver (an appropriate pre-clinical model for cardiothoracic proof-of-concept surgery) and was run once and reported exactly "as-it-happened" (to better simulate "real" surgical conditions). The HeartStamp is referred to as HeartStamp-HPBT (Heart Patch Bearer-Transplanter).

Supplementary Figure S1 | The Claw head technical details. The Claw head design would create a secure enclosed space for a patch without crushing it.

Supplementary Figure S2 | Outer body design for the "Claw" minimally invasive heart patch transplantation instrument in early-stage development. **(A)** Initial design with rounded-base triangle forming the claw compartment where patch would sit. **(B)** Initial design with tapering rectangular claw compartment. Both initial designs shown here do not completely enclose the patch compartment (a feature of the subsequent final design).

Supplementary Figure S3 | Rack and Pinion mechanism technical details.

Supplementary Figure S4 | Plate holder technical details.

Supplementary Figure S5 | Plate holder working mechanism with combination of linkages. **(A)** L-link **(B)** H-link **(C)** T-link.

Supplementary Figure S6 | Shell-Beak Design. First-generation **(A,B)** Shell-Beak design with a patch dispenser system. The cardiac patch is held in an infolded "shell" position and then outfolded with opening of the "beak." **(C)** External structure **(D)** Internal structure. This instrument was designed to deploy a patch with a diameter larger than the instrument. Elliptical patches with shape-memory could potentially be out-folded and deployed with this design.

Supplementary Figure S7 | "Umbrella" Design. Initial designs for a protrusion-based patch deployment instrument which were subsequently developed into the final HeartStamp instrument.

REFERENCES

Bai, W., Cao, Q., Wang, P., Chen, P., Leng, C., and Pan, T. (2017). Modular Design of a Teleoperated Robotic Control System for Laparoscopic Minimally Invasive Surgery Based on ROS and RT-Middleware. *Ir* 44 (5), 596–608. doi:10.1108/ir-12-2016-0351

Chachques, J. C., Trainini, J. C., Lago, N., Masoli, O. H., Barisani, J. L., Cortes-Morichetti, M., et al. (2007). Myocardial Assistance by Grafting a New Bioartificial Upgraded Myocardium (MAGNUM Clinical Trial): One Year Follow-Up. *Cel Transpl.* 16 (9), 927–934. doi:10.3727/096368907783338217

Cossu, G., Birchall, M., Brown, T., De Coppi, P., Culme-Seymour, E., Gibbon, S., et al. (2018). Lancet Commission: Stem Cells and Regenerative Medicine. *The Lancet* 391 (10123), 883–910. doi:10.1016/s0140-6736(17)31366-1

Crew, B. (2020). Worth the cost? A closer look at the da Vinci robot's impact on prostate cancer surgery. *Nature* 580, S5–S7. doi:10.1038/d41586-020-01037-w

Gao, L., Gregorich, Z. R., Zhu, W., Mattapally, S., Oduk, Y., Lou, X., et al. (2018). Large Cardiac Muscle Patches Engineered from Human Induced-Pluripotent Stem Cell-Derived Cardiac Cells Improve Recovery from Myocardial Infarction in Swine. *Circulation* 137 (16), 1712–1730. doi:10.1161/circulationaha.117.030785

Gilbert, F., O'Connell, C. D., Mladenovska, T., and Dodds, S. (2018). Print Me an Organ? Ethical and Regulatory Issues Emerging from 3D Bioprinting in Medicine. *Sci. Eng. Ethics* 24 (1), 73–91. doi:10.1007/s11948-017-9874-6

Gilbert, F., Viaña, J. N. M., O'Connell, C. D., and Dodds, S. (2018). Enthusiastic Portrayal of 3D Bioprinting in the media: Ethical Side Effects. *Bioethics* 32 (2), 94–102. doi:10.1111/bioe.12414

Güllü, A. Ü., Şenay, Ş., Ersin, E., Demirhisar, Ö., Kocyigit, M., and Alhan, C. (2021). Feasibility of Robotic-Assisted Atrial Septal Defect Repair in a 6-Year-Old Patient. *Int. J. Med. Robot* 17 (2), e2185. doi:10.1002/rcs.2185

Lim, E. K. S., Batchelor, T. J. P., Dunning, J., Shackcloth, M., Anikin, V., Naidu, B., et al. (2021). Video-assisted Thoracoscopic versus Open Lobectomy in Patients with Early-Stage Lung Cancer: One-Year Results from a Randomized Controlled Trial (VIOLET). *Jco* 39 (15_Suppl. l), 8504. doi:10.1200/jco.2021.39.15_suppl.8504

McBride, K., Steffens, D., Stanislaus, C., Solomon, M., Anderson, T., Thanigasalam, R., et al. (2021). Detailed Cost of Robotic-Assisted Surgery in the Australian Public Health Sector: from Implementation to a Multi-Specialty Caseload. *BMC Health Serv. Res.* 21 (1), 108. doi:10.1186/s12913-021-06105-z

Menasché, P., Vanneaux, V., Hagège, A., Bel, A., Cholley, B., Cacciapuoti, I., et al. (2015). Human Embryonic Stem Cell-Derived Cardiac Progenitors for Severe Heart Failure Treatment: First Clinical Case Report: Figure 1. *Eur. Heart J.* 36 (30), 2011–2017. doi:10.1093/eurheartj/ehv189

Menasché, P., Vanneaux, V., Hagège, A., Bel, A., Cholley, B., Parouchev, A., et al. (2018). Transplantation of Human Embryonic Stem Cell-Derived Cardiovascular Progenitors for Severe Ischemic Left Ventricular Dysfunction. *J. Am. Coll. Cardiol.* 71 (4), 429–438. doi:10.1016/j.jacc.2017.11.047

Moscarelli, M., Lorusso, R., Abdullahi, Y., Varone, E., Marotta, M., Solinas, M., et al. (2021). The Effect of Minimally Invasive Surgery and Sternotomy on Physical Activity and Quality of Life. *Heart Lung Circ.* 30 (6), 882–887. doi:10.1016/j.hlc.2020.09.936

Roche, C. D., and Gentile, C. (2020). Transplantation of a 3D Bioprinted Patch in a Murine Model of Myocardial Infarction. *J. Vis. Exp.*, e61675. doi:10.3791/61675

Roche, C. D., Sharma, P., Ashton, A. W., Jackson, C., Xue, M., and Gentile, C. (2021a). Printability, Durability, Contractility and Vascular Network Formation in 3D Bioprinted Cardiac Endothelial Cells Using Alginate-Gelatin Hydrogels. *Front. Bioeng. Biotechnol.* 9, 636257. doi:10.3389/fbioe.2021.636257

Roche, C. D., Brereton, R. J. L., Ashton, A. W., Jackson, C., and Gentile, C. (2020). Current Challenges in Three-Dimensional Bioprinting Heart Tissues for Cardiac Surgery. *Eur. J. Cardiothorac. Surg.* 58 (3), 500–510. doi:10.1093/ejcts/ezaa093

Roche, C. D., Zhou, Y., Gentile, C., and Zhao, L. 2021b, A World-First Thorascopic Surgical Instrument for Minimally Invasive Robotically-Enabled Transplantation of 3D Bioprinted Heart Patches for Myocardial Regeneration: A Brief Research Report. *Front. Surg.* 8, 653328. doi:10.3389/fsurg.2021.653328

Sawa, Y., Miyagawa, S., Sakaguchi, T., Fujita, T., Matsuyama, A., Saito, A., et al. (2012). Tissue Engineered Myoblast Sheets Improved Cardiac Function Sufficiently to Discontinue LVAS in a Patient with DCM: Report of a Case. *Surg. Today* 42 (2), 181–184. doi:10.1007/s00595-011-0106-4

Sawa, Y., Yoshikawa, Y., Toda, K., Fukushima, S., Yamazaki, K., Ono, M., et al. (2015). Safety and Efficacy of Autologous Skeletal Myoblast Sheets (TCD-51073) for the Treatment of Severe Chronic Heart Failure Due to Ischemic Heart Disease. *Circ. J.* 79 (5), 991–999. doi:10.1253/circj.cj-15-0243

Shademan, A., Decker, R. S., Opfermann, J. D., Leonard, S., Krieger, A., and Kim, P. C. (2016). Supervised Autonomous Robotic Soft Tissue Surgery. *Sci. Transl Med.* 8 (337), 337ra64. doi:10.1126/scitranslmed.aad9398

Torregrossa, G., and Balkhy, H. H. (2020). The Role of Robotic Totally Endoscopic Coronary Artery Bypass in the Future of Coronary Artery Revascularization. *Eur. J. Cardiothorac. Surg.* 58 (2), 217–220. doi:10.1093/ejcts/ezaa104

Trevis, J., Chilvers, N., Freystaetter, K., and Dunning, J. (2020). Surgeon-Powered Robotics in Thoracic Surgery; an Era of Surgical Innovation and its Benefits for the Patient and beyond. *Front. Surg.* 7 (109), 589565. doi:10.3389/fsurg.2020.589565

Wang, H., Roche, C. D., and Gentile, C. (2020). Omentum Support for Cardiac Regeneration in Ischaemic Cardiomyopathy Models: a Systematic Scoping Review. *Eur. J. Cardiothorac. Surg.* 58 (6), 1118–1129. doi:10.1093/ejcts/ezaa205

Wang, L., Liu, Y., Ye, G., He, Y., Li, B., Guan, Y., et al. (2021). Injectable and Conductive Cardiac Patches Repair Infarcted Myocardium in Rats and Minipigs. *Nat. Biomed. Eng.* doi:10.1038/s41551-021-00796-9

Zhou, X., Zhang, H., Feng, M., Zhao, J., and Fu, Y. (2018). New Remote centre of Motion Mechanism for Robot-Assisted Minimally Invasive Surgery. *Biomed. Eng. Online* 17 (1), 170. doi:10.1186/s12938-018-0601-6

Zhu, D., Li, Z., Huang, K., Caranasos, T. G., Rossi, J. S., and Cheng, K. (2021). Minimally Invasive Delivery Of Therapeutic Agents By Hydrogel Injection Into The Pericardial Cavity For Cardiac Repair. *Nat. Commun.* 12, 1412. doi:10.1038/s41467-021-21682-7

Conflict of Interest: The authors declare that the research was conducted in the absence of any commercial or financial relationships that could be construed as a potential conflict of interest.

Publisher's Note: All claims expressed in this article are solely those of the authors and do not necessarily represent those of their affiliated organizations, or those of the publisher, the editors and the reviewers. Any product that may be evaluated in this article, or claim that may be made by its manufacturer, is not guaranteed or endorsed by the publisher.

3.4 – Closing remarks to Part 3

This part of the thesis arguably has the potential to be the most impactful in terms of shaping the future directions of the field. The early work contained in Part 3 shows that it is possible to transplant (robotically and minimally invasively) the type of patches used in Part 2 of this thesis. The complete dataset for this work is freely available for others to build upon in the spirit of open science. It remains to be seen if the specific approach we successfully demonstrated (uniportal VATS) becomes the approach others might adopt for this type of application. Gaining access to the pericardium and the heart via the thoracic (lung surgery) approach of uniportal VATS is not typical and this suggestion is itself innovative. We moved to this approach because the "keyhole" port used is larger (5 cm) compared to more "typical" 2 cm keyhole ports. We did this because it was easier to fabricate a functional prototype (the HeartStamp) and we could also place the patch on the instrument without having to fold it in on itself and then "outfold" it (as was envisaged in the preliminary report of Chapter 3.2). In the interim as we published this work, others published their highly manipulatable patches which could be rolled up inside a minimally invasive catheter of 7 mm diameter and then rolled out once on the heart surface (Wang et al., 2021). This demonstrates the level of control bioengineers can enact on the patches themselves. Our AlgGel patches would not be capable of being rolled up and unrolled in this way, which is why we successfully transplanted them using a 5 cm uniportal VATS incision (rather than 2 cm). In future, our work may provide the starting point for the field to move towards robotic minimally invasive patch transplantation. If it does, then the interplay of patch and instrument may be manipulatable in ways not currently imagined. If patches can be designed with extensive control over their "shape-memory" behaviour, our other 2 cm diameter instrument designs (which were not taken forward to surgery) may be adopted and/or adapted for various other surgical approaches (not necessarily uni-portal VATS). Nonetheless, the inventions presented in Part 3 have the potential to start a process which could lead to patches being transplanted by robotic minimally invasive approaches. If the surgical landscape continues to move towards more and more surgery being done by this sort of method, then it may not be useful to propose transplantation of patches by traditional open surgery.

PART 4 – DISCUSSION OF THE THESIS

4.1 – Introduction and relevance to Part 4

Part 4 discusses the ways in which this thesis has contributed to the field of myocardial regeneration. The original hypothesis was defined in broad terms as:

3D bioprinted heart patches will promote myocardial regeneration**.**

The articles/chapters within have addressed this hypothesis via the specific aims. Aim 1 sought to optimise patches (Chapters 2.2 and 2.3) and Aim 2 sought to evaluate the effect of patches in mice modelling MI (Chapter 2.4). Aim 3 (Chapters 3.2 and 3.3) addressed the question of how to actually transplant patches by minimally invasive robotic approaches to ensure they are maximally translatable in future.

In bringing together these aims and elaborating on how they address the central hypothesis, the following chapters of Part 4 will discuss (4.2), speculate on future directions (4.3) and conclude (4.4). The final section (4.5) proposes a take home message for the thesis as a whole. Whilst the hypothesis was defined in broad terms, the important more specific contributions of the thesis will be highlighted. Especially, the discussion will detail the considerations pertaining to the use of VCS in bioink (as this was the novel technique the experiments herein used).

4.2 – Thesis discussion

This thesis supports its central hypothesis that 3D bioprinted heart patches promote myocardial regeneration. It therefore adds to a growing body of literature suggesting that epicardial patch-based repair strategies improve cardiac functional outcomes after MI (Wang et al., 2021). The thesis also introduces several novel contributions to the scientific field which had not previously been addressed:

Firstly, the use of VCS in bioink seems to offer a small advantage compared to freely suspended mixed cardia cells in alginate-gelatin hydrogel patches. This is consistent with the hypothesis that allowing cells to culture in 3D before using them in bioink will promote the formation of cell-to-cell connections and a more physiological microenvironment for the cells. Patches with cells freely suspended in hydrogel (not in spheroids) were also associated with a marked improvement in cardiac function. To detect the small difference between the two groups would require very high numbers of mice (>100) and probably would not be ethical to detect a small difference of minimal *clinical* significance. The VCS group showed stronger electrical waveforms than the cellular group and a favourable gene expression profile which was closer to the sham group (without MI or patch). Therefore, the evidence provided herein suggests that there is no reason to choose freely suspended cells over VCS and that it is likely to be worth preculturing cells as VCS before mixing with hydrogel for similar experiments in future.

Importantly, even hydrogel alone without cells provided some improvement in cardiac function as measured by the median LVEF% for each experimental group. This suggests that the mechanism behind the efficaciousness of this treatment strategy is not fully explained by direct cell replenishment. This finding supports the hypothesis put forward by others that the mechanism underlying the beneficial effect of applying cells to the myocardium is stimulation of host immune cell responses, particularly of the innate immune system (Chachques et al., 2021; Vagnozzi et al., 2019). To further explore inflammatory mechanisms, we performed quantitative analysis (flow cytometry) of cell types in our RAG.1 (no mature B or T cells) mice. The fact that our mice lacked for mature B or T cells suggests that inflammatory mechanisms are not reliant on the B or T cell mediated mechanisms of the adaptive immune system. Our quantitative analysis identified a trend towards reversal of macrophage polarisation between sham and MI experimental groups and then a re-reversal back towards the sham ratio with any of our three treatment groups (MI+PATCH, MI+PATCH CELLS or MI+PATCH SPHEROIDS). We also identified an increase in the proportion of Natural Killer (NK) cells compared to other white blood cells. These changes support the hypothesis that host immune cell behaviour may be a central mechanism, perhaps *the* mechanism, by which epicardial patch transplantation improves cardiac function. This warrants a dedicated future study, not least because it is inadvisable to proceed to human trials without understanding the mechanism by which this treatment seems to work. Of note, an LVEF% ≥ 55 is often used as a cut off level for heart failure (with anything below classified as heart failure). Therefore, one reading of our results could be that all our treatment groups (MI+PATCH, MI+PATCH CELLS and MI+PATCH SPHEROIDS) raised the LVEF from 41% (MI group) to ≥ 55%. It is possible that differences might have emerged after 28 days, but it is more likely that the differences were small and therefore difficult to detect. It is arguable whether the difference between our treatment groups would be *clinically* significant, especially for CELLS vs SPHEROIDS (59% vs 64%, respectively, compared to the "healthy" baseline median of 66% for RAG1 mice before any intervention is done to them).

As well as providing clues as to inflammatory mechanisms, our transcriptomic analysis of mRNA from apical cardiac tissue samples throws up a fascinating discovery. It seems that the transcriptomic profile (gene regulation) was similar between mice having treatment with patches containing spheroids and sham mice (non-infarcted without a patch). As expected, the transcriptome of the MI group (infarcted without a patch treatment) was different to that of sham. This difference seemed to be restored /

returned to the "healthy" state represented by the non-infarcted sham mice. This suggests that genetic mechanisms may be important. Interestingly, the result was not seen for the mice receiving a patch without any cells (hydrogel only) nor for mice receiving a patch with cells freely suspended in hydrogel (not in spheroids). It is tempting to speculate that only the spheroid group induced a return to the "healthy" gene expression profile represented by sham mice. If so, this could be because the advantage of 3D culturing our human cardiac cells (as VCS, microtissues) manifested as an ability to restore the genetic expression profile to approach that of non-infarcted mice. The transcriptomic profile was that of the host mouse tissue underlying the patch containing human cells (not therefore the human cells themselves). It would require a dedicated study to examine this finding, but if true, it would add a new "story" to the story of innate immune responses being *the* mechanism, as others have argued it is (Vagnozzi et al., 2019).

As well as understanding the mechanism, translatability to patients relies on the practical consideration of how to transplant patches (Wang et al., 2021; Zhu et al., 2021). The two reviews undertaken as part of this thesis (Chapter 1.2 and 1.3) revealed that the field has been working towards a model of open cardiac surgery for the transplantation of patches to the heart. This is problematic because heart failure patients may not be fit for a traditional major incision to access the heart (such as a median sternotomy) but may be fit for a less invasive procedure (Moscarelli et al., 2021). Patients may also push back against having traditional open surgery, especially in a changing surgical landscape where more surgeries are done by robotic and/or minimally invasive approaches (Torregrossa & Balkhy, 2020). If patches suitable for clinical use are unveiled after decades of research, it is likely to be important that they can be transplanted by minimally invasive and robotic approaches and not just traditional open surgery. If patch transplant for heart failure is proposed as a standalone procedure, then it would be easier to justify if the method of transplantation carried as little risk of complication (pain, blood loss, infection, prolonged hospital stay, poor healing) as possible. If patch transplantation is to be proposed as an adjunct to a patient already having a cardiac procedure for another reason, then patches need to be compatible with the primary method of the patient's surgery (that is, if the patient is having a minimally invasive robotic procedure, you cannot realistically propose to "add on" a major open surgical incision). In this context, we invented minimally invasive robotic instruments to transplant patches to the heart surface. Since this whole approach is novel, we introduced it by publishing our preliminary brief research report (Chapter 3.2) and then published the full proof-of-concept study (Chapter 3.3). This early work is the first time this approach has been published and could potentially be an important moment if the field pivots from its focus on open surgery towards minimally invasive robotic approaches.

In terms of limitations, it is worth discussing some of the insights this thesis offers for the mouse model of MI we used. Different species of mice react differently to LAD ligation (van den Borne et al., 2009) and mice within the same experiment have different infarct sizes and patterns, with different effects on myocardial function. It is not known how this relates to human myocardial response to coronary artery blockage. Additionally, we showed that individual mice across all our experimental groups (including sham surgery) can present different cardiac function (LVEF%) progression from baseline to midpoint to endpoint in this protocol. This could reflect intrinsic variability in the LVEF%, some variability factor intrinsic to the protocol itself (such as passing a needle and suture through heart tissue under the LAD), or variability in measurement techniques (such as mouse echocardiography in the presence of adhesions after cardiac surgery).

Another important limitation is that only mice surviving to the end of the experiment contributed to our full set of day 28 analyses. Day 28 values may be influenced by attrition bias due to some mice dying in the operative or postoperative period. Our mortality rate of 44% was exactly the same as the literature rate for non-immune suppressed C57Bl/6 mice having LAD ligation without a patch (van den

Borne et al., 2009). The choice of male mice was based on a pilot study which determined that female mice and mice with body weight below 22g seemed to have higher mortality and abandonment rates from intubation of smaller tracheas (data not shown). We detected no difference in our protocol (or mortality rate) with immune competent C57Bl/6 mice compared to mature B and T cell deplete RAG1.Bl6 mice (data not shown). Future murine studies must choose their mouse model very carefully (ideally only using male mice with body weight over 22 g) and critical considerations include: 1) more severely immune suppressed mice such as NOD/SCID gamma are not required and so may be unethical; 2) immune competent BALB/c mice have a reported mortality rate of only 15% with a wall-thinning dominant pattern of ventricular response to MI(van den Borne et al., 2009) and these are available as T-cell depleted (BALB/c-Fox1nu) allowing for acceptance of xenografts, so therefore this strain may be preferable; and 3) different mouse strains may show different macrophage responses (C57Bl/6 show easier activation to produce M1 whereas Balb/c tend towards M2 polarisation (Orecchioni, Ghosheh, Pramod, & Ley, 2019) and there may be tissue specific responses as well (Bleul et al., 2021)) which should be evaluated carefully, especially for dedicated mechanistic studies. Overall, if carefully designed, murine studies for patch transplantation may have a place for mechanistic studies, new treatments and studies where feasibility and high numbers of repeats are important (Christopher D. Roche & Gentile, 2020).

4.3 – Future directions

Epicardial patch transplantation is not the only approach to restoring some of the cardiac function lost after MI (Chachques et al., 2020; MacQueen et al., 2018; Mattapally et al., 2018). It is possible that another approach may yield benefits, for example advances might be possible in ventricular assist devices, mechanical blood pumps, synthetic acellular patches, xenotransplantation, pharmaceuticals, preventative medicine, a new surgical technique or even biomaterial or cellular injection. These approaches are not necessarily mutually exclusive and there is no reason why they could not be combined.

It has been observed that the field of myocardial regeneration and cardiac tissue engineering may be particularly susceptible to ethical pitfalls such as media hyping of patient expectations (Cossu et al., 2018; Gilbert, O'Connell, Mladenovska, & Dodds, 2018). It is critical therefore that the field moves forward based on robust science and well-communicated messaging (Cossu et al., 2018). It is also critical to obtain a greater understanding of the mechanism behind the benefit of potential treatments (Vagnozzi et al., 2019). For instance, if the mechanism turns out to be stimulation of host inflammatory responses by applying foreign cells to the epicardium, then moving forward with strategies focused on cell number replenishment, electrochemical integration (contractility), vascularisation or mechanical reinforcement may be non-aligned with the underlying mechanism (Vagnozzi et al., 2019). This could result in significant resources being wasted and/or patients being subjected to mechanistically irrelevant procedures (Gilbert, Viana, O'Connell, & Dodds, 2018). If inflammation is shown to be a primary mechanism, then it might make no sense to strive for patient-specific tissue which would be immunocompatible and result in minimal inflammation. It might also make no sense to create biobanks of stored tissue and then select the closest match to the patient. Even the pursuit of vascularisation to keep patches “alive” by providing a blood supply (considered by many to be a *sine qua non* for cardiac tissue engineering) might become irrelevant. The only way to answer these questions is by focused mechanism-focused research. The immediate next step for this work is therefore a dedicated mechanistic study. That study should examine our contention that the mechanism relies on host immune cell changes combined with gene expression changes. Going forward, similar studies should incorporate the optimisation points from our mouse model (for example, using BALB/c-Fox1nu mice rather than RAG1 to potentially reduce the death rate and therefore minimise attrition bias).

This thesis has focused on heart failure following MI (ischaemic cardiomyopathy) but there are other causes of cardiac failure. It remains to be seen if other causes of reduced LVEF% (for example inherited cardiomyopathies, diastolic heart failure, rhythm disturbances, inflammation, drug-induced and so on) could benefit from this approach as well. This has not been explored and future studies should examine whether patches which have so far seemed to benefit MI-induced heart failure can be used in other-cause heart failure as well.

Our surgical instruments (detailed in Part 3) provide an important reminder to the field that it needs to keep one eye on the patients it intends to benefit. In other words, future studies should always consider translatability and the end goal of benefiting patients. In this way, it is arguable that all patches currently being developed should now be transplantable by minimally invasive (and/or robotic) methods. To out-pace alternative, sometimes directly competing, technologies, patch-based repair strategies will need to develop patches alongside transplantation techniques. Notably, Wang et al (2021) recently published a long-awaited study where they transplanted patches to the epicardium using a catheter in a minimally invasive (keyhole) procedure in mini-pigs (Wang et al., 2021). Using pig feasibility models, others have injected hydrogel into the pericardial space and allowed it to form a patch in situ (Zhu et al., 2021) and our own group (Roche et al, 2021) pioneered

the concept of robotic minimally invasive surgical approaches to epicardial patch transplantation (C. Roche et al., 2021). As well as a focus on mechanistic understanding (Cossu et al., 2018; Vagnozzi et al., 2019), which the mouse model presented herein can support (Christopher D. Roche & Gentile, 2020), the future for this therapeutic avenue for heart failure patients is likely to require that patches are transplanted by minimally invasive (and/or robotic) approaches (C. Roche et al., 2021). Without this, the field risks moving forward with patches designed for traditional open surgical approaches which might limit their useability and clinical translatability (C. Roche et al., 2021; Zhu et al., 2021). This is especially important given that other therapeutic approaches, such as ventricular pump devices, have also reached human feasibility trials ('Impella ECP Early Feasibility Study (ECP EFS)'; https://clinicaltrials.gov/ct2/show/NCT04477603). Given that media hype and over-statement of results is a particular ethical pitfall contributing to patient risk for this field (Cossu et al., 2018; Gilbert, O'Connell, et al., 2018; Gilbert, Viana, et al., 2018), it would be better to fully understand why patch-based myocardial regeneration treatments seem to work before transplanting them in human patients (Cossu et al., 2018; Vagnozzi et al., 2019). For those human patients, it would be optimal to transplant patches by the least invasive method possible (C. Roche et al., 2021; Wang et al., 2021).

In summary, for successful translation of epicardial patches, more understanding is needed. This includes understanding of the mechanism, the types of heart failure to which this treatment might be applied, and the practicalities of the transplantation method itself.

4.4 – Thesis conclusion

Epicardial transplantation of 3D bioprinted heart patches improves cardiac function in mice modelling MI. The use of VCS in alginate-gelatin bioink seems to offer an advantage compared to freely suspended cells or hydrogel alone. Hydrogel alone without cells confers some restoration of myocardial function suggesting that the mechanism is not fully accounted for by the cellular portion of the bioink. The inflammatory cell profile induced by hydrogel alone was similar to the cellular treatment groups, suggesting that innate immune responses were similar whether or not patches contained cells. By contrast, genetic changes were seen in the spheroid treatment group which were not seen for other groups and this group seemed to have the greatest improvement in LVEF%. Therefore the mechanism may have been related to both host immune cell changes and gene expression changes. Further studies are needed with a focus on the mechanism underlying the benefit of this approach. For translatability and to avoid redundant experimentation, patch development should work towards being compatible with robotic and/or minimally invasive transplantation.

4.5 – Thesis take home message

Transplanting a heart patch to the epicardium is a promising approach to restore some of the function lost after myocardial infarction. For this purpose, 3D bioprinted AlgGel patches containing VCS seem to offer an advantage compared to freely suspended cells or hydrogel alone. Many challenges remain before the dream can be realised of “on-demand repair” of the myocardium by patching it.

This thesis adds extensive analysis of the current challenges for the field (Part 1), a promising new approach using direct suspension of spheroids in bioink for 3D bioprinting of heart patches (Part 2) and a new proof-of-concept proposal for robotic minimally invasive transplantation of patches by cardiothoracic surgery (Part 3). This makes a significant contribution as a step towards the vision of heart patch transplant on demand as needed to protect the myocardium after infarction. For translation to the operating theatre, mechanisms need to be understood and the surgical method of transplantation optimised.

Appendix A1

Omentopexy may not be enough

Ismail Yurekli *, Mert Kestelli and Habib Cakir
Department of Cardiovascular Surgery, Izmir Ataturk Education and Research Hospital, Izmir, Turkey

Received 26 January 2021; accepted 1 March 2021

Keywords: Omentopexy • Cardiac regeneration

Congratulations to the authors for their effort in this interesting field of cardiac surgery. Some concerns raised in our heads after we read their article thoroughly. Table 1 makes a list of the associated studies with cardiac omentopexy. The investigated studies differ in terms of in vivo animal models, the coronary artery selected for occlusion to induce ischaemia, the time of intervention after induction of myocardial infarction and bioengineered cardiac tissue. These parameters are all different in each study. There is a lack of standardization, obviously.

There is another issue that we want to put emphasis on. Table 2 demonstrates the outcomes of engraftment. In the study by Kainuma *et al.*, the engrafted area shrinks two-fold from day 7 to day 28 in animals with omentopexy whereas it remains almost the same in control group (although smaller from the beginning) throughout this period. Likewise, Lilyanna *et al.* found that 'donor cell attrition rate in vivo over time comparable with or without omentum support' in their bioluminescence photon emission flux of labelled live donor cells with minimal difference in scar with or without omentum support [1]. These findings demonstrated that it seems to be pretentious to claim that '. . .this promising tissue may boost progress in cardiac regeneration'. Nevertheless, this technique is promising but should be modified or supported with some medications.

Reference

[1] Wang H, Roche CD, Gentile C. Omentum support for cardiac regeneration in ischaemic cardiomyopathy models: a systematic scoping review. Eur J Cardiothorac Surg. 2020;58:1118–1129.

* Corresponding author. 6436 Sok 82/3, Karsiyaka, Izmir 35540, Turkey. Tel: +90-505-5251202; fax: +90-232-2431530; e-mail: ismoyurekli@yahoo.com (I. Yurekli).

doi:10.1093/ejcts/ezab159

Appendix A2

European Journal of Cardio-Thoracic Surgery 00 (2021) 1–1

Reply to Yurekli *et al.*

Hogan Wang [a], **Christopher D. Roche** [a,b,c,d] **and Carmine Gentile** [a,c,*]

[a] Northern Clinical School of Medicine, University of Sydney, Kolling Institute, St Leonards, Sydney, NSW, Australia
[b] Department of Cardiothoracic Surgery, Royal North Shore Hospital, St Leonards, Sydney, NSW, Australia
[c] School of Biomedical Engineering, Faculty of Engineering and IT, University of Technology Sydney (UTS), Ultimo, Sydney, NSW, Australia
[d] Department of Cardiothoracic Surgery, University Hospital of Wales, Cardiff, UK

Received 19 February 2021; accepted 1 March 2021

Keywords: Omentum • Cardiac regeneration • Omental flap • Omentopexy • In vivo models • Vascularization

We would like to express our thanks for your correspondence [1] about our article: *Omentum support for cardiac regeneration in ischaemic cardiomyopathy models: a systematic scoping review* [2] and for this opportunity to reply.

In our article, we addressed the following question: what potential effects may the omentum have *as a supporting tissue* for bioengineered myocardial regeneration? The scoping review included a heterogenous set of 11 studies, consistent with current techniques in myocardial regeneration and bioengineering research [3]. Six additional studies were separated out into Tables 5 and 6 (as they were too different to be comparable).

It was our utmost interest to ensure we were able to analyse these studies using the most unbiased criteria. Despite the heterogeneity of the approaches used, we were still able to compare the effects of a pedicled omental flap as support for bioengineering aimed at myocardial regeneration—according to reported findings of each study (regardless of the exact bioengineering technique used). It is *because* of the heterogenous nature of the studies, not despite it, that a systematic *scoping* review was chosen as the method to assess whether the wide variety of techniques anticipated by our search criteria might benefit from omental reinforcement. We are therefore confident that we addressed the central question regarding these studies, which could also be re-stated as: 'is the use of a pedicled omental flap a promising adjunct for bioengineering approaches to myocardial regeneration (based on the existing literature)?'.

Regarding your comment about the study by Kainuma *et al.* [4] and the engrafted area (Table 2) [2]; we compared the effects at day 7 and day 28 (similar intervals to those presented in many other studies). We do acknowledge that at day 3, there was not a statistically significant effect—engrafted area remaining of 0.35 mm^2 with omentum support and 0.25 mm^2 without [4]. Graphical representation of this (Figure 3h of the original article) [4] makes it clear that the omentum-supported myoblast cell sheets had a more gradual loss of donor cells (reducing engraftment area) up to day 28. In contrast, without omentum support, there was a steep drop off of donor cells (engrafted area) before day 7. The starting number (on 'day zero') of labelled donor cells was similar in all their bioengineered cell sheet groups. These effects were statistically significant only by day 7 and persisted until day 28, with the absolute numbers clearly favouring omentum support.

Regarding the study by Lilyanna *et al.* [5], this was the *only* study we found reporting that omentum support did not result in an increase in cell retention. We emphasized this in our paragraph titled 'Transplanted Cell Retention' where we concluded that most studies presented improved engraftment outcomes with supportive omentopexy, except for this one.

We would like to acknowledge the importance of your comments, especially your mention of modification with 'some medications', which in the tissue engineering space may be extended to signalling factors, cells and biomaterials. In summary, we agree that omentopexy alone may be insufficient based on the current literature, but *as a support* for bioengineered tissue, it may help for the translation of findings from the bench to the bedside.

REFERENCES

[1] Yurekli I, Kestelli M, Cakir H. Omentopexy may not be enough. Eur J Cardiothorac Surg 2021; doi:10.1093/ejcts/ezab159.
[2] Wang H, Roche C, Gentile C. Omentum support for cardiac regeneration in ischaemic cardiomyopathy models: a systematic scoping review. Eur J Cardiothorac Surg 2020;58:1118–29.
[3] Roche CD, Brereton RJL, Ashton AW, Jackson C, Gentile C. Current challenges in three-dimensional bioprinting heart tissues for cardiac surgery. Eur J Cardiothorac Surg 2020; doi:10.1093/ejcts/ezaa093.
[4] Kainuma S, Miyagawa S, Fukushima S, Pearson J, Chen YC, Saito A *et al.* Cell-sheet therapy with omentopexy promotes arteriogenesis and improves coronary circulation physiology in failing heart. Mol Ther 2015;23:374–86.
[5] Lilyanna S, Martinez EC, Vu TD, Ling LH, Gan SU, Tan AL *et al.* Cord lining-mesenchymal stem cells graft supplemented with an omental flap induces myocardial revascularization and ameliorates cardiac dysfunction in a rat model of chronic ischemic heart failure. Tissue Eng Part A 2013;19:1303–15.

* Corresponding author. Building 11, Level 10, Room 115, School of Biomedical Engineering, Faculty of Engineering and IT, 81 Broadway St, Ultimo, NSW 2007, Australia. Tel: +61-2-95144502; e-mail: carmine.gentile@uts.edu.au (C. Gentile).

doi:10.1093/ejcts/ezab152

Bibliography

Abad M, Mosteiro L, Pantoja C, Canamero M, Rayon T, Ors I, et al. Reprogramming in vivo produces teratomas and iPS cells with totipotency features. Nature. 2013;502(7471):340-5.

Abbasalizadeh S, Larijani MR, Samadian A, Baharvand H. Bioprocess development for mass production of size-controlled human pluripotent stem cell aggregates in stirred suspension bioreactor. Tissue Eng Part C Methods. 2012;18(11):831-51.

Adler CP, Costabel U. Cell number in human heart in atrophy, hypertrophy, and under the influence of cytostatics. Recent Adv Stud Cardiac Struct Metab. 1975;6:343-55.

Alonzo M, AnilKumar S, Roman B, Tasnim N, Joddar B. 3D Bioprinting of cardiac tissue and cardiac stem cell therapy. Transl Res. 2019;211:64-83.

Alvarez-Argote S, O'Meara CC. The evolving roles of cardiac macrophages in homeostasis, regeneration, and repair. Int J Mol Sci. 2021;22(15).

Amano Y, Nishiguchi A, Matsusaki M, Iseoka H, Miyagawa S, Sawa Y, et al. Development of vascularized iPSC derived 3D-cardiomyocyte tissues by filtration Layer-by-Layer technique and their application for pharmaceutical assays. Acta Biomater. 2016;33:110-21.

Asai H, Shingu Y, Yamakawa T, Niwano H, Wakasa S, Ooka T, et al. Left-Ventricular Plication Reduces Wall Stress and Cardiomyocyte Hypertrophy in a Rat Model of Ischemic Cardiomyopathy. European surgical research Europaische chirurgische Forschung Recherches chirurgicales europeennes. 2017;58(1-2):69-80.

Ascheim DD, Gelijns AC, Goldstein D, Moye LA, Smedira N, Lee S, et al. Mesenchymal precursor cells as adjunctive therapy in recipients of contemporary left ventricular assist devices. Circulation. 2014;129(22):2287-96.

Bai W, Cao Q, Wang P, Chen P, Leng C, Pan T. Modular design of a teleoperated robotic control system for laparoscopic minimally invasive surgery based on ROS and RT-Middleware. Ind Rob. 2017;44(5):596-608.

Barth AS, Zhang Y, Li T, Smith RR, Chimenti I, Terrovitis I, et al. Functional impairment of human resident cardiac stem cells by the cardiotoxic antineoplastic agent trastuzumab. Stem Cells Transl Med. 2012;1(4):289-97.

Bartulos O, Zhuang ZW, Huang Y, Mikush N, Suh C, Bregasi A, et al. ISL1 cardiovascular progenitor cells for cardiac repair after myocardial infarction. JCI Insight. 2016;1(10).

Batista RJ. Reduction ventriculoplasty. Z Kardiol. 2001;90 Suppl 1:35-7.

Beauchamp P, Moritz W, Kelm JM, Ullrich ND, Agarkova I, Anson BD, et al. Development and Characterization of a Scaffold-Free 3D Spheroid Model of Induced Pluripotent Stem Cell-Derived Human Cardiomyocytes. Tissue Eng Part C Methods. 2015;21(8):852-61.

Bejleri D, Streeter BW, Nachlas ALY, Brown ME, Gaetani R, Christman KL, et al. A Bioprinted Cardiac Patch Composed of Cardiac-Specific Extracellular Matrix and Progenitor Cells for Heart Repair. Adv Healthc Mater. 2018;7(23):e1800672.

Bergmann O, Zdunek S, Felker A, Salehpour M, Alkass K, Bernard S, et al. Dynamics of cell generation and turnover in the human heart. Cell. 2015;161(7):1566-75.

Beyersdorf F. Three-dimensional bioprinting: new horizon for cardiac surgery. Eur J Cardiothorac Surg. 2014;46(3):339-41.

Bishop ES, Mostafa S, Pakvasa M, Luu HH, Lee MJ, Wolf JM, et al. 3-D bioprinting technologies in tissue engineering and regenerative medicine: current and future trends. Genes Dis. 2017;4(4):185-95.

Blaeser A, Duarte Campos DF, Puster U, Richtering W, Stevens MM, Fischer H. Controlling shear stress in 3D bioprinting is a key factor to balance printing resolution and stem cell integrity. Adv Healthc Mater. 2016;5(3):326-33.

Blakely AM, Manning KL, Tripathi A, Morgan JR. Bio-Pick, Place, and Perfuse: A New Instrument for Three-Dimensional Tissue Engineering. Tissue Eng Part C Methods. 2015;21(7):737-46.

Bleul T, Zhuang X, Hildebrand A, Lange C, Böhringer D, Schlunck G, et al. Different innate immune responses in BALB/c and C57BL/6 strains following corneal transplantation. Journal of Innate Immunity. 2021;13(1):49-59.

Blinova K, Schocken D, Patel D, Daluwatte C, Vicente J, Wu JC, et al. Clinical Trial in a Dish: Personalized Stem Cell-Derived Cardiomyocyte Assay Compared With Clinical Trial Results for Two QT-Prolonging Drugs. Clin Transl Sci. 2019.

Bociaga D, Bartniak M, Grabarczyk J, Przybyszewska K. Sodium alginate/gelatine hydrogels for direct bioprinting-the effect of composition selection and applied solvents on the bioink properties. Materials. 2019;12(17):2669.

Bohl S, Medway DJ, Schulz-Menger J, Schneider JE, Neubauer S, Lygate CA. Refined approach for quantification of in vivo ischemia-reperfusion injury in the mouse heart. American journal of physiology Heart and circulatory physiology. 2009;297(6):H2054-H8.

Bulanova EA, Koudan EV, Degosserie J, Heymans C, Pereira FD, Parfenov VA, et al. Bioprinting of a functional vascularized mouse thyroid gland construct. Biofabrication. 2017;9(3):034105.

Bursac N, Papadaki M, Cohen RJ, Schoen FJ, Eisenberg SR, Carrier R, et al. Cardiac muscle tissue engineering: toward an in vitro model for electrophysiological studies. Am J Physiol. 1999;277(2):H433-44.

Bursac N, Parker KK, Iravanian S, Tung L. Cardiomyocyte cultures with controlled macroscopic anisotropy: a model for functional electrophysiological studies of cardiac muscle. Circ Res. 2002;91(12):e45-54.

Butcher JT, Penrod AM, Garcia AJ, Nerem RM. Unique morphology and focal adhesion development of valvular endothelial cells in static and fluid flow environments. Arterioscler Thromb Vasc Biol. 2004;24(8):1429-34.

Campbell M, Chabria M, Figtree GA, Polonchuk L, Gentile C. Stem cell-derived cardiac spheroids as 3D in vitro models of the human heart microenvironment. In: Walker J, editor. Methods in Molecular Biology. 2018/08/31 ed: Humana Press; 2018. p. 1-9.

Campbell M, Surija L, Peceros K, Sharma P, Figtree G, Gentile C. Stem cell spheroids. In: Reis RL, editor. Encyclopedia of Tissue Engineering and Regenerative Medicine. Oxford: Academic Press; 2019. p. 387-93.

Cashman TJ, Josowitz R, Johnson BV, Gelb BD, Costa KD. Human Engineered Cardiac Tissues Created Using Induced Pluripotent Stem Cells Reveal Functional Characteristics of BRAF-Mediated Hypertrophic Cardiomyopathy. PLoS One. 2016;11(1):e0146697.

Cattelan G, Guerrero Gerbolés A, Foresti R, Pramstaller PP, Rossini A, Miragoli M, et al. Alginate formulations: current developments in the race for hydrogel-based cardiac regeneration. Frontiers in Bioengineering and Biotechnology. 2020;8(414).

Chachques JC, Gardin C, Lila N, Ferroni L, Migonney V, Falentin-Daudre C, et al. Elastomeric cardiowrap scaffolds functionalized with mesenchymal stem cells-derived exosomes induce a positive modulation in the inflammatory and wound healing response of mesenchymal stem cell and macrophage. Biomedicines. 2021;9(7).

Chachques JC, Lila N, Soler-Botija C, Martinez-Ramos C, Valles A, Autret G, et al. Elastomeric cardiopatch scaffold for myocardial repair and ventricular support. Eur J Cardiothorac Surg. 2020;57(3):545-55.

Chachques JC, Trainini JC, Lago N, Masoli OH, Barisani JL, Cortes-Morichetti M, et al. Myocardial assistance by grafting a new bioartificial upgraded myocardium (MAGNUM clinical trial): one year follow-up. Cell Transplant. 2007;16(9):927-34.

Chakravarty T, Makkar RR, Ascheim DD, Traverse JH, Schatz R, DeMaria A, et al. ALLogeneic Heart STem Cells to Achieve Myocardial Regeneration (ALLSTAR) Trial: Rationale and Design. Cell Transplant. 2017;26(2):205-14.

Chang R, Nam J, Sun W. Effects of dispensing pressure and nozzle diameter on cell survival from solid freeform fabrication–based direct cell writing. Tissue Engineering Part A. 2008;14(1):41-8.

Chaudhry SP, Stewart GC. New pharmacological and technological management strategies in heart failure. Vascular health and risk management. 2017;13:111-21.

Chen L, Pan Y, Zhang L, Wang Y, Weintraub N, Tang Y. Two-step protocol for isolation and culture of cardiospheres. Methods Mol Biol. 2013;1036:75-80.

Cheng G, Liao S, Kit Wong H, Lacorre DA, di Tomaso E, Au P, et al. Engineered blood vessel networks connect to host vasculature via wrapping-and-tapping anastomosis. Blood. 2011;118(17):4740-9.

Chimenti I, Gaetani R, Barile L, Forte E, Ionta V, Angelini F, et al. Isolation and expansion of adult cardiac stem/progenitor cells in the form of cardiospheres from human cardiac biopsies and murine hearts. Methods Mol Biol. 2012;879:327-38.

Chimenti I, Gaetani R, Forte E, Angelini F, De Falco E, Zoccai GB, et al. Serum and supplement optimization for EU GMP-compliance in cardiospheres cell culture. J Cell Mol Med. 2014;18(4):624-34.

Chimenti I, Massai D, Morbiducci U, Beltrami AP, Pesce M, Messina E. Stem Cell Spheroids and Ex Vivo Niche Modeling: Rationalization and Scaling-Up. J Cardiovasc Transl Res. 2017;10(2):150-66.

Chong JJ, Yang X, Don CW, Minami E, Liu YW, Weyers JJ, et al. Human embryonic-stem-cell-derived cardiomyocytes regenerate non-human primate hearts. Nature. 2014;510(7504):273-7.

Choudhury D, Anand S, Naing MW. The arrival of commercial bioprinters - Towards 3D bioprinting revolution! International Journal of Bioprinting. 2018;4(2).

Christoffersson J, Meier F, Kempf H, Schwanke K, Coffee M, Beilmann M, et al. A Cardiac Cell Outgrowth Assay for Evaluating Drug Compounds Using a Cardiac Spheroid-on-a-Chip Device. Bioengineering (Basel). 2018;5(2).

Cossu G, Birchall M, Brown T, De Coppi P, Culme-Seymour E, Gibbon S, et al. Lancet Commission: stem cells and regenerative medicine. Lancet. 2018;391(10123):883-910.

Cowie MR, Wood DA, Coats AJ, Thompson SG, Suresh V, Poole-Wilson PA, et al. Survival of patients with a new diagnosis of heart failure: a population based study. Heart. 2000;83(5):505-10.

Crean PA, Pratt T, Davies GJ, Myers M, Lavender P, Maseri A. The fractional distribution of the cardiac output in man using microspheres labelled with technetium 99m. Br J Radiol. 1986;59(699):209-15.

Crew B. Worth the cost? A closer look at the da Vinci robot's impact on prostate cancer surgery. Nature. 2020;580:S5.

Cui H, Miao S, Esworthy T, Zhou X, Lee SJ, Liu C, et al. 3D bioprinting for cardiovascular regeneration and pharmacology. Advanced drug delivery reviews. 2018.

Cui H, Zhu W, Huang Y, Liu C, Yu ZX, Nowicki M, et al. In vitro and in vivo evaluation of 3D bioprinted small-diameter vasculature with smooth muscle and endothelium. Biofabrication. 2019;12(1):015004.

Curfman G. Stem cell therapy for heart failure: an unfulfilled promise? JAMA. 2019;321(12):1186-7.

Davis DR, Zhang Y, Smith RR, Cheng K, Terrovitis J, Malliaras K, et al. Validation of the cardiosphere method to culture cardiac progenitor cells from myocardial tissue. PLoS One. 2009;4(9):e7195.

De Bank PA, Hou Q, Warner RM, Wood IV, Ali BE, Macneil S, et al. Accelerated formation of multicellular 3-D structures by cell-to-cell cross-linking. Biotechnol Bioeng. 2007;97(6):1617-25.

Derakhshanfar S, Mbeleck R, Xu K, Zhang X, Zhong W, Xing M. 3D bioprinting for biomedical devices and tissue engineering: a review of recent trends and advances. Bioact Mater. 2018;3(2):144-56.

Díaz CE, Fernández R, Armada M, García Gutiérrez FdJ. State of the art in robots used in minimally invasive surgeries. Natural Orifice Transluminal Surgery (NOTES) as a particular case. Industrial Robot: An International Journal. 2015;42(6):508-32.

DiMasi JA, Feldman L, Seckler A, Wilson A. Trends in Risks Associated With New Drug Development: Success Rates for Investigational Drugs. Clinical Pharmacology & Therapeutics. 2010;87(3):272-7.

Domenech M, Polo-Corrales L, Ramirez-Vick JE, Freytes DO. Tissue engineering strategies for myocardial regeneration: acellular versus cellular scaffolds? Tissue Eng Part B Rev. 2016;22(6):438-58.

Dor V, Saab M, Coste P, Kornaszewska M, Montiglio F. Left ventricular aneurysm: a new surgical approach. Thorac Cardiovasc Surg. 1989;37(1):11-9.

Duan B. State-of-the-Art Review of 3D Bioprinting for Cardiovascular Tissue Engineering. Annals of biomedical engineering. 2017;45(1):195-209.

Dunn KK, Reichardt IM, Simmons AD, Jin G, Floy ME, Hoon KM, et al. Coculture of Endothelial Cells with Human Pluripotent Stem Cell-Derived Cardiac Progenitors Reveals a Differentiation Stage-Specific Enhancement of Cardiomyocyte Maturation. Biotechnol J. 2019:e1800725.

Dvir T, Kedem A, Ruvinov E, Levy O, Freeman I, Landa N, et al. Prevascularization of cardiac patch on the omentum improves its therapeutic outcome. Proc Natl Acad Sci U S A. 2009;106(35):14990-5.

Dvir T, Timko BP, Brigham MD, Naik SR, Karajanagi SS, Levy O, et al. Nanowired three-dimensional cardiac patches. Nat Nanotechnol. 2011;6(11):720-5.

Ebert SN, Taylor DG, Nguyen HL, Kodack DP, Beyers RJ, Xu Y, et al. Noninvasive tracking of cardiac embryonic stem cells in vivo using magnetic resonance imaging techniques. Stem Cells. 2007;25(11):2936-44.

Edri R, Gal I, Noor N, Harel T, Fleischer S, Adadi N, et al. Personalized hydrogels for engineering diverse fully autologous tissue implants. Adv Mater. 2019;31(1):e1803895.

Eglen RM, Reisine T. Human iPS Cell-Derived Patient Tissues and 3D Cell Culture Part 2: Spheroids, Organoids, and Disease Modeling. SLAS Technol. 2019;24(1):18-27.

Ehler E, Moore-Morris T, Lange S. Isolation and culture of neonatal mouse cardiomyocytes. J Vis Exp. 2013(79):50154.

El-Battrawy I, Albers S, Cyganek L, Zhao Z, Lan H, Li X, et al. A cellular model of Brugada syndrome with SCN10A variants using human-induced pluripotent stem cell-derived cardiomyocytes. Europace. 2019.

Elliott NT, Yuan F. A review of three-dimensional in vitro tissue models for drug discovery and transport studies. J Pharm Sci. 2011;100(1):59-74.

Engler AJ, Sen S, Sweeney HL, Discher DE. Matrix elasticity directs stem cell lineage specification. Cell. 2006;126(4):677-89.

Eschenhagen T, Didie M, Munzel F, Schubert P, Schneiderbanger K, Zimmermann WH. 3D engineered heart tissue for replacement therapy. Basic Res Cardiol. 2002;97 Suppl 1:I146-52.

Fan Z, Xu Z, Niu H, Gao N, Guan Y, Li C, et al. An Injectable Oxygen Release System to Augment Cell Survival and Promote Cardiac Repair Following Myocardial Infarction. Sci Rep. 2018;8(1):1371.

Fennema E, Rivron N, Rouwkema J, van Blitterswijk C, de Boer J. Spheroid culture as a tool for creating 3D complex tissues. Trends Biotechnol. 2013;31(2):108-15.

Figtree GA, Bubb KJ, Tang O, Kizana E, Gentile C. Vascularized cardiac spheroids as novel 3D in vitro models to study cardiac fibrosis. Cells Tissues Organs. 2017;204(3-4):191-8.

Fisch P, Holub M, Zenobi-Wong M. Improved accuracy and precision of bioprinting through progressive cavity pump-controlled extrusion. bioRxiv. 2020:2020.01.23.915868.

Fleming PA, Argraves WS, Gentile C, Neagu A, Forgacs G, Drake CJ. Fusion of uniluminal vascular spheroids: a model for assembly of blood vessels. Dev Dyn. 2010;239(2):398-406.

Forsythe SD, Devarasetty M, Shupe T, Bishop C, Atala A, Soker S, et al. Environmental Toxin Screening Using Human-Derived 3D Bioengineered Liver and Cardiac Organoids. Front Public Health. 2018;6:103.

Foty R. A simple hanging drop cell culture protocol for generation of 3D spheroids. J Vis Exp. 2011;6(51):2720.

Freed LE, Langer R, Martin I, Pellis NR, Vunjak-Novakovic G. Tissue engineering of cartilage in space. Proc Natl Acad Sci U S A. 1997;94(25):13885-90.

Frey O, Misun PM, Fluri DA, Hengstler JG, Hierlemann A. Reconfigurable microfluidic hanging drop network for multi-tissue interaction and analysis. Nat Commun. 2014;5:4250.

Fu CY, Tseng SY, Yang SM, Hsu L, Liu CH, Chang HY. A microfluidic chip with a U-shaped microstructure array for multicellular spheroid formation, culturing and analysis. Biofabrication. 2014;6(1):015009.

Fujimoto KL, Tobita K, Merryman WD, Guan J, Momoi N, Stolz DB, et al. An elastic, biodegradable cardiac patch induces contractile smooth muscle and improves cardiac remodeling and function in subacute myocardial infarction. J Am Coll Cardiol. 2007;49(23):2292-300.

Gahwiler BH. Nerve cells in culture: the extraordinary discovery by Ross Granville Harrison. Brain Res Bull. 1999;50(5-6):343-4.

Gao L, Gregorich ZR, Zhu W, Mattapally S, Oduk Y, Lou X, et al. Large cardiac muscle patches engineered from human induced-pluripotent stem cell-derived cardiac cells improve recovery from myocardial infarction in swine. Circulation. 2018;137(16):1712-30.

Gentile C. Filling the gaps between the in vivo and in vitro microenvironment: engineering of spheroids for stem cell technology. Curr Stem Cell Res Ther. 2016;11(8):652-65.

Gettler BC, Zakhari JS, Gandhi PS, Williams SK. Formation of Adipose Stromal Vascular Fraction Cell-Laden Spheroids Using a Three-Dimensional Bioprinter and Superhydrophobic Surfaces. Tissue Eng Part C Methods. 2017;23(9):516-24.

GhavamiNejad A, Ashammakhi N, Wu XY, Khademhosseini A. Crosslinking strategies for 3D bioprinting of polymeric hydrogels. Small. 2020;16(35):2002931.

Ghosh D, Mehta N, Patil A, Sengupta J. Ethical issues in biomedical use of human embryonic stem cells (hESCs). Journal of Reproductive Health and Medicine. 2016;2:S37-S47.

Giannopoulos AA, Mitsouras D, Yoo SJ, Liu PP, Chatzizisis YS, Rybicki FJ. Applications of 3D printing in cardiovascular diseases. Nature reviews Cardiology. 2016;13(12):701-18.

Gilbert F, O'Connell CD, Mladenovska T, Dodds S. Print me an organ? Ethical and regulatory issues emerging from 3D bioprinting in medicine. Sci Eng Ethics. 2018;24(1):73-91.

Gilbert F, Viana JNM, O'Connell CD, Dodds S. Enthusiastic portrayal of 3D bioprinting in the media: ethical side effects. Bioethics. 2018;32(2):94-102.

Gillispie G, Prim P, Copus J, Fisher J, Mikos AG, Yoo JJ, et al. Assessment methodologies for extrusion-based bioink printability. Biofabrication. 2020;12(2):022003-.

Gnecchi M, He H, Liang OD, Melo LG, Morello F, Mu H, et al. Paracrine action accounts for marked protection of ischemic heart by Akt-modified mesenchymal stem cells. Nat Med. 2005;11(4):367-8.

Goldfracht I, Efraim Y, Shinnawi R, Kovalev E, Huber I, Gepstein A, et al. Engineered heart tissue models from hiPSC-derived cardiomyocytes and cardiac ECM for disease modeling and drug testing applications. Acta Biomater. 2019;92:145-59.

Goldstein TA, Epstein CJ, Schwartz J, Krush A, Lagalante DJ, Mercadante KP, et al. Feasibility of bioprinting with a modified desktop 3D printer. Tissue Eng Part C Methods. 2016;22(12):1071-6.

Gong R, Jiang Z, Zagidullin N, Liu T, Cai B. Regulation of cardiomyocyte fate plasticity: a key strategy for cardiac regeneration. Signal Transduct Target Ther. 2021;6(1):31.

Groll J, Boland T, Blunk T, Burdick JA, Cho DW, Dalton PD, et al. Biofabrication: reappraising the definition of an evolving field. Biofabrication. 2016;8(1):013001.

Gu Z, Fu J, Lin H, He Y. Development of 3D bioprinting: from printing methods to biomedical applications. Asian J Pharm Sci. 2019.

Güllü AÜ, Şenay Ş, Ersin E, Demirhisar Ö, Kocyigit M, Alhan C. Feasibility of robotic-assisted atrial septal defect repair in a 6-year-old patient. Int J Med Robot. 2021;17(2):e2185.

Guo Y, Pu WT. Cardiomyocyte maturation. Circ Res. 2020;126(8):1086-106.

Gutierrez-Aranda I, Ramos-Mejia V, Bueno C, Munoz-Lopez M, Real PJ, Mácia A, et al. Human induced pluripotent stem cells develop teratoma more efficiently and faster than human embryonic stem cells regardless the site of injection. Stem Cells. 2010;28(9):1568-70.

Halbert SP, Bruderer R, Lin TM. In vitro organization of dissociated rat cardiac cells into beating three-dimensional structures. J Exp Med. 1971;133(4):677-95.

Hancock PC, Koduru SV, Sun M, Ravnic DJ. Induction of scaffold angiogenesis by recipient vasculature precision micropuncture. Microvascular Research. 2021;134:104121.

Hansen A, Eder A, Bonstrup M, Flato M, Mewe M, Schaaf S, et al. Development of a drug screening platform based on engineered heart tissue. Circ Res. 2010;107(1):35-44.

Harary I, Farley B. In vitro studies of single isolated beating heart cells. Science. 1960;131(3414):1674-5.

Hatzistergos KE, Selem S, Balkan W, Hare JM. Chapter 17 - Cardiac stem cells: biology and therapeutic applications. In: Atala A, Lanza R, Mikos AG, Nerem R, editors. Principles of Regenerative Medicine (Third Edition). Boston: Academic Press; 2019. p. 247-72.

Hauton D, Winter J, Al-Shammari AA, Gaffney EA, Evans RD, Egginton S. Changes to both cardiac metabolism and performance accompany acute reductions in functional capillary supply. Biochim Biophys Acta. 2015;1850(4):681-90.

Hayakawa T, Kunihiro T, Ando T, Kobayashi S, Matsui E, Yada H, et al. Image-based evaluation of contraction-relaxation kinetics of human-induced pluripotent stem cell-derived cardiomyocytes: Correlation and complementarity with extracellular electrophysiology. J Mol Cell Cardiol. 2014;77:178-91.

He Y, Hou H, Wang S, Lin R, Wang L, Yu L, et al. From waste of marine culture to natural patch in cardiac tissue engineering. Bioactive Materials. 2021;6(7):2000-10.

Hedegaard CL, Collin EC, Redondo-Gómez C, Nguyen LTH, Ng KW, Castrejón-Pita AA, et al. Hydrodynamically Guided Hierarchical Self-Assembly of Peptide–Protein Bioinks. Advanced Functional Materials. 2018;28(16):1703716.

Helmy KY, Patel SA, Silverio K, Pliner L, Rameshwar P. Stem cells and regenerative medicine: accomplishments to date and future promise. Ther Deliv. 2010;1(5):693-705.

Hirsch JE. An index to quantify an individual's scientific research output. Proceedings of the National Academy of Sciences of the United States of America. 2005;102(46):16569-72.

Hirt MN, Boeddinghaus J, Mitchell A, Schaaf S, Bornchen C, Muller C, et al. Functional improvement and maturation of rat and human engineered heart tissue by chronic electrical stimulation. J Mol Cell Cardiol. 2014;74:151-61.

Ho JY, Hendi AS. Recent trends in life expectancy across high income countries: retrospective observational study. BMJ (Clinical research ed). 2018;362:k2562.

Hobbs FD, Roalfe AK, Davis RC, Davies MK, Hare R. Prognosis of all-cause heart failure and borderline left ventricular systolic dysfunction: 5 year mortality follow-up of the Echocardiographic Heart of England Screening Study (ECHOES). Eur Heart J. 2007;28(9):1128-34.

Hookway TA, Butts JC, Lee E, Tang H, McDevitt TC. Aggregate formation and suspension culture of human pluripotent stem cells and differentiated progeny. Methods. 2016;101:11-20.

Hourd P, Medcalf N, Segal J, Williams DJ. A 3D bioprinting exemplar of the consequences of the regulatory requirements on customized processes. Regen Med. 2015;10(7):863-83.

Hsiao AY, Tung YC, Kuo CH, Mosadegh B, Bedenis R, Pienta KJ, et al. Micro-ring structures stabilize microdroplets to enable long term spheroid culture in 384 hanging drop array plates. Biomed Microdevices. 2012;14(2):313-23.

Hsiao AY, Tung YC, Qu X, Patel LR, Pienta KJ, Takayama S. 384 hanging drop arrays give excellent Z-factors and allow versatile formation of co-culture spheroids. Biotechnol Bioeng. 2012;109(5):1293-304.

Huang NF, Serpooshan V, Morris VB, Sayed N, Pardon G, Abilez OJ, et al. Big bottlenecks in cardiovascular tissue engineering. Commun Biol. 2018;1:199.

Huang S, Yang Y, Yang Q, Zhao Q, Ye X. Engineered circulatory scaffolds for building cardiac tissue. J Thorac Dis. 2018;10(Suppl 20):S2312-s28.

Huang Y, Hunyor SN, Jiang L, Kawaguchi O, Shirota K, Ikeda Y, et al. Remodeling of the chronic severely failing ischemic sheep heart after coronary microembolization: functional, energetic, structural, and cellular responses. Am J Physiol Heart Circ Physiol. 2004;286(6):H2141-50.

Huebsch N, Loskill P, Deveshwar N, Spencer CI, Judge LM, Mandegar MA, et al. Miniaturized iPS-Cell-Derived Cardiac Muscles for Physiologically Relevant Drug Response Analyses. Sci Rep. 2016;6:24726.

Ibrahim AG, Cheng K, Marban E. Exosomes as critical agents of cardiac regeneration triggered by cell therapy. Stem Cell Reports. 2014;2(5):606-19.

Itzhaki I, Maizels L, Huber I, Zwi-Dantsis L, Caspi O, Winterstern A, et al. Modelling the long QT syndrome with induced pluripotent stem cells. Nature. 2011;471(7337):225-9.

Jakab K, Norotte C, Damon B, Marga F, Neagu A, Besch-Williford CL, et al. Tissue engineering by self-assembly of cells printed into topologically defined structures. Tissue Eng Part A. 2008;14(3):413-21.

Jana T, Khabbaz E, Bush CM, Prosser JD, Birchall MA, Nichols CA, et al. The body as a living bioreactor: a feasibility study of pedicle flaps for tracheal transplantation. Eur Arch Otorhinolaryngol. 2013;270(1):181-6.

Jatene AD. Left ventricular aneurysmectomy. Resection or reconstruction. J Thorac Cardiovasc Surg. 1985;89(3):321-31.

Ji S, Guvendiren M. Recent Advances in Bioink Design for 3D Bioprinting of Tissues and Organs. Front Bioeng Biotechnol. 2017;5:23.

Jiang L, Gentile C, Lauto A, Cui C, Song Y, Romeo T, et al. Versatile fabrication approach of conductive hydrogels via copolymerization with vinyl monomers. ACS Appl Mater Interfaces. 2017;9(50):44124-33.

Kainuma S, Miyagawa S, Fukushima S, Pearson J, Chen YC, Saito A, et al. Cell-sheet therapy with omentopexy promotes arteriogenesis and improves coronary circulation physiology in failing heart. Mol Ther. 2015;23(2):374-86.

Kalmykov A, Huang C, Bliley J, Shiwarski D, Tashman J, Abdullah A, et al. Organ-on-e-chip: Three-dimensional self-rolled biosensor array for electrical interrogations of human electrogenic spheroids. Sci Adv. 2019;5(8):eaax0729.

Kang C, Qiao Y, Li G, Baechle K, Camelliti P, Rentschler S, et al. Human Organotypic Cultured Cardiac Slices: New Platform For High Throughput Preclinical Human Trials. Scientific Reports. 2016;6:28798.

Kant RJ, Coulombe KLK. Integrated approaches to spatiotemporally directing angiogenesis in host and engineered tissues. Acta Biomater. 2018;69:42-62.

Katt ME, Placone AL, Wong AD, Xu ZS, Searson PC. In vitro tumor models: advantages, disadvantages, variables, and selecting the right platform. Front Bioeng Biotechnol. 2016;4.

Kawaguchi H. Micro hydrogels: preparation, properties, and applications. J Oleo Sci. 2013;62(11):865-71.

Kawaguchi N. Adult cardiac-derived stem cells: differentiation and survival regulators. Vitam Horm. 2011;87:111-25.

Kawaguchi N. Stem cells for cardiac regeneration and possible roles of the transforming growth factor-beta superfamily. Biomol Concepts. 2012;3(1):99-106.

Kawaguchi N, Hatta K, Nakanishi T. 3D-culture system for heart regeneration and cardiac medicine. Biomed Res Int. 2013;2013:895967.

Kawaguchi N, Machida M, Hatta K, Nakanishi T, Takagaki Y. Cell shape and cardiosphere differentiation: a revelation by proteomic profiling. Biochem Res Int. 2013;2013:730874.

Kawaguchi N, Nakanishi T. Cardiomyocyte regeneration. Cells. 2013;2(1):67-82.

Kawamura M, Miyagawa S, Fukushima S, Saito A, Miki K, Funakoshi S, et al. Enhanced therapeutic effects of human iPS cell derived-cardiomyocyte by combined cell-sheets with omental flap technique in porcine ischemic cardiomyopathy model. Sci Rep. 2017;7(1):8824.

Kelm JM, Diaz Sanchez-Bustamante C, Ehler E, Hoerstrup SP, Djonov V, Ittner L, et al. VEGF profiling and angiogenesis in human microtissues. J Biotechnol. 2005;118(2):213-29.

Kelm JM, Ehler E, Nielsen LK, Schlatter S, Perriard JC, Fussenegger M. Design of artificial myocardial microtissues. Tissue Eng. 2004;10(1-2):201-14.

Kelm JM, Fussenegger M. Microscale tissue engineering using gravity-enforced cell assembly. Trends Biotechnol. 2004;22(4):195-202.

Kempf H, Olmer R, Kropp C, Ruckert M, Jara-Avaca M, Robles-Diaz D, et al. Controlling expansion and cardiomyogenic differentiation of human pluripotent stem cells in scalable suspension culture. Stem Cell Reports. 2014;3(6):1132-46.

Khademhosseini A, Eng G, Yeh J, Kucharczyk PA, Langer R, Vunjak-Novakovic G, et al. Microfluidic patterning for fabrication of contractile cardiac organoids. Biomedical Microdevices. 2007;9(2):149-57.

Khoushhal Z, Hussain MA, Greco E, Mamdani M, Verma S, Rotstein O, et al. Prevalence and causes of attrition among surgical residents: a systematic review and meta-analysis. JAMA Surg. 2017;152(3):265-72.

Kim TY, Kofron CM, King ME, Markes AR, Okundaye AO, Qu Z, et al. Directed fusion of cardiac spheroids into larger heterocellular microtissues enables investigation of cardiac action potential propagation via cardiac fibroblasts. PLoS One. 2018;13(5):e0196714.

Kimura W, Sadek HA. The cardiac hypoxic niche: emerging role of hypoxic microenvironment in cardiac progenitors. Cardiovasc Diagn Ther. 2012;2(4):278-89.

Kinney MA, Saeed R, McDevitt TC. Systematic analysis of embryonic stem cell differentiation in hydrodynamic environments with controlled embryoid body size. Integr Biol (Camb). 2012;4(6):641-50.

Kiraly L. Three-dimensional modelling and three-dimensional printing in pediatric and congenital cardiac surgery. Translational pediatrics. 2018;7(2):129-38.

Kizawa H, Nagao E, Shimamura M, Zhang G, Torii H. Scaffold-free 3D bio-printed human liver tissue stably maintains metabolic functions useful for drug discovery. Biochemistry and biophysics reports. 2017;10:186-91.

Klaourakis K, Vieira JM, Riley PR. The evolving cardiac lymphatic vasculature in development, repair and regeneration. Nature reviews Cardiology. 2021;18(5):368-79.

Klotz S, Drees G. Foreword. New therapeutic strategies for the medical and surgical management of end-stage heart failure patients. Thorac Cardiovasc Surg. 2010;58 Suppl 2:S165-6.

Kobuszewska A, Tomecka E, Zukowski K, Jastrzebska E, Chudy M, Dybko A, et al. Heart-on-a-Chip: An Investigation of the Influence of Static and Perfusion Conditions on Cardiac (H9C2) Cell Proliferation, Morphology, and Alignment. SLAS Technol. 2017;22(5):536-46.

Kodama H. Automatic method for fabricating a three-dimensional plastic model with photo-hardening polymer. Review of Scientific Instruments. 1981;52(11):1770-3.

Koti P, Muselimyan N, Mirdamadi E, Asfour H, Sarvazyan NA. Use of GelMA for 3D printing of cardiac myocytes and fibroblasts. Journal of 3D Printing in Medicine. 2019;3(1):11-22.

Koudan EV, Korneva JV, Karalkin PA, Gladkaya IS, Gryadunova AA, Mironov VA, et al. The Scalable Standardized Biofabrication of Tissue Spheroids from Different Cell Types Using Nonadhesive Technology. 3D Printing and Additive Manufacturing. 2017;4(1):53-60.

Kurup HK, Samuel BP, Vettukattil JJ. Hybrid 3D printing: a game-changer in personalized cardiac medicine? Expert review of cardiovascular therapy. 2015;13(12):1281-4.

Laflamme MA, Chen KY, Naumova AV, Muskheli V, Fugate JA, Dupras SK, et al. Cardiomyocytes derived from human embryonic stem cells in pro-survival factors enhance function of infarcted rat hearts. Nat Biotechnol. 2007;25(9):1015-24.

Lamb EK, Kao GW, Kao RL. Cellular cardiomyoplasty: its past, present, and future. Methods Mol Biol. 2013;1036:1-17.

LaPietra A, Grossi EA, Derivaux CC, Applebaum RM, Hanjis CD, Ribakove GH, et al. Robotic-assisted instruments enhance minimally invasive mitral valve surgery. The Annals of Thoracic Surgery. 2000;70(3):835-8.

Lee KY, Mooney DJ. Alginate: properties and biomedical applications. Prog Polym Sci. 2012;37(1):106-26.

Lee TJ, Kang S, Jeong GJ, Yoon JK, Bhang SH, Oh J, et al. Incorporation of gold-coated microspheres into embryoid body of human embryonic stem cells for cardiomyogenic differentiation. Tissue Eng Part A. 2015;21(1-2):374-81.

Legere SA, Haidl ID, Légaré JF, Marshall JS. Mast cells in cardiac fibrosis: New insights suggest opportunities for intervention. Front Immunol. 2019;10(MAR).

Leonard JR, Rahouma M, Abouarab AA, Schwann AN, Scuderi G, Lau C, et al. Totally endoscopic coronary artery bypass surgery: A meta-analysis of the current evidence. International Journal of Cardiology. 2018;261:42-6.

Leong YY, Ng WH, Ellison-Hughes GM, Tan JJ. Cardiac Stem Cells for Myocardial Regeneration: They Are Not Alone. Frontiers in cardiovascular medicine. 2017;4:47.

Lesman A, Habib M, Caspi O, Gepstein A, Arbel G, Levenberg S, et al. Transplantation of a Tissue-Engineered Human Vascularized Cardiac Muscle. Tissue Engineering Part A. 2009;16(1):115-25.

Leung BM, Lesher-Perez SC, Matsuoka T, Moraes C, Takayama S. Media additives to promote spheroid circularity and compactness in hanging drop platform. Biomater Sci. 2015;3(2):336-44.

Li Y, Li H, Pei J, Hu S, Nie Y. Transplantation of murine neonatal cardiac macrophage improves adult cardiac repair. Cell Mol Immunol. 2021;18(2):492-4.

Lietz K, Miller LW. Improved survival of patients with end-stage heart failure listed for heart transplantation: analysis of organ procurement and transplantation network/U.S. United Network of Organ Sharing data, 1990 to 2005. J Am Coll Cardiol. 2007;50(13):1282-90.

Lilyanna S, Martinez EC, Vu TD, Ling LH, Gan SU, Tan AL, et al. Cord lining-mesenchymal stem cells graft supplemented with an omental flap induces myocardial revascularization and ameliorates cardiac dysfunction in a rat model of chronic ischemic heart failure. Tissue Eng Part A. 2013;19(11-12):1303-15.

Lim EKS, Batchelor TJP, Dunning J, Shackcloth M, Anikin V, Naidu B, et al. Video-assisted thoracoscopic versus open lobectomy in patients with early-stage lung cancer: One-year results from a randomized controlled trial (VIOLET). J Clin Oncol. 2021;39(15_suppl):8504-.

Liu Y, Moller B, Wiltfang J, Warnke PH, Terheyden H. Tissue engineering of a vascularized bone graft of critical size with an osteogenic and angiogenic factor-based in vivo bioreactor. Tissue Eng Part A. 2014;20(23-24):3189-97.

Lund LH, Khush KK, Cherikh WS, Goldfarb S, Kucheryavaya AY, Levvey BJ, et al. The registry of the International Society for Heart and Lung Transplantation: thirty-fourth adult heart transplantation report-2017; focus theme: allograft ischemic time. J Heart Lung Transplant. 2017;36(10):1037-46.

Lutolf MP, Lauer-Fields JL, Schmoekel HG, Metters AT, Weber FE, Fields GB, et al. Synthetic matrix metalloproteinase-sensitive hydrogels for the conduction of tissue regeneration: engineering cell-invasion characteristics. Proc Natl Acad Sci U S A. 2003;100(9):5413.

Lv D, Hu Z, Lu L, Lu H, Xu X. Three-dimensional cell culture: A powerful tool in tumor research and drug discovery. Oncol Lett. 2017;14(6):6999-7010.

Ma J, Guo L, Fiene SJ, Anson BD, Thomson JA, Kamp TJ, et al. High purity human-induced pluripotent stem cell-derived cardiomyocytes: electrophysiological properties of action potentials and ionic currents. Am J Physiol Heart Circ Physiol. 2011;301(5):H2006-17.

Ma Z, Huebsch N, Koo S, Mandegar MA, Siemons B, Boggess S, et al. Contractile deficits in engineered cardiac microtissues as a result of MYBPC3 deficiency and mechanical overload. Nat Biomed Eng. 2018;2(12):955-67.

MacGowan GA, Crossland DS, Hasan A, Schueler S. Considerations for patients awaiting heart transplantation—insights from the UK experience. J Thorac Dis. 2015;7(3):527-31.

MacQueen LA, Sheehy SP, Chantre CO, Zimmerman JF, Pasqualini FS, Liu X, et al. A tissue-engineered scale model of the heart ventricle. Nat Biomed Eng. 2018;2(12):930-41.

Mahmoud AI, O'Meara CC, Gemberling M, Zhao L, Bryant DM, Zheng R, et al. Nerves regulate cardiomyocyte proliferation and heart regeneration. Dev Cell. 2015;34(4):387-99.

Maiullari F, Costantini M, Milan M, Pace V, Chirivi M, Maiullari S, et al. A multi-cellular 3D bioprinting approach for vascularized heart tissue engineering based on HUVECs and iPSC-derived cardiomyocytes. Sci Rep. 2018;8(1):13532.

Maizels L, Huber I, Arbel G, Tijsen AJ, Gepstein A, Khoury A, et al. Patient-Specific Drug Screening Using a Human Induced Pluripotent Stem Cell Model of Catecholaminergic Polymorphic Ventricular Tachycardia Type 2. Circ Arrhythm Electrophysiol. 2017;10(6).

Makkar RR, Smith RR, Cheng K, Malliaras K, Thomson LE, Berman D, et al. Intracoronary cardiosphere-derived cells for heart regeneration after myocardial infarction (CADUCEUS): a prospective, randomised phase 1 trial. Lancet. 2012;379(9819):895-904.

Maltsev VA, Wobus AM, Rohwedel J, Bader M, Hescheler J. Cardiomyocytes differentiated in vitro from embryonic stem cells developmentally express cardiac-specific genes and ionic currents. Circ Res. 1994;75(2):233-44.

Mancha Sánchez E, Gómez-Blanco JC, López Nieto E, Casado JG, Macías-García A, Díaz Díez MA, et al. Hydrogels for bioprinting: A systematic review of hydrogels synthesis, bioprinting parameters, and bioprinted structures behavior. Frontiers in Bioengineering and Biotechnology. 2020;8(776).

Martens A, Rojas SV, Baraki H, Rathert C, Schecker N, Hernandez SR, et al. Macroscopic fluorescence imaging: a novel technique to monitor retention and distribution of injected microspheres in an experimental model of ischemic heart failure. PLoS One. 2014;9(8):e101775.

Mathur A, Loskill P, Shao K, Huebsch N, Hong S, Marcus SG, et al. Human iPSC-based cardiac microphysiological system for drug screening applications. Sci Rep. 2015;5:8883.

Mattapally S, Zhu W, Fast VG, Gao L, Worley C, Kannappan R, et al. Spheroids of cardiomyocytes derived from human-induced pluripotent stem cells improve recovery from myocardial injury in mice. Am J Physiol Heart Circ Physiol. 2018;315(2):H327-h39.

Mauretti A, Spaans S, Bax NAM, Sahlgren C, Bouten CVC. Cardiac progenitor cells and the interplay with their microenvironment. Stem Cells Int. 2017;2017:7471582.

Mawad D, Artzy-Schnirman A, Tonkin J, Ramos J, Inal S, Mahat MM, et al. Electroconductive hydrogel based on functional poly(ethylenedioxy thiophene). Chem Mater. 2016;28(17):6080-8.

Mawad D, Figtree G, Gentile C. Current technologies based on the knowledge of the stem cells Microenvironments. Adv Exp Med Biol. 2017;1041:245-62.

Mawad D, Mansfield C, Lauto A, Perbellini F, Nelson GW, Tonkin J, et al. A conducting polymer with enhanced electronic stability applied in cardiac models. Sci Adv. 2016;2(11):e1601007.

McAllister TN, Dusserre N, Maruszewski M, L'Heureux N. Cell-based therapeutics from an economic perspective: primed for a commercial success or a research sinkhole? Regen Med. 2008;3(6):925-37.

McBride K, Steffens D, Stanislaus C, Solomon M, Anderson T, Thanigasalam R, et al. Detailed cost of robotic-assisted surgery in the Australian public health sector: from implementation to a multi-specialty caseload. BMC Health Serv Res. 2021;21(1):108.

Mehesz AN, Brown J, Hajdu Z, Beaver W, da Silva JV, Visconti RP, et al. Scalable robotic biofabrication of tissue spheroids. Biofabrication. 2011;3(2):025002.

Mehta G, Hsiao AY, Ingram M, Luker GD, Takayama S. Opportunities and challenges for use of tumor spheroids as models to test drug delivery and efficacy. J Control Release. 2012;164(2):192-204.

Menasché P, Vanneaux V, Hagege A, Bel A, Cholley B, Cacciapuoti I, et al. Human embryonic stem cell-derived cardiac progenitors for severe heart failure treatment: first clinical case report. Eur Heart J. 2015;36(30):2011-7.

Menasché P, Vanneaux V, Hagege A, Bel A, Cholley B, Parouchev A, et al. Transplantation of human embryonic stem cell-derived cardiovascular progenitors for severe ischemic left ventricular dysfunction. J Am Coll Cardiol. 2018;71(4):429-38.

Messina E, De Angelis L, Frati G, Morrone S, Chimenti S, Fiordaliso F, et al. Isolation and expansion of adult cardiac stem cells from human and murine heart. Circ Res. 2004;95(9):911-21.

Michler RE. Stem cell therapy for heart failure. Methodist Debakey Cardiovasc J. 2013;9(4):187-94.

Miller JS, Stevens KR, Yang MT, Baker BM, Nguyen DH, Cohen DM, et al. Rapid casting of patterned vascular networks for perfusable engineered three-dimensional tissues. Nat Mater. 2012;11(9):768-74.

Mironov V, Kasyanov V, Markwald RR. Organ printing: from bioprinter to organ biofabrication line. Curr Opin Biotechnol. 2011;22(5):667-73.

Mironov V, Visconti RP, Kasyanov V, Forgacs G, Drake CJ, Markwald RR. Organ printing: tissue spheroids as building blocks. Biomaterials. 2009;30(12):2164-74.

Moldovan NI, Hibino N, Nakayama K. Principles of the Kenzan method for robotic cell spheroid-based three-dimensional bioprinting. Tissue Eng Part B Rev. 2017;23(3):237-44.

Mondal A, Gebeyehu A, Miranda M, Bahadur D, Patel N, Ramakrishnan S, et al. Characterization and printability of sodium alginate -gelatin hydrogel for bioprinting NSCLC co-culture. Scientific Reports. 2019;9(1):19914.

Mongkoldhumrongkul N, Flanagan JM, Jayasinghe SN. Direct jetting approaches for handling stem cells. Biomed Mater. 2009;4(1):015018.

Montgomery M, Ahadian S, Davenport Huyer L, Lo Rito M, Civitarese RA, Vanderlaan RD, et al. Flexible shape-memory scaffold for minimally invasive delivery of functional tissues. Nat Mater. 2017;16:1038.

Moon du G, Christ G, Stitzel JD, Atala A, Yoo JJ. Cyclic mechanical preconditioning improves engineered muscle contraction. Tissue Eng Part A. 2008;14(4):473-82.

Morgan S, Grootendorst P, Lexchin J, Cunningham C, Greyson D. The cost of drug development: a systematic review. Health Policy. 2011;100(1):4-17.

Mosadegh B, Xiong G, Dunham S, Min JK. Current progress in 3D printing for cardiovascular tissue engineering. Biomed Mater. 2015;10(3):034002.

Moscarelli M, Lorusso R, Abdullahi Y, Varone E, Marotta M, Solinas M, et al. The effect of minimally invasive surgery and sternotomy on physical activity and quality of life. Heart Lung Circ. 2021;30(6):882-7.

Moscona A, Moscona H. The dissociation and aggregation of cells from organ rudiments of the early chick embryo. J Anat. 1952;86(3):287-301.

Moya M, Tran D, George SC. An integrated in vitro model of perfused tumor and cardiac tissue. Stem Cell Res Ther. 2013;4 Suppl 1:S15.

Mukouyama YS, Shin D, Britsch S, Taniguchi M, Anderson DJ. Sensory nerves determine the pattern of arterial differentiation and blood vessel branching in the skin. Cell. 2002;109(6):693-705.

Mummery C, Oostwaard DW-v, Doevendans P, Spijker R, Brink Svd, Hassink R, et al. Differentiation of human embryonic stem cells to cardiomyocytes. Circulation. 2003;107(21):2733-40.

Munarin F, Coulombe KL. A novel 3-dimensional approach for cardiac regeneration. Conf Proc IEEE Eng Med Biol Soc. 2015;2015:1741-4.

Murphy SV, Atala A. 3D bioprinting of tissues and organs. Nat Biotechnol. 2014;32(8):773-85.

Neto AI, Correia CR, Oliveira MB, Rial-Hermida MI, Alvarez-Lorenzo C, Reis RL, et al. A novel hanging spherical drop system for the generation of cellular spheroids and high throughput combinatorial drug screening. Biomater Sci. 2015;3(4):581-5.

Nguyen DC, Hookway TA, Wu Q, Jha R, Preininger MK, Chen X, et al. Microscale generation of cardiospheres promotes robust enrichment of cardiomyocytes derived from human pluripotent stem cells. Stem Cell Reports. 2014;3(2):260-8.

Noguchi R, Nakayama K, Itoh M, Kamohara K, Furukawa K, Oyama J, et al. Development of a three-dimensional pre-vascularized scaffold-free contractile cardiac patch for treating heart disease. J Heart Lung Transplant. 2016;35(1):137-45.

Noor N, Shapira A, Edri R, Gal I, Wertheim L, Dvir T. 3D printing of personalized thick and perfusable cardiac patches and hearts. Adv Sci. 2019;0(0):1900344.

Nunes SS, Miklas JW, Liu J, Aschar-Sobbi R, Xiao Y, Zhang B, et al. Biowire: a platform for maturation of human pluripotent stem cell-derived cardiomyocytes. Nat Methods. 2013;10(8):781-7.

Oliveira MB, Neto AI, Correia CR, Rial-Hermida MI, Alvarez-Lorenzo C, Mano JF. Superhydrophobic chips for cell spheroids high-throughput generation and drug screening. ACS Appl Mater Interfaces. 2014;6(12):9488-95.

Ong CS, Fukunishi T, Nashed A, Blazeski A, Zhang H, Hardy S, et al. Creation of Cardiac Tissue Exhibiting Mechanical Integration of Spheroids Using 3D Bioprinting. J Vis Exp. 2017(125).

Ong CS, Fukunishi T, Zhang H, Huang CY, Nashed A, Blazeski A, et al. Biomaterial-free three-dimensional bioprinting of cardiac tissue using human induced pluripotent stem cell derived cardiomyocytes. Scientific Reports. 2017;7(1):4566.

Ong CS, Nam L, Ong K, Krishnan A, Huang CY, Fukunishi T, et al. 3D and 4D Bioprinting of the Myocardium: Current Approaches, Challenges, and Future Prospects. Biomed Res Int. 2018;2018:6497242.

Onofrillo C, Duchi S, O'Connell C, Blanchard R, O'Connor AJ, Scott M, et al. Biofabrication of human articular cartilage: a path towards the development of a clinical treatment. Biofabrication. 2018.

Orecchioni M, Ghosheh Y, Pramod AB, Ley K. Macrophage polarization: different gene signatures in M1(LPS+) vs. classically and M2(LPS–) vs. alternatively activated macrophages. Front Immunol. 2019;10(1084).

Osidak EO, Karalkin PA, Osidak MS, Parfenov VA, Sivogrivov DE, Pereira F, et al. Viscoll collagen solution as a novel bioink for direct 3D bioprinting. J Mater Sci Mater Med. 2019;30(3):31.

Owens AT, Brozena SC, Jessup M. New Management Strategies in Heart Failure. Circ Res. 2016;118(3):480-95.

Owens CM, Marga F, Forgacs G, Heesch CM. Biofabrication and testing of a fully cellular nerve graft. Biofabrication. 2013;5(4):045007.

Parfenov VA, Koudan EV, Bulanova EA, Karalkin PA, F DASP, Norkin NE, et al. Scaffold-free, label-free and nozzle-free biofabrication technology using magnetic levitational assembly. Biofabrication. 2018;10(3):034104.

Parker KK, Ingber DE. Extracellular matrix, mechanotransduction and structural hierarchies in heart tissue engineering. Philos Trans R Soc Lond B Biol Sci. 2007;362(1484):1267-79.

Parrish J, Lim KS, Baer K, Hooper GJ, Woodfield TBF. A 96-well microplate bioreactor platform supporting individual dual perfusion and high-throughput assessment of simple or biofabricated 3D tissue models. Lab Chip. 2018;18(18):2757-75.

Pendyala L, Goodchild T, Gadesam RR, Chen J, Robinson K, Chronos N, et al. Cellular cardiomyoplasty and cardiac regeneration. Curr Cardiol Rev. 2008;4(2):72-80.

Pinto AR, Ilinykh A, Ivey MJ, Kuwabara JT, D'Antoni ML, Debuque R, et al. Revisiting cardiac cellular composition. Circ Res. 2016;118(3):400-9.

Polley C, Kussauer S, David R, Barkow P, Mau R, Seitz H. Printing of vessels for small functional tissues-A preliminary study. Current Directions in Biomedical Engineering. 2020;6(3).

Polonchuk L, Chabria M, Badi L, Hoflack JC, Figtree G, Davies MJ, et al. Cardiac spheroids as promising in vitro models to study the human heart microenvironment. Sci Rep. 2017;7(1):7005.

Polonchuk L, Surija L, Lee MH, Sharma P, Liu Chung Ming C, Richter F, et al. Towards engineering heart tissues from bioprinted cardiac spheroids. Biofabrication. 2021;13(4):045009.

Pope AJ, Sands GB, Smaill BH, LeGrice IJ. Three-dimensional transmural organization of perimysial collagen in the heart. Am J Physiol Heart Circ Physiol. 2008;295(3):H1243-h52.

Puluca N, Lee S, Doppler S, Münsterer A, Dreßen M, Krane M, et al. Bioprinting approaches to engineering vascularized 3D cardiac tissues. Curr Cardiol Rep. 2019;21(9):90.

Purpura KA, Bratt-Leal AM, Hammersmith KA, McDevitt TC, Zandstra PW. Systematic engineering of 3D pluripotent stem cell niches to guide blood development. Biomaterials. 2012;33(5):1271-80.

Qian F, Huang C, Lin YD, Ivanovskaya AN, O'Hara TJ, Booth RH, et al. Simultaneous electrical recording of cardiac electrophysiology and contraction on chip. Lab Chip. 2017;17(10):1732-9.

Qureshi ZP, Seoane-Vazquez E, Rodriguez-Monguio R, Stevenson KB, Szeinbach SL. Market withdrawal of new molecular entities approved in the United States from 1980 to 2009. Pharmacoepidemiol Drug Saf. 2011;20(7):772-7.

Redfors B, Shao Y, Omerovic E. Myocardial infarct size and area at risk assessment in mice. Exp Clin Cardiol. 2012;17(4):268-72.

Reichert K, Colantuono B, McCormack I, Rodrigues F, Pavlov V, Abid MR. Murine left anterior descending (LAD) coronary artery ligation: an improved and simplified model for myocardial infarction. J Vis Exp. 2017(122).

Reid JA, Mollica PA, Johnson GD, Ogle RC, Bruno RD, Sachs PC. Accessible bioprinting: adaptation of a low-cost 3D-printer for precise cell placement and stem cell differentiation. Biofabrication. 2016;8(2):025017.

Reinecke H, Zhang M, Bartosek T, Murry CE. Survival, integration, and differentiation of cardiomyocyte grafts: a study in normal and injured rat hearts. Circulation. 1999;100(2):193-202.

Roche C, Iyer G, Nguyen M, Mabroora S, Dome A, Sakr K, et al. Cardiac patch transplantation instruments for robotic minimally invasive cardiac surgery: initial proof-of-concept designs and surgery in a porcine cadaver [preprint]. Front Robot AI. 2021.

Roche CD, Brereton RJL, Ashton AW, Jackson C, Gentile C. Current challenges in three-dimensional bioprinting heart tissues for cardiac surgery. Eur J Cardiothorac Surg. 2020;58(3):500-10.

Roche CD, Dobson JS, Williams SK, Quante M, Popoola J, Chow JWM. Malignant and noninvasive skin tumours in renal transplant recipients. Dermatol Res Prac. 2014;2014:409058.

Roche CD, Gentile C. Transplantation of a 3D bioprinted patch in a murine model of myocardial infarction. J Vis Exp. 2020:e61675.

Roche CD, Sharma P, Ashton AW, Jackson C, Xue M, Gentile C. Printability, durability, contractility and vascular network formation in 3D bioprinted cardiac endothelial cells using alginate-gelatin hydrogels. Front Bioeng Biotechnol. 2021;9:e636257.

Roche CD, Zhou Y, Zhao L, Gentile C. A world-first surgical instrument for minimally invasive robotically-enabled transplantation of heart patches for myocardial regeneration: a brief research report. Frontiers in Surgery. 2021;8(436).

Rodness J, Mihic A, Miyagi Y, Wu J, Weisel RD, Li RK. VEGF-loaded microsphere patch for local protein delivery to the ischemic heart. Acta Biomater. 2016;45:169-81.

Romagnuolo R, Masoudpour H, Porta-Sanchez A, Qiang B, Barry J, Laskary A, et al. Human embryonic stem cell-derived cardiomyocytes regenerate the infarcted pig heart but induce ventricular tachyarrhythmias. Stem Cell Reports. 2019;12(5):967-81.

Ronaldson-Bouchard K, Ma SP, Yeager K, Chen T, Song L, Sirabella D, et al. Advanced maturation of human cardiac tissue grown from pluripotent stem cells. Nature. 2018;556(7700):239-43.

Ruytinx P, Proost P, Van Damme J, Struyf S. Chemokine-induced macrophage polarization in inflammatory conditions. Front Immunol. 2018;9(1930).

Salvi M, Morbiducci U, Amadeo F, Santoro R, Angelini F, Chimenti I, et al. Automated Segmentation of Fluorescence Microscopy Images for 3D Cell Detection in human-derived Cardiospheres. Sci Rep. 2019;9(1):6644.

Sawa Y, Miyagawa S, Sakaguchi T, Fujita T, Matsuyama A, Saito A, et al. Tissue engineered myoblast sheets improved cardiac function sufficiently to discontinue LVAS in a patient with DCM: report of a case. Surg Today. 2012;42(2):181-4.

Sawa Y, Yoshikawa Y, Toda K, Fukushima S, Yamazaki K, Ono M, et al. Safety and efficacy of autologous skeletal myoblast sheets (TCD-51073) for the treatment of severe chronic heart failure due to ischemic heart disease. Circ J. 2015;79(5):991-9.

Sawkins MJ, Saldin LT, Badylak SF, White LJ. ECM hydrogels for regenerative medicine. In: Berardi AC, editor. Extracellular Matrix for Tissue Engineering and Biomaterials. Cham: Springer International Publishing; 2018. p. 27-58.

Sazer D, Miller J. Vascular networks within 3D printed and engineered tissues. In: Ovsianikov A, Yoo J, Mironov V, editors. 3D Printing and Biofabrication. Cham: Springer International Publishing; 2018. p. 79-105.

Schlick SF, Spreckelsen F, Tiburcy M, Iyer LM, Meyer T, Zelarayan LC, et al. Agonistic and antagonistic roles of fibroblasts and cardiomyocytes on viscoelastic stiffening of engineered human myocardium. Prog Biophys Mol Biol. 2019;144:51-60.

Schofield R. The relationship between the spleen colony-forming cell and the haemopoietic stem cell. Blood cells. 1978;4(1-2):7-25.

Schroer A, Pardon G, Castillo E, Blair C, Pruitt B. Engineering hiPSC cardiomyocyte in vitro model systems for functional and structural assessment. Prog Biophys Mol Biol. 2019;144:3-15.

Shademan A, Decker RS, Opfermann JD, Leonard S, Krieger A, Kim PC. Supervised autonomous robotic soft tissue surgery. Sci Transl Med. 2016;8(337):337ra64.

Shadrin IY, Allen BW, Qian Y, Jackman CP, Carlson AL, Juhas ME, et al. Cardiopatch platform enables maturation and scale-up of human pluripotent stem cell-derived engineered heart tissues. Nat Commun. 2017;8(1):1825.

Shafiee A, Atala A. Printing technologies for medical applications. Trends Mol Med. 2016;22(3):254-65.

Shevach M, Fleischer S, Shapira A, Dvir T. Gold nanoparticle-decellularized matrix hybrids for cardiac tissue engineering. Nano Lett. 2014;14(10):5792-6.

Shevach M, Soffer-Tsur N, Fleischer S, Shapira A, Dvir T. Fabrication of omentum-based matrix for engineering vascularized cardiac tissues. Biofabrication. 2014;6(2):024101.

Shevach M, Zax R, Abrahamov A, Fleischer S, Shapira A, Dvir T. Omentum ECM-based hydrogel as a platform for cardiac cell delivery. Biomed Mater. 2015;10(3):034106.

Shin HS, Shin HH, Shudo Y. Current status and limitations of myocardial infarction large animal models in cardiovascular translational research. Frontiers in Bioengineering and Biotechnology. 2021;9(321).

Shin'oka T, Imai Y, Ikada Y. Transplantation of a tissue-engineered pulmonary artery. N Engl J Med. 2001;344(7):532-3.

Shri M, Agrawal H, Rani P, Singh D, Onteru SK. Hanging Drop, A Best Three-Dimensional (3D) Culture Method for Primary Buffalo and Sheep Hepatocytes. Sci Rep. 2017;7(1):1203.

Simon MC, Keith B. The role of oxygen availability in embryonic development and stem cell function. Nat Rev Mol Cell Biol. 2008;9(4):285-96.

Singelyn JM, Sundaramurthy P, Johnson TD, Schup-Magoffin PJ, Hu DP, Faulk DM, et al. Catheter-deliverable hydrogel derived from decellularized ventricular extracellular matrix increases endogenous cardiomyocytes and preserves cardiac function post-myocardial infarction. J Am Coll Cardiol. 2012;59(8):751-63.

Sirenko O, Hancock MK, Crittenden C, Hammer M, Keating S, Carlson CB, et al. Phenotypic Assays for Characterizing Compound Effects on Induced Pluripotent Stem Cell-Derived Cardiac Spheroids. Assay Drug Dev Technol. 2017;15(6):280-96.

Skardal A. Perspective: “Universal” bioink technology for advancing extrusion bioprinting-based biomanufacturing. Bioprinting. 2018:e00026.

Smith RR, Barile L, Cho HC, Leppo MK, Hare JM, Messina E, et al. Regenerative potential of cardiosphere-derived cells expanded from percutaneous endomyocardial biopsy specimens. Circulation. 2007;115(7):896-908.

Soonpaa MH, Koh GY, Klug MG, Field LJ. Formation of nascent intercalated disks between grafted fetal cardiomyocytes and host myocardium. Science. 1994;264(5155):98-101.

Sperelakis N. Cultured heart cell reaggregate model for studying cardiac toxicology. Environ Health Perspect. 1978;26:243-67.

Stoehr A, Neuber C, Baldauf C, Vollert I, Friedrich FW, Flenner F, et al. Automated analysis of contractile force and Ca2+ transients in engineered heart tissue. American journal of physiology Heart and circulatory physiology. 2014;306(9):H1353-H63.

Su M, Luo Z, Yu J, Zhang R, Wang J, Huang C, et al. Effects of fastigial nucleus electrostimulation on cardiac nerve regeneration, neurotransmitter release, and malignant arrhythmia inducibility in a post-infarction rat model. Eur J Neurosci. 2021.

Su Q, Li L, Zhou Y, Wang J, Liu Y, Ma G. Induction of myocardial PDCD4 in coronary microembolization-related cardiac dysfunction: evidence from a large-animal study. Cell Physiol Biochem. 2014;34(2):533-42.

Suzuki R, Hattori F, Itabashi Y, Yoshioka M, Yuasa S, Manabe-Kawaguchi H, et al. Omentopexy enhances graft function in myocardial cell sheet transplantation. Biochemical and biophysical research communications. 2009;387(2):353-9.

Tabei R, Kawaguchi S, Kanazawa H, Tohyama S, Hirano A, Handa N, et al. Development of a transplant injection device for optimal distribution and retention of human induced pluripotent stem cellderived cardiomyocytes. J Heart Lung Transplant. 2019;38(2):203-14.

Takagawa J, Zhang Y, Wong ML, Sievers RE, Kapasi NK, Wang Y, et al. Myocardial infarct size measurement in the mouse chronic infarction model: comparison of area- and length-based approaches. Journal of Applied Physiology. 2007;102(6):2104-11.

Takahashi K, Yamanaka S. Induction of pluripotent stem cells from mouse embryonic and adult fibroblast cultures by defined factors. Cell. 2006;126(4):663-76.

Tan Y, Richards D, Coyle RC, Yao J, Xu R, Gou W, et al. Cell number per spheroid and electrical conductivity of nanowires influence the function of silicon nanowired human cardiac spheroids. Acta Biomater. 2017;51:495-504.

Tan Y, Richards D, Xu R, Stewart-Clark S, Mani SK, Borg TK, et al. Silicon nanowire-induced maturation of cardiomyocytes derived from human induced pluripotent stem cells. Nano Lett. 2015;15(5):2765-72.

Tao H, Chen X, Wei A, Song X, Wang W, Liang L, et al. Comparison of teratoma formation between embryonic stem cells and parthenogenetic embryonic stem cells by molecular imaging. Stem Cells Int. 2018;2018:7906531.

Taylor M, Jefferies J, Byrne B, Lima J, Ambale-Venkatesh B, Ostovaneh MR, et al. Cardiac and skeletal muscle effects in the randomized HOPE-Duchenne trial. Neurology. 2019;92(8):e866-e78.

Teng CJ, Luo J, Chiu RC, Shum-Tim D. Massive mechanical loss of microspheres with direct intramyocardial injection in the beating heart: implications for cellular cardiomyoplasty. J Thorac Cardiovasc Surg. 2006;132(3):628-32.

Tiburcy M, Hudson JE, Balfanz P, Schlick S, Meyer T, Chang Liao ML, et al. Defined Engineered Human Myocardium With Advanced Maturation for Applications in Heart Failure Modeling and Repair. Circulation. 2017;135(19):1832-47.

Tiburcy M, Meyer T, Soong PL, Zimmermann WH. Collagen-based engineered heart muscle. Methods Mol Biol. 2014;1181:167-76.

Tomlinson L, Lu ZQ, Bentley RA, Colley HE, Murdoch C, Webb SD, et al. Attenuation of doxorubicin-induced cardiotoxicity in a human in vitro cardiac model by the induction of the NRF-2 pathway. Biomed Pharmacother. 2019;112:108637.

Torregrossa G, Balkhy HH. The role of robotic totally endoscopic coronary artery bypass in the future of coronary artery revascularization. Eur J Cardiothorac Surg. 2020;58(2):217-20.

Transplant Service NHS. Organ donation and transplantation annual activity report 2018/20192019 29 November 2019. Available from: https://nhsbtdbe.blob.core.windows.net/umbraco-assets-corp/16537/organ-donation-and-transplantation-activity-report-2018-2019.pdf.

Trevis J, Chilvers N, Freystaetter K, Dunning J. Surgeon-Powered Robotics in Thoracic Surgery; An Era of Surgical Innovation and Its Benefits for the Patient and Beyond. Frontiers in Surgery. 2020;7(109).

Trivedi JR, Schumer E, Black M, Massey HT, Cheng A, Slaughter MS. Risk factors of waiting list mortality for patients awaiting heart transplant. J Heart Lung Transplant. 2016;35(4):S214.

Tseliou E, Pollan S, Malliaras K, Terrovitis J, Sun B, Galang G, et al. Allogeneic Cardiospheres Safely Boost Cardiac Function and Attenuate Adverse Remodeling After Myocardial Infarction in Immunologically Mismatched Rat Strains. Journal of the American College of Cardiology. 2013;61(10):1108-19.

Tu C, Chao B, Wu J. Strategies for improving the maturity of human induced pluripotent stem cell-derived cardiomyocytes. Circ Res. 2018;123(5):512-4.

Tulloch NL, Muskheli V, Razumova MV, Korte FS, Regnier M, Hauch KD, et al. Growth of engineered human myocardium with mechanical loading and vascular coculture. Circ Res. 2011;109(1):47-59.

Tung YC, Hsiao AY, Allen SG, Torisawa YS, Ho M, Takayama S. High-throughput 3D spheroid culture and drug testing using a 384 hanging drop array. Analyst. 2011;136(3):473-8.

Turnbull IC, Karakikes I, Serrao GW, Backeris P, Lee JJ, Xie C, et al. Advancing functional engineered cardiac tissues toward a preclinical model of human myocardium. FASEB J. 2014;28(2):644-54.

Uosaki H, Taguchi YH. Comparative gene expression analysis of mouse and human cardiac maturation. Genomics Proteomics Bioinformatics. 2016;14(4):207-15.

Vadivelu RK, Kamble H, Shiddiky MJA, Nguyen N-T. Microfluidic Technology for the Generation of Cell Spheroids and Their Applications. Micromachines (Basel). 2017;8(4):94.

Vagnozzi RJ, Maillet M, Sargent MA, Khalil H, Johansen AK, Schwanekamp JA, et al. An acute immune response underlies the benefit of cardiac stem-cell therapy. Nature. 2019.

Valls-Margarit M, Iglesias-García O, Di Guglielmo C, Sarlabous L, Tadevosyan K, Paoli R, et al. Engineered macroscale cardiac constructs elicit human myocardial tissue-like functionality. Stem Cell Reports. 2019;13(1):207-20.

van den Borne SWM, van de Schans VAM, Strzelecka AE, Vervoort-Peters HTM, Lijnen PM, Cleutjens JPM, et al. Mouse strain determines the outcome of wound healing after myocardial infarction. Cardiovasc Res. 2009;84(2):273-82.

Varzideh F, Mahmoudi E, Pahlavan S. Coculture with noncardiac cells promoted maturation of human stem cell-derived cardiomyocyte microtissues. J Cell Biochem. 2019.

Verissimo AR, Nakayama K. Scaffold-Free Biofabrication. In: Ovsianikov A, Yoo J, Mironov V, editors. 3D Printing and Biofabrication. Cham: Springer International Publishing; 2017. p. 1-20.

Vermeulen N, Haddow G, Seymour T, Faulkner-Jones A, Shu W. 3D bioprint me: a socioethical view of bioprinting human organs and tissues. J Med Ethics. 2017;43(9):618-24.

Vijayavenkataraman S, Yan WC, Lu WF, Wang CH, Fuh JYH. 3D bioprinting of tissues and organs for regenerative medicine. Advanced drug delivery reviews. 2018;132:296-332.

Visconti RP, Kasyanov V, Gentile C, Zhang J, Markwald RR, Mironov V. Towards organ printing: engineering an intra-organ branched vascular tree. Expert Opin Biol Ther. 2010;10(3):409-20.

Visone R, Ugolini GS, Vinarsky V, Penati M, Redaelli A, Forte G, et al. A Simple Vacuum-Based Microfluidic Technique to Establish High-Throughput Organs-On-Chip and 3D Cell Cultures at the Microscale. Advanced Materials Technologies. 2019;4(1):1800319.

Vunjak-Novakovic G, Tandon N, Godier A, Maidhof R, Marsano A, Martens TP, et al. Challenges in cardiac tissue engineering. Tissue Eng Part B Rev. 2010;16(2):169-87.

Walker RL, Eggel M. From mice to monkeys? Beyond orthodox approaches to the ethics of animal model choice. Animals (Basel). 2020;10(1).

Walther G. Printing Insecurity? The Security Implications of 3D-Printing of Weapons. Sci Eng Ethics. 2015;21(6):1435-45.

Wang H, Roche CD, Gentile C. Omentum support for cardiac regeneration in ischaemic cardiomyopathy models: a systematic scoping review. Eur J Cardiothorac Surg. 2020;58(6):1118-29.

Wang L, Liu Y, Ye G, He Y, Li B, Guan Y, et al. Injectable and conductive cardiac patches repair infarcted myocardium in rats and minipigs. Nat Biomed Eng. 2021.

Wang L, Serpooshan V, Zhang J. Engineering human cardiac muscle patch constructs for prevention of post-infarction LV remodeling. Frontiers in cardiovascular medicine. 2021;8(111).

Wang S, Lee JM, Yeong WY. Smart hydrogels for 3D bioprinting. Int J Bioprinting. 2015;1(1):3-14.

Wang X, Ao Q, Tian X, Fan J, Tong H, Hou W, et al. Gelatin-based hydrogels for organ 3D bioprinting. Polymers. 2017;9(9):401.

Waters R, Alam P, Pacelli S, Chakravarti AR, Ahmed RPH, Paul A. Stem cell-inspired secretome-rich injectable hydrogel to repair injured cardiac tissue. Acta Biomater. 2018;69:95-106.

Whitehead AJ, Engler AJ. Regenerative cross talk between cardiac cells and macrophages. Am J Physiol Heart Circ Physiol. 2021;320(6):H2211-h21.

Wobus AM, Wallukat G, Hescheler J. Pluripotent mouse embryonic stem cells are able to differentiate into cardiomyocytes expressing chronotropic responses to adrenergic and cholinergic agents and Ca2+ channel blockers. Differentiation. 1991;48(3):173-82.

Wu LY, Di Carlo D, Lee LP. Microfluidic self-assembly of tumor spheroids for anticancer drug discovery. Biomed Microdevices. 2008;10(2):197-202.

Wu PH, Giri A, Sun SX, Wirtz D. Three-dimensional cell migration does not follow a random walk. Proc Natl Acad Sci U S A. 2014;111(11):3949-54.

Wu W, DeConinck A, Lewis JA. Omnidirectional printing of 3D microvascular networks. Adv Mater. 2011;23(24):H178-83.

Xu B, Han X, Hu Y, Luo Y, Chen CH, Chen Z, et al. A remotely controlled transformable soft robot based on engineered cardiac tissue construct. Small. 2019;15(18):e1900006.

Xu L, Varkey M, Jorgensen A, Ju J, Jin Q, Park JH, et al. Bioprinting small diameter blood vessel constructs with an endothelial and smooth muscle cell bilayer in a single step. Biofabrication. 2020;12(4).

Xu Y, Guan J. Biomaterial property-controlled stem cell fates for cardiac regeneration. Bioact Mater. 2016;1(1):18-28.

Xu Y, Patnaik S, Guo X, Li Z, Lo W, Butler R, et al. Cardiac differentiation of cardiosphere-derived cells in scaffolds mimicking morphology of the cardiac extracellular matrix. Acta Biomater. 2014;10(8):3449-62.

Xue M, Lin H, Liang HPH, McKelvey K, Zhao R, March L, et al. Deficiency of protease-activated receptor (PAR) 1 and PAR2 exacerbates collagen-induced arthritis in mice via differing mechanisms. Rheumatology (Oxford). 2020.

Yang B, Lui C, Yeung E, Matsushita H, Jeyaram A, Pitaktong I, et al. A net mold-based method of biomaterial-free three-dimensional cardiac tissue creation. Tissue Eng Part C Methods. 2019;25(4):243-52.

Yechiel E, Barenholz Y. Cultured heart cell reaggregates: a model for studying relationships between aging and lipid composition. Biochim Biophys Acta. 1986;859(1):105-9.

Yee K, Malliaras K, Kanazawa H, Tseliou E, Cheng K, Luthringer DJ, et al. Allogeneic cardiospheres delivered via percutaneous transendocardial injection increase viable myocardium, decrease scar size, and attenuate cardiac dilatation in porcine ischemic cardiomyopathy. PloS one. 2014;9(12):e113805-e.

Yoo SJ, Thabit O, Kim EK, Ide H, Yim D, Dragulescu A, et al. 3D printing in medicine of congenital heart diseases. 3D printing in medicine. 2015;2(1):3.

Yoshida S, Miyagawa S, Fukushima S, Kawamura T, Kashiyama N, Ohashi F, et al. Maturation of human induced pluripotent stem cell-derived cardiomyocytes by soluble factors from human mesenchymal stem cells. Mol Ther. 2018;26(11):2681-95.

Yoshikawa Y, Miyagawa S, Toda K, Saito A, Sakata Y, Sawa Y. Myocardial regenerative therapy using a scaffold-free skeletal-muscle-derived cell sheet in patients with dilated cardiomyopathy even under a left ventricular assist device: a safety and feasibility study. Surg Today. 2018;48(2):200-10.

Yoshioka N, Dowdy SF. Enhanced generation of iPSCs from older adult human cells by a synthetic five-factor self-replicative RNA. PLoS One. 2017;12(7):e0182018.

Yoshioka N, Gros E, Li HR, Kumar S, Deacon DC, Maron C, et al. Efficient generation of human iPSCs by a synthetic self-replicative RNA. Cell stem cell. 2013;13(2):246-54.

Yu C, Ma X, Zhu W, Wang P, Miller KL, Stupin J, et al. Scanningless and continuous 3D bioprinting of human tissues with decellularized extracellular matrix. Biomaterials. 2019;194:1-13.

Yurekli, Kestelli, Cakir. EJCTS-2021-100278 - omentopexy may not be enough, Experimental, Letter to the Editor (received: 26.01.2021). Eur J Cardio-Thorac Surg. 2021.

Zhang B, Montgomery M, Chamberlain MD, Ogawa S, Korolj A, Pahnke A, et al. Biodegradable scaffold with built-in vasculature for organ-on-a-chip engineering and direct surgical anastomosis. Nat Mater. 2016;15(6):669-78.

Zhang D, Shadrin IY, Lam J, Xian HQ, Snodgrass HR, Bursac N. Tissue-engineered cardiac patch for advanced functional maturation of human ESC-derived cardiomyocytes. Biomaterials. 2013;34(23):5813-20.

Zhang J, Zhu W, Radisic M, Vunjak-Novakovic G. Can we engineer a human cardiac patch for therapy? Circ Res. 2018;123(2):244-65.

Zhang Y, Kumar P, Lv S, Xiong D, Zhao H, Cai Z, et al. Recent advances in 3D bioprinting of vascularized tissues. Materials & Design. 2021;199:109398.

Zhang YS, Arneri A, Bersini S, Shin SR, Zhu K, Goli-Malekabadi Z, et al. Bioprinting 3D microfibrous scaffolds for engineering endothelialized myocardium and heart-on-a-chip. Biomaterials. 2016;110:45-59.

Zhang YS, Pi Q, van Genderen AM. Microfluidic Bioprinting for Engineering Vascularized Tissues and Organoids. J Vis Exp. 2017(126).

Zhao H, Chen Y, Shao L, Xie M, Nie J, Qiu J, et al. Airflow-Assisted 3D Bioprinting of Human Heterogeneous Microspheroidal Organoids with Microfluidic Nozzle. Small. 2018;14(39):e1802630.

Zhao Y, Rafatian N, Feric NT, Cox BJ, Aschar-Sobbi R, Wang EY, et al. A Platform for Generation of Chamber-Specific Cardiac Tissues and Disease Modeling. Cell. 2019;176(4):913-27.e18.

Zhou G, Jiang H, Yin Z, Liu Y, Zhang Q, Zhang C, et al. In vitro regeneration of patient-specific ear-shaped cartilage and its first clinical application for auricular reconstruction. EBioMedicine. 2018;28:287-302.

Zhou P, Pu William T. Recounting cardiac cellular composition. Circulation Research. 2016;118(3):368-70.

Zhou Q, Zhou J-Y, Zheng Z, Zhang H, Hu S-S. A novel vascularized patch enhances cell survival and modifies ventricular remodeling in a rat myocardial infarction model. J Thorac Cardiovasc Surg. 2010;140(6):1388-96.e3.

Zhou X, Zhang H, Feng M, Zhao J, Fu Y. New remote centre of motion mechanism for robot-assisted minimally invasive surgery. Biomed Eng Online. 2018;17(1):170.

Zhu D, Li Z, Huang K, Caranasos TG, Rossi JS, Cheng K. Minimally invasive delivery of therapeutic agents by hydrogel injection into the pericardial cavity for cardiac repair. Nature Communications. 2021;12(1):1412.

Zimmermann WH, Schneiderbanger K, Schubert P, Didie M, Munzel F, Heubach JF, et al. Tissue engineering of a differentiated cardiac muscle construct. Circ Res. 2002;90(2):223-30.

Zuppinger C. Measurement of contractility and calcium release in cardiac spheroids. Methods Mol Biol. 2019;1929:41-52.